Investigating opiate-induced changes on respiratory pattern and brain blood flow in mice

Majdi Mohammedzaki Damanhori MD, MSc

Submitted in fulfilment of the requirements for the Degree of Doctor of Philosophy

The Institute of Neuroscience and Psychology
College of Medical, Veterinary and Life Sciences

University of Glasgow

August 2021

Abstract

Breathing is a rhythmic motor process that starts at the perinatal age, influenced by other physiological measures, and continues throughout the life course of a mammal. Failure to produce a respiratory rhythm can be fatal and understanding the mechanism of the respiratory rhythm generation by the brainstem is crucial. In vitro and in vivo studies have disclosed evidence of a region within the ventrolateral medulla, known as the pre-Bötzinger complex (preBötC), and assumes it to be the respiratory rhythmogenesis originator. Also, some studies suggest the retrotrapezoid nucleus/parafacial respiratory group (RTN/pFRG) as a second respiratory rhythm generator that plays a certain role in in the neonatal rodent.

At neonatal age in rodents and humans, the breathing pattern is irregular and respiratory system is immature, which signifies that it is vulnerable to external environmental challenges during this period. Nevertheless, the maturity step occurs early in life and breathing becomes stable and constant. The mechanisms of respiratory rhythm generation perinatally remains elusive, and it is hypothesised that the RTN/pFRG acts as the dominant respiratory rhythm generator during the early days of life when the respiratory system is immature. After that, preBötC takes the role of the rhythm generation, and breathing becomes more stable. However, the interaction between preBötC and RTN/pFRG in vivo during postnatal development is not fully understood.

Fentanyl is widely used on a clinical basis to control chronic and acute pain. Despite the fact that respiratory depression is a common side effect of fentanyl, the long-term respiratory consequences of repeated fentanyl exposure is unknown. Concerning the immaturity of the respiratory system during neonatal life in mammals, the thesis was designed to understand the long-term effects of fentanyl exposure during this vulnerable period in neonatal rodents, which is a suitable model for understanding long-lasting changes in humans. Therefore, the fentanyl-exposure at postnatal stage was categorised into two groups, which are neonatal mice (NN) exposed to fentanyl (0.04 mg/kg daily) from P1-P5 and juvenile mice (JUV) exposed from P9-P13.

The first aim of the thesis was to investigate the influence of fentanyl on the postnatal maturation step of the central respiratory control. Fentanyl, a potent μ opioid receptor agonist, was introduced to evoke respiratory frequency depression in vivo by targeting preBötC neurons, which are sensitive to μ opioids, while the RTN/pFRG neurons are insensitive to μ opioids. Therefore, fentanyl was used to suppress the preBötC in vivo throughout the postnatal developmental phase. Then, the effect of the early fentanyl exposure was evaluated during adulthood via plethysmography. The plethysmography data showed differences in the respiratory rate at rest between the NN and the control group. Also, the awake fentanyl challenge showed an increase in the tidal volume response to fentanyl in the NN group.

The fentanyl challenge was applied to the study groups to evaluate the vulnerability and sensitivity to fentanyl under anaesthesia. The vulnerability to fentanyl was observed in the NN and JUV groups, which shows low survival rates of the fentanyl challenge. This indicates that the anaesthetised state is more sensitive to respiratory depression. Also, cerebral blood flow (CBF) was analysed during the same challenge to investigate the effect of opioids on CBF. An increase in the CBF was recorded via the laser speckle technique as a response to opioid exposure, and the fentanyl-exposed groups (NN and JUV) showed an attenuated response to opioid exposure within the parietal regions.

The second aim of the thesis was to highlight the chronic effect of early-life fentanyl exposure on endogenous opioids and stress hormones by utilising the enzyme-linked immunosorbent assay (ELISA) technique. The study showed low detection of the endogenous opioid level (β -endorphin) due to the small blood volume used for the analysis. Yet, the JUV-FEN group had more detectable levels of endogenous opioids, which could support the effect of earlier opioids exposure on endogenous opioids level. Weighted average trends were obtained in the JUV-FEN group compared to JUV-SAL, which were not statistically significant. In addition, a trend of the stress hormone (corticosterone) collected from hair follicle samples was noted in the JUV-FEN group.

The third aim of the thesis was to investigate the long-lasting effect of early-life fentanyl exposure on the μ opioid receptor (μOR) neural expression and distribution within the CNS. Unfortunately, the initial group had cross-contamination on the films, and the samples were discarded. Therefore, other groups were involved in the study that showed a slight decrease of μOR density across the brain regions in the JUV-FEN group compared to JUV-SAL. Nevertheless, the presented data were underpowered regarding the small sample size involved in this other group. The last study of μOR neural expression was planned to be investigated via Immunohistochemistry (IHC) for brainstem and cerebral regions. Still, due to the national lockdown and the pandemic situation, it was not completed as planned.

In conclusion, repeated early-life exposure to fentanyl possibly leads to long-lasting changes that may affect the breathing pattern at rest and last into adulthood. Those changes are attenuated under anaesthetic and may lead to respiratory arrest.

Table of Contents

List of Tables

List of Figures

Acknowledgements

I would like to thank the Saudi government for offering me the opportunity and providing the unconditional funds to pursue my postgraduate studies. Also, I would like to thank Dr Leanne McKay, my first supervisor, for supporting and guiding me through my PhD research. It has been my pleasure to know her in person and work with her through the past four years. I would like to extend my thanks to Dr Christopher McCabe and Dr David Hughes, who contributed to my PhD research and assisted me with my lab work.

I would like to thank my wife Nojoud and my little daughter Yosr for supporting me and participating in the wondrous PhD experience. Without them, it would have been difficult to get to this point by the end of my PhD journey. I would like to extend my thanks to my parents-in-law, Adnan Faqerah and Elham Istanbouli, for their advice and support.

A massive thanks to Wellcome Surgical Institute's staff, especially Linda Carberry and Lindsay Gallagher. It has been my honour to work alongside with you. Also, I would like to thank my Garscube friends, Haitham, Abdulrahman and Mohammed. It is so special to work with you all, and I hope the friendship remains forever.

I would like to dedicate this work to my family: my father Mohammed Zaki Damanhori, my mother Amirah Saleh Damanhori, and my siblings Hazar, Ghassan and Abdulelah. Your endless support has been unrivalled.

Author’s Declaration

I declare that this dissertation is the result of my personal work and has not been submitted for any other degree at the University of Glasgow or any other institution.

Majdi Damanhori,

June 2021

Definitions/Abbreviations

5-HT	Serotonin
a.u.	Arbitrary units
BC	Bötzinger complex
bpm	Breath/minute
CA	Cerebral autoregulation
CBF	Cerebral blood flow
CNS	Central nervous system
CO_2	Carbon dioxide
CPG	Central pattern generator
CPP	Cerebral perfusion pressure
cVRG	Caudal ventral respiratory group
DAMGO	d-Ala(2),NMePhe(4),Gly-ol(5)enkephalin
Dbx1	Developing brain homeobox protein 1
DRG	Dorsal respiratory group
E	Embryonic day
e-pF	Embryonic parafacial oscillator
EEG	Electroencephalography
ELISA	Enzyme-linked immunosorbent assay

FBMs	Fetal breathing movements
FFA	Flufenamic acid
fMRI	Functional magnetic resonance imaging
GABA	Gamma-Aminobutyric acid type A
GPCRs	G protein coupled receptors
GRKs	G protein-coupled receptor kinases
i.p.	Intraperitoneal
ICA	Internal carotid artery
ICP	Intracranial pressure
IHC	Immunohistochemistry
INaP	Persistent sodium current
K-F	Kölliker-Fuse
LC	Locus coeruleus
LRN	Lateral reticular nucleus
MABP	Mean arterial blood pressure
MCA	Middle cerebral artery
μOR	μ-opioid receptor
MRI	Magnetic resonance imaging
NA	Nucleus ambiguus

NK1R	Neurokinin-1 receptor
nREM	Non-rapid eye movement
NTS	Nucleus tractus solitarius
O_2	Oxygen
P	Postnatal day
PBc	Parabrachial complex
PBS	Phosphate buffered saline
PCA	Posterior cerebral artery
Pre-I	Pre-inspiratory
PreBötC	PreBötzinger complex
PRG	Pontine respiratory group
rCBF	Regional cerebral blood flow
REM	Rapid eye movement
ROI	Regions of interest
RTN/pFRG	Retrotrapezoid nucleus/parafacial respiratory group
rVRG	Rostral ventral respiratory group
SIDS	Sudden infant death syndrome
SP	Substance P
SST	Somatostatin

TSA	Tyramide Signal Amplification
VGLUT2	Vesicular glutamate transporter 2
VLM	Ventrolateral medulla
VRC	Ventral respiratory column
VRG	Ventral respiratory group
XII	Hypoglossal nucleus

Chapter 1 Introduction

1.1 The breathing process

Breathing is the critical function; in humans it starts in utero and advances after birth to balance with the environmental settings and physiological requirements. Essentially, breathing interacts with various other tasks that rely on respiratory function, such as speaking, sneezing, crying and coughing. Each of these tasks requires a coordination between the on-going rhythmicity of breathing and the emerged parallel task, in order to maintain a breathing pattern that is fluent in all conditions. Additionally, the breathing pattern is affected by other physiological challenges, such as body temperature, blood PH and metabolic rate. Yet, to compensate for the variable physiological demands, a closed neural circuit takes place in order to link the feedback received from peripheral and central sensors to the assigned breathing neural kernel, which modifies the breathing pattern as a response to the variable signals obtained (Feldman et al., 2013).

The breathing cycle in human is driven by three main actions which are inflate, deflate and airway resistance. Inflation, which is inspiration, is triggered by the diaphragm muscle contraction that is assisted by the external intercostal muscles. On the other hand, the oblique abdominal muscle accompanied by the transversus abdominus and internal intercostals are the expiratory muscles, which are intended to create the deflation force of the thoracic cavity during the expiratory phase. Also, breathing accessory muscles (scalene muscle and sternocleidomastoid) join the role of inspiration or expiration according to the physiological demands, such as the changes of the metabolic rate and blood gases' levels. Hence, the airway resistance has a role in the breathing series and it is participated by the genioglossus, hyoglossus and styloglossus muscles, which facilitate the air passage across the respiratory tract (Milici-Emili and Petit, 1960, Feldman, 1986).

The respiratory process is monitored by neural circuits that receive the feedback from chemosensors that are distributed peripherally and centrally. For instance, carotid bodies are peripheral chemosensors that monitor the oxygen pressure. The chemosensor signals are transferred to the brainstem via the glossopharyngeal nerve toward the glia of the ventral parafacial nucleus, where the alterations of the blood gases are interpreted initially see Figure 1-1.

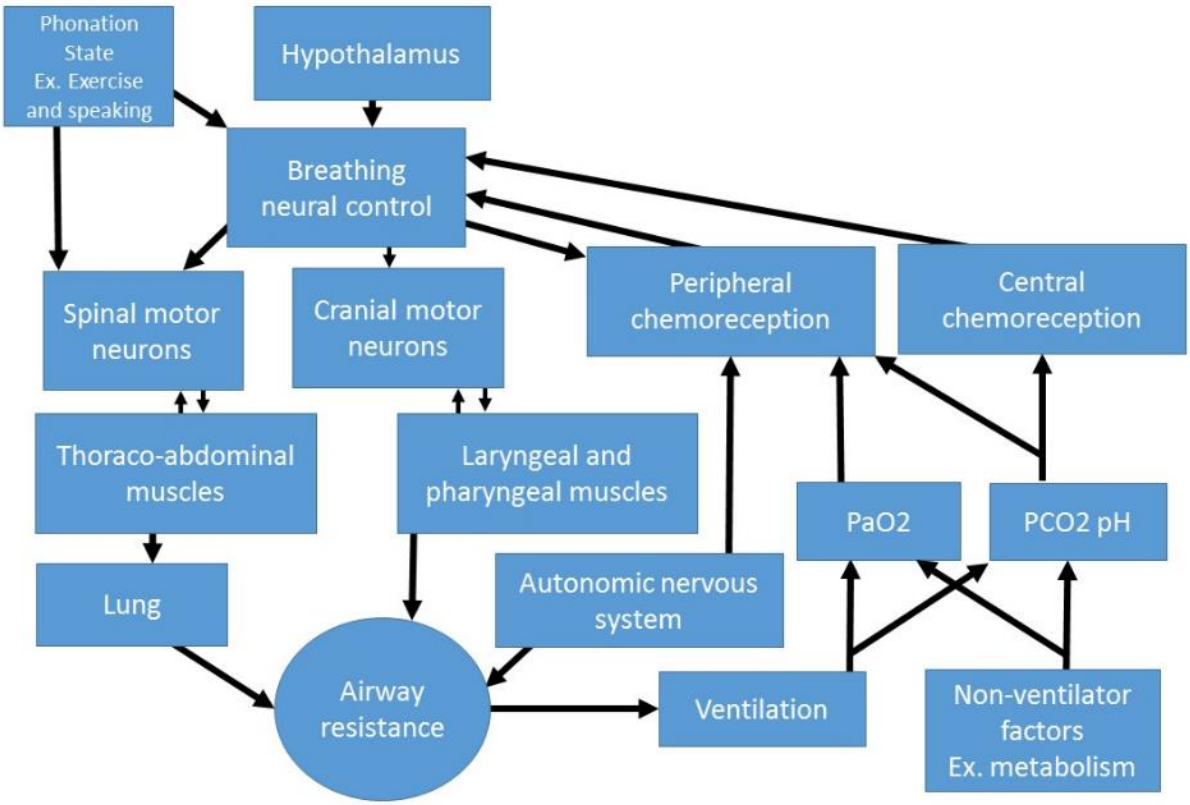

Figure 1-1 Schematic illustration of the breathing mechanism

Neural breathing centres trigger the respiratory cycle by sending signals to the spinal and cranial motor centres. Accordingly, an output signal is transmitted from the motor neuron centres towards the respiratory muscles including the thoraco-abdominal and laryngeal muscles. The respiratory muscles initiate the breathing mechanical function by contracting the diaphragm and expanding the lung capacity, to commence inhalation. Hence, the airway resistance is decreased as part of the inhalation process, after receiving the breathing motor signals too. As the ventilation process started, a feedback process provides the control mechanism of the breathing rhythm. Indeed, there are several factors that control the ventilation process, such as Pa_{O2}, P_{CO2} and blood pH. The change of these parameters is delivered to neural breathing centres via the peripherally and centrally distributed sensors, in the form of chemoreceptors and mechanoreceptors. Those receptors provide the details of blood gas levels and blood pH, which guide the respiratory neural centres to adapt to the alterations by adjusting the rhythm and pace of the breathing pattern (Del Negro et al., 2018).

To understand the origin of breathing control, several studies were conducted on the central nervous centre to reveal the brain's critical role in initiating and maintaining breathing rhythm. An earlier observation by Legallois in 1809 linked the control of blood pressure and respiratory activity to "medulla and spinalis", which emphasised the role of the central nervous system in controlling the breathing function. It was later published in 1813 (Experiments on the Principles of Life). Marckwald backed up the medullary inspiratory centre at 1888 and included the fact that the expiratory centre is located within the medulla too (Marckwald, 1888). Both findings ascertained the central role of the medulla oblongata in monitoring breathing. Later in 1923, Lumsden conducted a study on an anesthetised cat brain, where a micro-segmentation of a cat's brain was performed during anaesthesia, while observing the breathing function alterations. The study was conducted to localise the specified brainstem region that is responsible for breathing control when a complete breathing cessation is achieved during the coronal micro-sectioning of the brainstem. Prolonged inspiratory silences were observed when they reached the caudal pons and rostral medulla; the neural breathing centres are assumed to be located within this region (Lumsden, 1923).

Lumsden's work inspired many scientists to explore the breathing control centres, and two pontine regions were linked to respiratory control which are Kolliker–Fuse (K-F) and parabrachial nuclei (PB) (Lara et al., 1994). Later, respiratory neurons were categorised as two main groups: the ventral respiratory group (VRG) and the dorsal respiratory group (DRG). Both named groups have neural axons travelling caudally towards the thoracic area, where the neural signal is delivered to the phrenic nerve and intercostal muscles (Spyer, 2009).

1.2 Respiratory neurons in brainstem

The respiratory control neurons, which are located within the brainstem, are categorised into three main clusters, which are the pontine respiratory group (PRG), the dorsal respiratory group (DRG) and the ventral respiratory group (VRG). The PRG comprises the PB and K-F nuclei, whose role in breathing pattern generation remains unclear. However, electrophysiological studies have shown the synaptic input of the PRG into the medulla (Ezure et al., 1998, Jiang et al., 2004) and also computational modelling analyses asserted the regulation role of PRG on the PreBötzinger complex (preBötC) signal output (Rybak et al., 2004). DRG is found within the Nucleus Tractus Solitarius (NTS), and it receives the afferent signals from the mechanoreceptors and chemoreceptors, which are distributed peripherally across respiratory airways. Also, it is presumed that DRG provides the relay input phase of the respiratory control, which allows the adjustment of respiratory activity (Alheid et al., 2011). VRG is located within the ventral respiratory column (VRC) and comprises several neural clusters that are accountable for variable roles in controlling respiratory patterns. The neural clusters localised across the VRG are (caudal-rostral) caudal ventral respiratory group (cVRG), rostral ventral respiratory group (rVRG), preBötzinger complex (preBötC), Bötzinger complex (BötC) and retrotrapezoid nucleus/parafacial respiratory group (RTN/pFRG). See Figure 1-2.

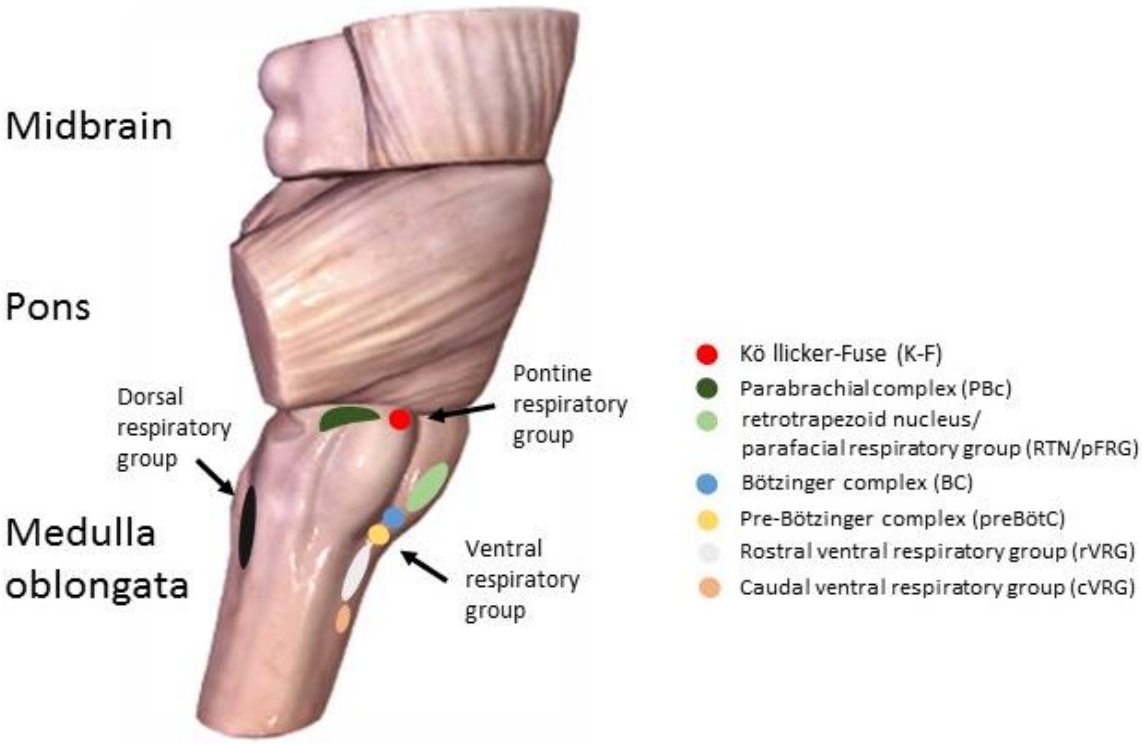

Figure 1-2 Respiratory neurons distribution within the brainstem
A sagittal view of the human brainstem that shows the main respiratory neural groups distribution through the brainstem, which are ventral respiratory group (VRG), dorsal respiratory group (DRG) and pontine respiratory group (PRG). Adapted from (Spyer, 2009).

1.3 PreBötC and the respiratory rhythm generation

1.3.1 Location of preBötC and neural projections

The preBötC region is identified as the essential inspiratory rhythm generator located in the ventrolateral medulla. The motor output originates from preBötC and is transmitted by the neural projections to the premotor regions that are responsible for controlling the respiratory muscles and facilitating breathing airway resistance. The neural projections arise from preBötC and transmit the signals to the ponto-medullary and supra-pontine regions (Smith et al., 1991).

Recognising the shape and borders of preBötC has drawn attention in order to understand its impact on breathing phases and rhythm. Therefore, many neural markers were taken into account to be linked to preBötC and to shape its borders. An example of these neural markers is neurokinin-1 receptor (NK1R).See Figure 1-3. Anatomically, NK1R is distributed along preBötC caudally and rostrally to the rostral ventral respiratory group, which comprises the phrenic pre-motor neurons . Also, NK1R is extended dorsolaterally to the nucleus ambiguus and ventrolaterally to the parafacial neurons (Wang et al., 2001).

The NK1R neurons express vesicular glutamate transporter 2, which indicates that the preBötC has an excitatory glutamatergic role. Also, some NK1R neurons express glutamic acid decarboxylase 67 (GAD67) and a γ-aminobutyric acid (GABA) which highlights the excitatory function of preBötC. Anatomically NK1R neurons extend to other neighbouring regions that may express a different role in the breathing cycle, which may interfere with understanding the accurate role of PreBötC in the breathing rhythm and recognising the distinct borders of the inspiratory oscillator (Del Negro et al., 2018). Additionally, the NK1R neurons express other neuropeptides such as somatostatin and the glycoprotein reelin, which forces the research groups to look for neural subgroups that are distinct to an isolated breathing oscillator (Pantaleo et al., 2011).

A subpopulation which showed the expression of the transcription factor developing brain homeobox protein 1 (Dbx1) is linked to the inspiratory rhythm generated from preBötC (Kottick et al., 2017). Accordingly, Dbx1-knockout mice were studied and died instantly after birth when they failed to generate a distinct breathing pattern (Picardo et al., 2013). Also, an optogenetic photoinhibition was applied on the Dbx1 neural population through in vitro and in vivo preparations, and a gradual depression of the inspiratory rhythm was observed as a result of the photoinhibition (Vann et al., 2016, Wang et al., 2014). Additionally, a photosimulation of channel rhodopsin-expressing Dbx1 cells triggered a premature inspiratory rhythm through the expiratory phase (Cui et al., 2016). This evidence may support the role of Dbx1 precursor in the inspiratory rhythm generation. Nevertheless, the detailed Dbx1 precursor role is not fully understood, concerning the rise of the preBötC neurons.

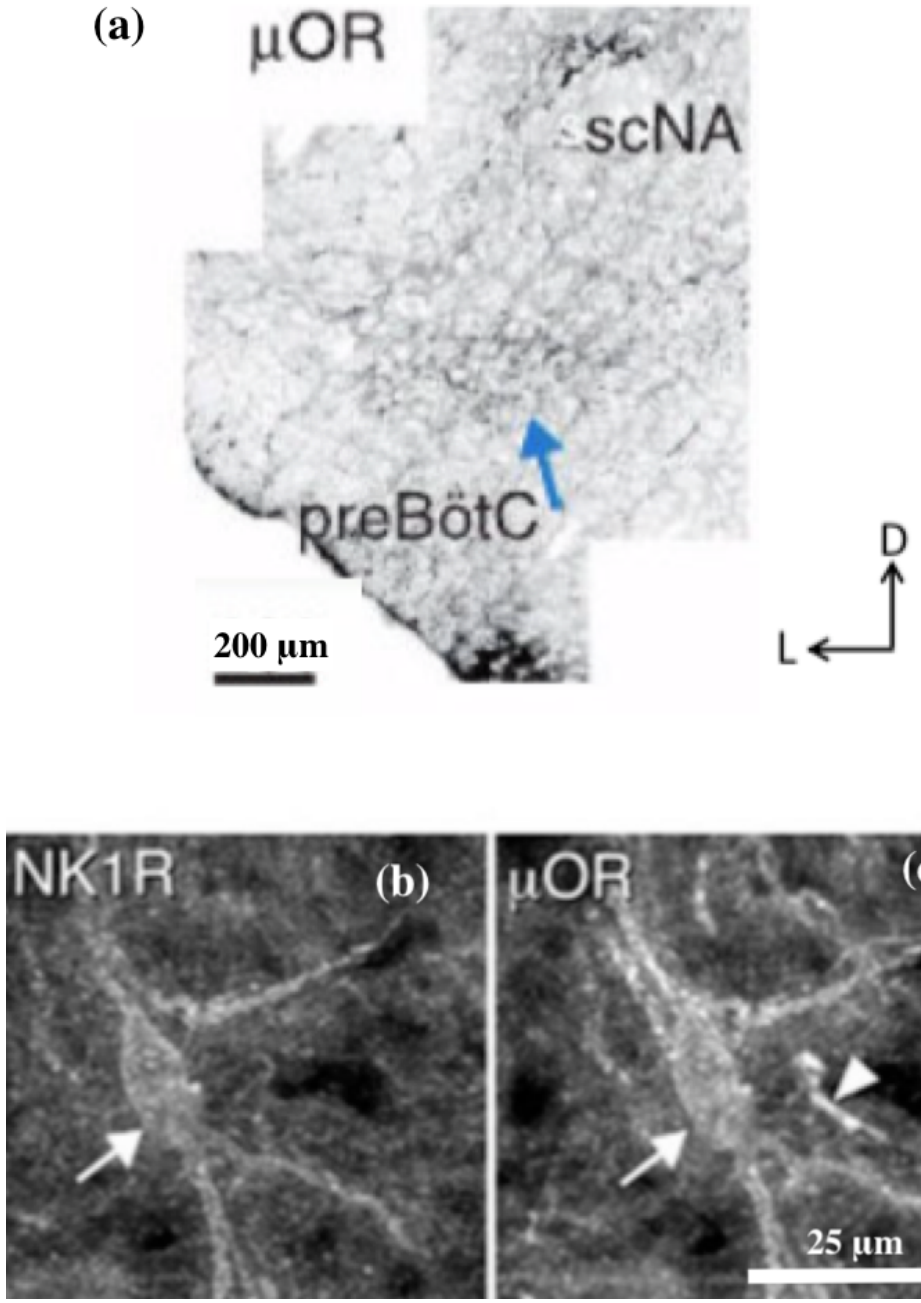

Figure 1-3 Neurons expressing μOR within preBötC
(a) A confocal microscopic image that shows the stained μOR within preBötC. (b) A confocal image presenting NK1R-expressing neurons within preBötC cell soma. (c) The arrow ↑ indicates a co-expression of NK1R and μOR in preBötC cell soma and process, while the arrowhead ∇ points to the absence of co-expression. scNA, subcompact nucleus ambiguous. Modified from (Gray et al., 1999).

1.3.2 Mechanism of respiratory rhythm generation in preBötC (pacemaker hypothesis)

PreBötC pacemaker neurons are persistent sodium currents (INaP) dependent (Smith et al., 1991), which are voltage-dependent, and are suppressed by riluzole (INaP blocker) (Del Negro et al., 2002). An additional type of pacemaker activity that is sensitive to calcium ion channel blocker (cadmium) was found within the preBötC (Thoby-Brisson and Ramirez, 2001). Experiments employing pharmacological interventions have been conducted to investigate the potential influence of pacemaker neurons on the respiratory rhythm generation. Blocking both INaP and the calcium-activated nonspecific cation current (ICAN) were done pharmacologically, and the changes in network activity were measured to determine if either or both types of pacemaker neurons' respiratory rhythm generation was affected. Only 5% of neurons within preBötC were found to rely on INaP (Del Negro et al., 2005). Riluzole administration to in-vitro medullary slice preparation including preBötC from neonatal rats does not alter the frequency of the rhythmic motor output (Del Negro et al., 2005). Nevertheless, riluzole blocks the fictive gasping under anoxic conditions in vitro, which indicates that respiratory rhythm generation during gasping is INaP dependent (Peña et al., 2004, Paton et al., 2006).This supports the fact that the role of pacemaker neurons in respiratory rhythmogenesis is likely to be state-dependent.

The administration of riluzole and the ICAN blocker, flufenamic acid (FFA), stops the respiratory rhythm in vitro (Peña et al., 2004, Del Negro et al., 2005). Accordingly, it was suggested that ICAN-dependent pacemakers are vital for controlling the respiratory rhythm in vitro. Yet, preBötC neurons express both INaP and ICAN (Del Negro et al., 2002), which means that the failure of rhythm generation could be linked to riluzole and FFA affecting the excitability of all neurons as possible induvial pacemakers. Therefore, it is difficult to conclude the significance of pacemaker neurons to rhythm generation relying on the riluzole and FFA effect only. In fact, blocking the rhythmic motor output in the slice preparation using riluzole and FFA, and the application of SP, depolarises preBötC membrane potential and resumes the respiratory rhythm (Del Negro et al., 2005). This suggests that high levels of cellular excitability are necessary to maintain respiratory rhythmogenesis.

1.3.3 Prenatal development of the preBötC

Breathing is one of the first detectable physiological functions in the mammalian foetus. During prenatal life, the mammalian foetus produces a series of rhythmic foetal breathing movements (FBMs) that involves respiratory muscular contractions (Jansen and Chernick, 1983, Kobayashi et al., 2001), which are assumed to originate from the respiratory rhythm generator. FBMs are hypothesised to encourage the maturation of the lungs, and to influence the development of respiratory motoneurons to facilitate synchronised breathing at birth (Kitterman, 1988).

1.3.3.1 Anatomical development

The preBötC comprises several population of rhythmically active neurons that are linked together through a glutamate-mediated network of synaptic input (Hilaire and Duron, 1999, Feldman and Del Negro, 2006). These neural populations are known to have distinct bursting pacemaker properties, which are driven by the persistent sodium current (INaP) and the calcium-activated nonspecific cation current (ICAN) (Del Negro et al., 2005, Thoby-Brisson and Ramirez, 2001). The pacemaker neurons play a role in generating the respiratory rhythm in accordance with different age and environmental changes (Peña et al., 2004, Thoby-Brisson and Greer, 2008).

To investigate the prenatal development of preBötC, NK1R expression was examined in rodents by labelling a region below NA, in addition to other markers, such as SST and TrkB. A weak NK1R labelling was detected at the embryonic age of E14 in mice and E16 in rats, which increases in intensity in newborn rodents. A similar increase of intensity from the embryonic age was obtained on other neural populations (SST and TrkB), while NK1R-expressing neurons originate at E12-E13 and migrate to their final location around E17 to E18 (Pagliardini et al., 2003). However, preBötC only expresses Nk1R neurons at their final site within the ventrolateral population (Thoby-Brisson and Greer, 2008). Despite the fact that Nk1R-expressing neurons are vital for respiratory rhythm generation, they represent a subpopulation of all preBötC neural groups (Guyenet et al., 2002). Other respiratory neurons (which do not express Nk1R)

could participate in breathing rhythm regulation during the earlier days of life or specific developmental stages.

In rodents, preBötC is defined anatomically as a region containing neurons that express neurokinin-1 receptor (NK1R), μ-opioid receptor (μOR), tyrosine kinase B receptor (TrkB), somatostatin (SST) and type 2 vesicular glutamate transporter (VGlut2) (Gray et al., 1999, Stornetta et al., 2003, Thoby-Brisson et al., 2003) (see Table 1-1). Accordingly, respiratory rhythm is regulated by a group of substances, such as substance P, opioid agonists and brain-derived neurotropic factor (BDNF) (Manzke et al., 2003, Rekling et al., 1996, Thoby-Brisson et al., 2003). The anatomical borders of the preBötC remain indistinct and may indicate an overlap between preBötC breathing function and other neurological roles (Del Negro et al., 2018). Outlining preBötC neuronal sub-populations regarding the anatomical features, electrophysiology and transmitter phenotype has helped us to recognise the role of preBötC in breathing. For instance, silencing NK1R-expressing preBötC neurons (within days) results in breathing irregularity in adult rats (Gray et al., 2001, McKay et al., 2005). Also, inhibiting the SST-expressing preBötC neurons within a short duration (minutes) ceases the breathing function (Tan et al., 2008). Peptide receptors are not perfect markers, because their neural expression is not an indication of their roles in breathing rhythm generation, or in synchronising breathing with other functions, such as whisking or licking (Moore et al., 2013, Moore et al., 2014).

Additional neuronal subpopulations are classified concerning the genetic transcription factors. Accordingly, Dbx1-knockout mice did not develop an active preBötC, and die at birth due to breathing failure; also, following in vitro preparations from the same mice group, which retained the medulla, no inspiratory rhythm was obtained (Gray et al., 2010, Bouvier et al., 2010). In fact, Dbx1 preBötC neurons express rhythmogenic membrane properties in vitro (Picardo et al., 2013), and the optogenetic photoinhibition in the preBötC of mice expressing archaerhodopsin in Dbx1 cells leads to the inspiratory rhythm gradually reducing and stopping, in vitro and in vivo (Koizumi et al., 2016, Vann et al., 2016), while the transient photo stimulation of channel rhodopsin-expressing Dbx1 cells at expiration produces premature inspiration (Cui et al., 2016). Consequently, it is suggested that Dbx1 preBötC neurons are accountable

for these effects, and that the Dbx1 neuronal population includes non-rhythmogenic neurons, rhythmogenic neurons (Cui et al., 2016) and signal-transmitting neurons throughout preBötC (Tan et al., 2010, Yackle et al., 2017).

Marker	*Overlapping marker*	*Relevance*	*Reference*
NK1R	SST and μOR	Peptide receptor that depolarises rhythmogenic neurons	(Tan et al., 2008, Thoby-Brisson et al., 2005)
μOR	NK1R	Peptide receptor that hyperpolarises preBötC neurons	(Gray et al., 1999, Liu et al., 2004)
SST	NK1R, VGLUT2and Dbx1	Marker of pattern-generating output neurons	(Stornetta et al., 2003, Cui et al., 2016, Koizumi et al., 2016)
VGLUT 2	Dbx1 and SST	Marker for glutamatergic neurons	(Koizumi et al., 2016, Gray et al., 2010)
Dbx1	VGLUT2, SST, SSTR2A and NK1R	Transcription factor expressed by glutamatergic rhythm-generating neurons, premotor neurons and midbrain-projecting neurons	(Wu et al., 2017, Yackle et al., 2017, Revill et al., 2015)

Table 1-1 Selected markers for interneurons in preBötC.
NK1R, neurokinin 1 receptor, μOR, μ-opioid receptor; SST, somatostatin; VGLUT2, vesicular glutamate transporter 2, Dbx1, developing brain homeobox protein 1, SST2AR, somatostatin 2A receptor.

1.3.3.2 Functional development

Respiratory recordings were performed in vivo, in vitro and in utero, which stressed the emergence of the rhythmogenic respiratory neurons at the age of E15 in mice and E17 in rats (Abadie et al., 2000, Di Pasquale et al., 1992, Kobayashi et al., 2001, Viemari et al., 2003). Thus, it suggests a strong link between the anatomical emergence of preBötC and the functionality of respiratory rhythm motor output. At the beginning of the respiratory rhythm activity the burst frequency is low, and it increases with the gestational age (Di Pasquale et al., 1996, Onimaru and Homma, 2002, Viemari et al., 2003). Before commencing the respiratory neural activity, the associated neurons are gathered to originate regular motor pattern along the full extent of the spinal cord and medulla. The developed motor pattern plays a key role in the early neural developmental networks and motor neural phenotypes. Nevertheless, no evidence supports its part in the early respiratory activity (Gust et al., 2003, O'Donovan and Landmesser, 1987, Ren and Greer, 2003, Yvert et al., 2004).

In mammals, GABA and glycine are neurotransmitters that are known to have a fast inhibitory action on the nervous system. However, chloride-mediated inhibition has the principal effect on the neural output that modifies the respiratory rhythm (Brockhaus and Ballanyi, 1998, Parkis et al., 1999, Ritter and Zhang, 2000). Due to the immaturity of the neural transmembrane at early embryonic days, chloride-mediated transmission enhances the respiratory neurons and increases the burst frequency (Ren and Greer, 2003). Once the neuron transmembrane develops at E19 in rats, a transition of the action is inherited from excitation to inhibition of the synaptic input on respiratory rhythm. At birth, the activation of GABA and glycine receptors results in a decrease of the respiratory rhythm (Thoby-Brisson and Greer, 2008). These transitional periods are the key events of the maturation of preBötC respiratory function prenatally.

1.4 The retrotrapezoid nucleus/parafacial respiratory group

1.4.1 RTN/pFRG and respiratory rhythm generation

The Retrotrapezoid nucleus (RTN) is a cluster of neurones which have chemoresponsive properties. It transmits the feedback of the chemoreception to preBötC and brainstem in order to compensate with the metabolic demands (Rose et al., 2009, Dubreuil et al., 2009). Indeed, Ventral parafacial nucleus (VpF) generates a late active expiratory rhythm beside the inspiratory preBötC signals earlier at postnatal and late embryonic age (Onimaru and Homma, 2003). The rhythmogenic output from these neurones is not detected in later ages; however the chemosensation role remain unchanged (Onimaru et al., 2008). Despite the fact that VpF expresses an active expiratory role in the breathing rhythm of mature rodents, Lateral parafacial nucleus (LpF) does not show a similar characterisations earlier in life at the same age window (Pagliardini et al., 2011). Indeed, LpF neurons remain silent at rest, but late expiratory signals are triggered alongside the preBötC inspiratory bursts with an unsolved mechanism of action (Huckstepp et al., 2016, Zhang et al., 2016). In fact, LpF expiratory bursts are associated with the preBötC signals in adult rodents, but in neonatal rodents the LpF expiratory activity remains without the obligation of preBötC inspiratory bursts, which may suggest a maturation step that occurs earlier in life regarding the breathing rhythm coordination (Janczewski and Feldman, 2006).

Regarding the neural breathing centres, it is hypothesised that the retrotrapezoid nucleus and parafacial respiratory group (RTN/pFRG) is the main oscillator for breathing in the early days of life (P1-P3) in rodents, when breathing is vulnerable and unstable. Later on, pre-Bötzinger complex (preBötC) takes the lead of breathing control and breathing becomes more rhthmic with less variable patterns (Greer et al., 1995; kennedy, 2015). PreBötC is rich with neurokin (Gray et al., 1999; Inturrisi, 2002; Montandon et al., 2011; Smith et al., 1991a).

Systemic administration of μ-opioid agonists to neonatal rodent (P1-P5) causes a slight depression in breathing compared to the effect in adult rodents; thus, suggesting that the dominant respiratory oscillator is the opioid insensitive RTN/pFRG during this neonatal/early life period. (Smith et al., Science, 1991; Gray et al., Science, 1999) (see Figure 1-4).

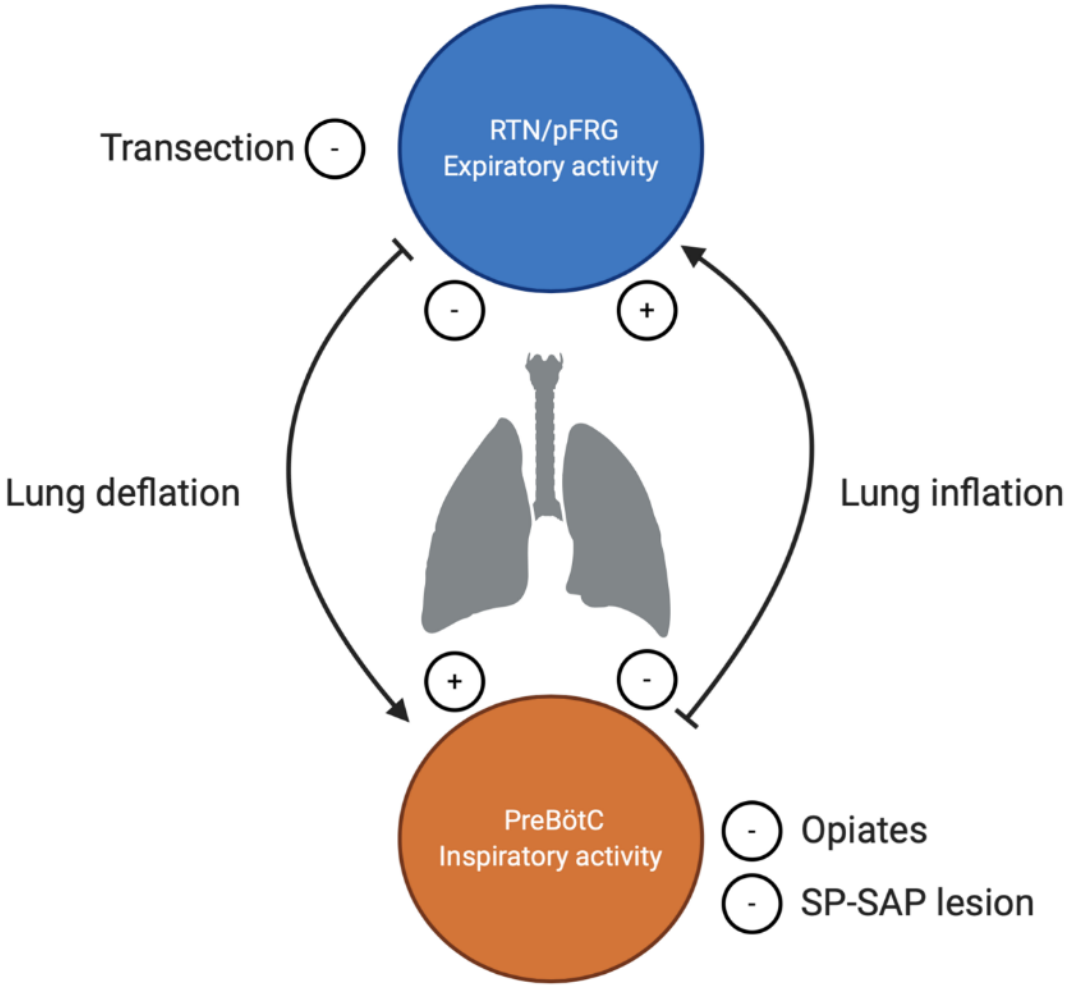

Figure 1-4 An illustration of respiratory rhythmogenesis theory in a mammal's brainstem This assumes that the two respiratory oscillators are affected by different inputs. For instance, inspiration has a negative feedback on preBötC (inspiratory active drive) but a positive influence on RTN/pFRG (expiratory active drive), while expiration (lung deflation) has the opposite effect on both oscillators. In addition, opiates and substance P-saporin (SP-SAP) supress breathing, which has a negative effect on preBötC. A transaction between RTN/pFRG (rostral centre) and preBötC (caudal centre) disrupts the expiratory activity, but the inspiratory oscillator (preBötC) remains unabated. Thus, a group of pacemakers is suggested to speculate the rhythmogenesis of the respiratory drive (Feldman and Del Negro, 2006).

1.4.2 Prenatal development of RTN/pFRG

In vitro, a rhythmic activity within the parafacial region was identified by utilising the calcium imaging and neuronal population recordings in the isolated embryonic mouse brainstem (Thoby-Brisson et al., 2009). This rhythmic neuron activity occurs at the border of the facial motor nucleus and is recognised as the embryonic parafacial oscillator (e-pF). The activity of the e-pF develops at E14.5, which is one day before the onset of preBötC rhythmic activity at E15.5 (Thoby-Brisson et al., 2005). Administration of riluzole blocks rhythmic activity of the e-pF, indicating that the firing of these neurons is INaP dependent. Yet, preBötC is identified anatomically by its expression of NK1R and Phox2b (Thoby-Brisson et al., 2009). In regard to the anatomical features and the expression of histological markers, it is expected that e-pF rhythmic activity is unaffected by μ opioid receptor agonists. In fact, the e-pF neurons are the embryonic origin to the RTN/pFRG. Also, the e-pF and preBötC become functionally synchronous when both oscillators are active at E15.5. Once the e-pF is suppressed by riluzole, the frequency of rhythmic activity from the preBötC is decreased, which indicates that preBötC receives inputs from the e-pF (Thoby-Brisson et al., 2009). These findings illustrate that analogous with postnatal life (Mellen et al., 2003), during embryonic development a network of dual respiratory rhythm generators is formed by a couple of spatially distinct neuronal groups.

1.4.3 RTN/pFRG and the active expiration

Depending on the variable sensitivity of the preBötC and RTN/pFRG to μ opioids, RTN/pFRG may play an important role in generating active expiration. Normally, expiration is a passive process in mammals which becomes active in some conditions, when the metabolic demand increases as a response to vigorous exercise or a drop in O2 levels. Indeed, the active expiration decreases the lung volume below the resting levels, which increases the tidal volume of the following inspiration and delivers more O2 to the lung by the end of the breathing cycle (Del Negro et al., 2018).

The active expiration is primarily linked to the parafacial respiratory group (pF) that extends on the lateral and ventral borders of the facial nucleus dorsally to the pyramidal tract and medial to spinal trigeminal tract, and contains the NK1R glutamatergic-expressing neurons. In fact, the pF nuclei are divided into two groups: the ventral parafacial nucleus (VpF) and the lateral parafacial nucleus (LpF). Both nuclei are hypothesised to have an essential role in CO_2 central chemoreception and active expiration (Huckstepp et al., 2016). Furthermore, transection of the brainstem caudal to the RTN/pFRG interrupts the abdominal muscle expiratory activity, but has a negligible effect on inspiratory motor activity (Janczewski and Feldman, 2006). Therefore, it was suggested that inspiratory and expiratory phases of respiration are not derived from a single oscillator. To support this, a study was performed on adult anaesthetised rats and it was found that stimulating the RTN/pFRG changes the normal silent RTN/pFRG neurons into rhythmically active neurons, which exhibit an expiratory-modulated rhythm. This stimulation of RTN/pFRG rhythmic activity produces active expiration, by affecting the expiratory-related abdominal muscles (Pagliardini et al., 2011). These observations suggest that the rhythm-generating features of the RTN/pFRG remain into adulthood, but under resting conditions synaptic inhibition supresses these neurons.

1.5 Developmental plasticity of the respiratory control neural centres

The key feature of developmental plasticity is the time of the environmental stimulus, which affects a specific age or developmental process (Carroll, 2003, Bavis and Mitchell, 2008). As the individual matures they may acquire developmental plasticity due to the ceasing of the maturation process, or exhibit inconstant physiological capacity of adaptation between individuals (Burggren and Reyna, 2011). For example, new-born rats were exposed to hyperoxia challenge at ages one, two, and four weeks old. Later, an assessment of the carotid body response to the hypoxic challenge was applied once the rats were adult. An impaired response to hypoxic challenge was obtained in the group involved in the hyperoxia challenge at two weeks old compared to other groups (Bisgard et al., 2003). The experiment emphasises the critical window of the developmental changes that occur through the first two weeks of life (Bavis et

al., 2002). Indeed, the carotid body emerges into rapid maturation steps early in life and the environmental stimuli at this age could lead to hyperoxia-induced hypoplasia (Dmitrieff et al., 2012, Bavis et al., 2013).

In order to emphasise the respiratory neural plasticity, the critical maturation window must be reviewed at the time when the breathing pattern is immature, and characterised by irregularity and vulnerability (Fisher et al., 1982, Read and Henderson-Smart, 1984). The mammals develop neural plasticity as a long-term change in the mature adult respiratory system, which is triggered by environmental challenges that occurred at the critical maturation time windows. Yet, no chronic changes were obtained after the exposure to similar environmental challenges later in life (post-maturational age) (Carroll, 2003, Bavis and Mitchell, 2008). Thus, the chronic effect and plasticity may develop at this stage as the neural breathing centres are not fully mature (Wong-Riley and Liu, 2008, Wong-Riley and Liu, 2005).

The postnatal maturation of the respiratory controls within the brainstem alters the expression of neurochemical factors, such as GABA, Glutamate and 5-HT (Wong-Riley et al., 2013). Those significant changes take place at the age of P11-P13 (Wong-Riley and Liu, 2005), and the functional abnormality could be related to the disappearance of the hypoxic ventilatory response (HVR) at P13 (Liu et al., 2009, Holley et al., 2012). Other studies had obtained an increase of the HVR magnitude between P10-P15 (OHTAKE et al., 2000), so the receptors' adjustment and neurotransmitters are affected at this critical window, and the adaptation to hypoxic challenge at this age becomes insufficient (Stunden et al., 2001, Putnam et al., 2005). Additionally, an animal model had shown a vulnerability to hypoxic exposure at the second week postnatally, where a chronic sustained hypoxia (CSH) was introduced at the age of P11-P15 and caused a significant surge of mortality rate in neonatal rats (Mayer et al., 2014). Nevertheless, the younger (P1-P5) and older (P21-P25) groups were unaffected by the CSH exposure, which highlights the vulnerable transitional period that occurs at the age of P11-P15 (Wong-Riley and Liu, 2005, Wong-Riley and Liu, 2008).

The development of the respiratory rhythm generation during early life remains unclear. Indeed, preBötC and the RTN/pFRG are essential for postnatal breathing rhythm generation, and the inhibition or deletion of either of these neuronal groups leads to respiratory failure at birth in rodents (Blanchi et al., 2003, Dubreuil et al., 2009, Rose et al., 2009, Bouvier et al., 2010). At present, engagement of preBötC and the RTN/pFRG into the early life breathing rhythm generation remains elusive and understanding the mechanisms of the respiratory rhythm generation during the early postnatal development age is a crucial step to apprehend the pathophysiology of the central respiratory disorders that develop in early life.

1.6 Cerebral blood flow

1.6.1 Anatomy of cerebral blood supply

In humans more than 75% of the cerebral blood supply is delivered by the internal carotid artery (ICA), which is a branch of the common carotid artery (CCA) (Scheel et al., 2000). The CCA arises from the aortic artery, and it contributes two branches: the ICA and the external carotid artery (ECA). The ECA provides the blood supply to the face and neck structures. The ICA bifurcates into two branches: the anterior cerebral artery (ACA) and middle cerebral artery (MCA) which in mice supply blood to the frontal and parietal regions of the brain. (Watson et al., 2012). The posterior cerebral region is mainly supplied by vertebral arteries that join to form the basilar artery. The basilar artery gives off two branches (right and left posterior cerebral arteries), which provide the blood to the brainstem, midbrain, occipital cortex, cerebellum and hypothalamus. The main branches of cerebral blood supply are connected together by a ring-shaped network that joins ACA, MCA and the posterior cerebral artery, and it is called the arterial circle of Willis (Gillilan, 1974). See Figure **1-5**.

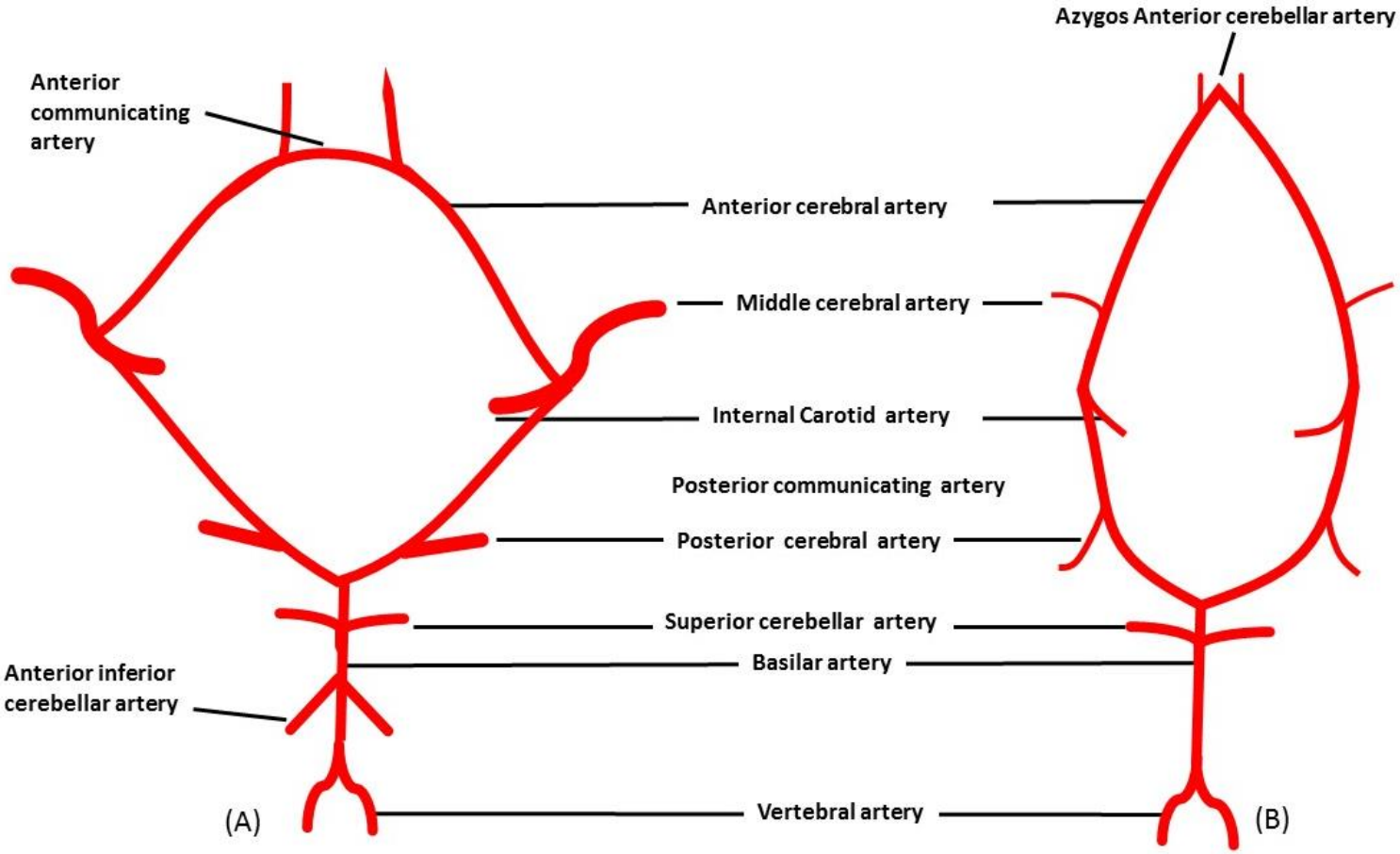

Figure 1-5 The arterial blood supply of the brain in humans and rats.
A schematic illustration of the major arterial blood supply of the brain and the circle of Willis in humans (A) and rats (B). Modified from (Lee, 1995)

1.6.1.1 Variation in the cerebrovascular anatomy

The circle of Willis has varying degrees of completeness in humans (Zhou et al., 2016). An approximate 30-50% showed a lack of either the anterior or posterior parts of the circle of Willis (Zhou et al., 2016, Romero et al., 2009, Hashemi et al., 2013). The nonexistence of anterior or posterior parts is believed to be found in 4-15% of individuals. In rodents, the mouse strain (C57BL/6) usually shows an inadequate formation of the posterior part of the circle of Willis (Hartkamp et al., 1999).

Morphologically, humans and rats share similar features of the circle of Willis formation (see Figure 1-5). Yet, some variations are obtained within the circle organisation. Starting with the internal carotid artery which forms the circle of Willis in rats, while it represents the continuation of the middle cerebral artery (MCA), and provide the posterior communicating branch to form the circle of Willis in humans. In addition, anterior communicating artery has no existence in rats and is found in humans (Lee, 1995). A wide variation of MCA communication patterns in rats was studied by (Fox et al., 1993). Accordingly, 80% of the rats showed a typical bifurcation of MCA, while 17% had atypical branching formations arise from the anastomotic connection to the branches of MCA.

1.6.2 Regulation of cerebral blood flow

Cerebral blood flow (CBF) delivers continuous and constant oxygen supply to the brain, which consumes around a fifth of the oxygen within the blood circulation. The need for oxygen supply may vary depending on different circumstances that affect brain function. A change in the brain vascular resistance occurs within the large arteries to regulate the blood supply in certain areas (Siegel, 1999). Henceforth, the function of increasing the blood supply to certain brain region is called hyperaemia, which raises the blood supply blood (oxygen) to a specific region in response to emerging metabolic demands in order to compensate the neural tissue requirement (Faraci and Heistad, 1990).

The necessity of cerebral oxygen supply may vary depending on different circumstances that affect the brain function. Cerebral blood flow is controlled by three key factors, which are arterial blood pressure (ABP), intracranial pressure (ICP) and cerebrovascular resistance (CVR). Starting with ABP, which is produced by the cardiac output and the peripheral vessels' resistance. Both factors act together in order to maintain the blood volume delivered to the brain (Meng et al., 2015). Nevertheless, the relationship between ABP and CBF is affected by an additional factor which is cerebral autoregulation, which influences the vascular tone of the cerebral arterioles (Donnelly et al., 2016). The cerebral autoregulation (CA) process aims to control the CBF, which remains constant when the mean arterial blood pressure (MABP) ranges between 50/150 mmHg. Accordingly, a dilation of the cerebral arterial vessels occurs to lower the MABP, and a constriction of the arterial vessels is triggered by CA to increase the MABP when the lower limit is reached (Siegel, 1999, Panerai, 1998). Additionally, an increase in the ICP causes a decrease of the CBF by providing a reversed pressure within the vascular bed that is delivered by veins. Indeed, the increase of ICP influences the venous pressure, which passes the pressure to bigger veins and produces the resistance that affects the CBF (Ursino and Lodi, 1997).

1.6.3 Analysing cerebral blood flow changes

Non-invasive imaging techniques, such as near infra-red spectroscopy (NIRS) and trans-cranial Doppler (TCD), are used to provide a continuous monitoring data, to follow up the CBF fluctuations. The continuous recording of the CBF data is useful to analyse the changes of other physiological parameters such as P_{CO2} (Willie et al., 2011, Davies et al., 2015). In addition, invasive imaging techniques are used for critical patients, where they provide long-term data for the CBF changes, for instance laser Doppler flowmetry (Rajan et al., 2009). Analysing the CBF fluctuations may not reflect the entire process of CA, where it might be affected by external factors, such as MABP and ICP. Therefore, measuring the additional parameters is a key factor to evaluate the CBF changes and relate it with the events that trigger those alterations (Donnelly et al., 2016).The laser speckle (LS) device was introduced initially in the physiological tissue blood perfusion studies that intended to evaluate the changes in quantity of blood flow within the assigned areas in the course of the in vivo experiments. In fact, LS took advantage of other devices such as Doppler flowmetry, as it was preferred regarding its simplicity and measurement accuracy through the course of the study, and the live recording of CBF changes up to up to 120 minutes (Dunn, 2012, Perimed, 2018).

1.7 Opioids

Since 2015, drug overdose remained a serious public health crisis in the United States. Opioid prescriptions formerly forced the crisis, but by 2015, they contributed an equal share to heroin, synthetic opioids other than methadone (mostly illicit fentanyl), cocaine, and methamphetamine (Mattson et al., 2017). Approximate 47.7 million Americans aged 12 or older used illegal substances or abused prescription medications, a rate of 17.8 per 100 individuals. 2015 has seen a record number of drug overdose deaths, 52,404. While multiple drugs may contribute to death, prescription or illicit opioids were involved in 63.1% of these cases (Mattson et al., 2017).

Females are more likely to have opioids prescribed than men, and opioid could be consumed early in pregnancy, as most pregnancies are unplanned and commonly recognised by the sixth week of gestation (Ailes et al., 2015). This could lead to exposing a neonate to opioids in a critical development time. Indeed, opioid exposure during the gestation age leads to premature delivery, which is accompanied by a lower birth weight compared to the average, and the possibility of having a neonatal opioid withdrawal syndrome (NOWS) will range between 60-80% (Patrick et al., 2012). A neonate with an opioid withdrawal syndrome experiences several complications that include diminished brain volume and an increasing risk of the sudden unexpected death. Also, secondary complications may appear in forms of tachypnoea, respiratory distress and meconium aspiration (Ko et al., 2016). The estimated half-life of morphine in adults is one hour, and it takes a longer time in infants and reaches up to 6-12 hours. The prolonged half-life of morphine in infants is related to the slower elimination produced by the liver metabolism. Morphine elimination speeds up as the human body grows, and it reaches the adult elimination rate by the age of 6 months (Ainsworth, 2014). Yet, the slow elimination in infants leads to an accumulation of morphine metabolites within the brain blood barriers (BBB), which causes the chronic sensitivity to opioids that triggers the long-term neurological developmental consequences (Bhat et al., 1990).

1.7.1 Opioid receptors

Opioid receptors belong to the group of G-protein-coupled receptors (GPCRs), which consists of 100 types that depend on 7 trans-membrane subunits to activate the intracellular signalling process (Waldhoer et al., 2004). There are 4 main opioids receptors, which are μ, Κ, δ and the nociception/orphanin, and they are linked to the endogenous ligand such as endorphins and enkephalins (Meunier et al., 1995). The receptors are distributed through the CNS and could be found in several sites with variable expression. For instance, μ-opioid receptors (μOR) are expressed in the basal ganglia, spinal cord and brainstem (Gabilondo et al., 1995). The distribution and expression of opioid receptors could be altered by aging and the different physiological circumstances (Trescot et al., 2008).

1.7.2 Opioids' pharmacology

The affinity of receptors for opioids and membrane transportation are enhanced by the drug lipophilic profile and the ionisation at certain physiological pH. For instance, fentanyl has a higher lipophilicity than morphine, which improves the transportation through the lipophilic membranes. The latter increases the uptake of fentanyl through skin and mucous membrane. In general, opioids are highly absorbed within the gastrointestinal tract, following the oral intake (Stein, 2016). Yet, their bioavailability is determined by the first pass metabolism. Once absorbed, opioids target their effector sites, which are located within the central nervous system, such as spinal cord, brainstem and brain (Stein, 2016). After that, metabolism takes place employing the glucuronidation or methylation process in the liver. Some opioids, such as fentanyl, metabolised via cytochrome p450 (CYP) isoenzymes. The genetic variability of the cytochrome p450 significantly influences the metabolism process of the related opioids (Chaves et al., 2017). Opioids are mainly exerted through kidneys. Nevertheless, the accumulation of opioid metabolites in kidneys could result into renal impairment, and develops renal opioid toxicity (Niesters et al., 2013). The action of the commonly used opioids is reviewed in Table 1-2.

Name	Type	Action
Alfentanil	Fully synthetic	μ-opioid receptors (μOR) agonist
Codeine	Natural	μ-opioid receptors (μOR) weak agonist
Diamorphine (heroin)	Semi-synthetic	μ, Κ, δ receptors agonist, predominant to μOR
Fentanyl	Fully synthetic	μ, Κ, δ receptors agonist, predominant to μOR
Morphine	Natural	μ, Κ, δ receptors agonist, predominant to μOR
Pethidine (meperidine)	Fully synthetic	Κ receptors agonist
Tramadol	Fully synthetic	Weak μOR agonist

Table 1-2 The action of commonly used opioids
The data are retrieved from the DrugBank and PubChem database (http://www.drugbank.ca) (https://www.pubchem.ncbi.nlm.nih.gov)

1.7.2.1 Opioids' agonists/antagonists

Agonists of opioids modulate pain via the peripheral, neuraxial or systemic administration (Stein and Machelska, 2011, Stein and Zollner, 2009, Schumacher et al., 2004). The systemic administration of opioids results in side effects, such as respiratory depression, depending on the dose, route of admission and distribution. Some opioids, such as buprenorphine and butorphanol, are mixed agonists/antagonists, which act as agonists in small doses and antagonists at higher doses (Stein and Zollner, 2009). Opioid's receptors have the same analgesic effect but different side effects, which may result from the variability of regional expression and plasticity. For example, mu-receptors mediate respiratory depression, nausea and constipation, while kappa-receptors mediate diuretic and sedative effects (Stein, 2007). Opioid antagonists are mainly used to treat constipation, which is a common side effect of opioid intake. Opioid-linked constipation results from the stimulation of intestinal and central mu-opioid receptors. Laxatives represent an alternative solution for opioid-linked constipation (Holzer, 2009). Moreover, naloxone and its derivatives (methylnaltrexone) are introduced as mu-opioid antagonists and are used to reduce analgesia or drug overdose withdrawal (Diego et al., 2011, Pattinson, 2008).

1.7.2.2 Opioid's tolerance

Tolerance is defined as a decrease in the drug effect after repeated exposure of the same dose, and the need to increase the dose in order to produce an equivalent effect. All opioids are subjected to differing levels of tolerance development. For instance, respiratory depression tolerance develops faster than constipation (Collett, 1998, McNicol, 2008). Opioid-induced adaptation is linked to several procedures, which start with the alteration of opioid receptors signalling and extends to neural development of adapted behaviour. The intended pharmacodynamic mechanism involves opioid receptor–G protein uncoupling that causes the receptor's internalisation/recycling to subside and increases the N-methyl-D-aspartate (NMDA) receptor's sensitivity (Stein, 2007, Williams et al., 2013).

1.7.3 Endogenous opioids

Endogenous opioids (EO) are peptides that are distributed within the body and CNS. Those peptides interact with the CNS as neurotransmitters in order to control pain and enhance the neuroendocrine interaction (Adams et al., 1986, Toubia and Khalife, 2019). The key precursors of EO are pro-opiomelanocortin (POMC), pro-enkephalin (POE) and pro-dynorphin (POD), which produce 20 known types of EO that are categorised into four main categories (enkephalins, endomorphins, dynorphins and endorphins) (Corder et al., 2018, Vuong et al., 2010). In detail, opioid exposure, 75 mg pe pellet implanted in rats for 7 days, alters the β-endorphin levels and the HPA axis by affecting the regulation of the POMC gene in the hypothalamus (Bronstein et al., 1993b); therefore, it decreases the hypophyseal β-endorphin concentration (Gudehithlu et al., 1991). In contrast, a chronic administration of naltrexone (10 mg pellet for 8 days) significantly elevates POMC mRNA levels 140% from control level (Bronstein et al., 1993a). In fact, the increased level of plasma β-endorphin is linked with obesity in mice (Recant et al., 1983), and the decrease of μ opioid receptor binding sites may enhance the receptor's binding affinity and trigger hyperphagia (Khawaja et al., 1989).

The distribution of EO varies in relation to the main group. For example, endomorphin-1 is found in the brain while endomorphin-2 is distributed along the spinal cord (Waldhoer et al., 2004). In addition, Enkephalins are located within KF (Hermanson and Blomqvist, 1995) and distributed along KF neurons and the parabrachial plexus, which express pro-pro-enkephalin mRNA (PPEM) (Engström et al., 2001, Hermanson and Blomqvist, 1997). Also, β-endorphins were identified in a moderate to high level of distribution in the parabrachial plexus of the rodents, but no distribution was acknowledged within the KF neurons (Palkovits and Eskay, 1987). Despite the fact that exogenous opioid effect was reviewed among several studies (Prkic et al., 2012, Saunders and Levitt, 2020, Varga et al., 2020), not much research has been conducted to analyse the EO effect on KF.

The concentration of endogenous opioids is raised in both the foetus and the mother during pregnancy, thereafter it decreases to the postnatal control level. However, an exposure to exogenous opioids in the perinatal period will result in an increase of the EO level up to 100 times in the foetus. This elevation remains up to 40 days postnatal until it returns to the normal average (Panerai et al., 1983). μOR are ascertained to be the principal receptors for exogenous opioids, such as morphine and heroine, beside the endogenous β-endorphin. These receptors are found to be active within the CNS at 12-13 weeks of gestation (Ray and Wadhwa, 1999). Therefore, an exposure to exogenous opioids in utero will affect the affinity to EO. Indeed, some studies have indicated that altering the EO receptors earlier in life may lead to long-term effects on the cognitive function (Victoria et al., 2015).

1.8 Opioids' influence on the physiological process

1.8.1 The effect of opioids on the respiratory system

Opioids are known to cause a depressive effect on the respiratory pattern which includes a reduction in the breathing rate, a change in the tidal volume and a decrease of the upper airway patency (Ferguson and Drummond, 2006). Yet, some patients suffer from hypersensitivity to opioids that becomes remarkable with the extensive depression of the breathing pattern, such as elderly and obese patients (Desrosiers, 2006). Therefore, several studies have been conducted to understand the mechanism of opioid effect on respiratory patterns, beside the substantial hypersensitivity that patients develop when given the common clinical doses of opioids. Concerning the fact that opioid receptors have a major role in controlling respiratory neural centres in the brainstem (Akil et al., 1984), those receptors could be found in other higher centres such as the thalamus and anterior cingulate cortex (McKay et al., 2003). Hence, opioid receptors could be found in other sites around the body like the carotid body and the mechanoreceptors located in the respiratory tract linings (Kubin et al., 2006, LUNDBERG et al., 1979).

The opioid's effect on respiratory patterns is brought by the μOR, which is a subtype of GPCRs found within the preBötC neurons as a part of NKR1 neurons expression (Montandon et al., 2011, McKay et al., 2005). The systemic administration of fentanyl, μ opioid receptor agonist, results in a reduction of the respiratory rate. The respiratory depression is reversed by introducing a naloxone, μ opioid receptor antagonists, into the artificial cerebral spinal fluid (aCSF), which is perfused within the preBötC (see Figure 1-7). The activation of μOR is triggered by a negative coupling to adenylate cyclase, which starts the inhibitory cycle pathway (Law et al., 2000). This will lead to a closure of calcium channels and provoking of the potassium efflux (see Figure 1-6). According to the stated intracellular changes, the neural excitability is reduced and the breathing pattern is consequently affected (Lonergan et al., 2003).

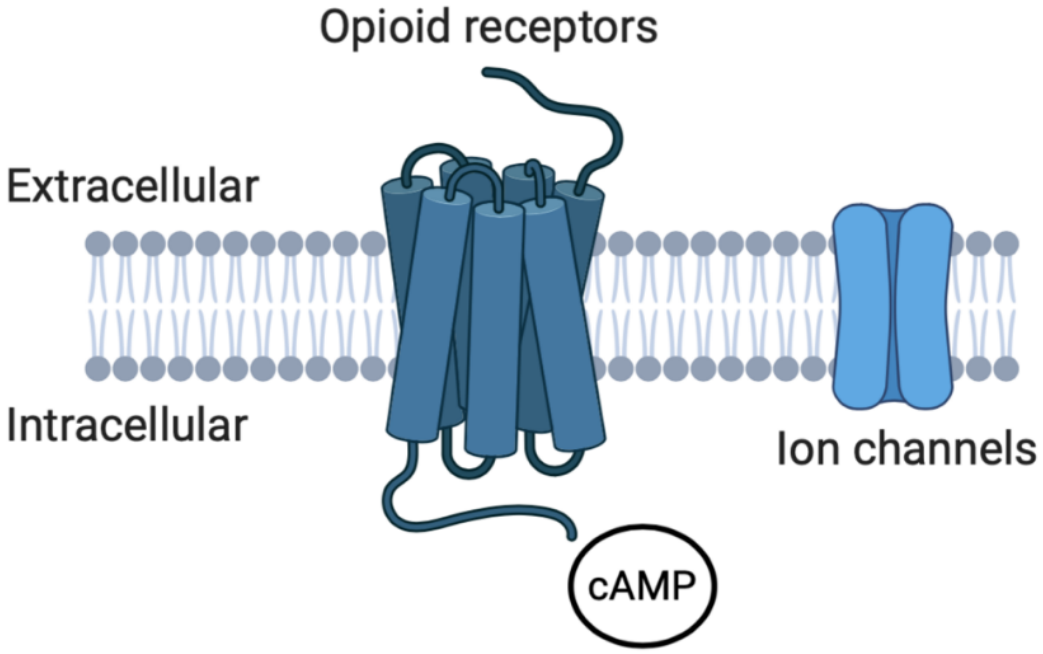

Figure 1-6 Opioid receptors' signalling process
The activation of μOR evokes changes that initiate an intracellular signalling process. The latter inhibits the adenyl cyclase and reduces cAMP, which results in closing of the calcium channels and stimulation of the potassium efflux. The end product of the mentioned intracellular changes is a reduction of the neural excitability that affects μOR in the CNS (Stein, 2016).

Despite the fact that opioid effect on respiratory neurons was linked to preBötC, the Kölliker-Fuse nucleus (KF) had shown an μOR expression under immunohistochemistry and in situ hybridisation in rodents (Erbs et al., 2014, Chamberlin et al., 1999, Ding et al., 1996). Also, a sufficient expression of delta opioid receptors (DOR) on site was documented by (Cahill et al., 2001). On a physiological basis, μOR expression neurons were linked to KF (Levitt et al., 2015, Varga et al., 2020) and parabrachial nuclei (Miller et al., 2017, Prkic et al., 2012). In addition, a lack of somatodendritic function of DOR was the result of μOR antagonist CTAP (d-Phe-Cys-Tyr-d-Trp-Arg-Thr-Pen-Thr-NH_2) (Levitt et al., 2015), and the deletion of μOR neurons (Varga et al., 2020).

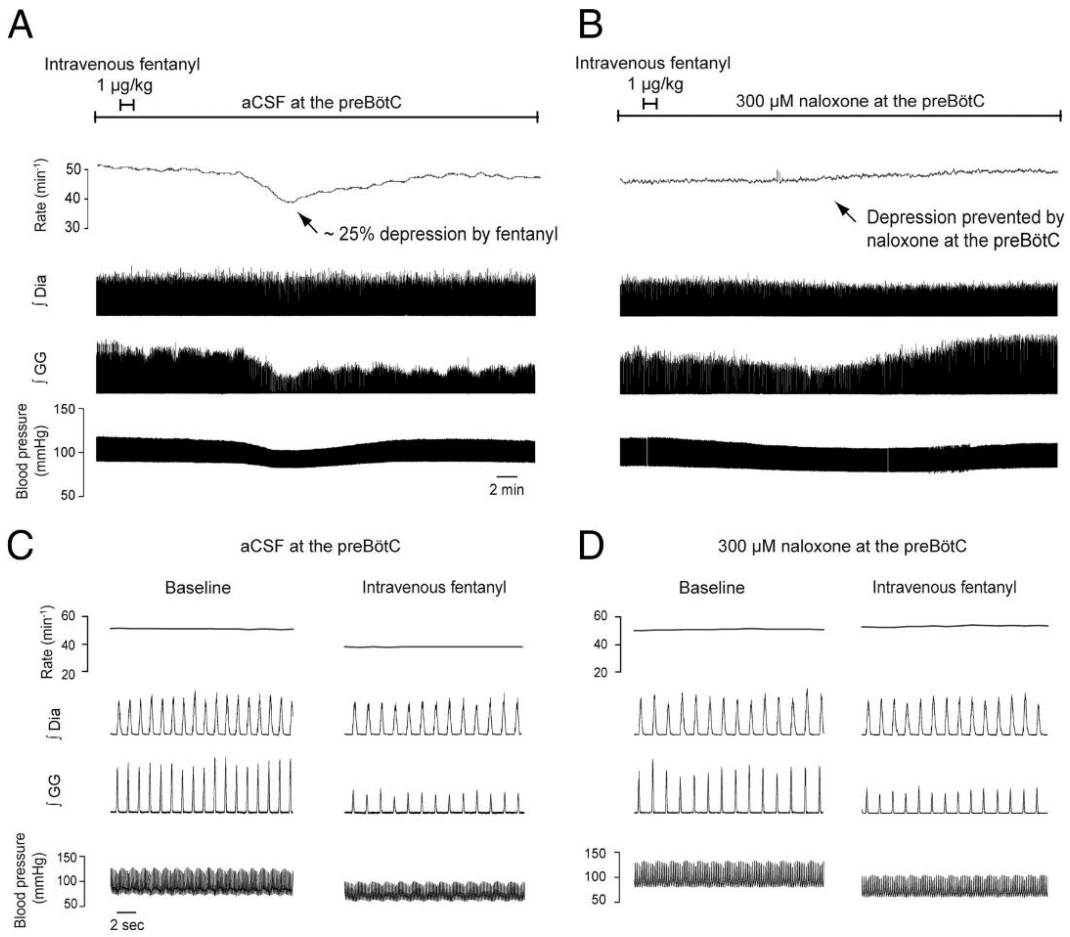

Figure 1-7 Systematic fentanyl administration depresses respiratory rate by targeting preBötC

A systemic administration of fentanyl (intravenous, IV) accompanied by artificial cerebrospinal fluid (aCSF) injection in the preBötC results in respiratory suppression and a decrease in the genioglossus (GG), diaphragm (Dia) muscles activity and blood pressure (a) and (c).However, naloxone administration prevents the respiratory rate suppression that is caused by the systematic fentanyl injection, and the drop of GG muscle and blood pressure remains unaffected (b) and (d). Reproduced from (Montandon et al., 2011)

1.8.2 The effect of opioids on CBF

In the beginning, opioids were considered to have no effect on CBF, as the studies conducted were backed by low-resolution techniques, such as TCD, which measures the blood flow velocity through the middle cerebral artery to estimate the CBF without considering the regional changes of CBF in certain cerebral areas. Thereafter, high-resolution techniques were utilised to analyse the regional changes of CBF, such as magnetic resonance imaging (MRI) and positron immersion tomography (PET). The latter had identified the changes of regional CBF after opioids administration, which differs in certain cerebral areas. For example, systematic fentanyl exposure in humans results in an increase of CBF in prefrontal cortex and caudate (Firestone et al., 1996, Zelaya et al., 2012). Also, morphine and hydromorphone revealed a similar effect on the regional CBF changes (Schlaepfer et al., 1998). Yet, remifentanil administration has a dual action on the regional CBF, which starts with an increase of CBF at low to moderate dose followed by a dose-dependent decrease of CBF under normocapnic conditions (Fodale et al., 2008, Lorenz et al., 2000). See Table 1-3 for the effect of opioids and other anaesthetic agents on CBF. The systemic administration of opioid's antagonist, such as naloxone, decrease the CBF (Theodore et al., 1993). Therefore, a neural protection utilisation was attributed by opioid antagonists (naloxone) in order to preserve the blood flow in spinal cord injuries (Flamm et al., 1982, Erman et al., 2004). The key role of the neural protection properties of opioid antagonists is based on the competition that arises between the opioid antagonists and endogenous opioid agonists on the opioid receptor signalling process (Slupe and Kirsch, 2018).

Anaesthetic agent	Cerebral Blood flow	References
Volatile anaesthetics (isoflurane)	Increase	(Kadoi et al., 2009, Jung et al., 2014, Li et al., 2014)
Nitrous oxide	Increase	(Reinstrup et al., 2008, Field et al., 1993)
Propofol	Decrease	(Kaisti et al., 2003, Schlünzen et al., 2012)
Ketamine	Increase	(Zeiler et al., 2016, Oren et al., 1987)
Opioids	Dose-specific	(Zelaya et al., 2012, Fodale et al., 2008, Lorenz et al., 2000)
Benzodiazepines	Decrease	(Matthew et al., 1995, Roy-Byre et al., 1993, Finelli et al., 2000)
Lidocaine	Dose-specific	(Adinoff et al., 2009, Kastrup et al., 1990, Lam et al., 1993)

Table 1-3 The effect of anaesthetic agents on CBF
A summary of the influence of common anaesthetic agents on CBF

1.8.3 Opioid effect on hormones, HPA axis and stress

Beside the increased demand of opioid prescriptions, many studies reviewed the side effects of the drugs. Some common side effects of opioids on the endocrine system have been acknowledged for more than four decades (Morley et al., 1980, Delitala et al., 1983), but the full picture of the endocrinopathies has not been revealed yet, because of the lack of symptoms reporting criteria and the awareness concerning the effect of opioids on the endocrine system (Hochberg et al., 2019, Saeed et al., 2019). See (Table 1-4) for more details about the effect of opioids on hormone secretions.

Opioid exposure stimulates the hypothalamic-pituitary-adrenal axis (HPA), which activates the secretion of corticotropin-releasing hormone (CRH). The latter stimulates the adrenocorticotropic hormone (ACTH) and results in producing corticosterone hormone in rodents and cortisol (CORT) in humans as a response to the stressful provocation. The end product, corticosterone and cortisol, acts as negative feedback towards the hypothalamus as a part of the stress adaptation (Ignar and Kuhn, 1990, Glahn et al., 2013) (see Figure 1-8). In rodents, acute exposure to morphine (0.06 mg/kg subcutaneous) leads to a significant increase in the plasma adrenocorticotropic hormone (ACTH) levels (Ježová et al., 1982). Also, acute morphine administration (0.02 mg/kg i.p.), in rats, exaggerates the stress response of hypothalamic–pituitary–adrenal axis (HPA axis) (Buckingham and Cooper, 1984). In rats, the chronic exposure to opioid analogues (morphine 2mg/kg daily for 7 days) results in a reduction of ACTH levels (Houshyar et al., 2001), and the treatment with morphine subcutaneously twice a day raises the corticosterone levels (Little and Kuhn , 1995). The effect of opioids on adrenal function is highly suggested, once naloxone administration increases the cortisol concentration in patients suffering from hypothalamo-pituitary malfunction (Coiro et al., 2011).

Hormone	Acute		Chronic	
	Animals	Humans	Animals	Humans
GH	+	+	=	?
PRL	+	+	+	+/=
TSH	-	+	?	?/=
ACTH	+	-	-/+	-/=
LH	-	--	-	--
FSH	=	=	=	=
Estradiol	-	--	=	-/=
Testosterone	-	--	-	--
AVP	+/-	+/-	+/-	+/-
OT	-	-	-/=	-/=

Table 1-4 The effect of opioids on the endocrine system
(+ stimulation) (- inhibition) (+- uncertain) (= no change) (? No studies obtained). Abbreviations, growth hormone (GH), prolactin (PRL), thyroid-stimulating hormone (TSH), adrenocorticotropic hormone (ACTH), luteinizing hormone (LH), follicle stimulating hormone (FSH) arginine vasopressin (AVP), oxytocin (OT). The table is extracted from (Vuong et al., 2010).

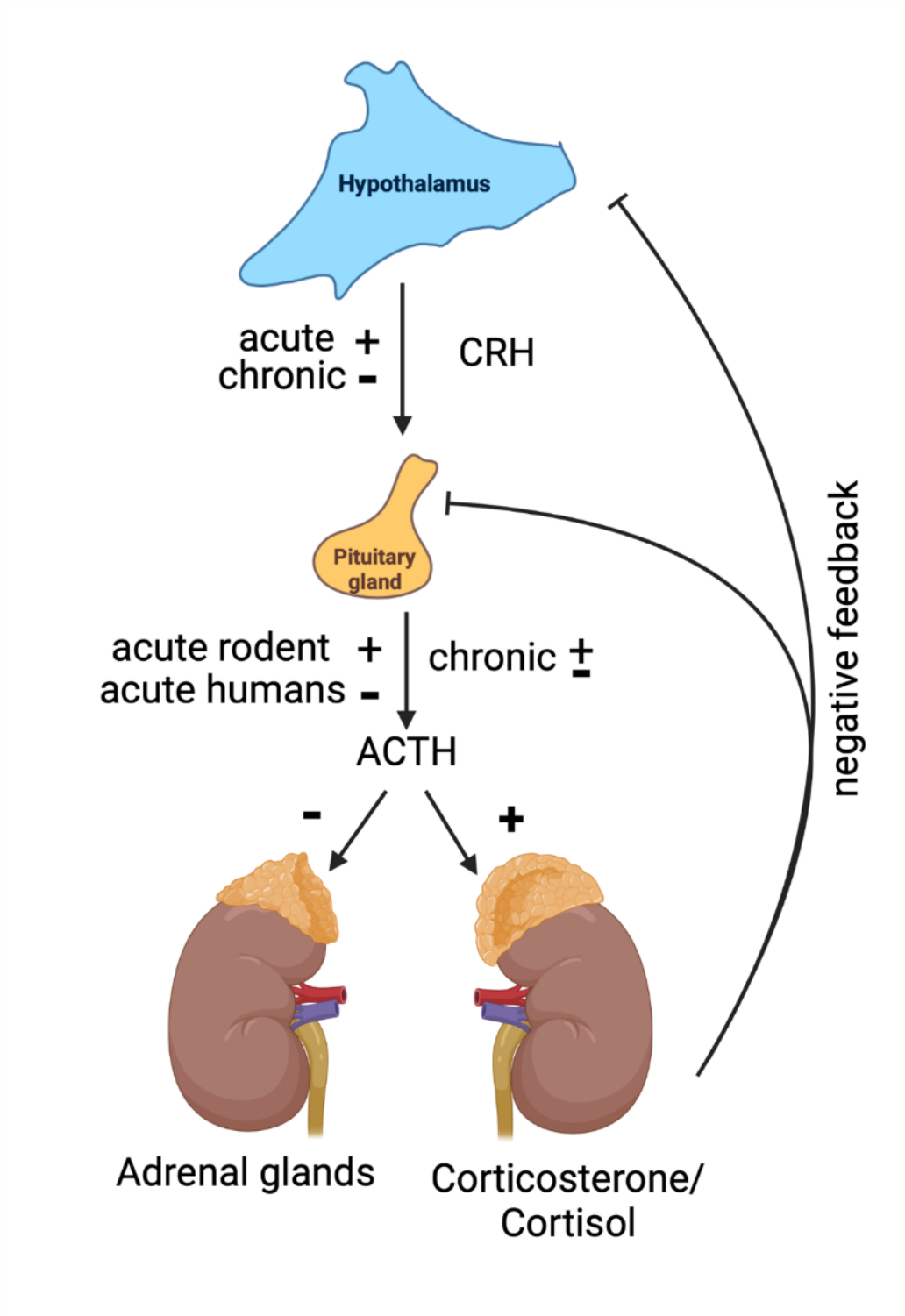

Figure 1-8 The effect of opioids on the HPA axis and stress response
The acute exposure to opioids triggers the HPA axis and enhance the secretion of CRH hormone. In rodents, acute exposure to opioids leads to increase of ACTH secretion, while humans studies showed a decrease of ACTH hormones after opioids administration. The increased level of stress hormones (corticosterone and cortisol) initiate a negative feedback pathway that inhibits the CRH and ACTH secretion.

The long-term use of opioids is associated with the suppressive effect on the HPA axis in patients with chronic pain. Two studies were conducted on the hypoadrenalism linked to the chronic use of opioids (Abs et al., 2000, Valverde-Filho et al., 2015). Despite the fact that studies backed the secondary biochemical adrenal insufficiency, several studies reported clinical manifestations of hypoadrenalism in patients who receive oral opioids (Debono et al., 2011, Das, 2014). In addition, hypoadrenalism was noticed with opioid addicts, who receive diamorphine treatment (Gerber et al., 2012). Also, heroin addicts are diagnosed with impaired ACTH circadian rhythm and reduction of the basal ACTH and cortisol concentration (Facchinetti et al., 1984).

To summarise, the inhibitory action of opioids on the HPA axis could be obtained with acute or chronic consumption of the drug. Nevertheless, a clear image and the actual process has not been defined yet. Indeed, the chronic exaggerated stress response may contribute to the HPA axis and may trigger changes in the hormonal concentration and responses.

1.9 Thesis aims

The aims of the thesis are as follows.

To investigate the chronic effect of opioids exposure, at the age of P1-P5 and P9-P13, on breathing pattern at adulthood.

To investigate the acute opioids effect on CBF, utilising a laser speckle device.

To analyse the chronic effect of repeated opioids exposure, at the age of P1-P5 and P9-P13, on cerebral blood flow.

To assess the vulnerability of respiratory function to fentanyl challenge under anaesthetic.

To analyse the chronic effect of the repeated opioids exposure, between P9-P13, on the HPA axis, endogenous β-endorphin level and weight gain.

To investigate the long-lasting effect of repeated opioids exposure, between P9-P13, on the μOR distribution within the brain, utilising autoradiography technique.

Investigating the chronic effect of opioids exposure, between P9-P13, on the μOR neural expression within the brain, utilising the IHC technique.

Chapter 2 Methodology

2.1 Animals

The experimental animal procedures were performed under the regulations of the UK Home Office (personal licence number i51F7C81D, and project licence number 60/4558). The studies were designed in correspondence with the Animal's Scientific Procedure Act, 1986. The experimental procedures were conducted on ICR mice, which were acquired from HARLAN. Pregnant dams were ordered and delivered to the housing facility at the Veterinary Research Facility, Garscube campus, University of Glasgow. The pups were kept with the mother up to the age of 21 days, when they were weaned. Then, the male and female mice were housed in separated cages, with a maximum of 4 mice per cage. Also, an ear-piercing technique was applied to identify individual mice within the cage. The light/dark cycle was 12 hours duration, with no dietary modifications. Day of birth is referred to as postnatal day (P0). The age categories used in this study were neonate (P0-P7), juvenile (P8-P21) and adults over P21.

2.2 Postnatal injection

The experimental groups were defined in regard to the age when the postnatal fentanyl exposure occurred:

- **Group 1 – Neonatal Fentanyl (NN-FEN)** This group received a daily injection of fentanyl (0.04 mg/kg i.p.) for 5 days from postnatal day 1 (P1) to postnatal day 5 (P5) injection at the age of (P1-P5) once daily).

- **Group 2 – Neonatal Saline (NN-SAL)** An equivalent volume of physiological saline was given once daily at the age of P1-P5.

- **Group 3 – Juvenile Fentanyl (JUV-FEN)** This group was introduced to a daily injection of fentanyl (0.04 mg/kg i.p.) between P9-P13.

- **Group 4 – Juvenile Saline (JUV-SAL)** A daily equivalent volume of the physiological saline was given to this group at the age of P9-P13.

Fentanyl citrate (μ-opioid receptor agonist) (Janssen-Cilag, UK) was acquired with a concentration of 50 μg/ml. It was administered intraperitoneally (i.p.). An essential dose was given after birth 0.04 μg/kg once daily in correspondence to the age group, and for the control group an equivalent volume of the normal saline was introduced as an alternative for fentanyl. The fentanyl was dose adjusted to 0.04 mg/kg as previous in vivo studies have found that this dose induces a significant respiratory depression in neonatal rodents without triggering significant side effects (Greer et al., 1995; Laferriere et al., 2005).

2.3 Plethysmography

Plethysmography apparatus was used to assess the awake respiratory function in mice, by measuring the pressure changes within the chamber in a freely behaving animal. The apparatus is made up of a group of devices that include two chambers, temperature monitor, calibration needle, pressure transducer and an air humidifier. Starting with the two chambers used in the plethysmography, the first one is a 700 ml recording chamber where the mouse is placed, and the second chamber is a reference chamber that has a similar volume. Both chambers are connected to the pressure transducer (model DP103-4, Validyne Engineering, Northridge, CA), which detects the pressure difference between the chambers and send it to the analogue-to-digital converter (CED, Cambridge Instruments, UK), executing a 100 Hz sampling frequency. The digital signals are analysed, once stored in the PC, using Spike 2 software (Cambridge Instruments, UK).

A plethysmography recording chamber is fitted with a temperature probe (RET-3, Physitemp Instruments Inc, USA) that indicates the chamber's temperature during the recording, and a humidified air is also delivered to the chamber at a rate of 2 L/min. A leak is set on each chamber (recording and reference), using a 26-gauge needle (Terumo, Exchange Supplies UK), which helps in standardising the thermal drift that disturbs the pressure signal. In addition, a calibration syringe is connected to the recording chamber to inject a known volume of 100 µl of room air at the end of the recording. See Figure 2-1.

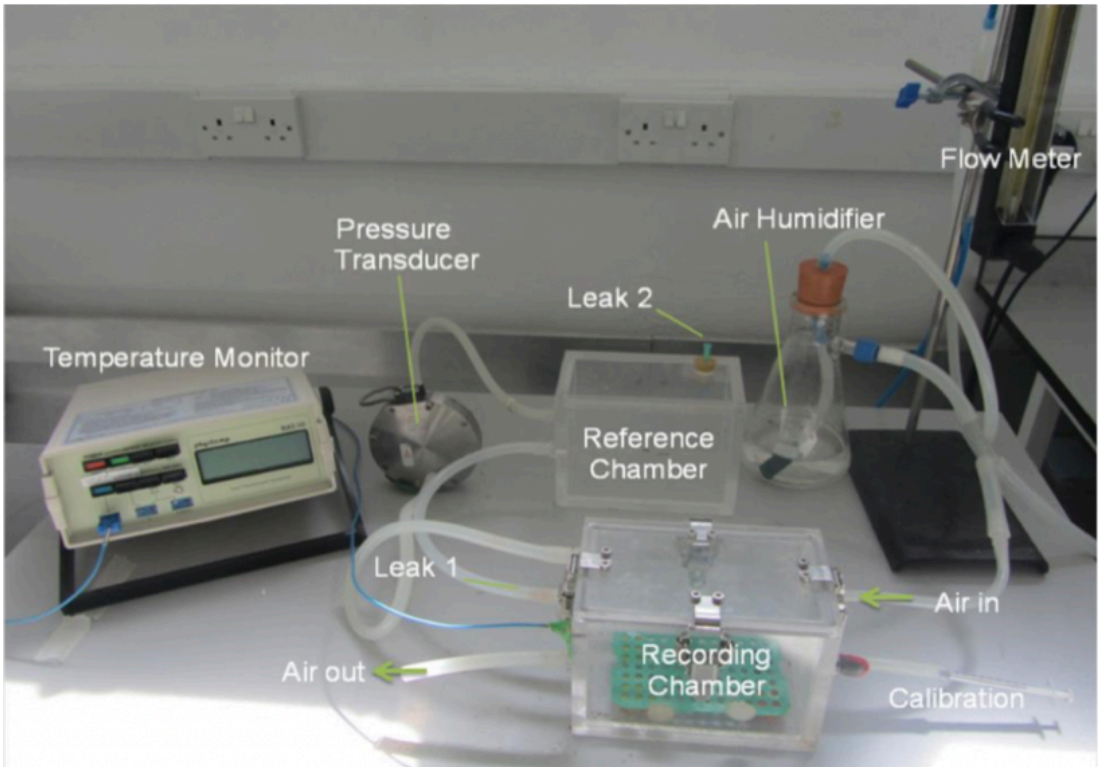

Figure 2-1 Plethysmography apparatus
The picture shows the plethysmography apparatus that comprises four main parts (recording champers, reference chamber, Validyne and the air humidifier). The recording chamber, where the mouse is placed through the experiment, receives the air from the humidifier at a rate of 2 L/min, and it is connected to the temperature monitor. It has three output tubes, one is for air output, the second is linked to the reference chamber and the last one is for the calibration needle. The reference chamber is connected to the recording chamber and Validyne.

The plethysmography experiment starts with habituation of mice to the plethysmography chamber. Mice are placed into the recording chambers for two hours on two separate days, so they become familiar with the surrounding environment and behave normally on the day of the procedure. A typical protocol for recording breathing pattern using plethysmography is as follows. Mice are habituated in the chamber for a period of 60-90 minutes. During this period the mouse settles within the recording chamber, and three control breathing recordings are taken to assess the baseline breathing parameters. Each recording lasts up to 2 minutes while airflow to the recording chamber is blocked at this point, to maintain a constant air pressure within the chamber, and deliver accurate pressure changes that are excreted by breathing movements caused by the mouse. After that, the mouse is removed from the recording chamber, and receives an injection of FEN 0.06 mg/kg IP. Once the injection is given, the mouse temperature is measured by a rectal probe (RET-3, Physitemp Instruments Inc, USA), and the mouse is put back into the chamber (Buxco Research Systems, USA). The effect of FEN on breathing function is measured right after the FEN injection is given at 5 minutes post injection (T5), 10 minutes post injection (T10) and 15 minutes post injection (T15). Then, additional breathing recordings are taken on specified time points after the FEN administration 30 minutes post injection (T30), 45 minutes post injection (T45) and 90 minutes post injection (T90). Each recording lasts for two minutes within the individual time point. See Figure 2-2.

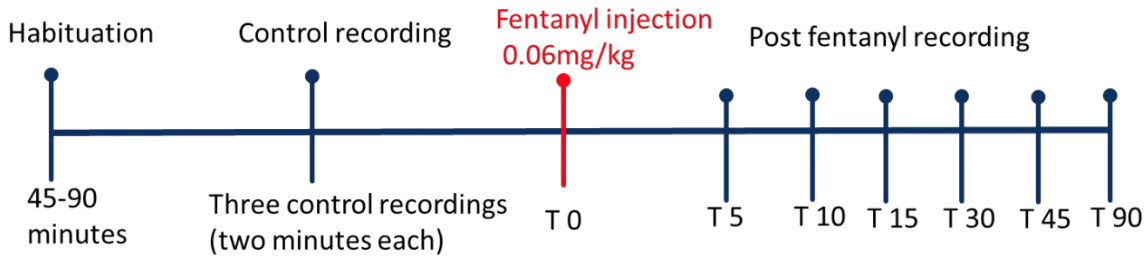

Figure 2-2 Plethysmography experiment timeline
The figure provides an illustration of the plethysmography experiment, which starts with a habituation period, that is followed by three control recordings to determine the baseline of the breathing function. After that, FEN is administrated, and breathing is evaluated in individual time points to follow up to 90 minutes post-injection.

2.4 Laser speckle imaging CBF

The laser speckle imaging technique (LS) has been used to record the real-time blood flow changes. It had been introduced into experimental models to analyse the CBF changes and the collateral blood flow dynamics. Generally, LS device is cheaper than MRI, CT and ultrasound, used for similar experimental purposes. The LS device has two main parts: the laser light source and the charged couple device camera (CCD). The laser light source produces a 785 nm wavelength, which illuminates the red blood cells (RBC) on the sample's surface. The surface vasculature reflects the laser light as a backscattering signal recorded by the CCD. The static RBCs, with no flow, produce a stationary speckle pattern. Yet, the moving RBCs produce a dynamic speckle pattern, which is a blurred image indicating the level of blood flow (Perimed, 2018).

Laser speckle experiment is conducted on 10-week-old ICR mice, one week after the awake fentanyl challenge study (plethysmography). The experiment is a continuation of the long-term assessment of the earlier exposure to fentanyl. In this part of the experiment, an adult ICR mouse is brought to the theatre, and an initial dose of urethane anesthetic is given (1.5 mg/kg i.p.). This dose of anesthetic is followed by three top-up doses (0.25 mg/kg i.p.) with 15 minutes between each top-up dose. Accordingly, urethane was chosen as the preferred anesthesia in these studies since it has a minor effect on respiration rate that mimics the rapid-eye-movement (REM) sleeping pattern, unlike other anesthetic agents, such as Isoflurane which is commonly used in rodent's anesthesia (Pagliardini et al., 2013). Mice were continually monitored throughout the experiment and paw reflex tested to check full anesthesia. See Figure 2-3.

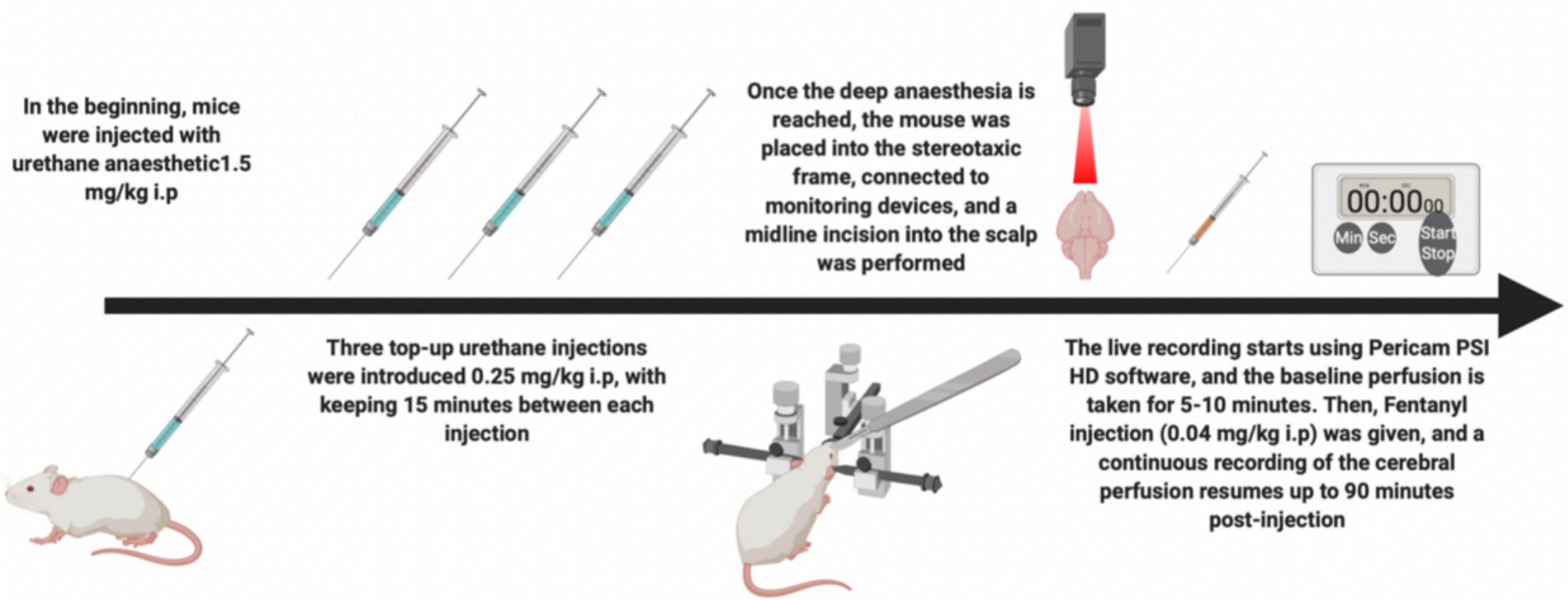

Figure 2-3 Laser speckle experiment timeline

Laser speckle study starts with anaesthetising the mouse with urethane injection 1.5 mg/kg i.p., which is followed by three top-up injections of urethane 0.25 mg/kg i.p. Once the mouse delves into deep state of anaesthesia, a placement within the stereotaxic frame takes place and followed by a scalp incision. The live recording starts right after, using PIM software to investigate the cerebral blood perfusion. Once the baseline data were taken (5-10 minutes), fentanyl injection (0.04 mg/kg i.p.) was given and CBF recording resumes up to 90 minutes.

2.4.1 Surgical preparations

Once a deep level of anaesthesia was maintained and paw reflex disappeared, the mice were then placed in a stereotaxic frame on prone position, where the head was secured using ear bars and a snout clamp to avoid any movement during laser speckle imaging. After that, a midline incision was made on the scalp to expose the skull. Additionally, monitoring devices were included in this stage in order to supervise the general state of the anaesthetised mouse, which are Pulsoxiometer, pressure pad, warming pad and a rectal thermometer. At the end of the experiment, the mouse was euthanised by cervical dislocation manoeuvre, as the experiment was a terminal procedure in this longitudinal study. See Figure 2-4.

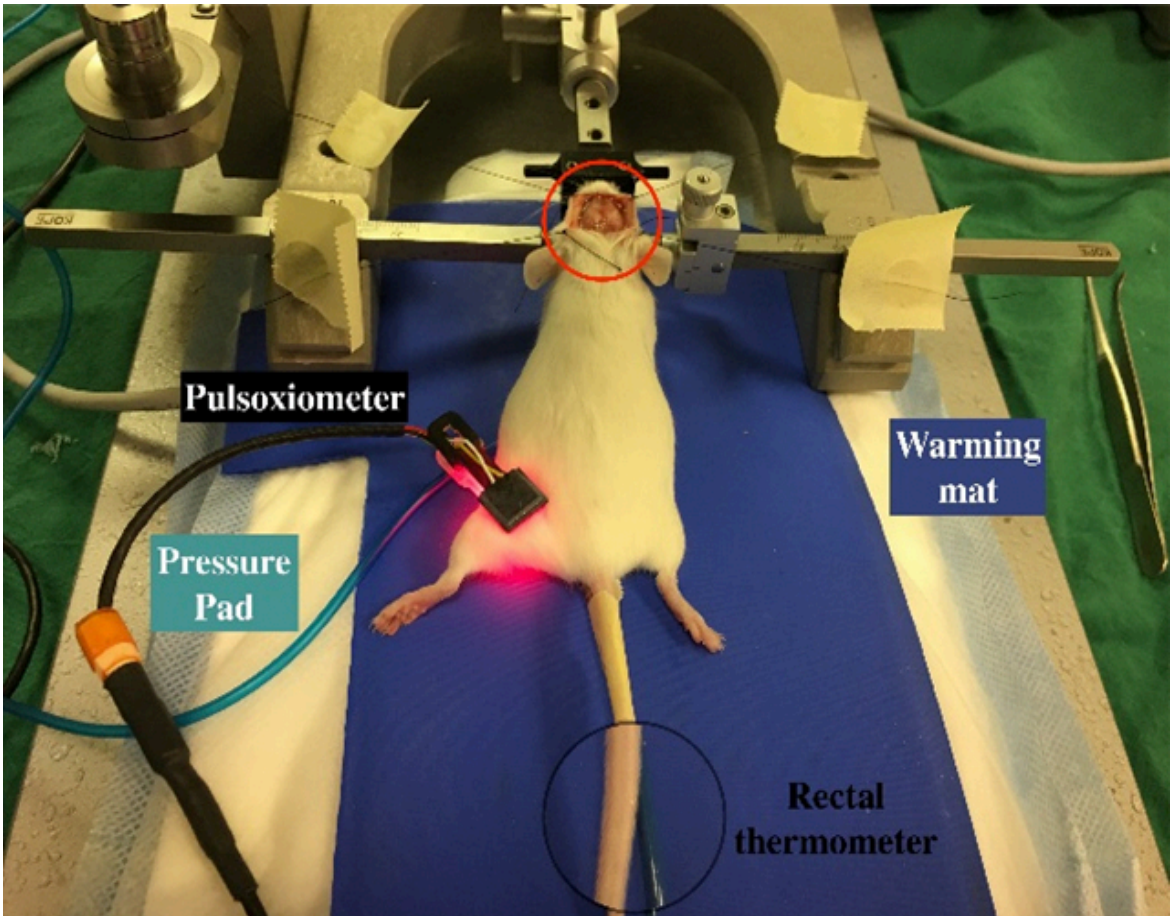

Figure 2-4 Anaesthetised fentanyl challenge set-up
The mouse was placed in a prone position, with the skull exposed for the laser speckle camera recording. Also, a warming mat was used to maintain the mouse temperature during the experiment, and a pulsoxiometre device attached to the left thigh in order to provide monitoring data about heart rate and approximate respiratory rate.

2.4.2 Live recording of the dynamic CBF changes

A live recording of the CBF dynamic changes is obtained by LS device, then it was analysed with PIM software that is provided by the manufacturer (Perimed, 2018). The recording cam was placed at 10 cm from the skull, the diffusion depth of the recording of the changes was 0.5 mm below the exposed skull (Tian et al., 2011; Davis et al., 2014). The imaging specifications were set to 1.4 * 1.4 field view, resolution 0.02 cm and 0.5 image/second. A 10-minute baseline period was used to set up the baseline perfusion rate, in reference to the arbitrary unit (a.u.). After the baseline recording was completed, a fentanyl injection was administered (0.04 mg/kg i.p.), and the recording was resumed up to 90 minutes post-fentanyl administration. See Figure 2-5.

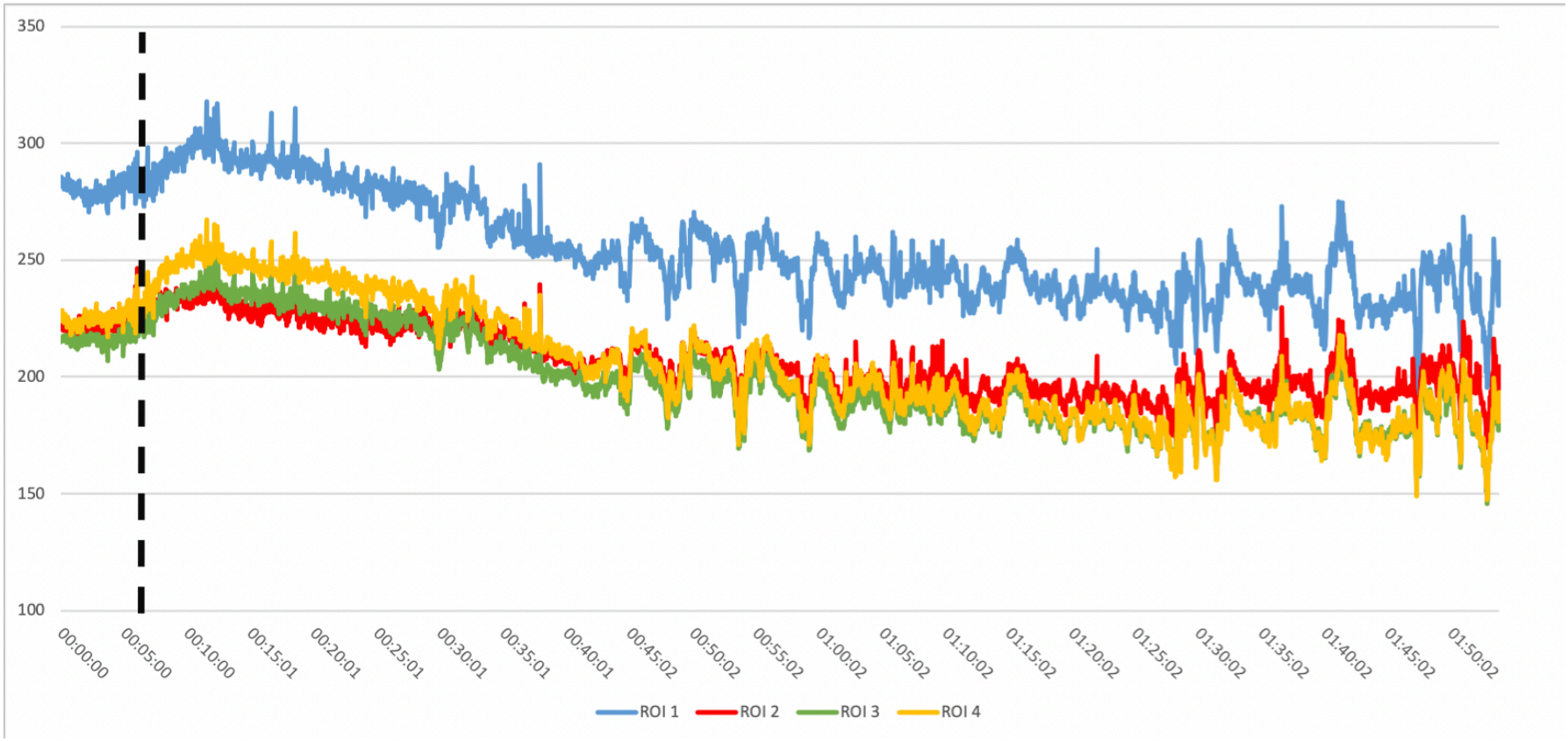

Figure 2-5 Laser speckle data presentation and analysis

The graph provides the data presentation within the PIMSoft software (PIM). The Y axis reflects the arbitrary unit of blood flow in the assigned ROI. The higher value is higher blood flow in the region. The X axis stands for the time, and the dashed line is the point when fentanyl was introduced into the study.

2.5 Enzyme-linked immunosorbent assay (ELISA)

2.5.1 Sample collection and processing

The ELISA test (Cusabio Biotech UK) was utilised in the study to follow up the chronic effect of the neonatal fentanyl exposure on the levels of the enzymes and stress response later in life. The sampling process starts by taking tail blood samples at weeks 6, 8 and 10 for β-endorphin levels analysis. Later, another tail vein sample is taken, at the termination point, at week 12 and it is accompanied with a cardiac puncture sample and hair sample. An illustration of the sampling process is provided at Figure 2-6, and more details are to be discussed later in the relevant chapter.

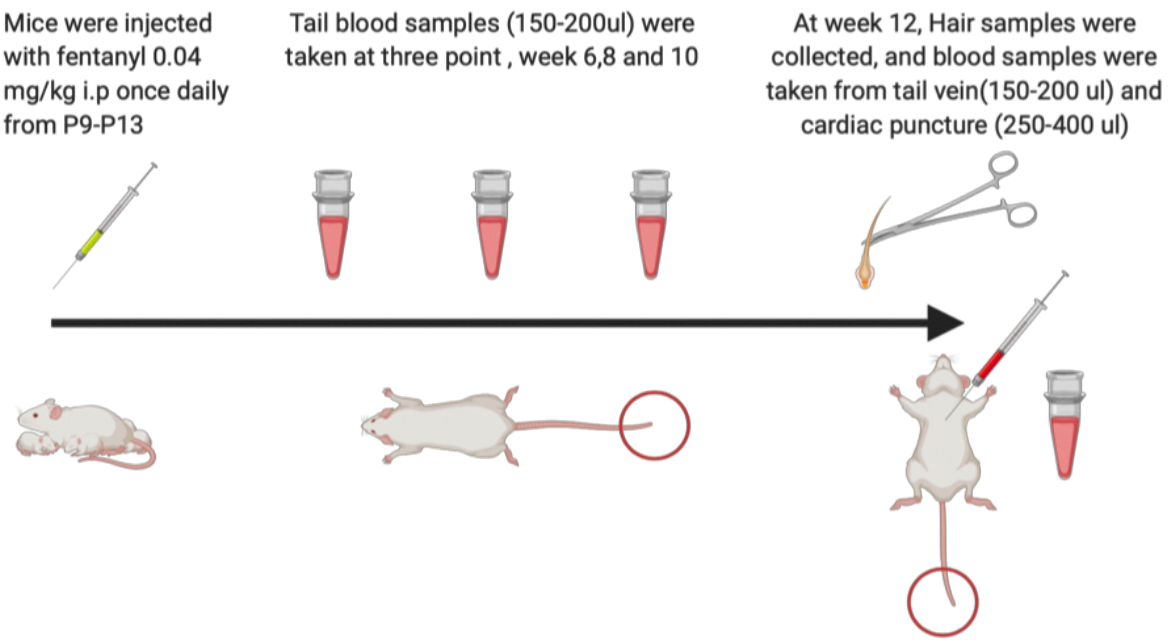

Figure 2-6 ELISA sampling (β -endorphin and corticosterone) process
Collecting the samples for ELISA analysis starts at 6 weeks old, and ends at the termination point (12 weeks old). Three tail vein samples are collected essentially at three different time points, and this is followed by a fourth sample that is taken beside cardiac puncture and hair sampling too.

2.5.2 Hair samples (corticosterone level)

At the age of 12 weeks, hair samples were collected from the mice group that received fentanyl injections between P1-P5 NN and P9-P13 JUV. The mice were injected with phenobarbital (0.1ml) intraperitoneal at the terminal phase of autoradiography and cryostat procedures. Hair samples were pulled from the back of the mice and stored in a dry vial at room temperature. Next, the samples were weighed, then washed with diluted methanol 20% (HPLC-grade methanol). Each wash required 2 ml of HPLC-grade methanol and placing the vial into the shaker set on 200 spins/minute for 2 minutes. Each hair sample took up to 3 washes, then vials were placed into the fume hood with no cap for 18-24 hours, so the remaining of the washing solution evaporated. After that, 2 ml of methanol (MeOH) was added to each vial, then placed on the orbital shaker at 52°C for 16 hours. The next day, MeOH was extracted from each vial and dispensed into a 12x75mm glass tube. Later, glass tubes were placed into the SpeedVac (Thermo Scientific, UK) , set on medium temperature, and kept for 2 hours, so the MeOH evaporated and the steroids dried at the bottom of the vials. The end product after evaporation process was sealed with a plastic cover and stored in the lab freezer for later analysis with an ELISA kit. See Figure 2-7.

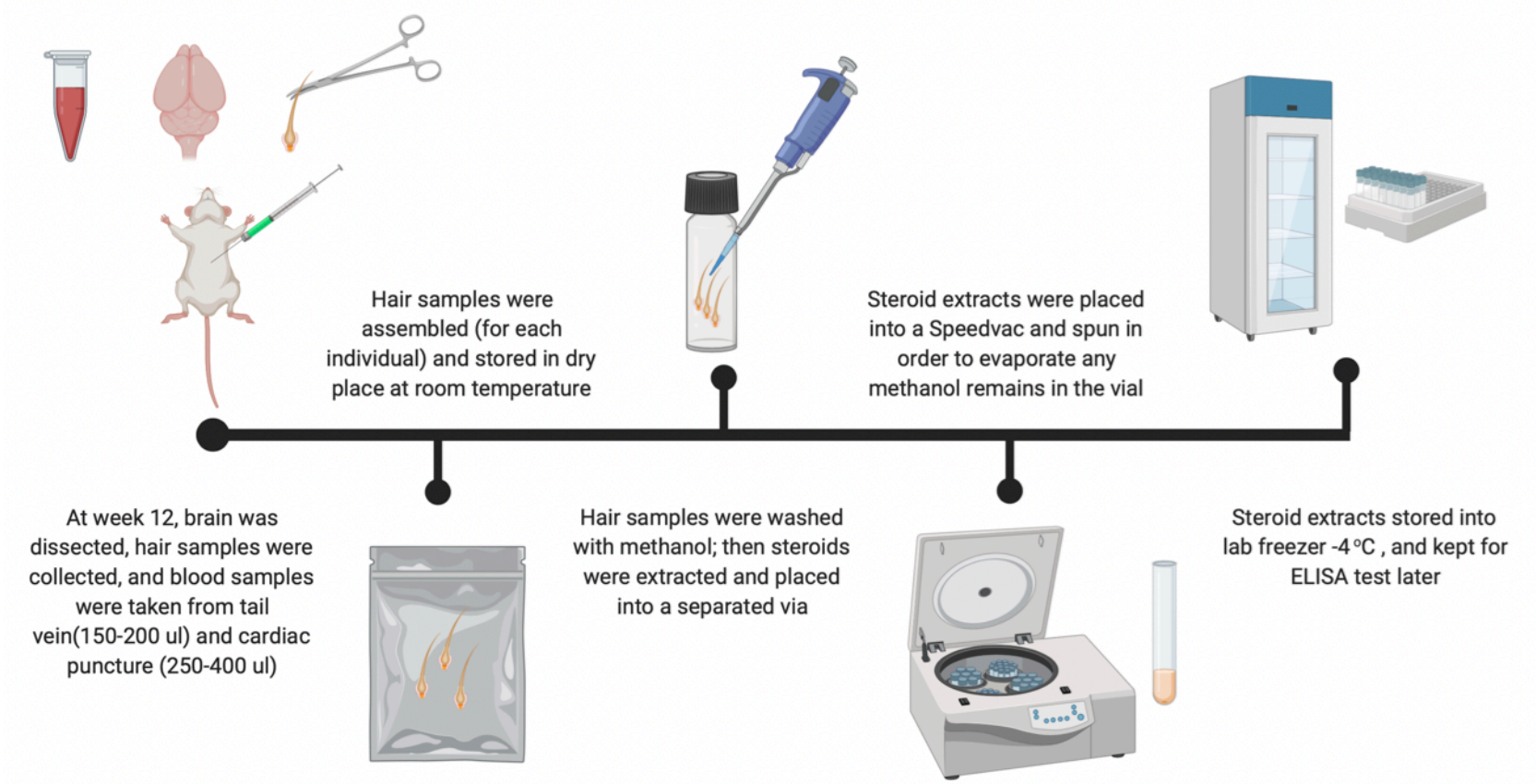

Figure 2-7 Hair sample preparation for ELISA test

Hair samples were collected at the age of 12 weeks old. It was stored in a dry place, then washed with methanol two times for 2 minutes. Methanol was aspirated and samples were left to dry for 18-24 hours at the fume hood. Then, 2 ml of methanol was added to the hair sample's vial and kept on the orbital shaker for 16 hours, set on 52°C. Methanol, containing steroids from hair samples, as aspirated again and placed into a separate vial, which as spun at the SpeedVac and dried. So, the methanol evaporated and steroids descended to the bottom of the vial, which as analysed later with ELISA test for corticosterone levels.

2.5.3 Blood samples (β-endorphin level)

Blood samples were collected in three different time points for each mouse. The mice group involved in this cohort was introduced to fentanyl earlier in life, the same group of mice that were involved in the autoradiography study. Hence, these mice were introduced to fentanyl at the age of P9-P13. Then, blood samples were collected at the age of 6, 8 and 10 weeks. Indeed, blood sampling was acquired by tail vein at each time point; moreover, a cardiac blood sample was collected at the age of 12 weeks, and the tail blood sample was taken the same day.

The blood sampling process was designed following the 3Rs recommendations, including the technique, sample volume and the timing of the sampling. Accordingly, mice were placed in the restraining apparatus that restricts the mouse movements and keeps the tail free for sampling. A side cut is made on the tail vein using a blade, then dripping blood is collected directly by heparinised Eppendorf. Once the 200 microliter blood sample is acquired, the samples are stored into an icebox. After that, samples were spun for 10 minutes at microcentrifuge (Sigma 1-14 Microfuge, Sigma®, Germany), and plasma was pipetted and kept on isolated Eppendorf. Then, plasma was stored in -60°C freezer in order to be analysed with ELISA kits later. See Figure 1-4.

The cardiac puncture was performed at the terminal experiment, when mice were euthanised by phenobarbital as a part of the brain dissection process, which is illustrated in detail at 1.6. In order to perform the cardiac puncture, a thoracotomy was mandatory and mid-clavicle cuts were done in parallel lines, so the rib cage could be everted and the heart exposed for sampling. Consequently, a 23-gate needle was used to pierce the heart at the left ventricle and blood was withdrawn gradually up to 1 ml. Once the samples were collected and stored in dry ice, center fusion was done for 10 minutes and serum extracted and stored in a separate tube at -60°C in a freezer, for later analysis.

2.6 Autoradiography

The brain samples used in this study were dissected from mice that are exposed to fentanyl after birth, at the age of (P9-P13). At the age of 10 weeks, the mice were injected with phenobarbital (0.1ml) intraperitoneal; as soon as the reflexes faded, brain dissection was carried out. Once the brain was excised from the skull, it was immersed in isopentane solution that was poured into a metal bucket which was surrounded by dry ice. This step may take up to 10 minutes. After that the brain sample was ready for preservation at – 80^{o}C in a freezer, and cryostat sectioning later.

2.6.1 Cryostat

Frozen brain samples were retrieved from the –80^{o}C freezer and each sample was cut into two parts (brainstem and cortex) by a blade. Each part was mounted on a separate chunk and fixed by Cryomatrix (Thermo Fisher Scientific, Cheshire, UK) at -20^{o}C, or dry ice. When the brain was fixed and enclosed by the Cryomatrix, the chunk was placed in the cryostat sectioning device at -20^{o}C. After that, micro-sectioning was commenced and set on a 20-micrometre width for both parts (brainstem and cortex), and the sections are collected to plates for future processing.

2.6.2 Incubation and film exposure

First of all, stored brain samples were retrieved from the –80 ^{o}C freezer and washed (50 mm Tris-HCl buffer) 3 times for 5 minutes each. After that, slides were incubated in 4 nm [3H] DAMGO for 60 minutes. Another wash (50 mm Tris-HCl) was conducted 3 times for 5 minutes each, after incubation with the [3H] DAMGO. Then, slides were left to dry at room temperature and placed into cassettes; exposed to Kodak bio-max films up to 15 weeks post-incubation. In the period of films exposure, cassettes were stored at 4°C, and test cassettes were opened at weeks 9, 12 and 15 to assess the film's development during the exposure period. Test cassettes were processed to develop and fix the film reaction; then the development level was measured and weighted against standard slides. Once an adequate level of development was obtained, the remaining cassettes were retrieved and analysed.

2.7 Immunohistochemistry

2.7.1 Perfusion

The perfusion procedure was carried out on mice that were involved in the immunohistochemistry study. This started with the administration of a single dose of phenobarbital (0.1ml) intraperitoneal, which was followed by testing the withdrawal reflexes. Once a suitable anesthetic state was attained, removal of the superficial ventral skin took place. Therefore, the thoracic and peritoneal cavity membrane became visible. A cut was made below the sternum in order to disclose the diaphragm. After that, an incision was made through the diaphragm on the lateral side, in order to expose the respiratory cavity and avoid damaging the internal organs (e.g. lungs and heart). Once the heart became visible, a butterfly needle (Butterfly-23 INT, Venisystems) was used to penetrate the left ventricle. The needle was attached to the perfusion system with the aim of replacing the circulatory blood with PBS by the end of the process. Once the butterfly needle was fixed through the left ventricle, a cut was made on the right atrium, and an influx of heparinised normal saline (10 ml heparin/1 l 0.9% saline solution) was commenced by the perfusion set, which was connected to the butterfly needle. The flushing process can take up to 30 seconds, and the constant pressure of influx was set to 80 mmHg. Accordingly, a changing of the liver's colour to pale is an early sign of successful clear out of blood from the vascular system. After that, the perfusion solution was switched to 4% paraformaldehyde, up to 250 ml with the same constant pressure. Stiffness of extremities is a useful indication of a successful perfusion, and this is followed by brain excision from the skull. After that, an immersion of the brain sample into 4% paraformaldehyde took place for up to 4 hours, then the sample was transferred to 30% sucrose vial.

2.7.2 Antibodies incubation (primary and secondary)

After perfusion and brain dissection, samples were immersed into sucrose and stored in the lab fridge. Next, brain samples were retrieved and rinsed into the PBS buffer. After that, the brain was cut coronally into two parts (brainstem and cortex), and both parts were placed on a separate plate and covered with agarose 5%. Agarose helps to segment samples via a vibratome and preserves the sample consistency. Once the sample is positioned in the vibratome, the micro-sectioning starts to segment 60- micrometer samples (caudal-cranial), for the brainstem; and (cranial-caudal) for the cortex part. Samples were collected in 48-well plates, in order, to select the required samples that take place when the micro-sectioning is over. After that, samples were allocated four vials and rinsed into glycerol in order to be stored at -20^{o}C in a fridge. On the day of antibody incubation, the vials are retrieved, and glycerol was rinsed with PBS (double salt) a couple of times. Then the samples were incubated into the primary antibodies for 48 hrs. After that, the samples were washed three times in PBS and incubated into secondary antibodies overnight. The next day, another washing with PBS (3 times) took place, then samples were mounted on anti-fade medium slides.

Chapter 3 The long-term effects on breathing pattern following opioid exposure in early life in ICR mice.

3.1 Introduction

The respiratory system is characterised as immature, vulnerable and unstable at birth and in the early days of life, with breathing pattern being susceptible to external environmental changes and distresses during this age window (Read and Henderson-Smart, 1984). Beyond the first week of life in rodents, the respiratory system matures leading to a breathing of increased frequency and rhythmicity (Hilaire and Duron, 1999). The retrotrapezoid nucleus/parafacial respiratory group (RTN/pFRG) is considered to be the origin of the breathing rhythm in the neonatal rodent. In the neonatal brainstem-spinal cord preparation, the RTN/pFRG produce rhythmic activity that is linked to the pre-inspiratory signals that precede the onset of inspiration (Onimaru et al., 2008, Onimaru and Homma, 2003). These pre-inspiratory signals are not observed from RTN/pFRG neurones in vivo studies conducted on adult rodents (Stornetta et al., 2006, Mulkey et al., 2004); which indicates a change in the breathing oscillator from neonatal to adult. On the other hand, the preBötC is acknowledged as a critical site for respiratory rhythmogenesis in mammals which drives the rhythmic contractions of the inspiratory muscles (Mellen et al., 2003; McKay et al., 2005; Janczewski and Feldman, 2006; McKay and Feldman, 2008; Tan et al., 2008).

Several studies have highlighted the role of preBötC in the opioid induced respiratory depression (Gray et al., 1999; Takeda et al., 2001; Mellen et al., 2003; Montandon et al., 2011),as applying DAMGO (a μOR agonist) directly to preBötC neurones in vitro results in a decrease in respiratory motor output; which is reversed by Naloxone (μOR antagonist) (Mellen et al., 2003, Takeda et al., 2001). In vivo, the systemic injections of DAMGO or fentanyl result in quantal slowing of the respiratory frequency, which leads to complete respiratory arrest if injected continuous and directly into preBötC (Montandon et al., 2011), while the administration of naloxone systemically or locally into preBötC will reverse the μOR agonists' effect and stop the respiratory depression (Montandon et al., 2011).

Clinically, respiratory function is monitored during the administration of opioids (Niesters et al., 2013); however, the long-term respiratory outcomes of repeated opioid exposure, especially during the first weeks of life, have never, to our knowledge been investigated clinically or in pre-clinical animal studies. To date, the pre-clinical rodent studies are focused on developing tolerance and reduced sensitivity to the drugs, which are resulted from repeated opioid exposure early in life (Thornton and Smith, 1998).

This study provides a novel insight into the long-term consequences of respiratory patterns triggered by early repeated exposure at neonate and infant age. Accordingly, fentanyl was introduced at the postnatal age P1-P5 and P9-P13 to disturb the maturation process and produce a long-term effect on the breathing pattern. After the repeated exposure to fentanyl early in life, mice were let to grow without any additional intervention for up to 10-12 weeks. Finally, at the adult age, respiratory measures (respiratory rate, tidal volume and minute volume) are assessed to investigate the long-term changes triggered by the early exposure to fentanyl.

3.2 Study aim

- To study the long-term effects on breathing pattern of postnatal (P1-P5) opioid exposure.

- To study the long-term effects on breathing pattern of postnatal (P9-P13) opioid exposure.

3.3 Hypothesis

The earlier exposure to opioids, postnatally, may cause alterations in breathing pattern later in life.

3.4 Materials and methods

3.5 Animals

The experimental animal procedures were performed under the regulations of the UK Home Office (personal licence number i51F7C81D, and project licence number 60/4558). The studies were designed in correspondence with the Animals (Scientific Procedures) Act 1986. The experimental procedures were conducted on ICR mice, which were acquired from HARLAN. Accordingly, pregnant dams were ordered and delivered to the housing facility at Veterinary Research Facility, Garscube campus, University of Glasgow. The pups were kept with the mother up to the age of 21 days, when they were weaned. Post weaning, male and female mice were housed in separated cages, with a maximum of 4 mice per cage. Ear-piercing allowed for identification of individual mice within the cage. The light/dark cycle was 12 hours duration, with no dietary modifications. Day of birth is referred to as postnatal day 0 (P0). The age categories used in this study were neonate (P0-P7), juvenile (P8-P21) and adults over P21.

3.6 Postnatal injection

The experimental groups were defined as follows:

- **Group 1 – Neonatal Fentanyl (NN-FEN) n=8** Each mouse received one daily injection of fentanyl (0.04 mg/kg i.p.) for 5 days from postnatal day 1 (P1) to postnatal day 5 (P5)

- **Group 2 – Neonatal Saline (NN-SAL) n=8** Each mouse received an equivalent volume of physiological saline was given once daily P1-P5.

- **Group 3 –Juvenile Fentanyl (JUV-FEN) n=8** Each mouse received one **daily** injection of fentanyl (0.04 mg/kg i.p.) P9-P13.

- **Group 4 Juvenile Saline (JUV-SAL) n=8** Each mouse received an equivalent volume of the physiological saline P9-P13.

Fentanyl citrate (μ opioid receptor agonist, 50 μg/ml, Janssen-Cilag, UK) was administered daily (0.04 μg/kg i.p.) P1-P5 for group 1 or P9-P13 for group 3. Control groups received an equivalent volume of the normal saline.

At week 10-12, all mice were habituated to the plethysmograph apparatus prior to recordings being made. On the day of recording, mice were given a period of time to settle before three control recordings of 2 minutes duration were taken to assess the baseline breathing parameters at rest. Upon completion of control recordings, mice received an injection of Fentanyl (0.06 mg/kg IP), rectal temperature was recorded, and mice were placed back into the plethysmography chamber. Two-minute recordings of breathing pattern were taken at the following time points post injection: 5 minutes (T5), 10 minutes (T10), 15 minutes (T15), 30 minutes (T30), 45 minutes (T45) and 90 minutes (T90); see Figure 3-1.

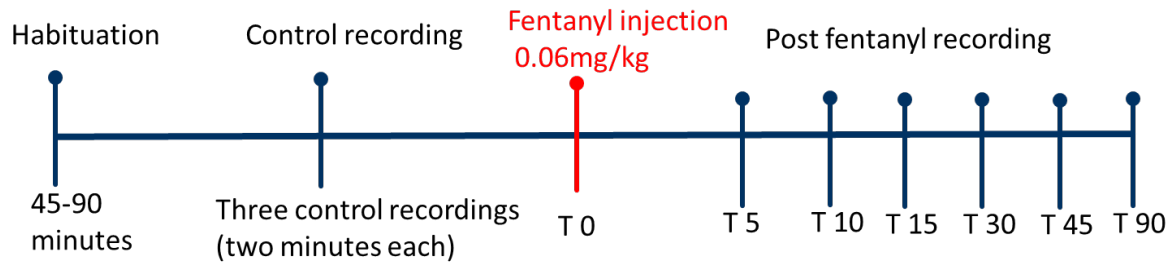

Figure 3-1 Plethysmography experiment
Plethysmography experiment timeline starts with a habituation period of 45-90 minutes, that is followed by three control recordings that are taken to determine the baseline of the breathing measures. Once the Fentanyl was administrated, breathing was evaluated in individual time points across 90 minutes time window post-injection.

3.7 Data analysis

The key software used for the Pleth study was Spike software (Cambridge, 2018). Plethysmography data were exhibited as a waveform signal that was obtained via the pressure changes delivered by the validyne (see Figure 3-2). The tidal volume (Vt) was measured via (Drorbaug and Fenn, 1955) equation that was set for the closed plethysmography pressure oscillation. The breathing cycle within the closed chamber will change the pressure inside the chamber by a magnitude proportional to the volume difference from the chamber to the airway conditions. In order to calculate the Vt, other variables were taken at the time of the recording, such as the mice and room temperature (see Figure 3-3). The mean average of the three control recordings was taken as a baseline record of respiratory parameters for each mouse in both groups (SAL and FEN). After that, the baseline data were set up as an average line to evaluate any change of respiratory measures during the course of the in-vivo experiment.

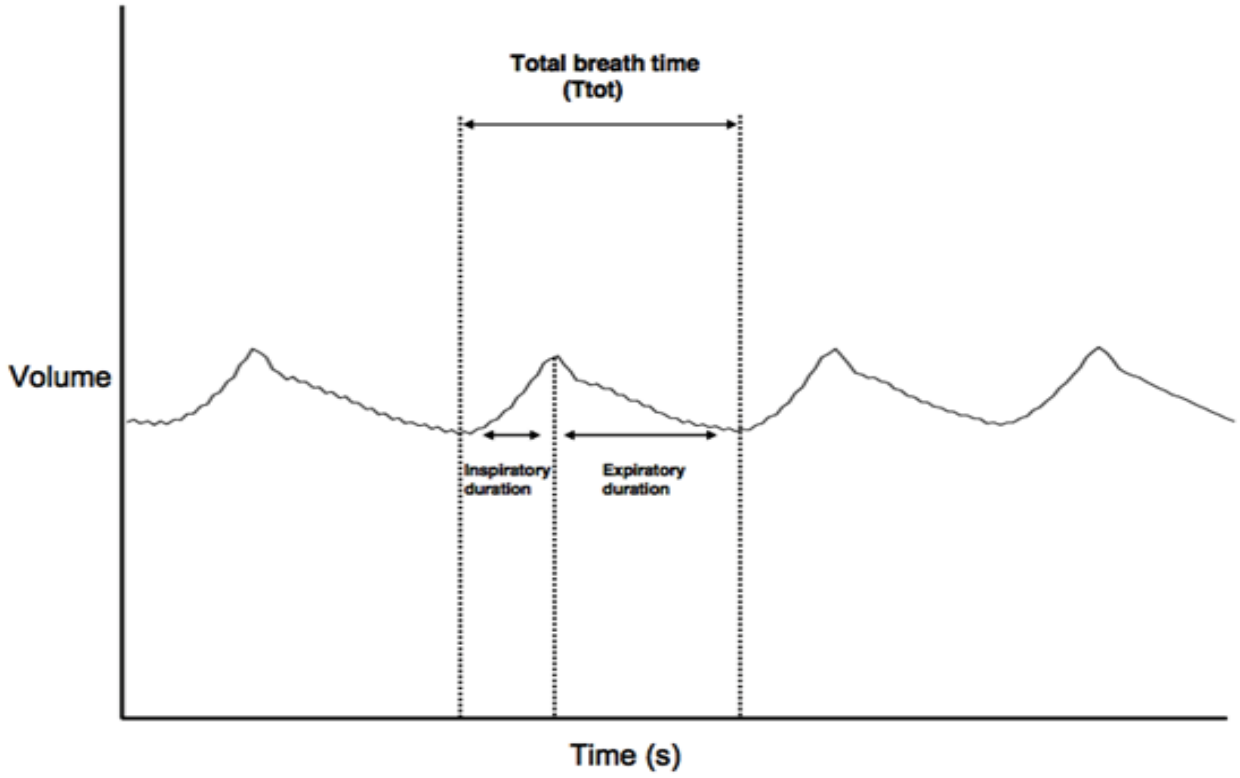

Figure 3-2 Plethysmography data presentation and analysis
The graph shows the raw data extracted from the Pleth experiment and it is presented in a waveform signal that illustrates the breathing cycle which starts with inspiratory and ends with expiratory.

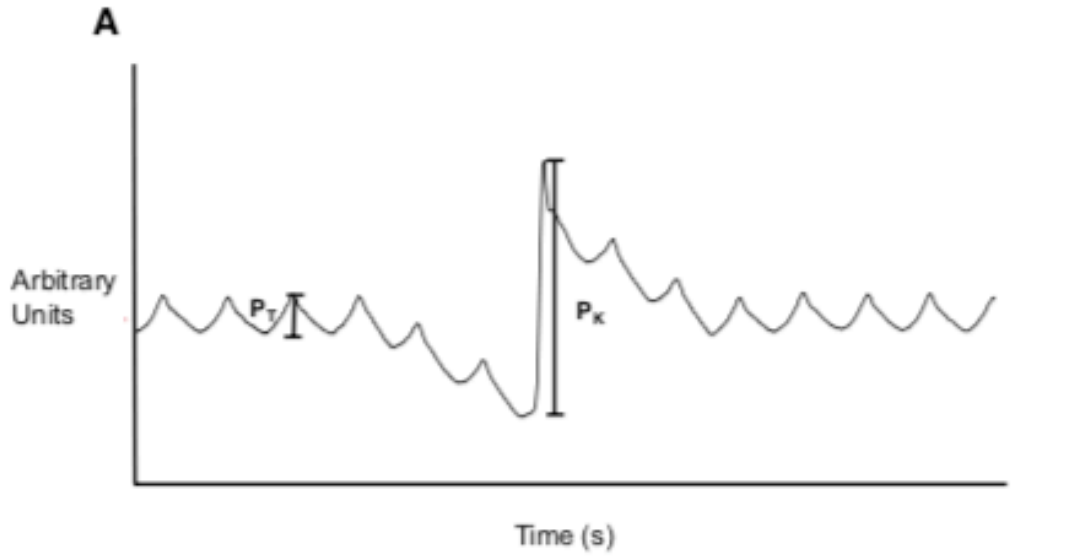

B

$$V_t = \frac{P_T}{P_K} \times V_K \times \left(\frac{T_R (P_B - P_C)}{T_R (P_B - P_C) - T_C (P_B - P_R)} \right)$$

Figure 3-3 Obtaining the tidal volume through plethysmography data
Tidal volume (V_t) was calculated by using the equation developed by (Drorbaug and Fenn, 1955). It started by converting the pressure change exerted by the calibrating needle P_K into volume V_k. Also, P_T stands for the pressure change with the respiratory cycle. The remaining variables at the equation are (T_R) the mouse body temperature, (T_c) recording chamber temperature, (P_B) barometric pressure, (P_R) pressure of water vapour at body temperature (50mmHg) and (P_C) pressure of water vapour in the recording chamber (50mmHg).

3.8 Statistical analysis

The statistical analysis was executed using GraphPad Prism 4 software. Data were presented as mean ± SD, and the level of statistical significance was set at $p<0.05$. Unpaired t-test were used to analyse the difference in baseline mean average for respiratory measures (respiratory rate, tidal volume and minute volume) between the FEN groups and the SAL from the same age category (NN and JUV). After that, the mean was taken from the respiratory measures at several time points (T5, T10, T15 … T90), and two-way Analysis of Variance (ANOVA) test was performed to analyse the difference between (NN-FEN vs NN-SAL, and JUV-FEN vs JUV-SAL) groups that is followed by a post hoc Bonferroni correction, for multiple comparison. Respiratory data were presented as normalised ratio to take account of the individual baseline variability. A coefficient variation (Co-Var) was performed to evaluate the variability of baseline respiratory rate within the study groups.

3.9 Results

3.9.1 Results of awake respiratory analysis (plethysmography)

Plethysmography breathing traces, collected at the age of 10-12 weeks, are presented in the figure Figure 3-4, which shows variable breathing patterns observed from different time points during the experiment. The top trace in both graphs shows the control breathing which presents the baseline breathing pattern in both groups, NN and JUV. Breathing traces are displayed from T15 and T30 post FEN injection 0.06 mg/kg i.p. or saline injections. T30 trace post fentanyl shows a decrease in number of peaks and amplitude in comparison to the baseline breathing pattern, as a result of the respiratory depression induced by the FEN injection.

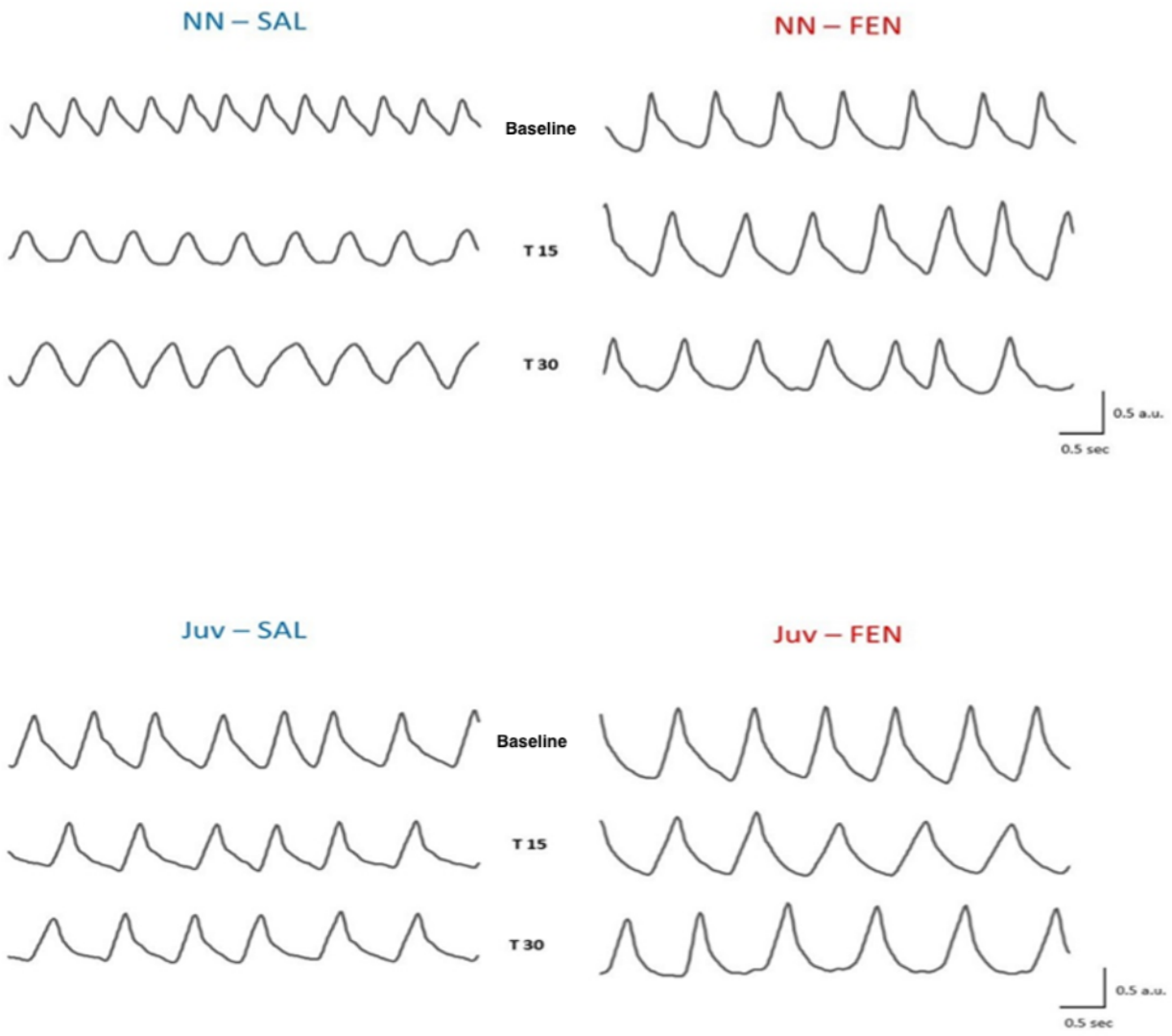

Figure 3-4 Plethysmography raw data
A schematic illustration of plethysmography raw data. The pressure waveforms illustrate breathing pattern and frequency pre-fentanyl injection (baseline) and post injection: T15 and T30 from one representative mouse from each of the 4 groups.

3.9.2 Baseline breathing data

Baseline respiratory frequency was significantly decreased in NN-FEN (n=8) compared to NN-SAL (n=8) (136.5 ± 5.63 bpm *vs* 153.1 ± 4.25 bpm, $p<0.05$) There was no significant difference in tidal volume when comparing NN-FEN with NN-SAL (0.24 ± 0.02 ul/g vs 0.25 ± 0.02 ul/g, $p>0.05$). The significant decrease in minute volume in NN-FEN (VALUE) compared to NN-SAL (29.56 ± 2.41ul/min/g vs 37.76 ± 2.86 ul/min/g, $p<0.05$) is driven by the decreased respiratory frequency. On the other hand, the baseline respiratory frequency showed no significant difference in JUV-SAL (n=8) compared to JUV-FEN (n=8) (173.3 ± 19 bpm vs 176.9 ± 14.84 bpm, $P > 0.05$). The tidal volume showed no significant difference between the JUV-SAL (n=8) and JUV-FEN (n=8) (0.29 ± 0.03 ul/g vs 0.33 ± 0.03 ul/g, $P<0.05$). The minute volume showed no significant difference when JUV-SAL (n=8) compared to JUV-FEN (n=8) (49.35 ± 8.74 ul/min/g vs 58.01 ± 7.23 ul/min/g JUV- $P<0.05$). See Figure 3-5.

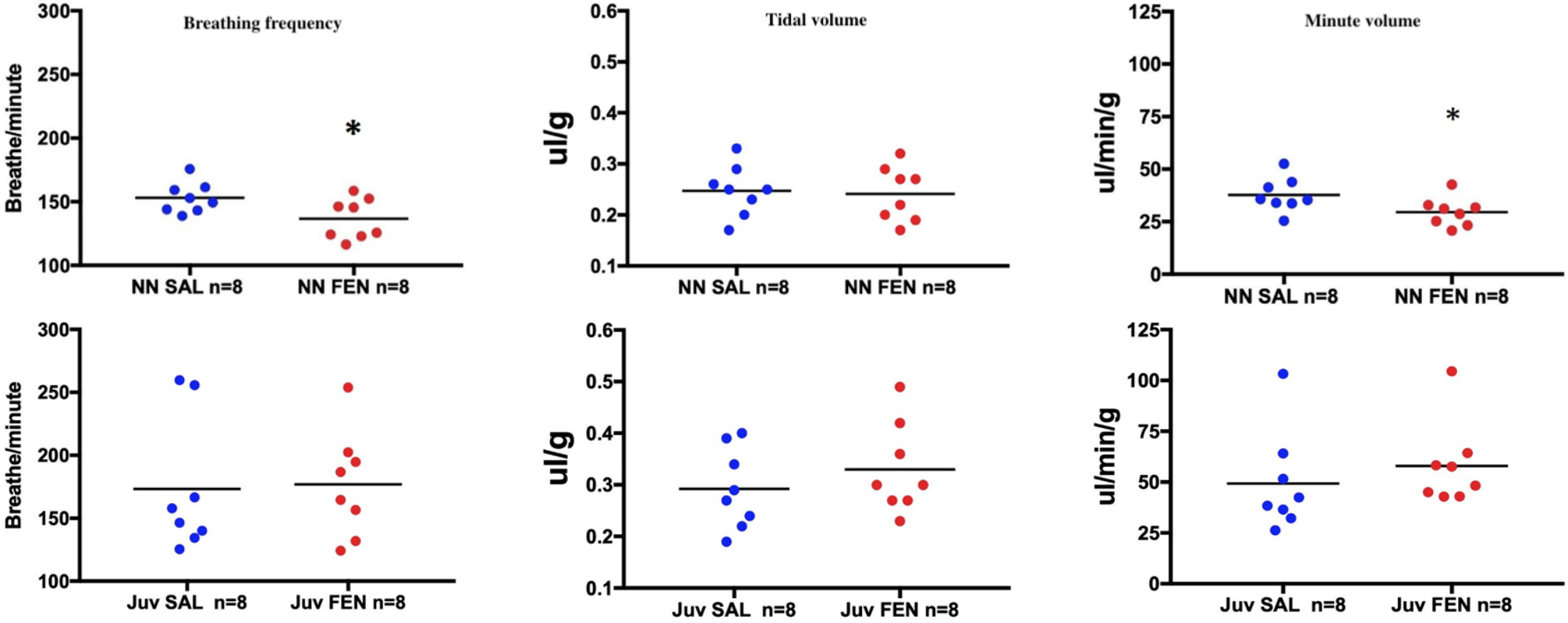

Figure 3-5 Breathing baseline data in NN and JUV groups

The breathing baseline measures are plotted for all experimental groups, and NN-FEN had exhibited a lower breathing frequency, when compared to NN-SAL. The same effect was obtained on the minute volume data. However, the JUV groups had brought a similar breathing data concerning the different parameters (breathing frequency, tidal volume and minute volume).

3.9.3 Awake fentanyl challenge

3.9.3.1 NN-SAL and NN-FEN

The NN-SAL baseline average was 153.1 bpm and it had declined to 141.8, then 148 at T15, 134.7 at T30, 128.5 at T45 and recorded a 149.6 bpm at T90. The NN-FEN baseline average was 136.5 bpm, and it had increased to 146.8, then declined to 126.7, 117.6 at, 130.3 at and ended at 117.4 bpm. See Figure 3-6 . No significant change was obtained between each time point and the baseline average of the breathing frequency at the awake fentanyl challenge conducted on both groups (NN-SAL and NN-FEN). Additionally, normalised ratio was applied to trace the changes of respiratory measures, starting from a baseline of 1. NN-SAL breathing frequency dropped to 0.93 at T10, then it raised to 0.97 at T15, followed by 0.88 T30, 0.84 T45 and 0.98 at T90. Besides, NN-FEN breathing frequency starts as 1 at baseline point, and raises to 1.06 at T10, then 0.93 at T15, 0.87 at T30, 0.96 at T45 and 0.86 at T90. Again, time factor was significant, with a P value < 0.05, and no significant change was obtained in between the groups' P value > 0.05. No significant differences were found between each time point and baseline for both NN groups. See Figure 3-6 (A)

Tidal volume average in NN-FEN showed an increase from baseline (0.24 ul/g) toward T15 (0.29 ul/g) and slowly decrease toward T30 (0.28 ul/g) T45 (0.27 ul/g) till (0.25 ul/g) at T90. NN-FEN showed a significant difference between T15 and baseline normalised ratio, as an increase in the tidal volume recorded from 1 at baseline to 1.25. The trend had declined at the following time points T30 (1.2), T45 (1.125) till reached (1.05) at T90. No significant change found by the time factor (P value > 0.05), but a difference between the groups was pointed with a (P value < 0.05). In addition, NN-SAL exhibited no increase in the tidal volume, where baseline average was (0.248 ul/g), then it changed to (0.247 ul/g) at T10, (0.225) at T15, (0.249) T30, (0.258) T45 and (0.231 ul/g) at T90. No significance difference found between each time point and baseline average. Hence, NN-SAL tidal volume (normalised ratio) did not reveal a change from the baseline point (1), as the mean average across different time points was (1.01) at T10, (0.91) T15, (1.02) T30, (1.05) T45 and (0.94) at T90. The group factor was significant (P value < 0.05) as a

difference between NN-SAL and NN-FEN, and tidal volume response to fentanyl is shown in Figure 3-6 B,

Minute volume showed a significant difference between the baseline and T10 at NN-FEN group, where the baseline mean average was (29.56 ul/min/g), T10 minute volume was (40.36 ul/min/g), and P value < 0.05. However, the remaining time points showed no difference from the baseline, as the mean averages were 35.57 at T15, 31.9 at T30, 32.28 at T45 and (28.18 ul/min/g) at T90. The control group (NN-SAL) showed no difference from the baseline average (37.76 ul/min/g), as the time points' averages were 35.76 at T10, 33.17 at T15, 33.65 at T30, 32.75 at T45 and (32.96 ul/min/g) at T90. Contrasting with the normalised ratio, NN-FEN group revealed the same significance change of minute volume at T10, where the mean average equals 1.414, compared to 1 at the baseline. The other time points showed a dropping slope from T10 points as the average was 1.229 at T15, 1.133 at T30, 1.108 at T45 and 0.960 at T90. The control group (NN-SAL) imposed a similar curve to the raw data, and the mean averages were 0.958 at 10, 0.887 at T15, 0.885 at T30, 0.883 at T45 and 0.912 at T90. See Figure 3-6 C.

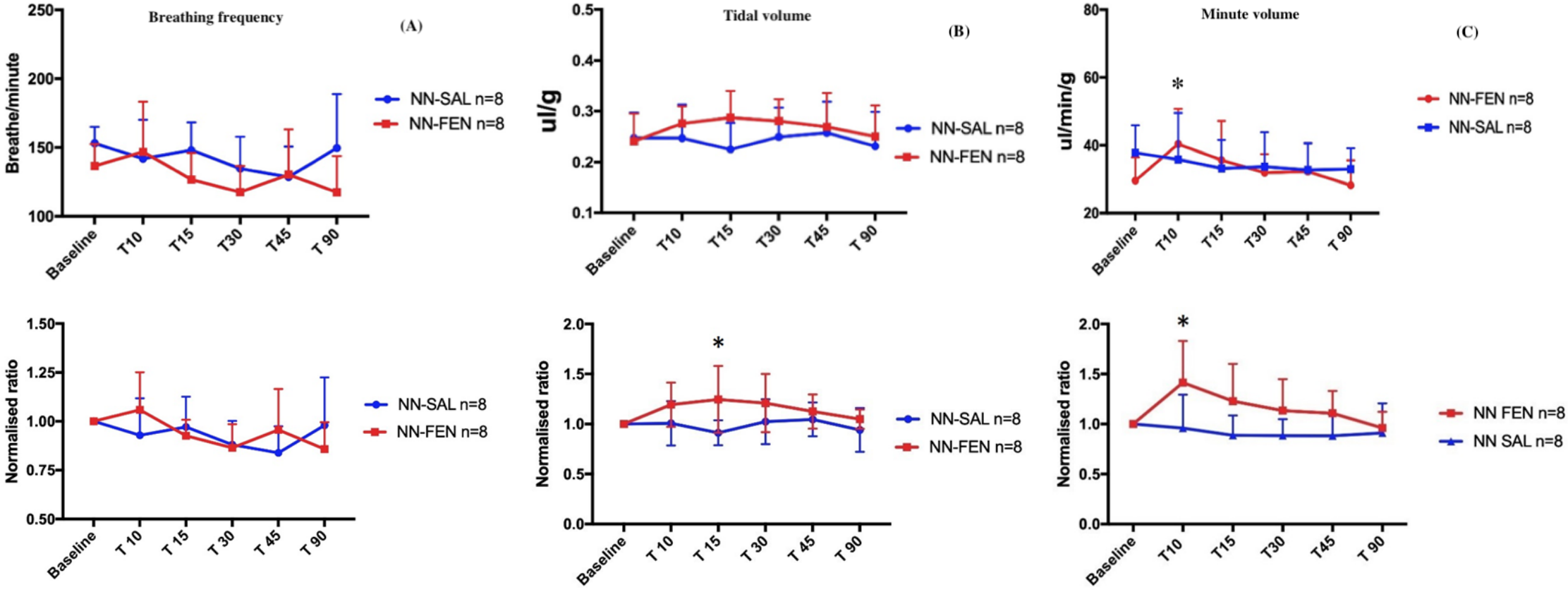

Figure 3-6 Awake fentanyl challenge in NN-FEN and NN-SAL groups

The graphs present the change of the breathing parameters (breathing frequency, tidal volume and minute volume) during the awake fentanyl challenge. The main finding is a decrease of the respiratory rate following the FEN injection. Hence, the decrease of respiratory rate is accompanied with an increase of the tidal volume, which is significantly seen at T15 on the (b) charts when the normalised ratio compared in the NN group . An asterisk highlights the increase of the minute volume (c) in NN-FEN group is detected at T10 and it reaches up to 1.5 increase from the baseline, where it was near the 1 (baseline records) in the NN-SAL. Two-way Analysis of Variance (ANOVA) test was performed to analyse the difference between the study groups that is followed by a post hoc Bonferroni test, for multiple comparison. Data is presented as mean ± SD,

3.9.3.2 JUV-SAL and JUV-FEN

JUV groups (JUV-FEN and JUV-SAL) showed similar results through the awake fentanyl challenge. Starting with the breathing frequency, the JUV-SAL mean average was (173.3 bpm) at baseline point, and after that it increased to 187.8 at T10, then a descent occurred and it reached 159.7 at T15, 145.7 at T30, 149.9 at T45 and ended at 180 bpm on T90 timepoint. No significant change was obtained between the breathing frequency average on different time points and the baseline. The other group (JUV-FEN) baseline average was (176.9 bpm), and it dropped to 151.8 bpm at T10. After that, an increase occurred and reached 165.6 at T15, then 148.2 at T30, 151 at T45 and 170.2 breaths/minute at T90. Again, no significant difference was highlighted between the time points and the baseline average. See Figure 3-7 A.Tidal volume on JUV-SAL group showed a slight rise at T10 and T30, beside a marked drop at T90 at the end of the challenge. Accordingly, the baseline average at JUV-FEN was (0.33 ul/g) and it rose to 0.36 at T10, then returned to 0.33 at T15 and another increase occurred at T30 0.35 ul/g that was followed by 0.33 at T45 and 0.26 ul/g at T90. JUV-SAL group had an average of (0.29 ul/g) at baseline, which lowered to 0.28 at T10 and rose to 0.28 at T15. It remained at 0.27 at T30 and 0.28 at T45, then ended at 0.24 ul/g at T90.

The normalised data of tidal volume change in JUV groups were similar to the raw data, as JUV-FEN showed an increase of the ration from 1 at baseline to 1.106 T10 and 1.085 at T30. Moreover, a significant drop was obtained at T90, where the normalised ratio had reached 0.8138, and (P value < 0.05) between baseline point and T90, which matches the same significant drop at the raw tidal volume at the same time point (*P* value < 0.05). The JUV-SAL group had no significant trends from the baseline point (0.293 ul/g) as the tidal volume at the different time points was 0.278 at T10, 0.284 at T15, 0.273 at T30, 0.281 at T45 and reached 0.24 ul/g at T90. Additionally, the normalised ratio of JUV-SAL was close to the baseline (1), T10 = 1.011, T15 = 0.95, T30 = 0.93, T45 = 0.923 and 0.811 at T90. Yet, T90 had a significant drop from the baseline (P value < 0.05), but no other time point had a significant change. See Figure 3-7 B.

No significant change was observed on the minute volume through the awake fentanyl challenge in both groups (JUV-SAL and JUV-FEN). The raw average minute volume of JUV-SAL was (49.35 ul/min/g), which rose at T10 to 50.82, then dropped to 42.39 at T15 and was followed by 38.84 at T30, 40.4 at T45 and 41.74 ul/min/g at T90. Plus, in the JUV-FEN group, the baseline average started at 58.01 ul/min/g and lowered to 52.97 at T10, then 53.79 at T15, 50.58 at T30, 47.91 at T45 and reached 44.24 ul/min/g at T90. No significant difference was observed between the time points and baseline in both groups (P value > 0.05). Additionally, the normalised ratio graph exhibited a steady slope after the awake fentanyl challenge for JUV-SAL and JUF-FEN groups, where JUV-SAL had an elevation at T10 = 1.165, which was followed by a reduction at T15 = 0.9791, T30 = 0.861, T45 = 0.9643, and T90 = 0.9489. Moreover, the JUV-FEN group had a decline at T10 = 0.9587, which was followed by a similar level at several time points T15 = 0.9741, T30 = 0.9198, T45 = 0.8438 and T90 = 0.79. No significant difference was obtained between the time points and baseline in both groups (P value > 0.05). See Figure 3-7 C.

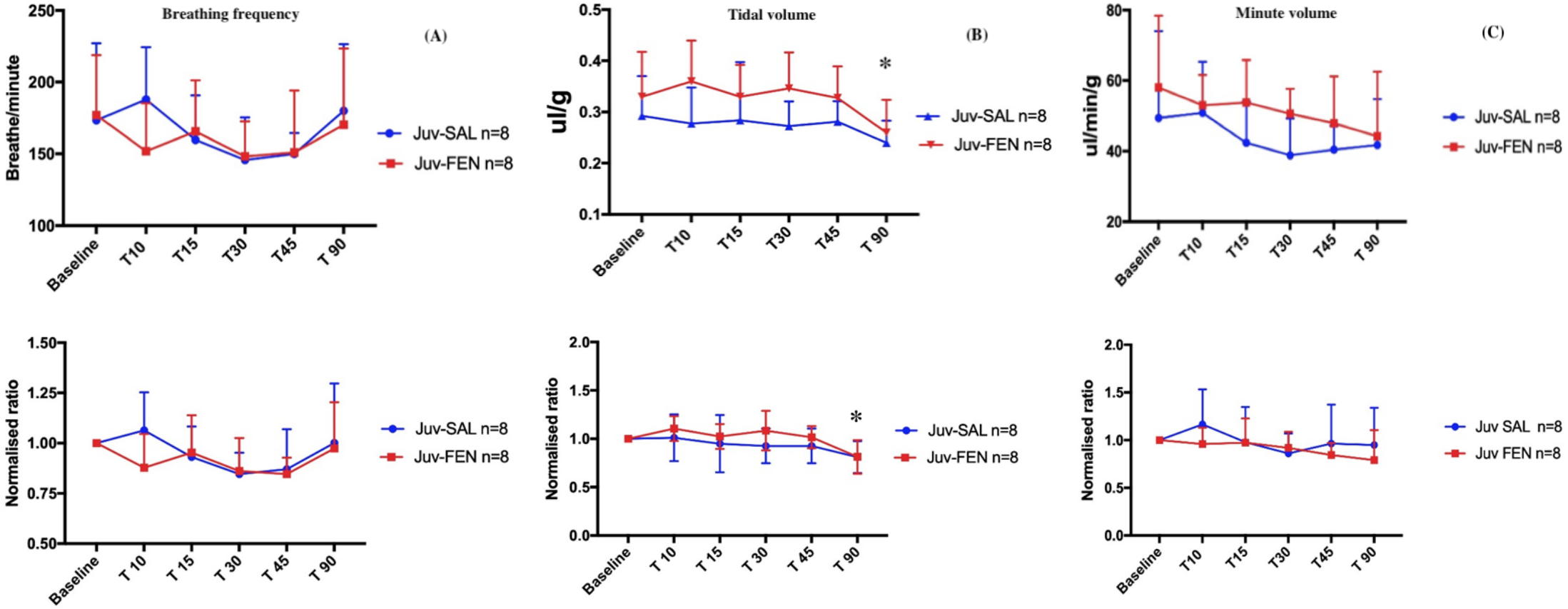

Figure 3-7 Awake fentanyl challenge in JUV-FEN and JUV-SAL groups

The graphs present the change of the breathing parameters (breathing frequency, tidal volume and minute volume) during the awake FEN challenge in JUV group. The main finding is a decrease of the respiratory rate that resulted from the FEN injection. Hence, the decrease in the respiratory rate is accompanied with an increase in the tidal volume. Two-way Analysis of Variance (ANOVA) test was performed to analyse the difference between the study groups that is followed by a post hoc Bonferroni test, for multiple comparison. Data is presented as mean ± SD,

A coefficient variation (Co-Var) was performed to evaluate the variability of the resting breathing data of each study group. In NN groups, the Co-Var range was 19% vs 21% in the JUV group. Those imply the variability of breathing data that could be produced within a single group as a part of an in vivo study. Therefore, a normalised ratio was used to evaluate the changes in breathing pattern from the baseline point in each mouse, to minimise the variability of the data of the study groups. See Figure 3-8.

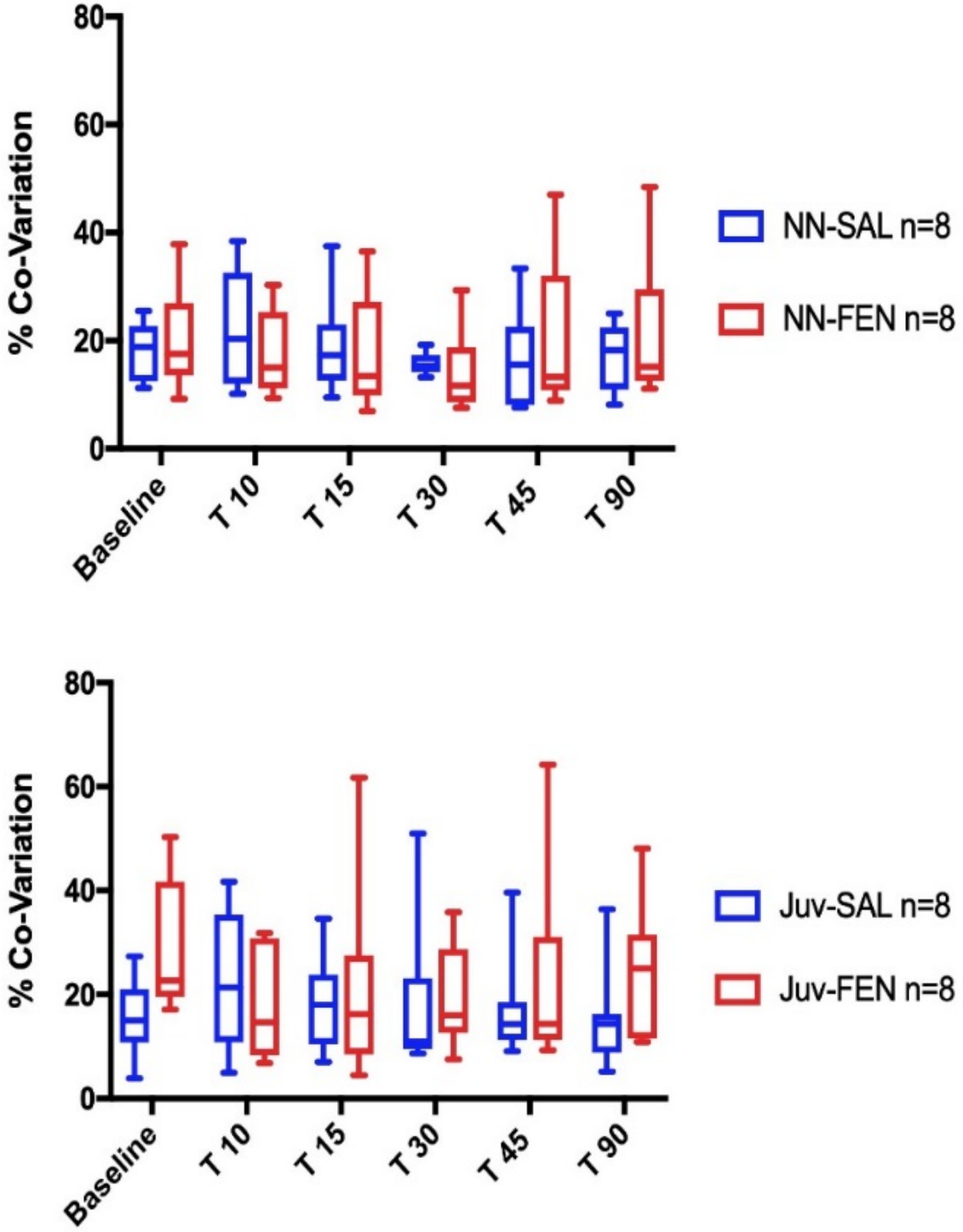

Figure 3-8 Co-variation of breathing pattern in the awake FEN challenge
The coefficient of variation shows an inconsistency of the breathing frequency across the recording period during the awake FEN challenge. The range of co-var falls between 10-45% and it is related to the nature of variation obtained in (in-vivo) studies. Data is presented as mean ± SD,

3.10 Discussion

The aim of the experiment was twofold i) to investigate if exposure to fentanyl in early life (P1-5 or P9-P13) would have long term effects on baseline breathing in adult hood; ii) if exposure to fentanyl in early life would alter how the respiratory system responds to further fentanyl exposure in adult hood. The results show a variable response; however, there is a clear indication that exposure to fentanyl during the neonatal period (NN-FEN) results in a long-term decrease in baseline respiratory frequency in adult hood, the response to further fentanyl challenge in adulthood is variable and will be further discussed.

3.10.1 Baseline breathing records

The baseline recording showed a decrease in breathing frequency and minute volume in the NN-FEN group compared to NN-SAL. The juvenile group exhibited no significant difference from the control group at the breathing measures taken. The decrease in breathing frequency is a similar finding to previous studies performed in the lab (Kennedy, 2015), investigating similar experimental groups and fentanyl doses. Opioids are known for their depressive effect on breathing frequency, which had been related to NK1R-expressing neuron within PreBötC (Montandon et al., 2011). Moreover, injecting μ-opioid antagonists into PreBötC reversed the depressive action of breathing frequency (Montandon et al., 2011). The power of the study is estimated between 50-80 % based on a standard deviation of 20 and an alpha level of 0.05. In order to have 95% of statistical power in future, a sample size of 22 mice would be recommended for the study design. Yet, the number may vary due to habituation period, mice movement and stress level during the recording of the awake fentanyl challenge (Fitts, 2011).

Concerning the fact that PreBötC is known to be the inspiratory rhythm generator, and it expresses a high level of NK1R neurons that are opioid-sensitive (Smith et al., 1991, Del Negro et al., 2018), an earlier enhancement of μ-opioid receptors could affect its function and sensitivity for future opioid exposure. Yet, the neural respiratory centre comprises a group of interacting neurons that act simultaneously to generate breathing bursts and control the rhythmogenesis (Feldman et al., 2013). Therefore, the long-lasting effect of a

systemically introduced opioid-agonist may involve a group of neural pacemakers instead of a single nucleus. As follows, the respiratory depressive effect of opioid-agonists on PreBötC could be triggered by another neural centre, Kolliker-Fuse nucleus (KF) (Lalley et al., 2014 Varga et al., 2020). Kolliker–Fuse nucleus is linked to VRG and ventrolateral medulla (Jiang et al., 2004), and a computational model analysis denoted its role in monitoring the PreBötC neural output (Rybak et al., 2004). Based on this, the chronic effect of postnatal opioid exposure may contribute to other nuclei in conjunction with PreBötC, to alter the respiratory frequency in the NN-FEN group.

3.10.2 Adult mice awake fentanyl challenge

Both groups (NN-FEN and NN-SAL) showed a decrease in breathing frequency as an expected outcome of opioid administration (Montandon et al., 2011, Pattinson, 2008) (see Figure 3-4). NN-FEN had a lower breathing frequency than NN-SAL at T15 and T30, which is associated with a marked increase in tidal volume at T15 (see Figure 3-6). The findings signify an attenuated response to opioid exposure. The increase in tidal volume as an outcome of systematic fentanyl administration was observed by (Lewanowitsch et al., 2006, Leino et al., 1999, Colman and Miller, 2001) as an acute response to opioid exposure, and the attenuated increase of tidal volume in a specific study group would suggest a higher sensitivity to opioid within the group. The JUV-FEN group had a similar response to the control group JUV-SAL after fentanyl administration (see Figure 3-7); both groups had an equivalent decrease in breathing frequency and a slight increase in tidal volume at T30. Although a postnatal exposure to opioids had resulted in a long-term alteration in breathing frequency, the breathing pattern remained intact, and no irregularity of breathing rhythm was obtained in the fentanyl-exposed groups (NN-FEN and JUV-FEN). This suggests that the early days of life are critical for developing breathing neural centres, which might be triggered by repeated opioid exposure between day 1 and day 5.

Previous studies have addressed the long-term effects of the perinatal environment on respiratory control in rodents and, consistent with the data discussed in this chapter, have found that exposure to various environmental stimuli in the neonatal period, such as hypoxia, hypercapnia, caffeine, and stressful events, can induce permanent changes in ventilatory control (Okubo and Mortola, 1988, Bavis et al., 2004, Montandon et al., 2006, Gulemetova and Kinkead, 2011). Our results are consistent with the hypothesis that manipulations of the developing respiratory system can result in long-lasting changes in respiratory activity. Furthermore, our findings suggest that neonatal repeated fentanyl exposure induces developmental plasticity, which in terms of respiratory control has been identified as long-term changes in the developed respiratory system that are induced by events that occur during a crucial developmental time frame, whereas the same experiences after this critical time window cause no changes (Carroll, 2003, Bavis and Mitchell, 2008). This theory is supported by the fact that juvenile exposure to fentanyl did not induce the same profound long-term respiratory changes, indicating that the first five days of a rodent's life represent a crucial developmental period vulnerable to opioid-induced developmental plasticity.

The mechanism underlying the postnatal chronic alterations of opioid exposure is uncertain. Nevertheless, a combination of several factors may contribute to the chronic changes in opioid exposure. Evidence suggests that chronic opioid exposure in rats induces glucocorticoid-dependent alterations in the expression of Fos transcription factors in stress-related brain regions, such as the central amygdala and the hypothalamic paraventricular nucleus may affect the stress-response system (Garcia-Perez et al., 2012). In addition, continuous fentanyl exposure to neonatal rats has been associated with withdrawal symptoms (Thornton and Smith, 1998), which may modulate anxiety levels. Therefore, the anxiety level was assessed in Chapter 5, and there was a trend of an increase of the stress marker, corticosterone, in the opioid exposed group, which support the increase in stress level in this specific group. In addition, the long-lasting effect of early opioid exposure might be triggered by hypoxemia, which fentanyl administration causes (Chen et al., 1996, Chevillard et al., 2009). The repeated hypoxic exposure in juvenile rats increases their respiratory sensitivity to future fentanyl exposure in adulthood (Moss et al., 2006), and the increased sensitivity

to opioid exposure might be triggered by the release of endogenous opiates induced by repeated hypoxic events. Thus, it could activate opioid receptors and sensitise them to future opioid administration exposure (Moss et al., 2006). If repeated fentanyl exposure in neonatal life provokes hypoxemia, this mechanism of enhanced endogenous opiate release and subsequent sensitisation of the opioid receptors within the preBötC may explain the increased respiratory responsiveness to future fentanyl application in adulthood. Therefore, recurrent hypoxemia in early life may have detrimental effects on the respiratory system.

3.11 Summary

The plethysmography study had emphasised the changes in respiratory pattern that are triggered by opioids exposure at the postnatal age. These findings had attracted attention regarding the long-term consequences of repeated opioids exposure, at the early days of life, on the respiratory function. The age-dependent factor was observed within the results, when the neonate group presented more vulnerability upon receiving fentanyl during the earlier days of life, compared to juvenile mice. This supports the hypothesis of the critical maturation step of breathing oscillators in the early days of life, when RTN/pFRG is responsible for the breathing drive after birth and followed by preBötC emerges into the breathing drive neural group. However, the long-lasting impact of opioids on respiratory pattern is uncertain, and it could be inherited by the increase of μOR sensitivity or the alteration of the brainstem's neural expression and distribution.

3.12 Study limitations

Due to the nature of the study, as the fentanyl should be administered at the early days of life, the sample size was restricted to the litter produced by each dam. A larger sample size would be suggested for future work, with the consideration of the time frame and staff support. In addition, a double blinded standard was not applied in the study, as the injection should be delivered for a specified mice group within a short time window. Yet, the mice assessment was done in random order, and the data was collected in reference to the ID number, without knowing the study group.

Chapter 4 The long-term effects on cerebral blood flow following opioid exposure in early life in ICR mice.

4.1 Introduction

Cerebral blood flow (CBF) is controlled by the autoregulation process, which preserves the blood supply to the brain by adjusting the resistance of blood vessels. The cerebral autoregulation process (CA) is influenced by several mechanisms, such as metabolism, neurovascular coupling, blood gases pressure and myogenic response (Claassen et al., 2021). Starting with the metabolic mechanism, which is linked to the neurovascular coupling activity (NVC) that influences changes in the level of CO_2, O_2, and adenosine (Iadecola, 2017). The activation of the NVC process results in vasodilation and an increase in regional CBF (O'Herron et al., 2016). For example, brain visual stimulation leads to NVC activation of the occipital cortex, which enhances the regional blood flow of the occipital lobe in humans (Aaslid, 1987).

The arterial blood gases and pH are essential in stabilising the brain perfusion (Ainslie and Duffin, 2009, Xie et al., 2009). In humans, the rise of PCO_2 levels results in hypercapnia and triggers the vasodilation process, reducing cerebrovascular resistance and increasing the regional CBF (Brian, 1998, Pandit et al., 2003). Moreover, the drop in PaO_2 increases the ventilation and results in hypocapnia, which induces vasodilation and attenuates the CBF response (Ainslie and Ogoh, 2010, Lucas et al., 2011). For example, a drop in the PaO2 level beyond 50 mmHg can cause a 400% increase in the CBF in a resting state, and inhalation of 7% of CO_2 in humans could lead to a CBF surge up to 100% (Bor-Seng-Shu et al., 2012, Walsh and Cunningham, 2004). See Figure 4-1. The mechanism of the blood gases effect on cerebrovascular resistance remains unclear. Nevertheless, it was related to the extracellular pH level, which enhances the vasodilation mechanism by activating the hyperpolarisation cascade and releasing vasodilators such as nitric oxide (NO) (Cipolla , 2016, Faraci et al., 2019).

Some drugs can manipulate the CBF and prompt an autoregulation response, such as ketamine, isoflurane and fentanyl, which are known to attenuate regional CBF when given instantly (Franceschini et al., 2010). Although the acute opioid exposure leads to an instant rise in CBF, the chronic exposure to opioids (opioid addiction) results in a decrease in the regional CBF (rCBF) within frontal, temporal and occipital lobes in the resting state (Botelho et al., 2006) (Pezawas et al., 2002). The long-term changes of rCBF are not fully understood, but some studies hypothesised that it could be triggered by the morphological and structural changes in the brain caused by opioids addition (Pezawas et al., 1998, Pezawas et al., 2002). Even though acute opioid exposure depresses the respiratory rate and increases the rCBF, the dominant cause remains elusive.It could be linked to the respiratory changes that alter blood gas levels.

The vascular smooth muscle plays a role in maintaining the CBF through the myogenic response, which is achieved by cerebrovascular resistance changes (Longden et al., 2017). Accordingly, vasorelaxation leads to the dilation of the cerebral arteries and arterioles, which increases CBF (O'Herron et al., 2016). The actual mechanism of the myogenic response is elusive, and it could be triggered by endothelial molecules that released by the endothelium tissue and enhance the vascular muscle contractions, such as NO, potassium ion and hydrogen peroxide (Faraci , 2011).

The nervous system is believed to control the CBF via the sympathetic pathway. The sympathetic activation enhances vasoconstriction, which decreases the CBF (Jeng et al., 1999). A study found that patients that have undergone superior cervical ganglionectomy are likely to demonstrate an increase in CBF (Suzuki et al., 1975). In humans, the systemic pharmacological ganglionic blockade (blocking sympathetic pathways) showed variable effects on CBF, although the majority stands with the increase of CBF effect (Willie et al., 2014). It is generally accepted that the activation sympathetic nervous system decreases the CBF under resting conditions (Heistad, 1980). Yet, the other mechanisms might significantly impact CA, such as myogenic response and chemical and metabolic (Ter Laan et al., 2013).

The current study was designed to analyse the changes in CBF, after the early exposure to opioids at the age of P1-P5 and P9-P13. Laser speckle will be introduced as a novel technique to evaluate the dynamic changes of CBF due to the systematic fentanyl administration. The resting-state CBF will be examined to evaluate the regional variations of CBF as a long-lasting effect. It will be followed by a fentanyl challenge to analyse the differences in the acute response within the experimental groups.

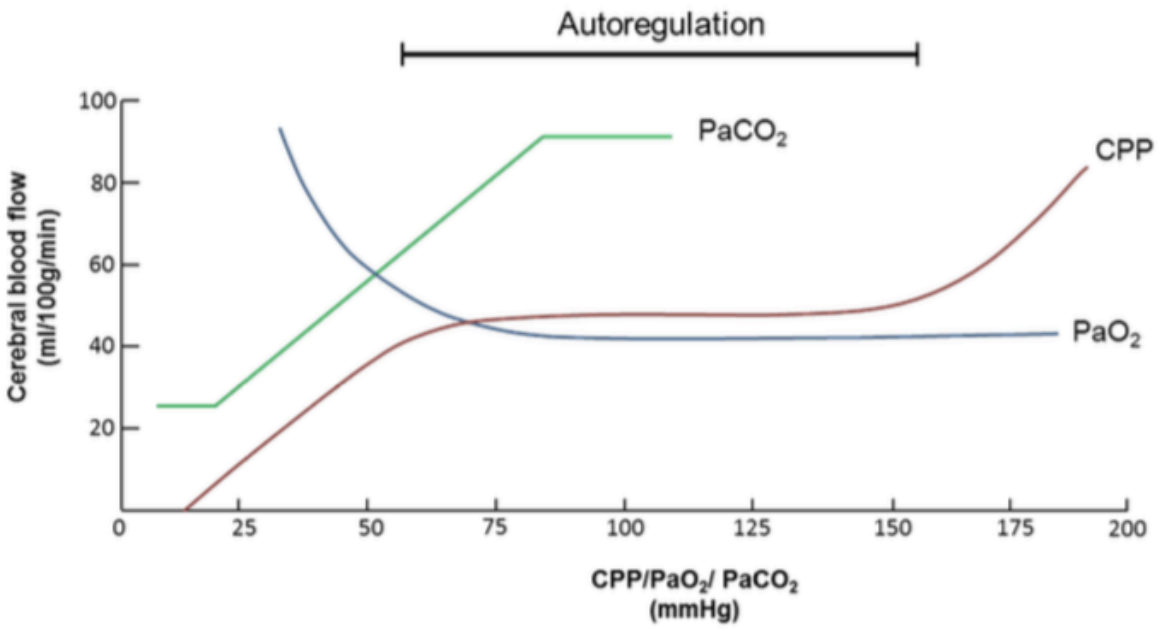

Figure 4-1 The effect of blood gases on CBF in the human brain under normal conditions. CBF remains stable when P_{aO2} is more than 60 mmHg and cerebral perfusion pressure (CPP) is 50-150 mmHg. Nevertheless, the increase of P_{aCO2} results in an increase of CBF, and the decrease of P_{aO2} leads to an increase of CBF. Modified from (Shardlow and Jackson, 2011)

4.2 Study aim

- Investigate the dynamic changes of CBF after opioid administration, utilising a continuous imaging technique laser speckle (LS).

- Study the chronic effect of the repeated postnatal opioid exposure on cerebral blood flow.

- Study the vulnerability to opioids under anaesthesia in adult mice, after the postnatal exposure to opioids at the ages of P1-P5 and P9-P13.

4.3 Hypothesis

Repeated exposure to opioids postnatally results in a long-term change in CBF, such as a decrease in the regional CBF and an attenuated response of CBF to opioid administration under anaesthesia.

4.4 Methodology

4.4.1 Animals

The experimental animal procedures were performed under the regulations of the UK Home Office (personal licence number i51F7C81D, and project licence number 60/4558). The studies were designed in correspondence with the Animals (Scientific Procedures) Act 1986. The experimental procedures were conducted on ICR mice, which were acquired from HARLAN. Accordingly, pregnant dams were ordered and delivered to the housing facility at Veterinary Research Facility, Garscube campus, University of Glasgow. The pups were kept with the mother up to the age of 21 days, when they were weaned. Post weaning, male and female mice were housed in separated cages, with a maximum of 4 mice per cage. Ear-piercing allowed for identification of individual mice within the cage. The light/dark cycle was 12 hours duration, with no dietary modifications. Day of birth is referred to as postnatal day 0 (P0). The age categories used in this study were neonate (P0-P7), juvenile (P8-P21) and adults over P21.

4.4.2 Postnatal injection

The experimental groups were defined as follows:

- **Group 1 – Neonatal Fentanyl (NN-FEN) n=7** Each mouse received one daily injection of fentanyl (0.04 mg/kg i.p.) for 5 days from postnatal day 1 (P1) to postnatal day 5 (P5)

- **Group 2 – Neonatal Saline (NN-SAL) n=10** Each mouse received an equivalent volume of physiological saline (i.p.) once daily P1-P5.

- **Group 3 –Juvenile Fentanyl (JUV-FEN) n=5** Each mouse received one daily injection of fentanyl (0.04 mg/kg i.p.) P9-P13.

- **Group 4 Juvenile Saline (JUV-SAL) n=8** Each mouse received an equivalent volume of the physiological saline (i.p.) once daily P9-P13.

4.4.3 Anaesthetic protocol

Urethane (ethyl carbamate) was used as an anaesthetic agent because it has the advantage of minimal effects on cardiorespiratory physiology and spinal neural reflexes compared to other anaesthetics. However, the disadvantage is Urethane is a carcinogenic and hepatotoxic agent; therefore, Home Office guidance is that all procedures conducted under Urethane anaesthesia are non-recoverable.

4.4.4 The study timeline

The mice were reused from the plethysmography experiment, see Chapter 3. They were brought to the surgical theatre at Wellcome Surgical Institute for the LS experiment a week after the awake fentanyl challenge was completed. Firstly, mice were anaesthetised with an initial dose of urethane (1.5 mg/kg i.p.), which was followed by three supplementary doses of 0.25 mg/kg i.p. Once the mouse was deeply anaesthetised, and the tail-flick sign disappeared, a sagittal incision was made through the skin to expose the skull. Bregma and Lambda were identified as anatomical landmarks on the skull surface, allowing for accurate placement of ROIs. ROI 4 and 5's centre was defined by identifying the midpoint between Bregma and Lambda, then measuring 2.5 mm lateral over right and left parietal bones, respectively. ROI 1 and 2 were determined by measuring 2 mm anterior and 2 mm lateral to Bregma, on the right and left, respectively. Each ROI is a 3 mm^2 surface area, fixed during the experiment. See Figure 4-2. A pressure pad RX110 (Biopac, UK) was placed below the mouse, in front of the mouse's chest. The pad was utilised as a non-invasive tool to measure the respiratory rate through the study, and follow-up the effect of opioid administration on respiratory rate. See Figure 4-4 Real-time changes in CBF were recorded by means of laser speckle contrast imaging (Perimed, 2018). After that, mice were allowed to stabilise for at least 10 minutes before baseline recording. Baseline recording was carried out for 5-10 minutes followed by fentanyl injection (0.04mk/kg i.p.). Following injection of fentanyl, LSCI was carried out for a further 90 minutes. Mice were euthanised with an overdose of pentobarbital (0.1 ml i.p.) at the end of recording, the brain was removed and frozen fixed in liquid Nitrogen (see Figure 4-3).

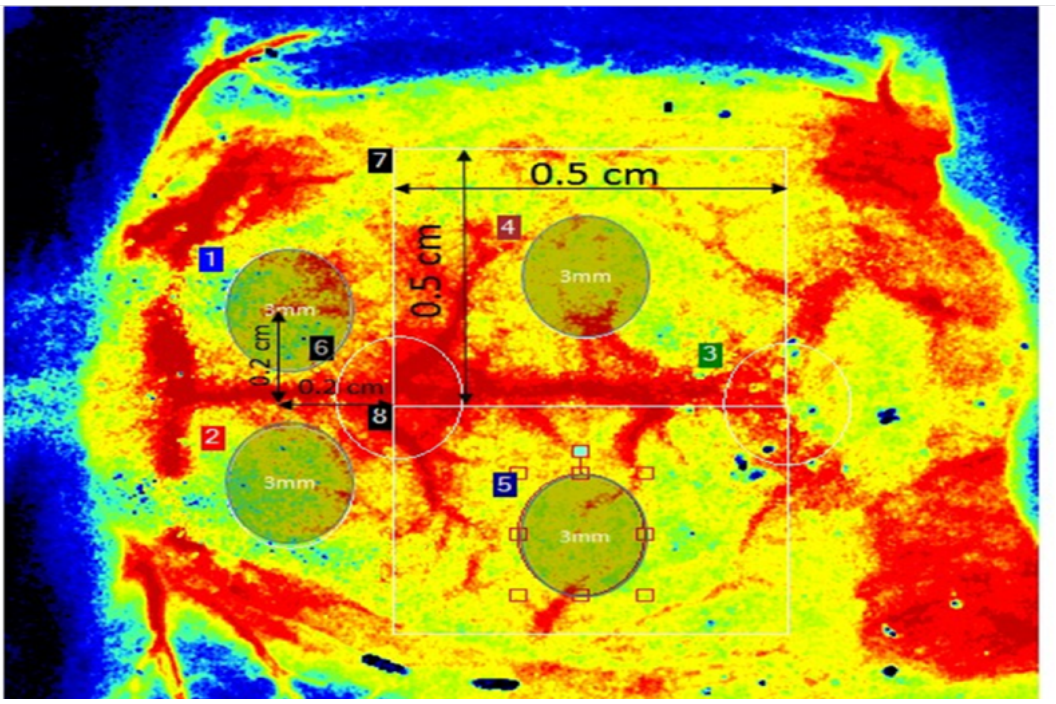

Figure 4-2 Cerebral blood flow ROI locations within the brain cortex
The picture shows the allocated ROIs used in the LS experiment, two located over the frontal cortex and two over the parietal areas. Locating ROI was aided by identifying the Bregma and Lambda at the beginning of the experiment as known anatomical markers.

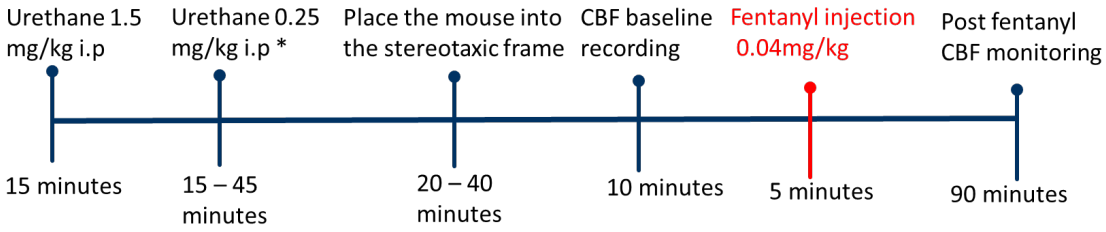

Figure 4-3 Laser speckle experiment timeline
The experiment started general anaesthesia which took around 45-60 minutes. After that, the mouse was placed into the stereotaxic frame and a sagittal incision was made on the scalp to expose the skull for the LS imaging. Then, a fentanyl 0.04 mg/kg i.p. injection was given, and a live recording of the dynamic changes of CBF was taken up to 90 minutes post-injection.

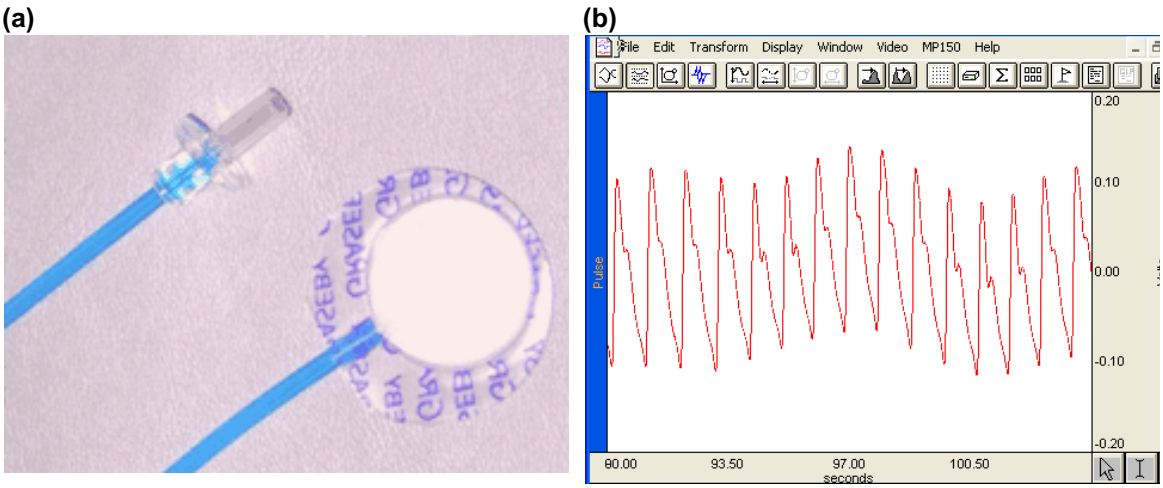

Figure 4-4 Pressure pad tool to measure the respiratory rate
(a) The pressure pad was placed beneath the mouse, in the right front of the chest in order to transduce the chest movement pressure as an electrical signal. The generated signals from the pressure pad were transmitted to ACQKNOWLEDGE software (b) and were presented in wave form.

4.5 Data analysis

PIM software was utilised to analyse the dynamic changes of CBF. See chapter 2.4 for details. The software presents the changes of CBF in a linear graph across the timeline, which traces the blood flow within the assigned area on the cortical surface. The changes of CBF in the course of the anaesthetised FEN challenge are presented through a number of graphs that provide longitudinal diagrams of the change contrasted to the normalised ratio (referred to in the baseline recording). The baseline recording took place once the mouse was fixed and stable within the stereotaxic frame, then fentanyl was injected and changes of CBF were traced across the 90 minutes post drug administration. The data are provided as an a.u., and the changes of the CBF are compared later to baseline blood flow in the same area to study the effect of μOR agonist administration on the CBF. See Figure 4-5.

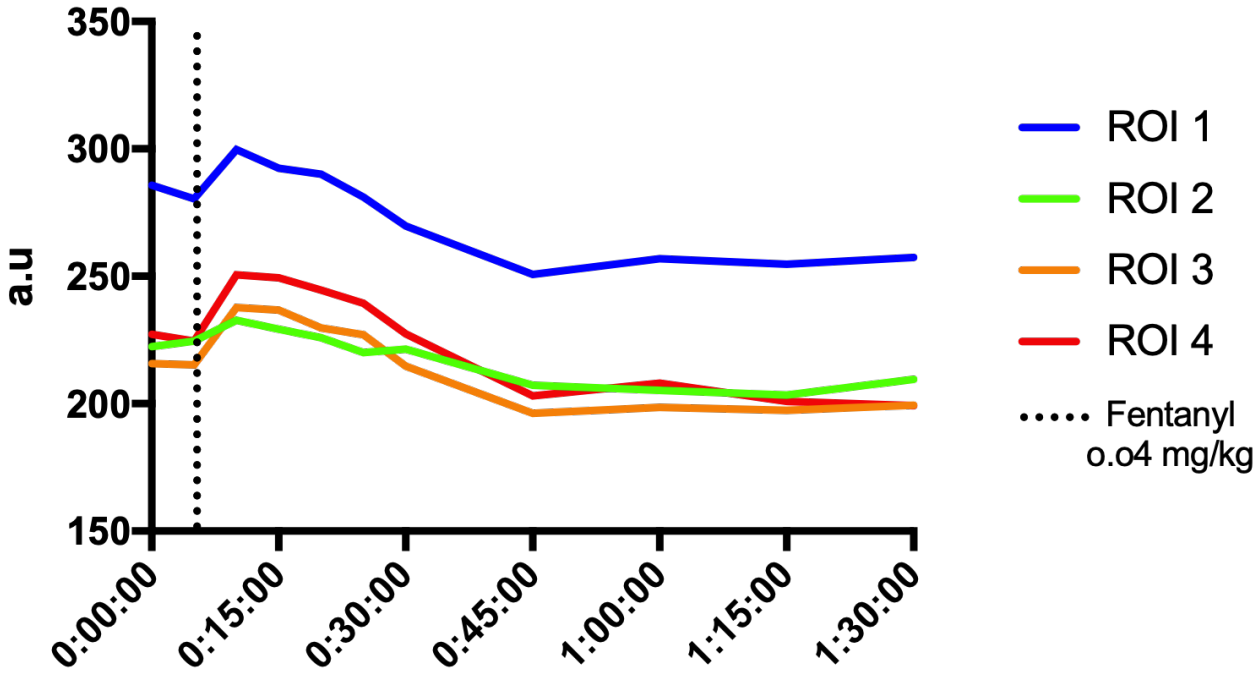

Figure 4-5 Laser speckle data presentation and analysis
The graph presents a smoothed version of the data collected by the Laser speckle device (five minutes averages). The X axis stands for the time (hours: minutes) and the Y axis stands represents CBF dynamic changes (a.u.). The dotted line indicates when the Fentanyl injection was performed.

4.6 Statistical analysis

All the statistical analyses were carried out by Graphpad Prism 6 (GraphPad Software, USA). The data are presented as mean ± SD, and an unpaired t-test was used to analyse the CBF at rest between the study groups within the same brain region. The data were normalised to the baseline record, and normalised blood flow was used to analyse the longitudinal changes of CBF due to the fentanyl challenge. The data were presented in a 5 min average for statistical analysis. 2-way ANOVA test was performed to analyse the CBF dynamic changes between the designed group. It is followed by a post hoc Bonferroni correction for multiple comparisons between each time point in both groups (NN-SAL vs NN-FEN and JUV-SAL vs JUV-FEN). An unpaired t-test comparison was used to analyse the 5 minutes-average difference, between the study groups, of the dynamic CBF changes at the following time points (T10, T20 and T30). The mice's survival rate through the anaesthetised FEN challenge was analysed by Chi-square test.

4.7 Results

NN FEN group and JUV FEN showed an increase of vulnerability to the FEN challenge under anaesthesia and the completion percentage was the lowest with 43% and 20% respectively. Nevertheless, the control group from the JUV age group (JUV SAL) had exhibited an increased number of mice dying through the challenge; and the completion percentage was 50% in JUV SAL (control group). This outcome was not expected. See Table 4-1.

Mice group	Urethane anaesthesia	Started baseline recording	Fentanyl injection 0.04mg/kg	Completed 90 minutes post FEN injection	Completion of 90 minutes anaesthetised FEN challenge %
NN SAL	10	10	10	8	80%
NN FEN	7	4	4	3	43%
JUV SAL	8	8	8	4	50%
JUV FEN	5	5	5	1	20%

Table 4-1 The percentage survival of anaesthetised FEN challenge of the study groups.
The table provides information about the mice numbers involved in the anaesthetised FEN challenge and how many mice completed 90 minutes challenge post FEN injection. Accordingly, NN-SAL (control group) had the higher completion rate, and the lowest rate was observed on the JUV-FEN (treated group). Nevertheless, JUV-SAL (control group) had a 50% completion rate. A Chi square test was performed to compare the survival rate between the groups (P value > 0.05). No statistically significant changes between the study groups.

Baseline CBF data showed a decrease in the CBF of the frontal region in NN group (NN-FEN n = 4 and NN-SAL n =10). The mean average of a.u. was 244.3 ± 1.993 in NN-SAL group, while NN-FEN group mean average was 206.7 ± 2.99. NN group parietal region averages were 235.6 ± 2.343 in NN-SAL, and 239.1 ± 4.833 in NN-FEN. The P value > 0.05 non-significant. JUV group (JUV-SAL n= 8 and JUV-FEN n= 5) had no significant difference in the CBF mean average at frontal and parietal regions P value > 0.05. Accordingly, JUV-SAL frontal a.u. average was 256.8 ± 2.364, and JUV-FEN 252.6 ± 2.53; parietal region averages were JUV-SAL = 252.1 ± 1.805 and JUV-FEN = 259 ± 2.717. See Table 4-2 and Figure 4-6.

Study group	Frontal region	Parietal region
NN-SAL n= 10	244.3 ± 1.99	235.6 ± 2.34
NN-FEN n= 4	206.7 ± 2.99	239.1 ± 4.83
JUV-SAL n= 8	256.8 ± 2.36	252.1 ± 1.81
JUV-FEN n= 5	252.6 ± 2.53	259 ± 2.72

Table 4-2 Regional CBF at rest in the study groups
The table presents the 5 minutes mean average of the CBF at rest within the study groups, as an arbitrary unit. The data are presented as mean ± SD, and t-test performed for the analysis. See Figure 4-6

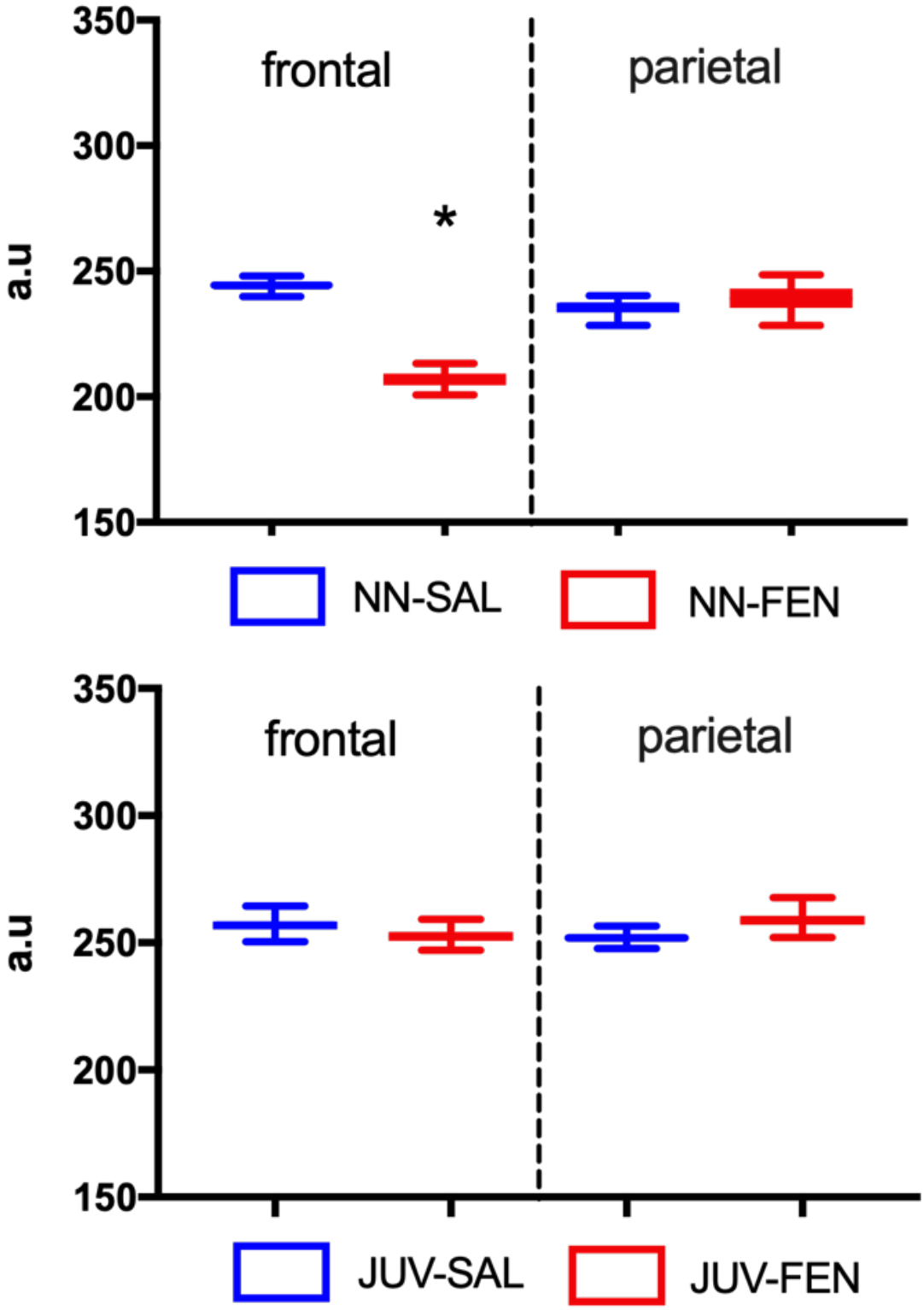

Figure 4-6 Baseline cerebral blood flow in the experimental groups
A comparison between the CBF baseline mean averages, at rest, of the 4 experimental groups (NN-SAL n=10, NN-FEN n=4, JUV-SAL n=8, and JUV-FEN n=5). A significant decrease was found on the frontal lobe CBF in NN groups, and P value < 0.05. No significant difference between the NN parietal CBF or JUV groups' baseline averages on the assigned ROIs (frontal and parietal). The data is presented as mean ± SD, and t-test was performed for analysis.

An increase of the dynamic CBF was observed post fentanyl injection under anaesthesia. In all groups a baseline recording was taken over 5 minutes, and it was set as reference for the normalised ratio. Once fentanyl was administered, while recording, a surge of CBF was observed (5% increase) in the CBF average of each of the study groups (NN-SAL n=10, NN-FEN n=4, JUV-SAL n=8, and JUV-FEN n=5). The elevation of CBF reaches maximum around 10-20 minutes after the fentanyl injection, followed by a gradual decrease takes place until it returns to the normal baseline average. See Figure 4-7.

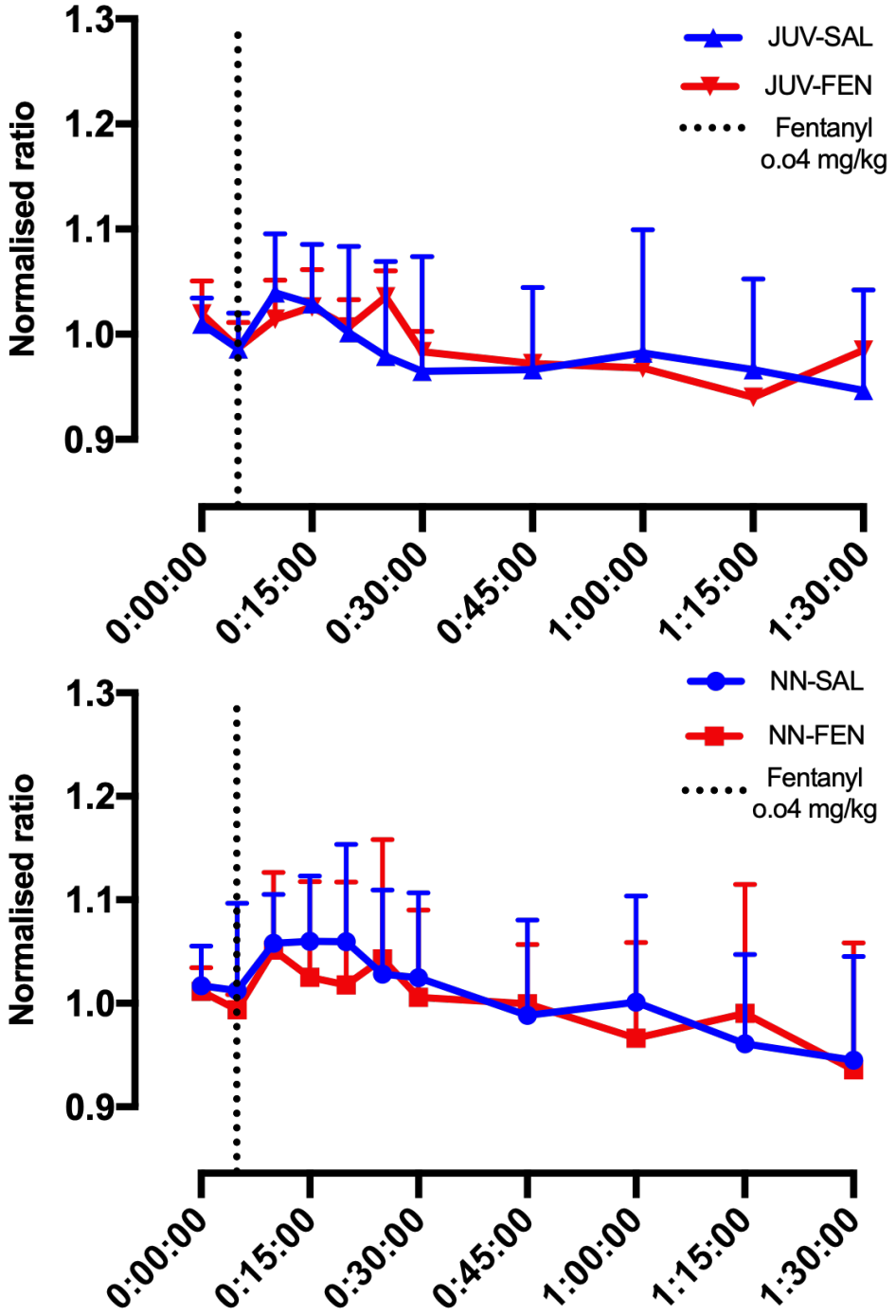

Figure 4-7 The effect of fentanyl administration on the cerebral blood flow
The main effect of the systematic fentanyl administration was an increase of the CBF, as shown in both graphs for the neonate group (NN-SAL and NN-FEN) and juvenile groups (JUV-SAL and JUV-FEN). The rise of CBF lasts for 20 minutes post fentanyl injection, then it returns to the normal average (1) gradually. The data is presented as mean + SD, and 2-way ANOVA test performed for analysis

Referring to the assigned ROIs, an average of each frontal and parietal regions was calculated for each group, and it was followed by a comparison of fentanyl exposed group and control group at specific time points (T10, T20 and T30) post fentanyl injection. Starting with the neonatal groups (NN-SAL n= 10 and NN-FEN n= 4), frontal region showed 5-10% increase of the CBF after fentanyl administration, which declined gradually after T30 to reach the baseline level (normalised ratio 1); that remains unchanged until the end of recording (T90). In addition, the change of CBF was not significant between NN-SAL and NN-FEN at T10, as the mean averages were NN-SAL = 0.9733 ± 0.0313 and NN-FEN = 0.9849 ± 0.0272. At the following time points (T20 and T30) the control group (NN-SAL = 10) showed a significant elevation of CBF T20 = 1.033 ± 0.006, T30 = 1.018 ± 0.007 when compared to the treated group (NN-FEN n= 4) T20 = 1.016 ± 0.0144 and T30 = 0.9977 ± 0.016 (P value <0.05) in both time points. See Figure 4-8 and Table 4-3.

In regard to parietal regions in neonatal groups (NN-SAL n=10 and NN-FEN n=4), 10-20% elevation of CBF was observed after the fentanyl injection, which was followed by a gradual decrease down to the baseline level (normalised ratio =1) after 30 minutes post fentanyl exposure. The control group (NN-SAL) showed a significant increase at T10 1.051 ± 0.04, and NN-FEN = 0.9902 ± 0.04 (P value > 0.05), then NN-FEN had a higher increase of CBF at T20, mean average = 1.077 ± 0.019 and NN-SAL = 1.084 ± 0.007 (P value > 0.05). No significance was obtained at the parietal region between neonatal groups at T30, NN-SAL mean = 1.056 ± 0.03 and NN-FEN = 1.059 ± 0.0234 (P value <0.05). See Figure 4-9 and Table 4-3.

Region	Study group	Time point		
		T10	T20	T30
Frontal	NN-SAL n=10	0.97 ± 0.03	1.03 ± 0.01	1.02 ± 0.01
	NN-FEN n=4	0.98 ± 0.02	1.02 ± 0.01	0.99 ± 0.02
Parietal	NN-SAL n=10	1.05 ± 0.04	1.08 ± 0.01	1.06 ± 0.03
	NN-FEN n=4	0.99 ± 0.04	1.08 ± 0.02	1.06 ± 0.02

Table 4-3 The dynamic changes of regional CBF after fentanyl administration at different timepoints in neonatal group

The table shows the regional dynamic changes of CBF in the neonatal group. The frontal region showed a similar change in both groups NN-FEN and NN-SAL at T10, followed by a 2-3% increase of CBF at T20 and returned to normal at T30 in the NN-FEN group, while NN-SAL maintained the 2% increase. NN-SAL showed a 5% increase in CBF in the parietal group, followed by an 8% increase from the baseline at T20, and remained 6% higher than the resting state at T30. The NN-FEN group mean average was close to normal at T10 ; then, it rose by 8% at T20, and maintained a 6% rise from baseline at T30. The data is presented as mean ± SD, and t-test was performed for the analysis See Figure 4-8 and Figure 4-9

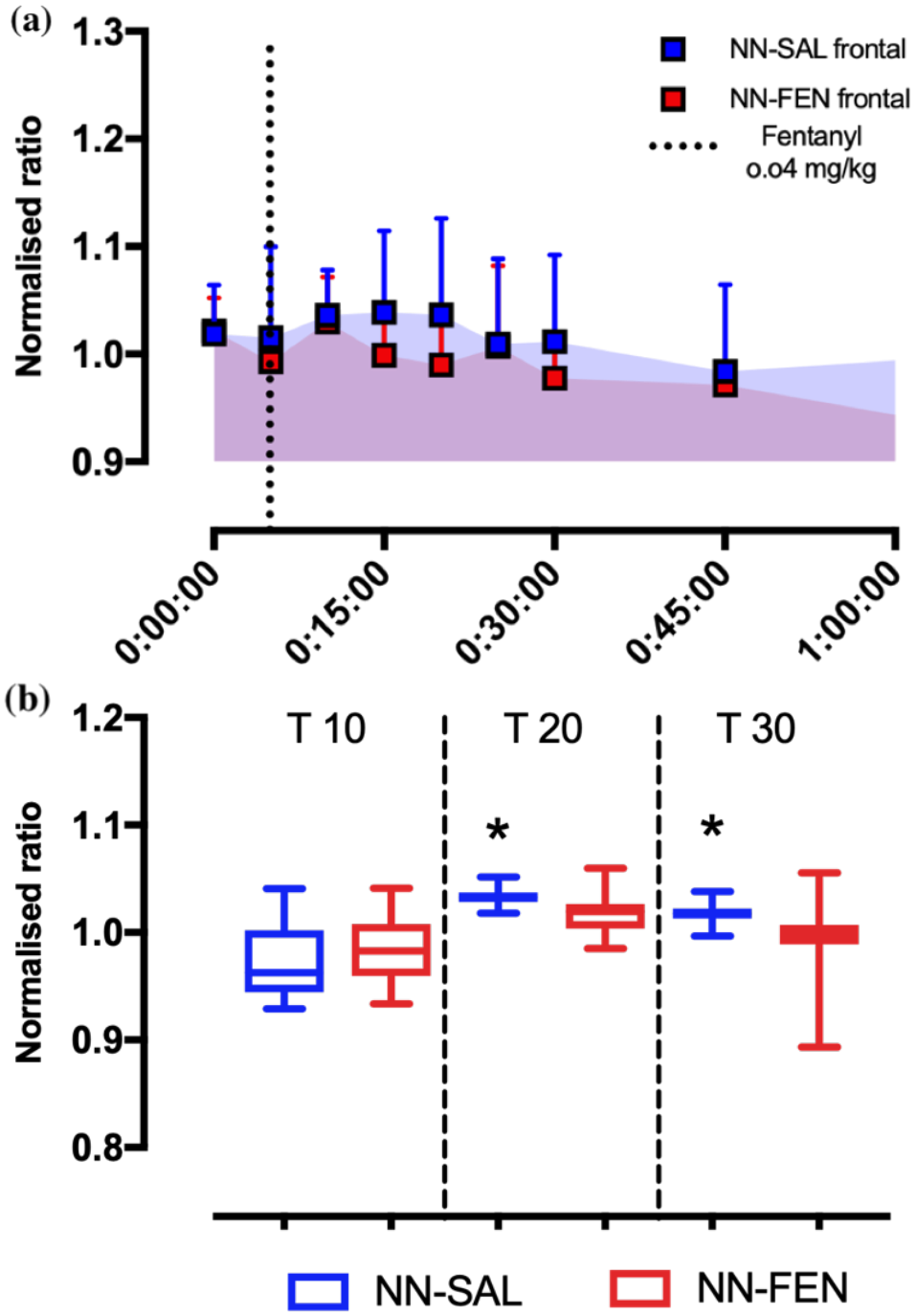

Figure 4-8 The effect of fentanyl administration on CBF at frontal ROI in neonatal group

(a) A longitudinal graph that shows the effect of systemic fentanyl administration on the frontal region CBF, which increases the CBF and followed by a gradual decrease. The data is presented as mean + SD, and the graph was executed regarding the 2-way ANOVA analysis which is followed by a post hoc Bonferroni correction test for multiple comparison. No significant different between the study groups (b) A comparison of the dynamic changes of CBF as a response to systemic fentanyl administration at specific timepoints (T10, T20 and T30). The data presented as mean ± SD, and t-test performed for analysis. A significant increase of CBF presented by NN-SAL at T20 and T30, compared to NN-FEN n= 4 (P value >0.05). for details, see Table 4-3

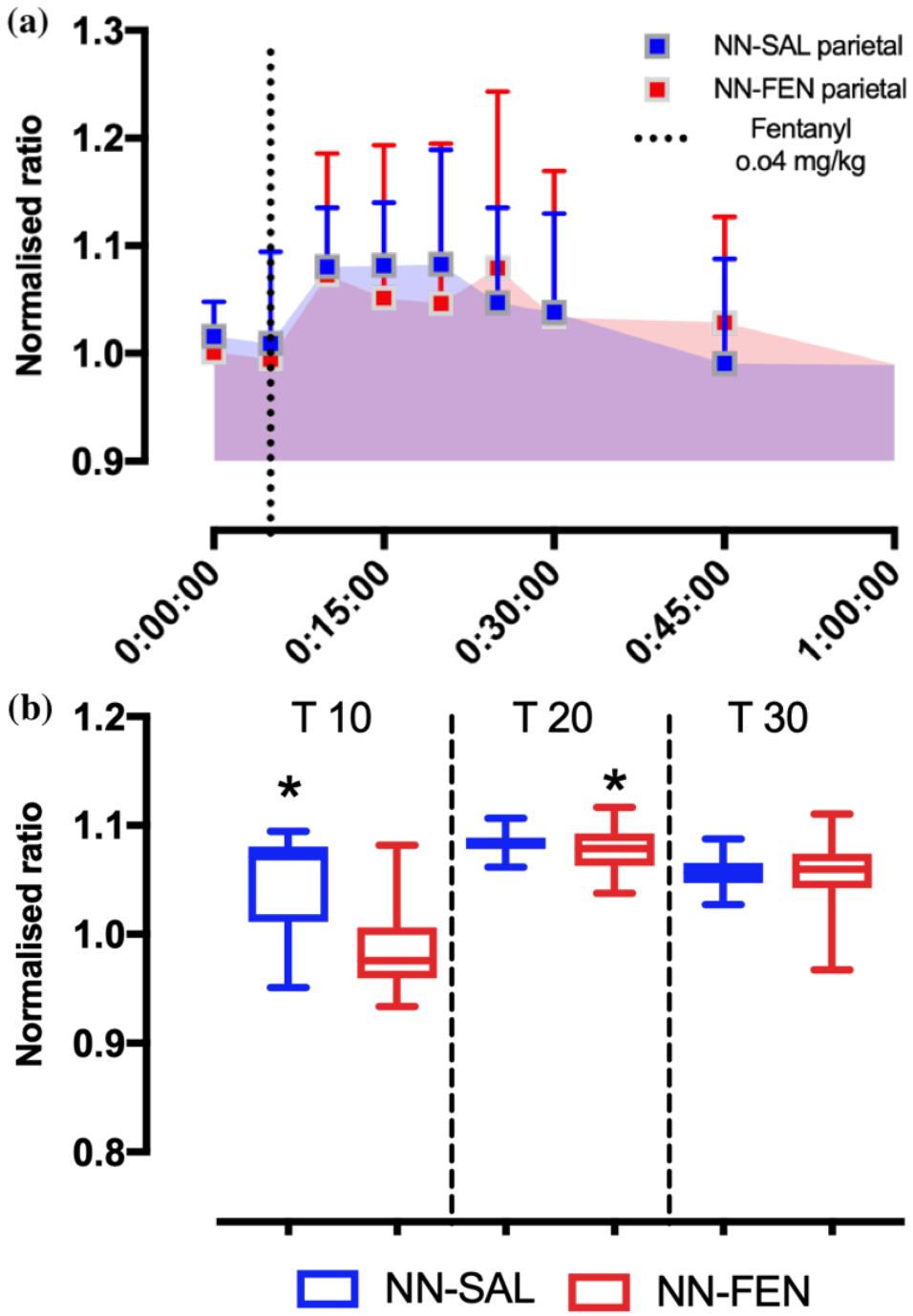

Figure 4-9 The effect of fentanyl administration on CBF at parietal ROI in neonatal group

(a) A longitudinal graph that shows the response of CBF, with a (10-20%) increase, which is observed on parietal region as a result of the systematic administration of fentanyl in both groups (NN-FEN and NN-SAL). The data is presented as mean + SD of the normalised ratio, and the value of (1) is referred to the CBF level at resting state (baseline). A 2-way ANOVA test performed for the analysis, and no significant change between the groups. (b) The graph shows a comparison of the CBF dynamic changes at specific timepoints (T10, T20 and T30). Each timepoint represent a 5 minutes average of the mean ± SD, and t-test used for the analysis. At T10 (NN-SAL) showed a significant increase, compared to (NN-FEN) at the same time point (P value >0.05). Then NN-FEN reflects a higher response with a significant increase of CBF at T20, and no obtainable significance between the groups at T30 (P value <0.05). See Table 4-3

The juvenile group (JUV-SAL n=8 and JUV-FEN n= 5) presented (5-15%) increase of the CBF within the frontal and parietal region, as an outcome of the systematic fentanyl exposure. Parietal showed a dominant increase, which is linked to the NN-SAL group mainly and exceeded 10% average at T20 and T30 post fentanyl injection. On the other hand, the frontal region revealed a similarity in the CBF response to fentanyl administration in both groups (JUV-SAL and JUV-FEN) at three different time points (T10, T20 and T30). Accordingly, the mean average of JUV-SAL at T10 = 1.005 $\pm$ 0.011, T20 = 1.001 $\pm$ 0.015 and T30 = 0.9579 $\pm$ 0.02; and the mean average of JUV-FEN at T10 = 1.01 $\pm$ 0.04, T20 = 1.001 $\pm$ 0.019 and T30 = 0.9721 $\pm$ 0.019. No significant difference was obtained between the juvenile group at the frontal region within the specified time points (P value <0.05). See Figure 4-10. The parietal region showed a significant increase of CBF between JUV-SAL and JUV-FEN at T20 and T30 (P value >0.05). The mean average of JUV-SAL at T10 was 1.037 $\pm$ 0.02, T20 = 1.053 $\pm$ 0.02 and T30 = 1.009 $\pm$ 0.013; and for the JUV-FEN at T10 = 1.032 $\pm$ 0.04, T20 = 1.016 $\pm$ 0.03 and T30 = 0.989 $\pm$ 0.024. See Figure 4-11 and Table 4-4.

Region	Study group	Time point		
		T10	T20	T30
Frontal	JUV-SAL n=8	1.01 ± 0.01	1.00 ± 0.02	0.96 ± 0.02
	JUV-FEN n=5	1.01 ± 0.04	1.00 ± 0.02	0.97 ± 0.02
Parietal	JUV-SAL n=8	1.04 ± 0.02	1.05 ± 0.02	1.01 ± 0.01
	JUV-FEN n=5	1.03 ± 0.04	1.02 ± 0.03	0.989 ± 0.02

Table 4-4 The dynamic changes of regional CBF, after fentanyl administration, at different timepoints in juvenile group

The table shows the changes in the regional CBF after fentanyl administration in the frontal and parietal areas. The frontal area increased CBF by 1% at T10, which returns to the average level at T30. The parietal groups showed a 2-4% increase of CBF at T10, followed by 2-5 % at T20, and returns to the average level (1) at T30. The data is presented as mean ± SD, and a t-test is used for the analysis. See the following figures for more information Figure 4-10 and Figure 4-11

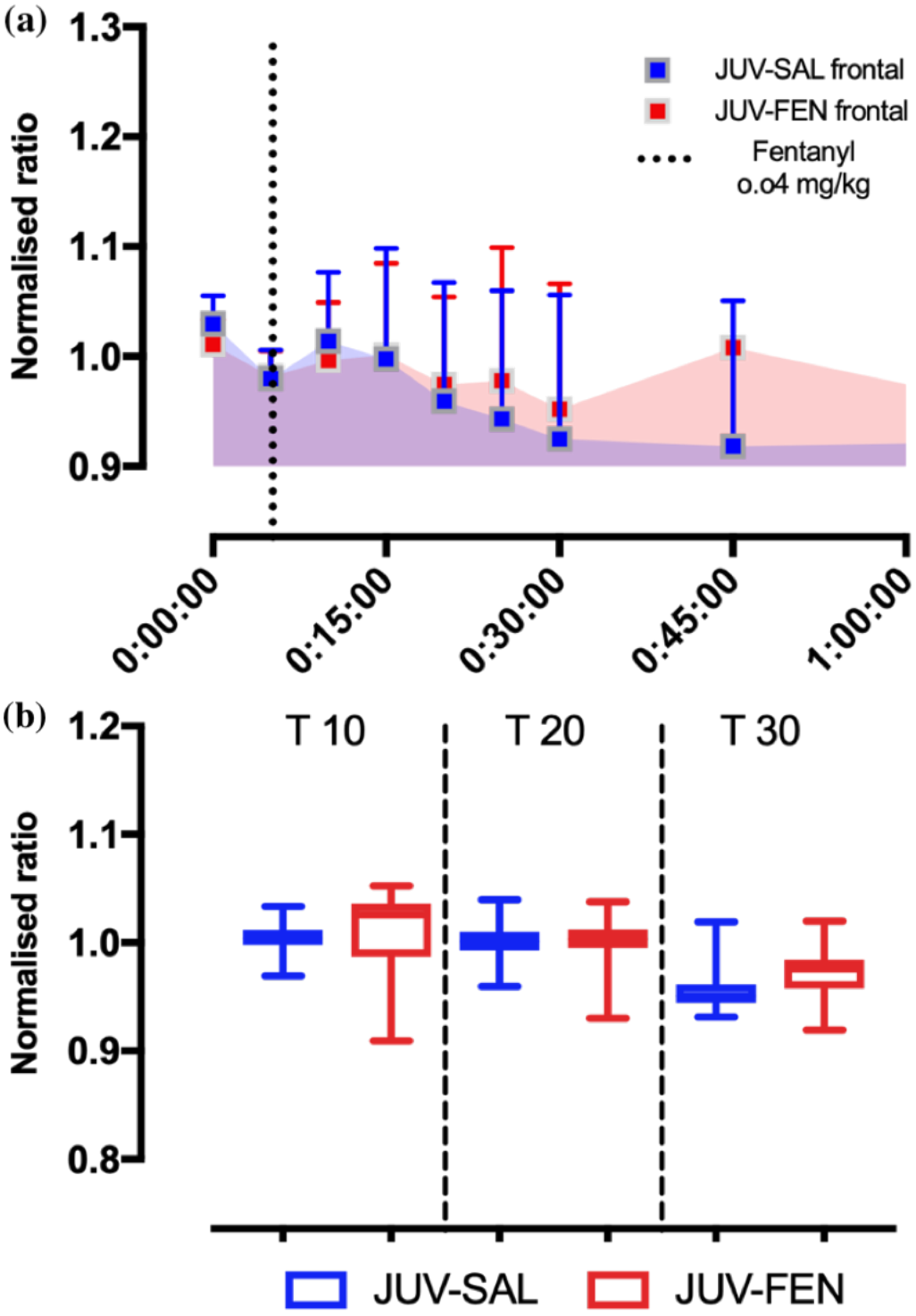

Figure 4-10 The effect of fentanyl dose on CBF at frontal ROI in juvenile group
(a) A longitudinal graph that shows the dynamic changes of the CBF at the frontal region, which is enhanced by the fentanyl injection. The data is presented as mean +SD, and 2-way ANOVA test used for the analysis. No significant changes of the CBF response between the study groups (NN-SAL and NN-FEN). (b) The 5 minutes average of CBF dynamic changes at specific points showed no significance between the study groups (JUV-SAL and JUV-FEN) at the specified time points, after the systematic fentanyl administration (P value < 0.05). The data presented as mean ± SD, and t-test performed for the comparison. See Table 4-4

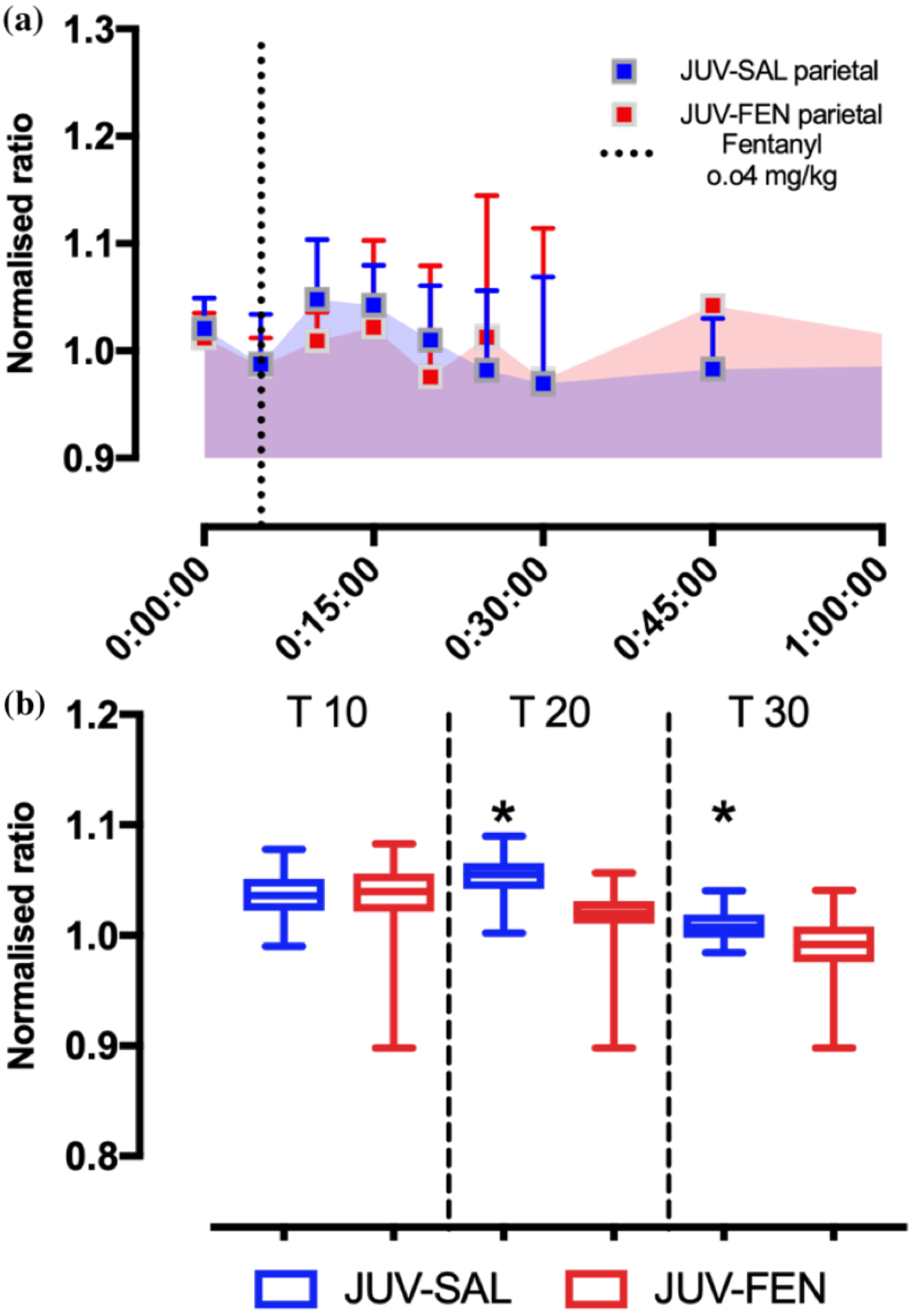

Figure 4-11 The effect of fentanyl dose on CBF at parietal ROI in juvenile group
(a) A longitudinal graph that shows the dynamic changes of parietal CBF, after fentanyl administration. An increase of CBF is obtained after fentanyl administration, which returned to normal level at 30 minutes post-fentanyl injection, and no significant different between the study groups. The data presented as mean + SD, and 2-way ANOVA test used for the analysis (b) The graph shows the 5 minutes average of CBF dynamic changes at specific points (T10, T20 and T30). Fentanyl administration increases the CBF within the parietal region by 5% at T10 and T20, post-injection. A significant different of the CBF response at T20 and T30 (P value >0.05). The data is presented as mean ± SD, and t-test performed for the analysis. See Table 4-4

Respiratory rate data were collected from some samples, alongside CBF, in order to analyse the dynamic response of CBF and respiration to fentanyl administration under anaesthesia. Mice included in the analysis were JUV-SAL n= 3, JUV-FEN n= 2, NN-SAL n= 3 and NN-=FEN n= 2. The initial observation was an increase of CBF in all groups that was accompanied by a decrease in respiratory rate during the first 10 minutes after fentanyl administration. This was followed by a gradual return to the baseline average (in both CBF and respiratory rate) at 20 minutes post fentanyl injection. The JUV-SAL group showed a 4% increase in CBF, accompanied by a decrease in the respiratory rate by 10% from the baseline. In the JUV-FEN group, CBF increased by 6% from the baseline, and the respiratory rate decreased by 10% from baseline when CBF took place. See Figure 4-13. The neonate group showed similar results, and NN-SAL had a 10% increase in CBF from the baseline, and breathing frequency dropped to 8% from the baseline. In addition, the NN-FEN showed a 10% increase in CBF, and the breathing rate decreased by 9% at the same time. See Figure 4-12.

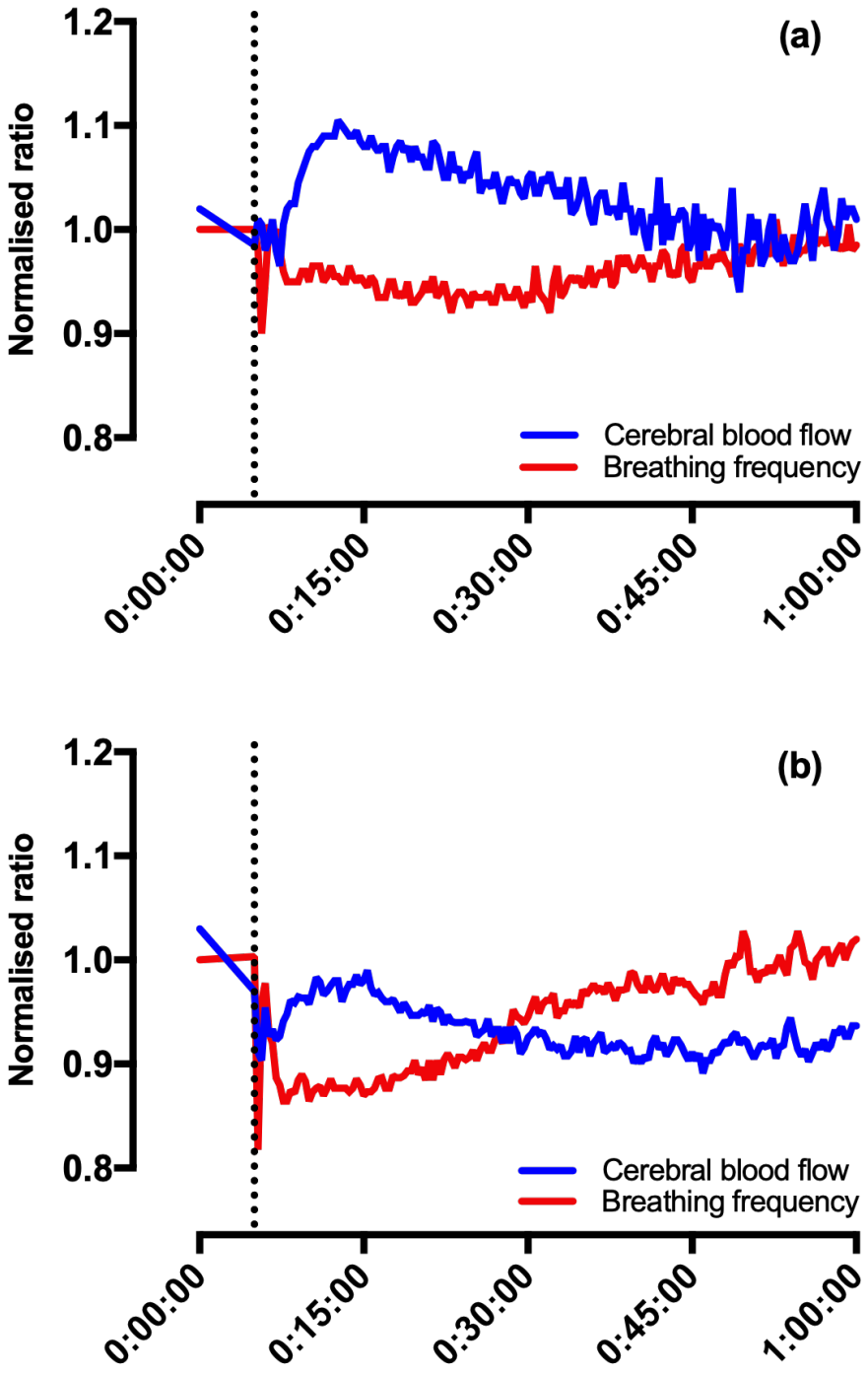

Figure 4-12 The change of respiratory rate and CBF after fentanyl administration in the neonatal group

The graph shows the changes of CBF and respiratory rate in (a) NN-FEN group n= 2, and NN-SAL group n = 3. An increase of CBF 10% from the baseline is observed in both graphs, and a 10% decrease of respiratory rate took place at the same time on both groups.

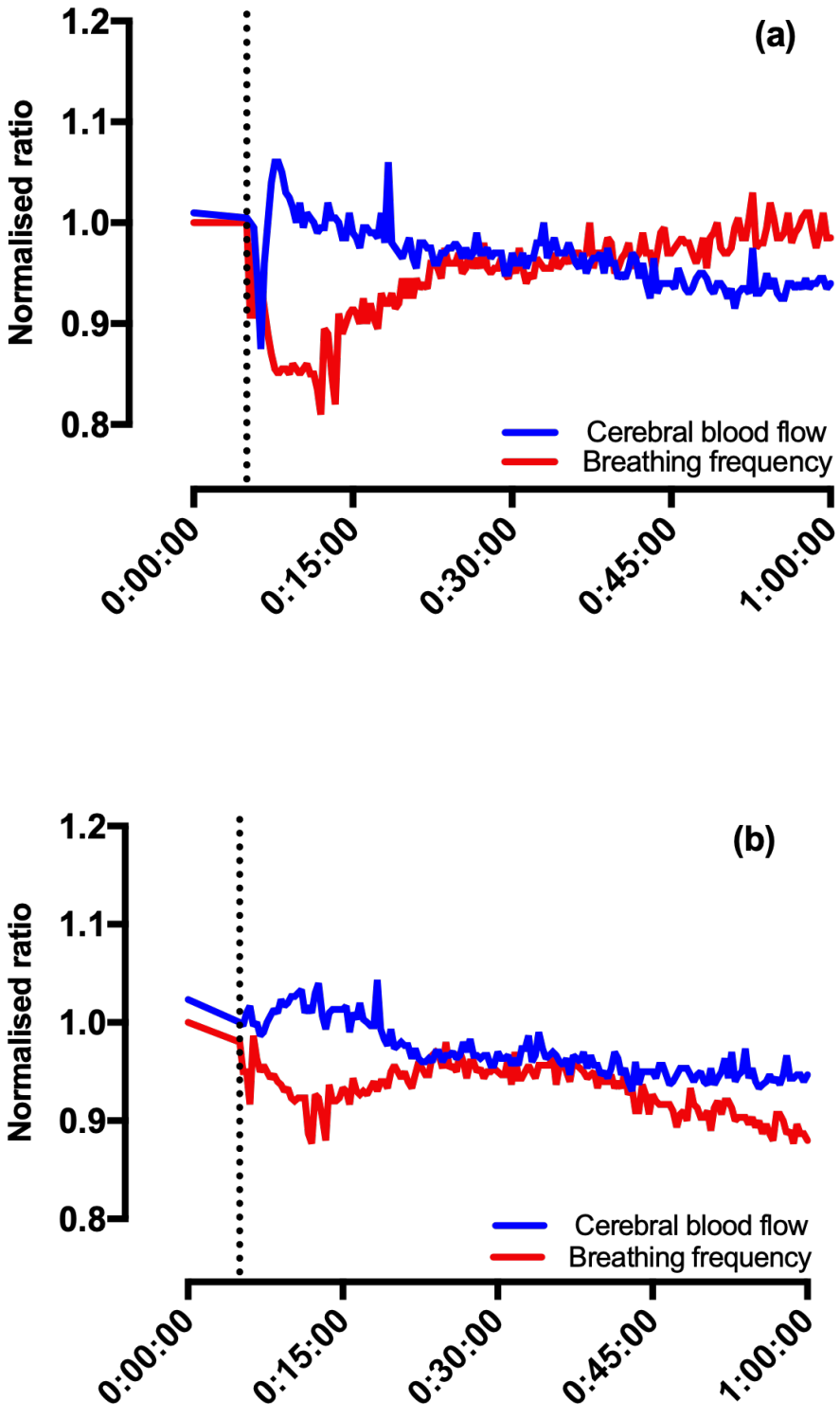

Figure 4-13 The change of respiratory rate and CBF after fentanyl administration in juvenile group

The graph illustrates the changes that occurred in CBF and respiratory rate, after fentanyl administration in the following groups (a) JUV-FEN group n= 2 and (b) JUV-SAL group n= 3. (a) showed a 5% increase of CBF and from baseline and 10% decrease of respiratory rate from the baseline average. (b) presented a 3% increase of CBF and 10% decrease of respiratory rate from the baseline average.

A fluctuating pattern was observed from the live recording of the CBF dynamic changes in the following mice (NN-SAL n= 2, NN-FEN n= 2, JUV-SAL n= 1, and JUV-FEN n= 1). The fluctuating pattern was synchronous among the identified ROIs, and the mice had completed the experiment 90 minutes post-fentanyl administration. The fluctuating pattern lasts between 180-300 seconds and remained consistent for most of the recording. See Figure 4-14

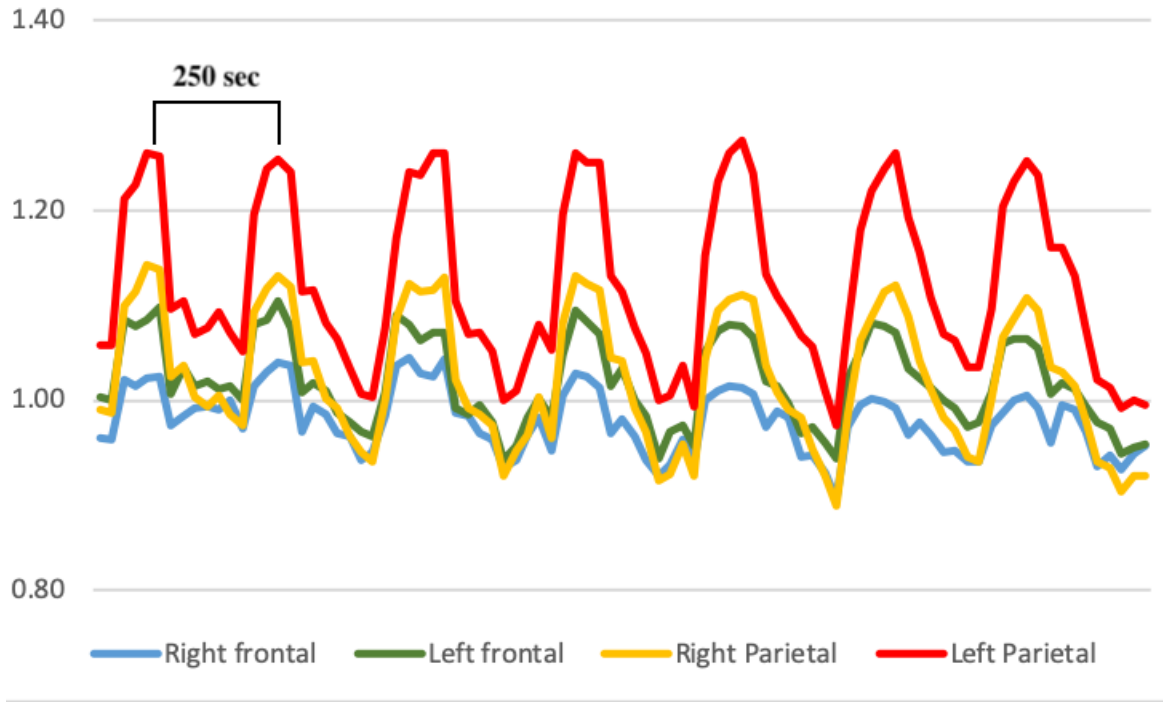

(a)

Figure 4-14 A fluctuating pattern obtained on CBF
A fluctuating pattern was observed in some of the recording, where a 10% increase of CBF occurred gradually and decreased after that, within a 180-300 second cycle. The fluctuation occurred in all regions in a rhythmic pattern.

4.8 Discussion

4.8.1 The effect of fentanyl on survival rates under anaesthesia

The preliminary results of the laser speckle experiment highlighted that groups of mice exposed to fentanyl were more vulnerable to death under anaesthesia than the control groups. There was 80% survival in the NN-SAL group vs 43% survival in the NN-FEN group. A similar difference was seen between JUV-SAL and JUV-FEN groups, though mortality was higher in both of these. See Table 4-1. Clearly, mice were vulnerable to fentanyl under anaesthesia. This finding matches the data provided by (Montandon et al., 2011, Montandon and Horner, 2019) concerning the opioid-induced respiratory depression relation to the level of cortical activity, which was determined by EEG. Montandon found that decreasing the cortical activity by anaesthesia leads to an attenuation of the respiratory depressive action of opioid exposure. This finding is backed by the wakefulness theory, which states that the excitatory drive supports the respiratory system to compensate the respiratory depressive action that is triggered by opioids (Phillipson and Bowes, 1986).. Concerning the fact that the μ-opioid receptor agonists act on the preBötC to suppress the respiratory frequency in vitro and in vivo (Montandon et al., 2011), it is speculated that the attenuated vulnerability of the opioid-exposed groups, under anaesthesia, is related to alterations at the level of the preBötC. Accordingly, the repeated exposure to opioids at the postnatal age may induce a long-term neural adaptation of preBötC that lasts up to adulthood. This neural alteration of preBötC is noticed as a hypersensitivity to future opioid exposure under anaesthesia and non-REM sleep, once the wakefulness cortical drive is absent as a compensation factor to respiratory suppression (Montandon and Horner, 2019). In fact, the destruction of NK1R-expressing neurons within preBötC results in breathing disturbances during a sleeping state in adult rats (McKay et al., 2005). Thus, a stand with the possibility of the preBötC neural alteration is involved with the opioid hypersensitive obtained under anaesthesia.

The study was stopped because of the unacceptably low survival rate. This followed direction from the Home Office and the Veterinary Research Facility. Subsequent post-mortem examination did not identify any obvious problem. Other projects experienced similar high mortality rates at the same time. As we referred to the VRF, they suggest that an external noise of construction work may have exposed the mice to stress during the VRF habituation period.

4.8.2 Opioids effect on CBF

An overall increase of the CBF was noted as a response to the FEN administration under urethane anaesthesia. See Figure 4-7. In fact, fentanyl exposure increases the CBF in general (Franceschini et al., 2010). Also, other μOR agonist drugs, such as heroin and cocaine, are known to increase the CBF (Safo et al., 1985). The mechanism which causes the increase in CBF is not fully understood. Accordingly, respiratory depression, which is a common side effect of exposure to opioids, results in a decrease of PO_2 that could lead to an increase of the CBF; also an increase of PCO_2 may lead to the same results (Kety and Schmidt, 1948, Walsh and Cunningham, 2004). To analyse respiratory depression and CBF response to fentanyl administration, these experiments recorded breathing frequency and dynamic CBF changes simultaneously. See Figure 4-12 and Figure 4-13. Both measures had changed at the same time. Neither obviously preceded the other. Yet, to understand the CBF autoregulation many factors should be considered beside the neural and circulatory system, such as arterial blood pressure and cerebral blood volume (Roy and Sherrington, 1890), and neurovascular coupling (Franceschini et al., 2010), and the intracranial pressure (Marina et al., 2020). Considering the mentioned factors beside the changes of oxygen and carbon dioxide partial pressure will help in future to understand the mechanism of opioid influence on the CBF.

The regional changes of CBF in ROI 3 and ROI 4, parietal region, revealed a higher CBF response to FEN injection compared to the ROI 1 and ROI 2, frontal regions. See Figure 4-9, Figure 4-11, Table 4-3 and Table 4-4. The data remain underpowered due to the low survival rate in the study groups discussed in section 4.8.1. Up to our knowledge, no similar studies were conducted on the same age window and fentanyl dose, followed by a CBF analysis later in adulthood. The literature backed the regional changes of CBF (Firestone et al., 1996, Zelaya et al., 2012) as the systemic fentanyl administration increases the CBF within prefrontal cortex and caudate. Also, morphine and hydromorphone presented similar results of the regional CBF influence (Schlaepfer et al., 1998). This regional effect of opioid on CBF is linked to the μOR distribution across the cortex (Lorenz et al., 2000, Jones et al., 1991), which could be analysed in future by introducing histological studies following the imaging protocol to investigate the changes at the level of μOR.

A decrease in the baseline average in the frontal region, as the NN-FEN group n=4 mean average was 206 ± 2.99 vs NN-SAL group n=10 mean average 244.3 ± 1.993, See Figure 4-6. The sample size was imbalanced due to the vulnerability of the NN-FEN mice group and low survival rate, which makes it difficult to have a statement to this finding. Yet, the reduction of the rCBF was obtained by (Pezawas et al., 1998, Pezawas et al., 2002) previously, as the chronic exposure to opioids leads to a decrease of the prefrontal cortex blood perfusion. (Botelho et al., 2006) observed a reduction of the CBF at the frontal, temporal, and occipital lobe. The temporal lobes showed no difference in the CBF data in the current study, and it was difficult to obtain the occipital cortex data as the scalp remnants appeared within the ROI and interfered with the CBF recordings. In fact, the parietal region in the fentanyl exposed groups presented an increase of the CBF as a response to fentanyl administration. See Figure 4-9 and Figure 4-11. The regional heterogenicity response to opioids administration was found by (Qiu et al., 2011), as the chronic exposure of opioids in heroin dependent patients lead to regional heterogeneity of CBF that included an increase of CBF within the thalamus, cuneus and lingual gyrus. Yet, the fentanyl effect on CBF was linked to the μOR population and location by (Lorenz et al., 2000), therefore, the alterations of μOR distribution may interfere with the chronic rCBF changes.

4.8.3 CBF fluctuating pattern

A fluctuating pattern was observed on some of the CBF data, as the CBF increases by 5-20% and then returns to normal.(See Figure 4-14 A fluctuating pattern obtained on CBF) The fluctuation cycle was observed in the mice that completed the 90 minutes post-fentanyl injection and lasted around 250 seconds and remained until the end of the recording. These fluctuations are identified as a vasomotion phenomenon (Obrig et al., 2000). Similar observations were recorded on rat's brain by Laser Doppler Flowmetry as the CBF changes by 5-20% (Hudetz et al., 1992, Golanov and Reis, 1996). Vasomotion were linked to several causes , such as the myogenic components (Wilkin, 1986, Bollinger et al., 1991, Kano et al., 1991), haemostatic stress, tissue oxygen delivery and the functional connectivity map (Biswal et al., 1997, Lowe et al., 1998).

4.9 Summary

Laser speckle (LS) experiment was designed investigate the dynamic changes of CBF after opioid administration. LS had provided the advantage of recording the live dynamic changes of CBF in response to pharmacological agents, which may help to broaden the utilisation of the tool in future study and have detailed understanding of the drugs impact on haemodynamic stability. NN-FEN showed a higher response of CBF to fentanyl administration (0.04 mg/kg i.p.), in comparison to the control group NN-SAL. Additionally, fluctuating pattern were obtained in some LS recordings, which is referred to the vasomotion activity. Opioid exposed mice were vulnerable to the generalised aesthesia procedure, and the mortality rate ranges between 60-80%.

4.10 Study limitation

The major limitation is that the number of mice that survived the experiment is low, limiting the data analysis and conclusion. The reason for the high mortality is still unclear, and the whole post-mortem report done by the VRF showed no elusive cause of the incident. The same protocol was used by (Kennedy, 2015), and the control group managed to complete the anaesthetised fentanyl challenge, which excludes fentanyl as a direct factor affecting the control group.

Chapter 5 The chronic impact of opioid exposure early in life on corticosterone, β-endorphin levels and weight in ICR mice.

5.1 Introduction

As discussed in Chapter 3, opioid exposure in the early days of life resulted in long-lasting changes in breathing patterns, such as the decreased resting breathing rate in the NN-FEN mice group compared to NN-SAL. In addition to changes in breathing pattern, it was observed that fentanyl exposed mice had an increased body weight. This suggests exposure to fentanyl may have wider systemic actions. The study reported in this chapter was conducted to analyse other physiological changes such as weight gain, endogenous opioid level, and chronic stress markers, corticosterone. Older literature contains conflicting reports about the effects of opiates on weight gain in rodents, which may reflect differences in the drugs used, the dosage schedules, other experimental differences and the widespread actions of opiates on hormone secretion (Levine et al., 1985, Buck and Marrazzi, 1987). As a part of the weight gain investigation, the plasma level of β-endorphin was measured to look after the cause of the weight gain observed on the mentioned study group from Chapter 3.

Endogenous opioids interact with different families of receptors to trigger a range of physiological responses. The three principal endogenous opioids are endorphin (END), enkephalin (ENK) and dynorphin (DYS), and they originate from three protein precursors (pro-opiomelanocortin (POMC), preproenkephalin A, and preproenkephalin B) (Vuong et al., 2010). In general, endogenous opioid peptides are linked to specific receptors; for example, END is known as a μ receptor agonist, ENK is selective to δ receptors, and DYS is associated with κ receptors. Opioids bind to three receptor types (α, δ, κ) to exert their actions, such as food intake, cognitive function, neuroendocrine and cardiovascular regulation (Fichna et al., 2007). See Table 5-1 Endogenous and exogenous opioid affinity to selective receptors, for the summary.

Concerning the chronic stress markers, exposure to opioid compounds (endogenous and exogenous) alters the secretion of the hormones by the endocrine system (See Table 1-4 The effect of opioids on the endocrine system). The literature review in section 1.8.3 described the short-term effects of opiates on the HPA axis in rodents.

The long-term effect could be noticed on the hormonal distribution after opioid exposure at the perinatal age. For instance, introducing rats to morphine at the day of birth produces a long-term effect on the stress reactions which could be obtained on the rat behaviour within the open field apparatus at the adulthood age (Victoria et al., 2015). A similar response is spotted in adult rats whose dams are treated with morphine throughout the gestation age (Ahmadalipour and Rashidy-Pour, 2015). Indeed, an early enhancement of the opioid may result in chronic changes that affect the CNS and stress adaptation. Again, range of experimental protocols have produced conflicting results. At the time of writing, there is no study conducted on the long-lasting changes of stress following an early repeated opioid exposure.

Ligand	Opioid receptor		
	μ	δ	κ
β-endorphin	++++	++	++
Met-enkephalin	++	+++	0
Dynorphin	++	0	+++
Endmorphin-1	+++++	0	0
Endmorphin-2	+++++	0	0
Morphine	+++	0	0
Fentanyl	+++	0	0
Methadone	+++	0	0
Naloxone	-	-	-
Naltrexone	-	-	-

Table 5-1 Endogenous and exogenous opioid affinity to selective receptors
Selective receptors were highlighted in relation to the specific opioid peptides. (+) Agonist, (-) antagonist and (0) have no specific affinity (Vuong et al., 2010).

5.2 Study aims

- To study the effect of repeated exposure of opioids, between P9-P13, on the plasma level of β-endorphin.

- To study the effect of repeated exposure of opioids, between P9-P13, on body weight.

- To study the long-term effect of opioid exposure between P9-P13 on corticosterone levels.

5.3 Hypothesis

The early exposure to opioid agonists, at the age of P9-P13, results in an increase in the plasma levels of β-endorphin, corticosterone and enhances weight gain.

5.4 Methodology

5.4.1 Animals

The experimental animal procedures were performed under the regulations of the UK Home Office (personal licence number i51F7C81D, and project licence number 60/4558). The studies were designed in correspondence with the Animals (Scientific Procedures) Act 1986. The experimental procedures were conducted on ICR mice, which were acquired from HARLAN. Accordingly, pregnant dams were ordered and delivered to the housing facility at Veterinary Research Facility, Garscube campus, University of Glasgow. The pups were kept with the mother up to the age of 21 days, when they were weaned. Post weaning, male and female mice were housed in separated cages, with a maximum of 4 mice per cage. Ear-piercing allowed for identification of individual mice within the cage. The light/dark cycle was 12 hours duration, with no dietary modifications. Day of birth is referred to as postnatal day 0 (P0). The age categories used in this study were juvenile (P8-P21) and adults over P21.

5.4.2 Postnatal injection

The experimental groups were defined as follows:

- **Group 1 –Juvenile Fentanyl (JUV-FEN) n=16** Each mouse received one **daily** injection of fentanyl (0.04 mg/kg i.p.) P9-P13.

- **Group 2 -Juvenile Saline (JUV-SAL) n=9** Each mouse received an equivalent volume of the physiological saline P9-P13.

Fentanyl citrate (μ opioid receptor agonist, 50 μg/ml, Janssen-Cilag, UK) was administered daily (0.04 μg/kg i.p.) for JUV-FEN. The control group JUV-SAL received an an equivalent volume of the normal saline.

5.4.3 Study timeline

Sampling started by taking tail vein blood samples at week 6, 8 and 10 for β-endorphin levels analysis. Another tail vein sample was taken, at the termination point, at week 12 and it is accompanied by a cardiac puncture sample and hair sample. The samples collected at 6th week were used as a to determine the suitable protocol and dilution level See Figure 5-1.

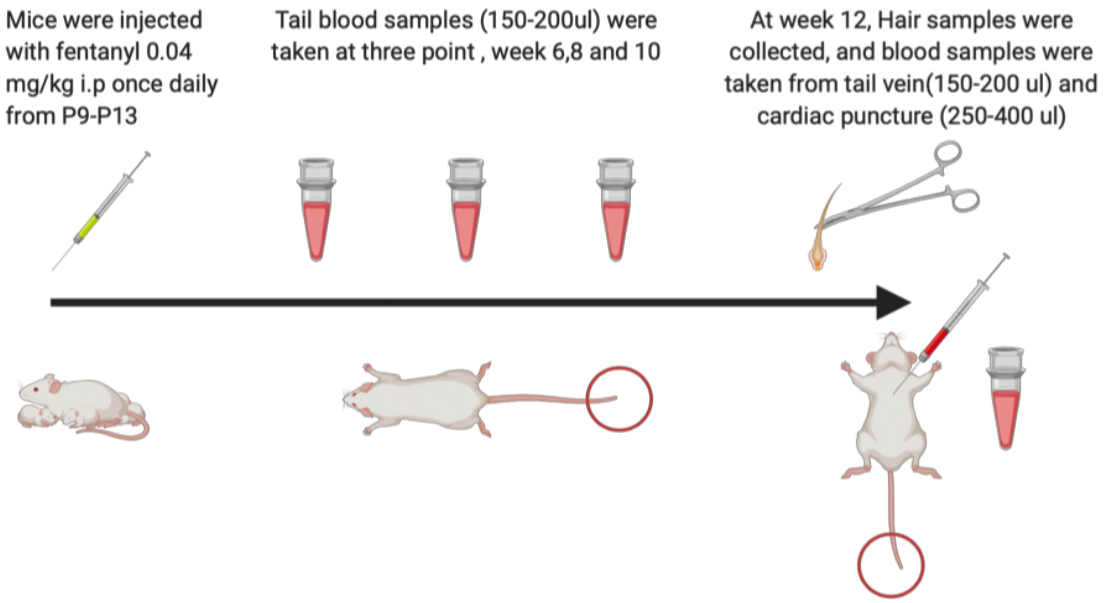

Figure 5-1 β-endorphin and Corticosterone sampling timeline
Collecting the samples for ELISA analysis started at week 6 old, and ended at the termination point (12 weeks old). Three tail vein samples were collected essentially at 6, 8 AND 10 weeks of age, followed by a fourth tail vein sample and cardia puncture, and hair samples at 12 weeks.

5.4.4 The level of plasma β-endorphin

Blood samples were collected at the ages of 6, 8, 10 and 12 weeks. Blood sampling was collected via the tail vein at each time point; a cardiac blood sample was collected at the age of 12 weeks. The blood samples collected at week 6 were used as a pilot to adjust the ELISA buffer concentration. β-endorphin level is known to be influenced by several factor, such as stress, age and sex (Pilozzi et al., 2020). Therefore, it was planned to collect the samples in several timepoints (10-12 am at the same day of the week) and compare the study groups at each timepoint. The blood sampling process was designed following the 3Rs recommendations, including the technique, sample volume and the timing of the sampling. Accordingly, mice were placed into the restraining apparatus that restrict the mouse movements and keep the tail free for sampling. A side cut is made on the tail vein using a blade; then dripping blood up to 200 microlitres was collected directly by heparinised Eppendorf. Once the 200-microlitre blood sample was acquired, the samples were stored in an icebox. After that, samples were spun for 10 minutes at microcentrifuge (Sigma 1-14 Microfuge, Sigma®, Germany), and plasma was pipetted and stored in isolated Eppendorf at -60°C in a freezer in order to be analysed with ELISA kits later. See Figure 5-2.

The cardiac puncture was performed at the terminal experiment, when mice were euthanised by phenobarbital as part of the brain dissection process, which is illustrated in detail in chapter 2.5.3. In order to perform the cardiac puncture, a thoracotomy was mandatory and mid-clavicle cuts were performed in parallel lines, so the rib cage could be everted, and the heart exposed for sampling. Consequently, a 23-gauge needle was used to pierce the left ventricle and blood was withdrawn gradually up to 1 ml. Samples were spun for 10 minutes and serum extracted and stored in a separate tube at -60°C freezer, for ELISA analysis.

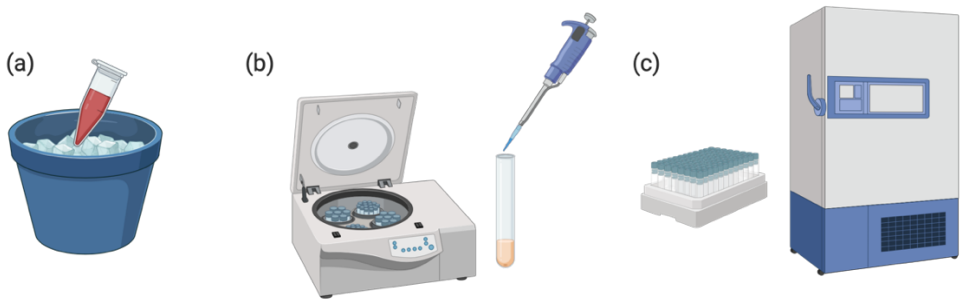

Figure 5-2 Plasma β-endorphin sampling process
Once a blood sample collected, it was kept on ice box (a). Then it was spun for 10 minutes at microcentrifuge (b). Right after the centrifuging, plasma was aspirated and stored in a separated vial. Both samples (blood and plasma) were kept in -60^{o}C for ELISA analysis later.

5.4.5 Measuring corticosterone level in hair samples

Hair samples were collected from mice aged 12 weeks. The corticosterone concentration in hair has been validated as a reliable biomarker for chronic stress in rodents. The hair corticosterone level in rodents reflects their plasma level for up to 14 days (Scorrano et al., 2015). The hair samples were collected at the terminal point to avoid the additional stressor of hair extraction and to manage collecting samples from the same site in each induvial mouse. The samples were pulled from the back of the stored in a dry vial at room temperature. Next, the samples were weighed, then washed with a diluted methanol 20% (HPLC-grade methanol) by 80% distilled water. Each wash requires 2 ml of HPLC-grade methanol and the vial placed into the shaker set on 200 spins/minute for 2 minutes. Each hair sample is washed 3 times, then vials are placed into the fume hood with no cap for 18-24 hours, so the remainder of the washing solution evaporates. After that, 2 ml of methanol (MeOH) is added to each vial, then to be placed on the orbital shaker at 52°C, set on 40 rpm, for 16 hours (4 pm-8 am). The next day, MeOH is extracted from each vial and dispensed into 12x75mm glass vial. Later, glass tubes are placed into the SpeedVac ('Thermo Scientific, UK), set on medium temperature, and kept for 2 hours, so the MeOH evaporates and the steroids precipitate at the bottom of the vials. The end product after the evaporation process is sealed with a plastic cover and stored in the lab freezer for later analysis with ELISA kit. See Figure 5-3. The extracted hair samples were reconstituted into an assay buffer, as duplicates, and the guidelines were followed through the user manual provided with each kit (Cusabio Biotech. Co., Ltd, UK). The samples' optical density was read at 405 wavelength using LT-4500 reader (Labtech, UK). Duplicate samples were taken from each mouse; the average of the duplicates was calculated for the analysis. See Figure 5-4.

5.4.6 Longitudinal weight follow-up

Body weight records were registered on a weekly basis for each mouse n= 9 and n=16 . The records started at the age of 3 weeks old until 12 weeks old. The weighting was done on the same day, each week, between 10-12 am, on the same scale provided by the VRF department.

An additional 4 groups were added to the weight comparison, which are NN-FEN, NN-SAL, JUV-FEN and JUV-SAL. The weight data were collected for the average weight between 10-12 weeks. The data were retrieved from the chapter 2, and the group's description is provided in the following section 2.2. The weight of this group was recorded at the day of the plethysmography experiment.

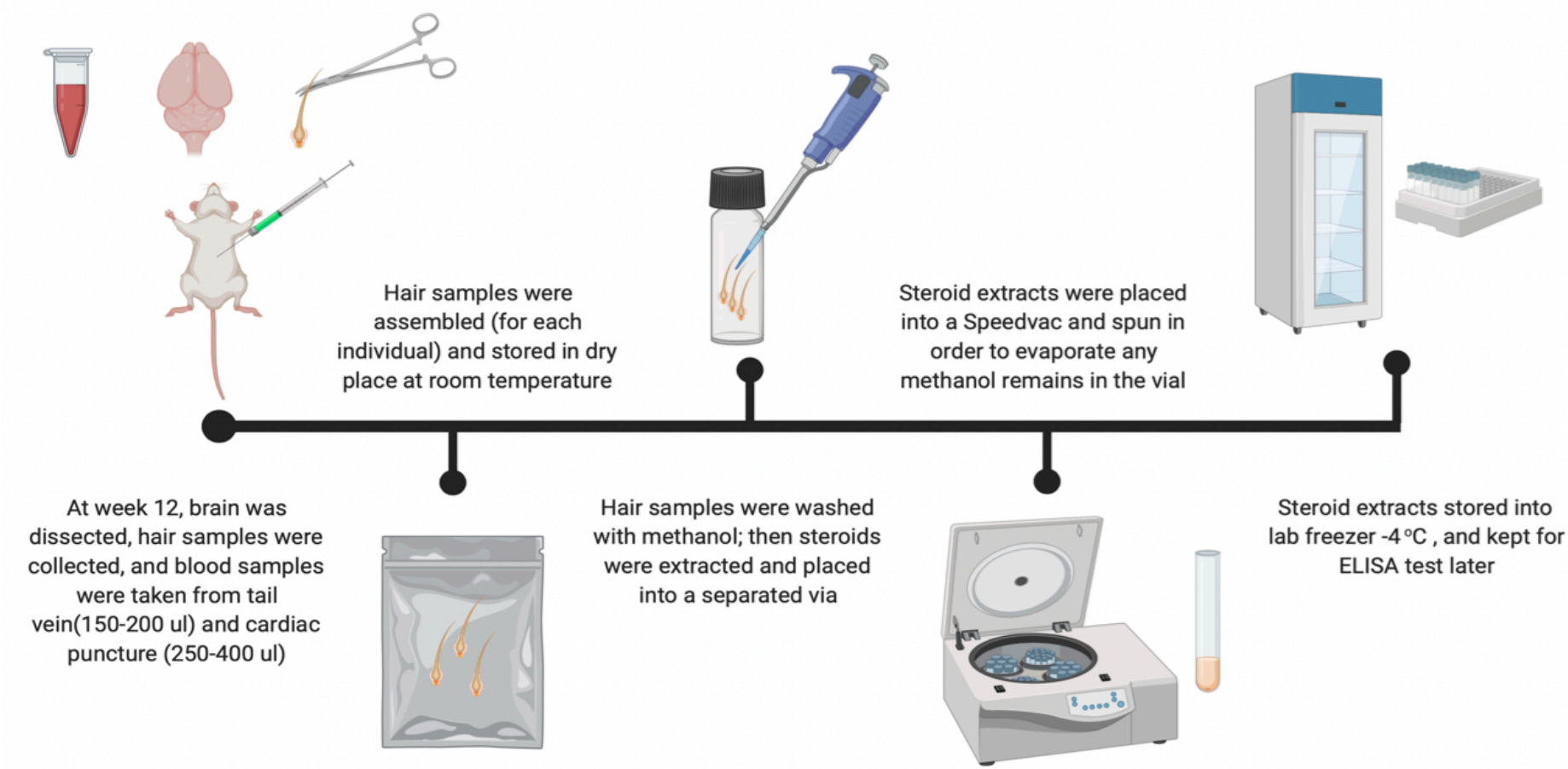

Figure 5-3 Hair sample preparation for ELISA test

Hair samples were collected at the age of 12 weeks. It was stored in a dry place then washed with methanol twice for 2 minutes. Methanol was aspirated and samples were left to dry for 18-24 hours at the fume hood. Then, 2 ml of methanol was added to the hair samples and kept on the orbital shaker for 16 hours, set on 52°C. Methanol, containing steroids from hair samples, was aspirated again and placed into a separate vial, which was spun using the Speedvac and dried. So, the methanol evaporated and steroids descended to the bottom of the vial, which was analysed later with an ELISA test for corticosterone levels.

(a)

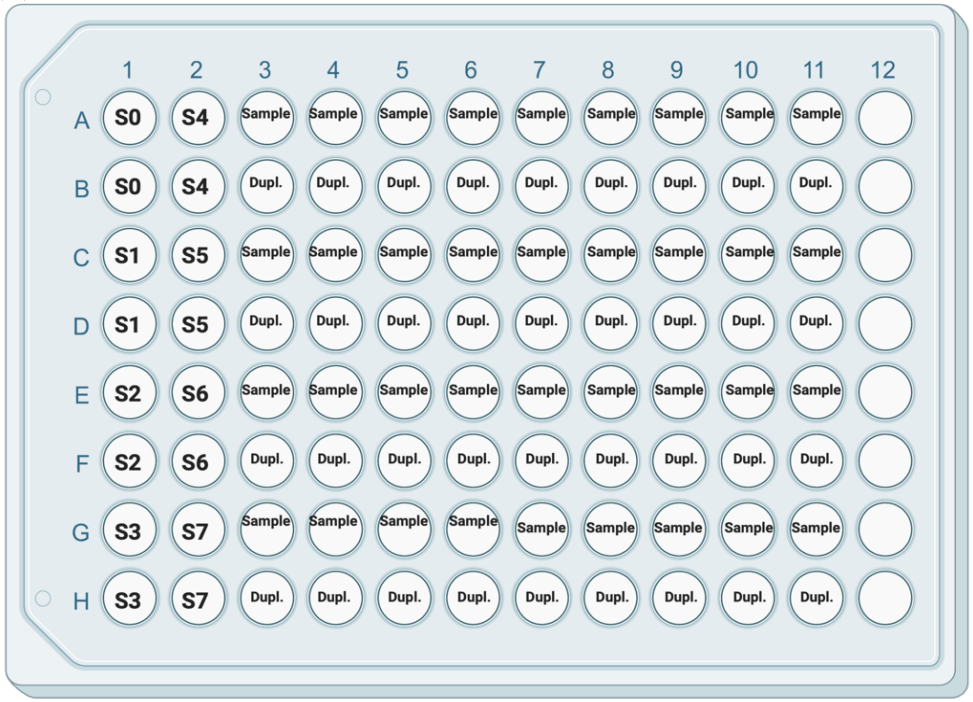

(b)

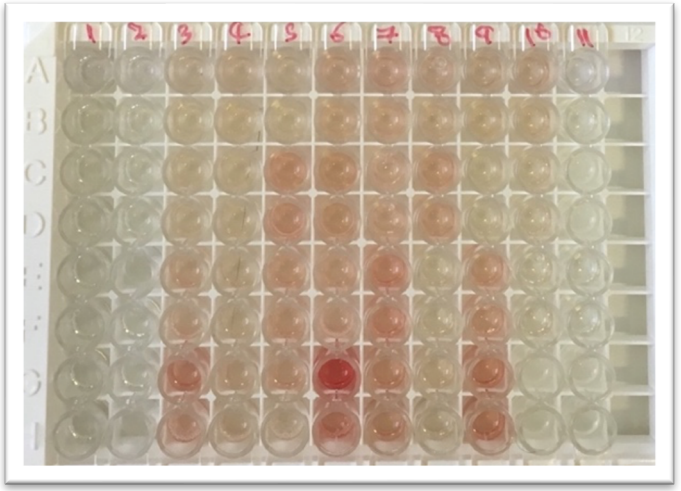

(c)

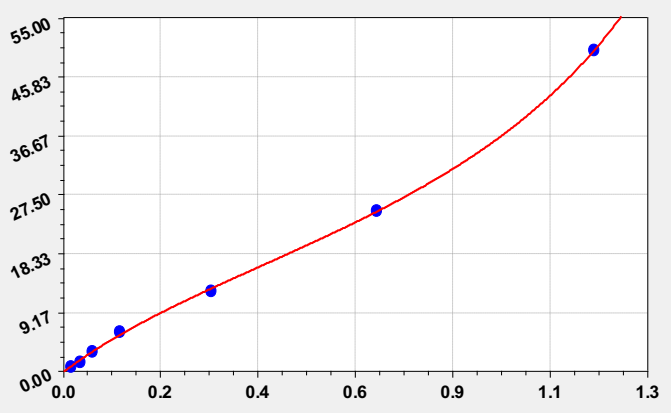

Figure 5-4 ELISA samples assay and stand curve

The samples were plotted as duplicates on the plate, beside the standard curve (a) and (b). Standard curve was measured using the software provided with the user manual (c). The X axis stands for the optic density that is measured by LT-4500 reader, and the Y axis stands for the certain concentrations reflected on different optic densities.

5.5 Statistical analysis

The statistical analysis was executed by GraphPad Prism 4 and significance was set at P value < 0.05. A non-paired t-test was used to compare the means of the corticosterone concentrations; Two-way ANOVA, which is followed by a post hoc Bonferroni correction, to compare the weight average of the study groups in each timepoint (JUV-SAL vs JUV-FEN). Plasma β-endorphin levels were assessed by two-way ANOVA, which is followed by a post hoc Bonferroni correction, for multiple comparisons between each time point in both groups (JUV-SAL vs JUV-FEN).

5.6 Results

5.6.1 Weekly weight assessment

The JUV-FEN group had a bigger spread of weight data along the longitudinal study. This bigger distribution could be related to the larger group size of n=16 in JUV-FEN vs n=9 in JUV-SAL. In addition, both groups have male and female mice, which could increase the variability of weight data because male mice are usually heavier than female mice (https://www.jax.org). The longitudinal graph showed a trend toward an increase in weight in JUV-FEN compared to JUV-SAL on a weekly basis. Two-way ANOVA, followed by a post hoc Bonferroni correction, was used to compare the weighted average of the study groups at each time point. No statistically significant difference was obtained between the experimental groups (JUV-FEN vs JUV-SAL) P value > 0.05. See Figure 5-5.

The additional 4 groups, whose data were retrieved from the plethysmography chapter (NN-FEN, NN-SAL, JUV-FEN and JUV-SAL), were added to the weight comparison and showed a significant difference between the mean weight, (NN-FEN (n=9) had an average of 43.06 grams ± 2.67 vs 33.18 grams ± 2.32 in NN-SAL (n=11), P value < 0.05). JUV-SAL group (n=11) had an average of 40.36 grams ± 5.89 vs 40.72 grams ± 5.45 in JUV-FEN (n=9), P value > 0.05). An additional JUV group was added with a new batch of mice later, and JUV-SAL weight average (n=9) = 34.83 grams ± 4.09, and JUV-FEN (n=16) average was 36.19 grams ± 4.86 (P value > 0.05). See Table 5-2 and Figure 5-6.

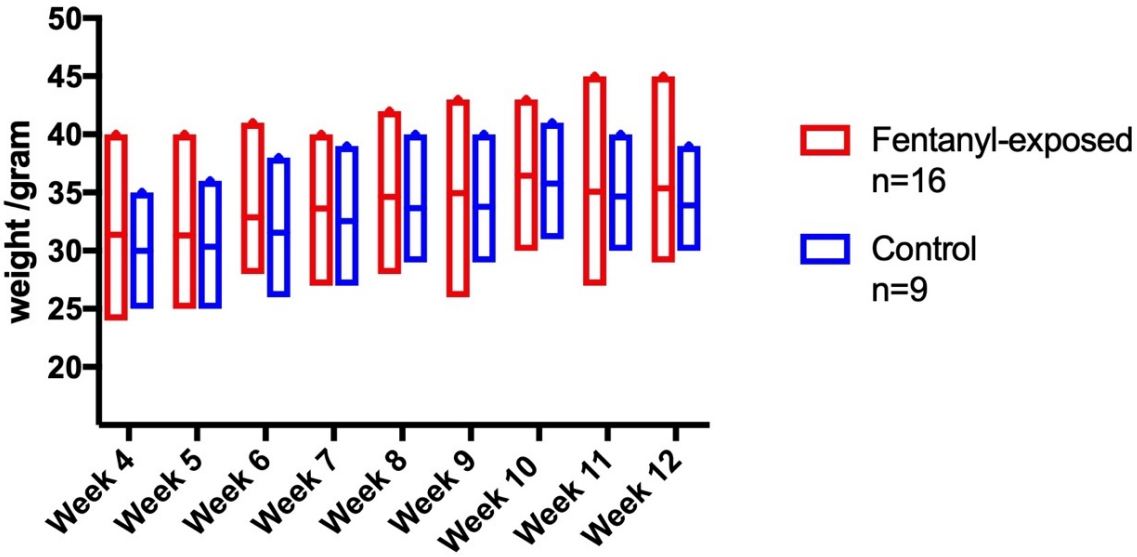

Figure 5-5 Mice weight weekly records

The figure presents the longitudinal weekly weight average for the study groups. The fentanyl-exposed group JUV-FEN had a higher spread compared to the control JUV-SAL group on a weekly basis. The JUV-FEN weight average was 31.38 grams at week 4 and reached 35.36 grams at 12 weeks old, while the JUV-SAL group weight average was 30 grams at week 4 and reached 33.89 grams at 12 weeks old. The data is presented as mean average ±SD

Study group	Weight average (gram)
NN-SAL n=11	33.18 ± 2.32
NN-FEN n=9	43.06 ± 2.67
JUV-SAL n=11	40.36 ± 5.89
JUV-FEN n=9	40.72 ± 5.45
** JUV-SAL n =9	34.83 ± 4.09
** JUV-FEN n=16	36.19 ± 4.86

Table 5-2 Average mice weight between week 10-12 in all study groups
The table presents the mice weight average taken between week 10-12 in all study groups. The NN-FEN group showed a higher weight average 43.06 ± 2.67 grams in comparison to the control group NN-SAL 33.18 ± 2.32 grams. ** Is the same longitudinal weight average group, which weight records were taken on weekly basis. The data of remaining groups were retrieved from the plethysmography study records that were taken between week 10-12.

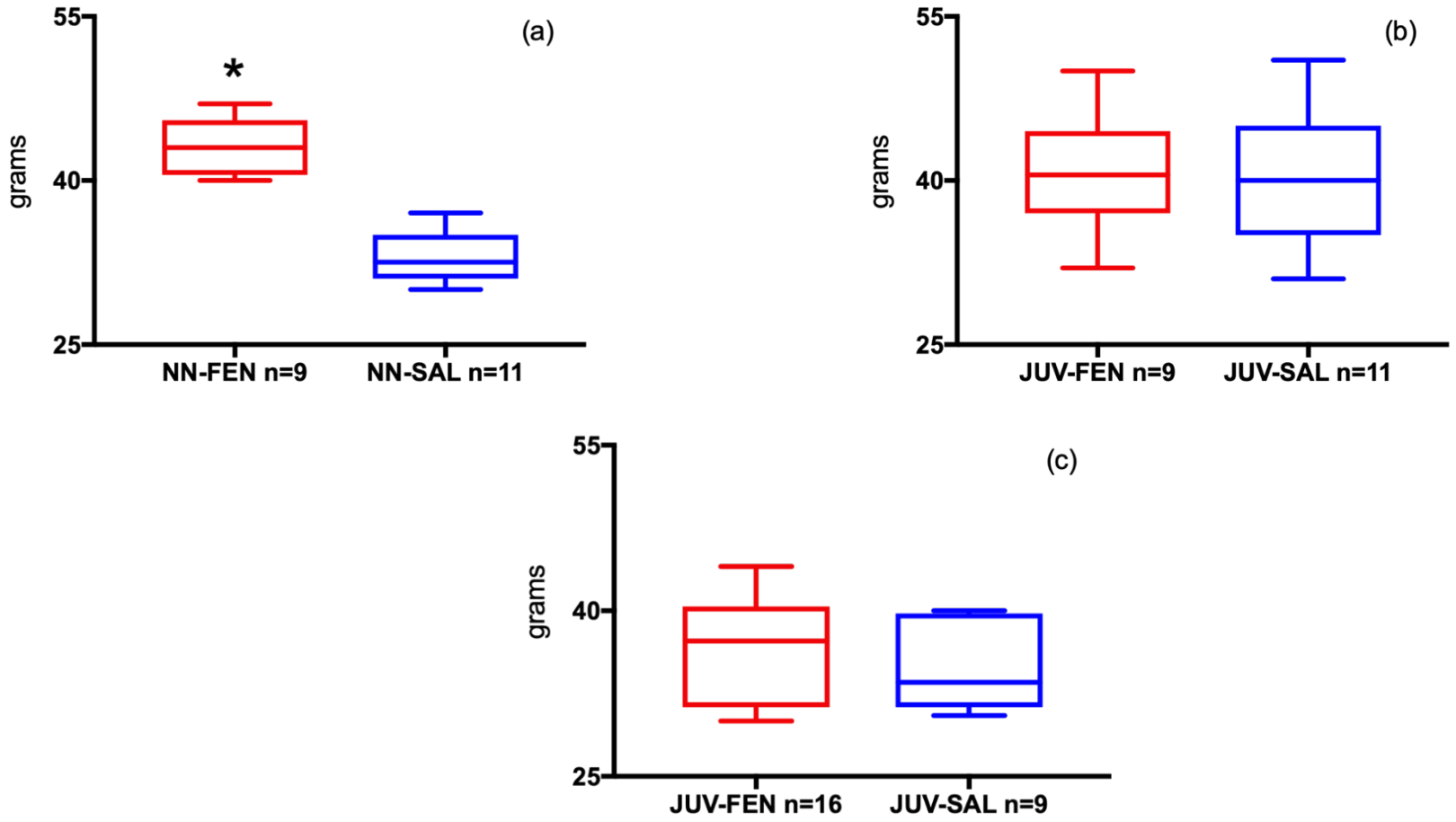

Figure 5-6 Average mice weight between week 10-12 in the study groups used in plethysmography study
(a) NN-FEN showed an increase in the weight average 43.06 grams, compared to NN-SAL 33.18 grams (P value < 0.05). (b) No significant difference was found between JUV-FEN 40.72 grams and JUV-SAL of 40.36. (c) No significant difference was found in the weight average between JUV-FEN 36.19 grams and JUV-SAL 34.83 grams. The data is presented as mean ±SD

Similar finding was obtained in previous work (with similar experimental groups) conducted by (Kennedy, 2015). Kennedy conducted her work on four mice groups, which went through the same protocol concerning fentanyl injection at P1-P5 and P9-P13. Kennedy's study aimed to investigate the long-lasting effect of opioid exposure early on in life, and mice weight was taken as a part of her assessment. Their study showed a trend of increase in the average weighted in the NN-FEN group compared to the control group, which was not statistically significant (P-value >0.05, two-way ANOVA). See Table 5-3 and Table 5-4.

Age	Weight (g)	
	NN-SAL	NN-FEN
P1	1.6±0.3	1.8±0.3
P2	2±0.5	2.2±0.2
P3	2.8±0.4	2.7±0.3
P4	3.3±0.4	3.1±0.5
P5	3.9±0.3	3.7±0.7
Adult	36.4±4.7	38.9±3.2

Table 5-3 Average body weight in fentanyl-exposed neonatal group
The table presents the data of body weight average of the experimental groups NN-SAL n =16 and NN-FEN n=16. No significant difference found between the study groups. The data presented as mean ±SD, and 2-way ANOVA test was used for the analysis. The table was amended from (Kennedy, 2015).

Age	Weight (g)	
	JUV-SAL	JUV-FEN
P9	5.4±1.9	6±1.3
P10	5.8±1.9	6.4±1.4
P11	6.2±1.8	6.7±1.4
P12	6.45±1.8	7±1.4
P13	6.9±1.8	7.3±1.5
Adult	33.4±2.9	35.2±4

Table 5-4 Average body weight in fentanyl-exposed juvenile group
The data represents the weight average of the study group across several ages. No significant difference was obtained in the body weight between the groups. The table was modified from (Kennedy, 2015).

Concerning the fact that male mice tend to have a bigger weight than females, as referred earlier in section 5.6.1, and the female mice could produce an exaggerated response to opioid exposure, preliminary data was presented, and mice were divided into subgroups depending on their sex. A small sample size was introduced between NN-FEN male (n=3) vs NN-SAL male (n=4) groups, which makes it difficult to justify the trend at the NN-FEN group. The JUV-FEN group male (n=6) had an average of 43.42 gram ± 3.8, and the JUV-SAL group male (n=6) average was 44.33 gram ± 4.32. The additional JUV group averages were JUV-FEN male (n =9) 39.94 gram ± 2.62 and JUV-SAL male (n=3) 39.83 gram ± 0.29, which is affected by the non-balanced group's size JUV-FEN (n=9) vs JUV-SAL (n=3). See Figure 5 9. The female mice data showed a trend in the NN-FEN (n=6) weight average of 43 gram vs 31.86 gram in NN-SAL (n=7). No difference was found between JUV-FEN (n=3) 35.33 gram vs 35.6 gram JUV-SAL (n=5). No difference was found in the weight average between JUV-FEN (n=7) 31.36 gram vs 32.33 gram JUV-SAL (n=6). See Figure 5-10. The subgroups data are underpowered by the small size number. The data were collected to present preliminary results to highlight the gender weight differences in the study groups in mice. This will be addressed with additional details in the discussion section.

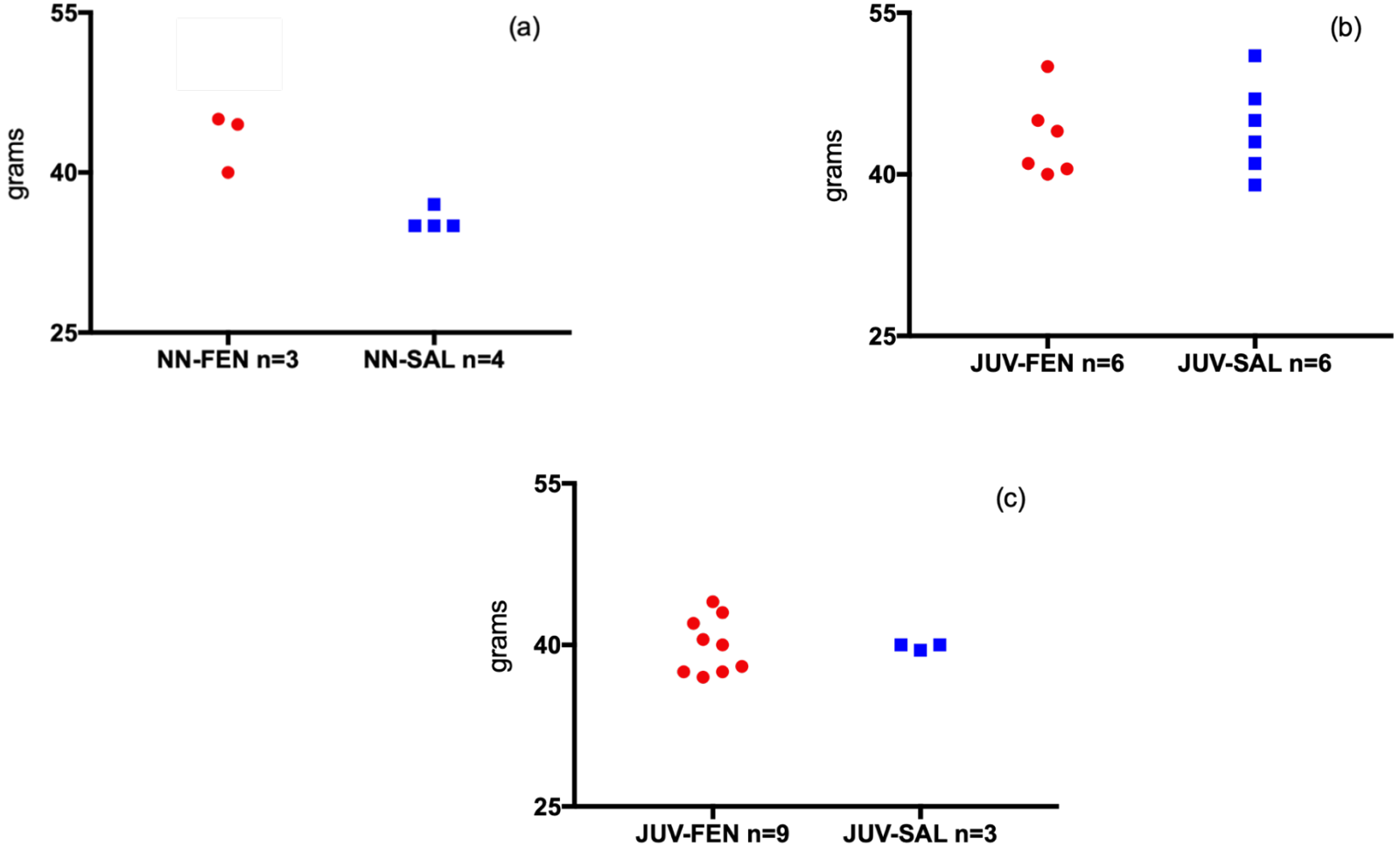

Figure 5-7 Average male mice weight between week 10-12 in all study groups
Awas observed in the mice weight on (a) NN-FEN average = 43.17, and NN-SAL average = 35.5 grams (b) A similar spread of the weight average was found between JUV-FEN 43.42 grams and JUV-SAL of 44.33. (c) No difference was found in the wight average between JUV-FEN 39.94 grams, and JUV-SAL 39.83 grams.

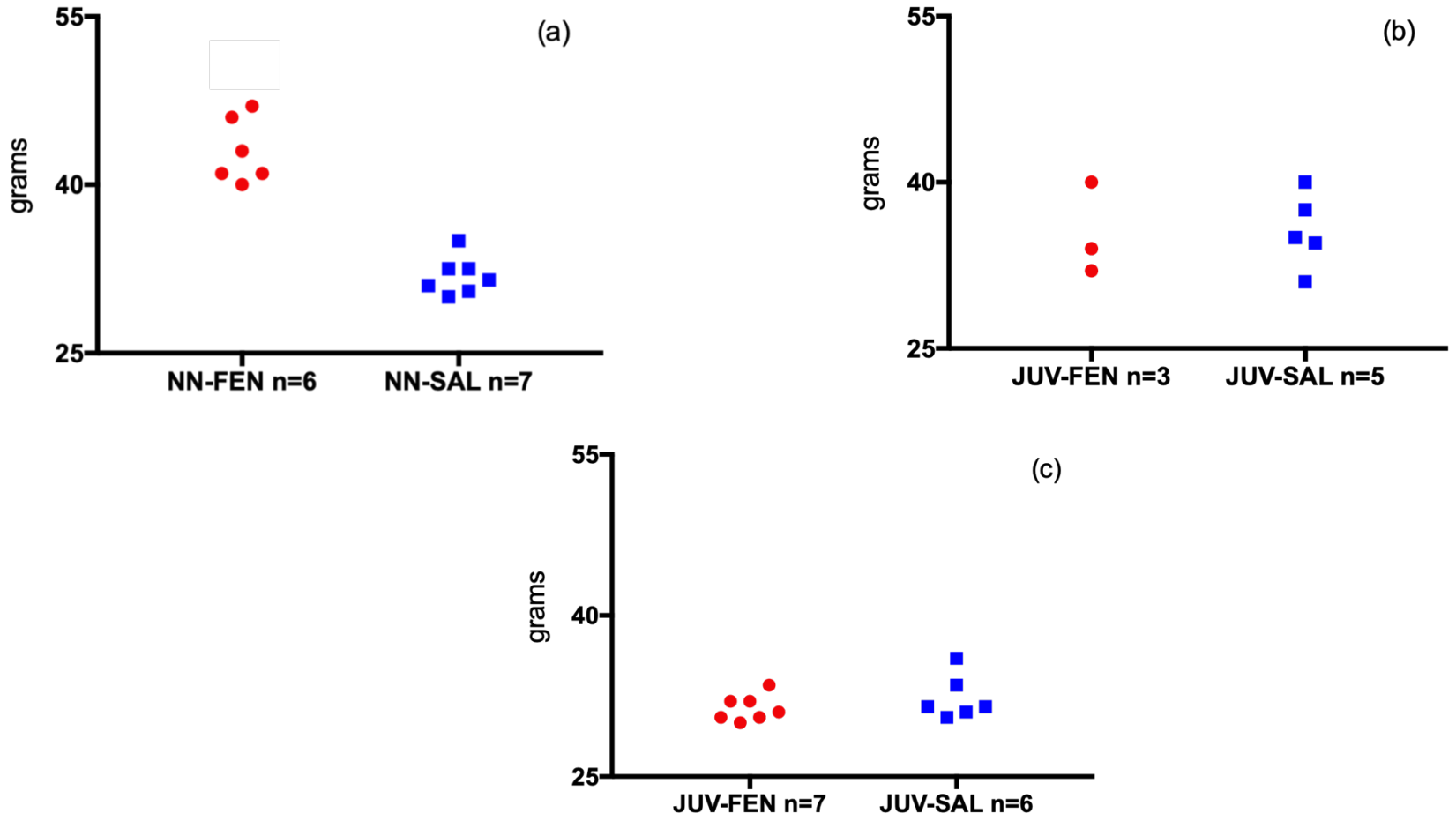

Figure 5-8 Average female mice weight between week 10-12 in all study groups
Ais found on (a) a trend towards an increase of body weight is found in fentanyl exposed group NN-FEN average = 43 vs 31.86 grams in control group NN-SAL . (b) No difference was found between JUV-FEN 35.33 grams and JUV-SAL of 35.6. (c) No difference was found in the weight average between JUV-FEN 31.36 grams, and JUV-SAL 32.33 grams

5.6.2 Hair corticosterone level

Figure 5.7 shows the concentrations of corticosterone in hair samples from mice in the JUV-FEN and JUV-SAL groups. There is big spread of concentrations in both groups, which ranges between 100-600.The mean average of the fentanyl-exposed group (JUV-FEN n= 14 was 321.6 ± 38.1 pg/ml vs 279.5 ± 40.6 pg/ml for the control group JUV-SAL n= 9). JUV-FEN showed a trend of an increase in hair corticosterone level. A non-paired t-test was used to compare the means of the corticosterone level and it was not statistically significant (P > 0.05). See Figure 5-9.

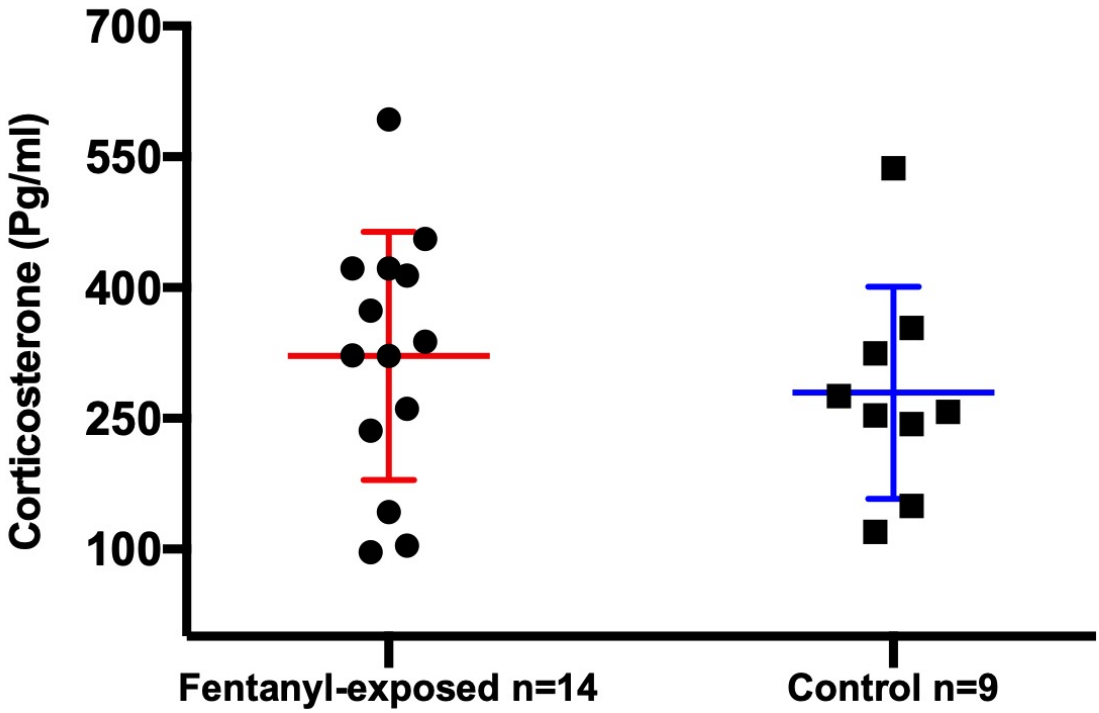

Figure 5-9 Hair corticosterone levels
The hair corticosterone level in the JUV-FEN group was 321.6 ± 38.1 pg/ml vs 279.5 ± 40.6 pg/ml for the control group JUV-SAL n= 9. The change was not statistically significant, and the data is presented as mean average ±SEM

5.6.3 Plasma β-endorphin

Plasma β-endorphin level was measured at 8, 10 and 12 weeks old. A duplicate sample were taken from each mouse; the duplicates average was calculated for the analysis. No significant results were found between the study groups at the different timepoints (P value > 0.05). The JUV-FEN group had a mean average of 1.175 pg/ml at week 8: 3.51 pg/ml at week 10: 1.85 pg/ml at week 12, and 1.91 pg/ml in the cardiac puncture sample. The JUV-SAL group had an average of 1.68 pg/ml at week 8: 2.03 pg/ml at week 10: 0.71 pg/ml week 12, and 1.22 pg/ml in the cardiac puncture sample.

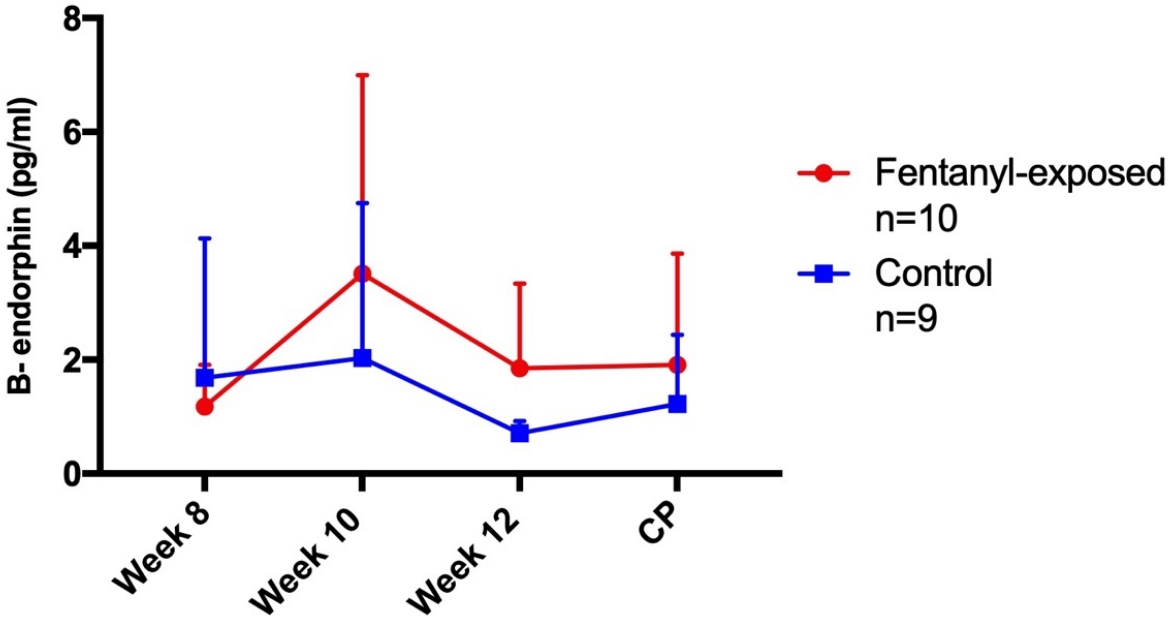

Figure 5-10 β-endorphin plasma levels in the study groups
The JUV-FEN group had a mean average of 1.175 pg/ml at week 8, which was followed by an increase of the β-endorphin levels up to 3.51 pg/ml, then a decrease to 1.85 pg/ml and 1.91 pg/ml in the cardiac puncture sample. The control mean average was 1.68 pg/ml at week 8, then 2.03 pg/ml at week 10, 0.71 pg/ml week 12 and 1.22 pg/ml in the cardiac puncture sample. The data was widely dispersed throughout the designed time points, which may affect the quality of the statistical analysis. There was no significant difference between the study groups at the same time points (P value > 0.05). The data is presented as mean average +SD

5.7 Discussion

The study investigated the long-lasting changes of repeated postnatal exposure to -opioid agonists (fentanyl) between (P9-P13). After that, a series of investigations were conducted to evaluate the chronic effect of opioid exposure early in life, such as weight, plasma β-endorphin and hair corticosterone levels. As a result, a higher trend was observed in the fentanyl exposed group at the longitudinal weight records, plasma β-endorphin and hair corticosterone levels, which were not statistically significant.

In Figure 5-5, The weight measures were taken weekly from 4 weeks old up to 12 weeks old. The mean average represented a 1-gram trend towards an increase in the JUV-FEN group compared to the JUV-SAL group on a weekly basis. However, no statistically significant difference was obtained between the groups. The G power of the study is estimated to be 50 % based on the standard deviation = 5 grams and an alpha level of 0.05. It is recommended to have at least 40 mice in a future study to produce robust statistical data analysing the weight difference between the study groups (Fitts, 2011). On the additional data retrieved from the plethysmography chapter, the fentanyl-exposed group showed a significant increase in body weight for the NN-FEN group vs NN-SAL. (See Table 5-2)

Additional analysis of mice weight was included in the study by comparing the same-sex mice from the study groups. (See Figure 5-7 and Figure 5-8) The idea was introduced to the work concerning the general difference in weight average between male/female mice, and the fact that Gender differences may affect the response to opioid administration and the severity of the side effects. Female rodents appear to be more vulnerable than males to the reinforcing effect of opiate addiction, such as acquisition, maintenance, and relapse (Lynch et al., 2002). Also, μ opioid receptor agonists showed a higher reinforcing effect in rats females than in males. Regarding the weight gain effect, male and female rats tend to have low birth weight after prenatal opioid exposure compared to the control group, which rises gradually and is equal to the control weight at the age of P21 (weaning age) (Timar et al., 2010, Kunko et al., 1996), similar to human studies of neonatal abstinence syndrome (Hunt et al., 2008). However, opioid-exposed rats tend to gain more weight, after weaning age, than

the control group, specifically females (Timar et al., 2010). The data presented in Figure 5-7 and Figure 5-8 are considered preliminary data to overview the weight average difference between mice sex within the study groups. The data remain underpowered, and no statement could be given for the latter analysis. The mechanism underlying the sex differences is unclear. Still, the preclinical and clinical studies suggested that hormonal effect, particularly oestrogen, plays a role in sex-related alterations in female rodents compared to males (Lynch et al., 2002).

Even though the literature was in conflict about the effect of opioid exposure on weight gain, some studies found that an increase in food intake and weight gain was noticed upon introducing opioid agonists to CNS, when the agonists bind to multiple opioid receptors and affect the food modulation centres (Baile et al., 1986, Levine et al., 1985). Accordingly, there was a trend toward an increase in plasma β-endorphin level in the JUV-FEN group compared to JUV-SAL, see Figure 5-10. The data showed a trend of an increased plasma β-endorphin level in the JUV-FEN group; however, a large distribution of the data was found along the samples analysed. Starting with the duplicate samples executed via the ELISA process, a 15% was set for each duplicate error, and the samples matched in general. The main issue concerning the collected data was the volume of tail blood samples of mice, which was restricted to 200 microlitre/mice. The low volume of blood samples had shown the lowest detectable level of plasma β-endorphin 0.78 pg/ml, mainly in the JUV-SAL group. Yet, the JUV-FEN group showed more traceable levels of plasma β-endorphin and produced the variability of data distribution too. This finding may suggest the increasing level of plasma β-endorphin in the JUV-FEN group. Still, the methods should be improved in future by collecting a larger volume of a blood sample or using another ELISA kit with higher sensitivity. A larger blood sample volume succeeded in producing more reliable data, as shown in Figure 5-10 at the cardiac puncture sample (CP). The cardiac puncture sample was collected at the terminal stage, and volume was not restricted to 200 microliters, and the JUV-FEN mean 1.91 pg/ml vs 1.22 pg/ml in JUV-SAL group. On week 10, the mean average of the plasma β-endorphin in JUV-FEN was 3.51 pg/ml vs 2.03 pg/ml in JUV-SAL. The marked rise in BEND level on week 10 had occurred in both study groups and it may be resulted by using a new ELISA kit for the assigned week.

Plasma BEND rises are an acute response to morphine (opioid agonist) administration (Martinez et al., 1990), and postnatal exposure to morphine could lead to a long-term increase in endogenous opioid levels (plasma BEND) that alters the affinity of μ-opioid receptors (LaPrairie and Murphy, 2010, LaPrairie and Murphy, 2009). The postnatal increase of endogenous opioids affects the HPA axis and triggers long-lasting changes in stress hormone levels (cortisol in humans and corticosterone in rodents) (CORT) (Victoria and Murphy, 2016, Ignar and Kuhn, 1990).

The corticosterone level was presented in Figure 5-9, and a trend toward an increase in the JUV-FEN group 321.6 ± 38.1 pg/ml vs 279.5 ± 40.6 pg/ml JUV-SAL was observed as an increase of the chronic marker for stress hormone release in JUV-FEN. In addition, the data was distributed between 100-550 pg/ml for both groups, which tend to be a big variance in a small study group. Similar results were provided in (Houshyar et al., 2001), which supported the increase of CORT level as an outcome of chronic morphine treatment. The significant variance in corticosterone levels was presented at several time points. As introduced earlier, postnatal opioid exposure results in significant stressful behaviour within the open field apparatus at adult rodent (Victoria et al., 2015), and similar stressful behaviours were observed in the offspring of morphine-treated dams, and an increase in CORT levels was attained (Ahmadalipour and Rashidy-Pour, 2015, Fodor et al., 2014). More details about the relation between opioid exposure, stress and corticosterone level could be found in section 1.8.3

Regarding the data presented in Figure 5-9, most of the data fell within a similar range of corticosterone level, but a single reading was higher in both groups, and 2-3 samples were markedly lower, which tend to be similar to (Ku Mohd Noor, 2017). An error in the preparations of the samples, such as hair weight, wash and buffer concentration, could result in a large distribution of the data. Yet, no significant difference was obtained through the sample's duplicate, which approves the quality of the ELISA technique conducted in the final stage. Due to the mice's small body size, short, thin hair coat, and uneven hair growth, the collection and analysis of mouse hair can be difficult. In humans and some larger veterinary species, hair grows significantly longer and, in some cases, at a predictable rate. So, the samples measured from different areas of the hair

shaft can indicate exposure over specific periods. Therefore, if the duration of the hair samples collected at a specific point in time is long enough, a degree of retrospective assessment of glucocorticoid exposure is viable. However, this would be challenging in C57BL/6 mice because the hair shaft has a maximum length of 1 mm (Erickson et al., 2017). In addition, different lifestyles and environments could affect the differences between humans and mice in hair sample assessment. For example, hair washing with shampoo solution and the use of cosmetic products may cause a decrease in cortisol in human hair (Stalder and Kirschbaum, 2012). Furthermore, humans are exposed to seasonal changes, whereas experimental rodents were kept in a cage with standard conditions, including constant temperature and light intensity (Dettenborn et al., 2012). A further methodological consideration is the methanol wash, which may dissolve some hair corticosterone before the extraction phase. Other solutions, such as isopropanol, could be used for the washing step in future studies (Erickson et al., 2017).

5.8 Summary

This chapter underlines the chronic effect of opioid exposure on the hypothalamic–pituitary–adrenal axis (HPA axis) and stress hormones. Opioid exposure is known to increase the secretion of the ACTH hormone and trigger the function of the HPA axis, which results in an increase in stress hormone concentration (cortisol in humans and corticosterone in rodents). In the current study, hair corticosterone, the chronic marker of the rodent's stress, showed a trend toward an increase in the JUV-FEN group. The plasma β-endorphins had a higher variation of data at different time points, and no statement could be given due to the low sample size. The weight data showed an increase in weight averages, collected at the age of 10-12 weeks, in the NN-FEN group.

5.9 Study limitations

The study was designed to have two groups besides JUV-FEN and JUV-SAL: NN-FEN and NN-SAL. The group NN group planned to have repeated opioid exposure at an earlier age (P1-P5). Yet, due to the time frame and licence renewal issues, the NN group could not be a part of the study. Due to the different means and nature of the studies conducted within this chapter on the mice group, it was challenging to meet the appropriate sample size in each group. For example, the weight data required a sample size of 40 mice to produce statistically robust data, while the sample size may differ in the other studies, hair corticosterone, for example. The plasma β-endorphins showed a variation in the data., which could be related to several factors, such as blood sample volume and sample bioavailability. Concerning the blood volume, the home office guidance was followed in mice species, and the only way to increase the sample volume was by conducting the experiment on rat species in a future study. The sample's bioavailability could be reserved in future work by completing the ELISA analysis on the same day of the sample's extraction. In this study, I had to arrange with an external lab to reserve the bench and tools for the ELISA experiment, and samples were stored in the fridge until the day of the analysis.

Chapter 6 The long-term effect of opioid exposure on μ-opioid receptor density within the CNS of ICR mice (autoradiography study)

6.1 Introduction

Mu opioid receptors (μOR) are distributed through the human CNS, with high densities in particular locations, such as the basal ganglia, cortex, thalamic nuclei, spinal cord and brainstem nuclei (Cross et al., 1987, Pilapil et al., 1987). The μOR distribution is based on the functional role of the receptors in controlling the behaviour, nociceptive modulation and physiological regulations (Gabilondo et al., 1995). See Table 6-1 for the full distribution of μOR within the rat brain In general, exogenous stimulation of the opioid receptor by the administration of opioid agonists impacts multiple cortical and subcortical sites. It influences the mesolimbic reward system within the nucleus accumbens (NaCC) and ventral tegmental region (VT) (Trigo et al., 2010).Also, μOR neural expression is identified within the amygdala, and it is conducted by GABAergic neurons of the central nucleus and intercalated cell mass (Winters et al., 2017). The μ-opioid agonists' inhibition of these neurons reduces the amygdala inhibitory input of the descending brainstem pain pathway (Han et al., 2015, Namburi et al., 2015). Those chronic changes of the μOR neural expression within the amygdala might affect the same receptors located at the neural breathing centres in the brainstem due to the systemic opioid exposure earlier in life and produce the long-term effect on the breathing pattern, which discussed in chapter 3.

In human studies, delayed maturity of the prefrontal cortex and a decrease in the subcortical projections may persist till adulthood, as a chronic change of CNS maturation, which are triggered by the early life opioid exposure (Squeglia et al., 2009). Also, changes in cortical thickness may occur after exposure to marijuana during early adolescence, diminishing in the middle, superior and frontal cortical regions accompanied by an increase of other brain regions' thickness, such as superior temporal and inferior parietal regions (Lopez-Larson et al., 2011). Methylphenidate (MP) as a medication example, which is used to treat the attention-deficit/hyperactivity disorder (ADHD), is categorised as norepinephrine–dopamine reuptake inhibitor (NDRI) and enhances the CNS by targeting dopamine the D2 receptor (D2R). Consuming MP in childhood results in chronic changes in D2R levels in the striatum, that affects the rewarding system, causing anxiety-like behaviour and affecting the plasma level of corticosterone (Bolanos et al., 2003, Thanos et al., 2007).Although morphological and structural

changes were triggered by early-life opioid exposure, the mechanism of these changes remains unclear.

Chronic exposure to exogenous opioids will result in alterations in the endogenous opioids system, where adaptive developmental changes occur and affect the tolerance to opioid compounds (Matthes et al., 1996). In addition, chronic exposure to opioid agonists leads to a decrease in the physiological response of the opioid's receptors, which is linked to three principal factors that are down-regulation, desensitisation and the loss of G-protein coupling (Zadina et al., 1995). Desensitisation and downregulation were reviewed due to chronic exposure to exogenous opioids (Trigo et al., 2010). Holaday et al. (1982) and Zadina et al. (1989) stated that μOR increased after the chronic exposure to opioids. Accordingly, μOR desensitisation and down-regulation start with the phosphorylation process triggered by G-protein-coupled receptor kinase (GRK). The phosphorylation process increases the μOR affinity to B-arrestin proteins, resulting in the uncoupling of G-protein signalling and internalisation (Trigo et al., 2010).The mentioned factors are hypothesised to cause the changes in μOR density, which could be triggered by the early life opioid exposure.

The chronic physiological changes were observed in the earlier chapters, for example, breathing pattern alterations, the attenuated anaesthesia vulnerability, and the hair corticosterone level trend. See chapters 3,4, and 5 for details. Therefore, the current study was designed to expose the mice to repeated opioid exposure at the age of P9-P13 to investigate the long-term neurological changes in the brainstem and cortex at the level of μOR distribution within the CNS.

Region	μOR	Region	μOR
Frontal cortex (laminar)	+++	Interpeduncular nucleus	++++
Piriform cortex (laminar)	++	Substantia nigra (pars compacta)	+++
Entorhinal Cortex (laminar)	++	Substantia nigra (pars reticula)	++
Amygdala	+++	Ventral tegmental area	++
Hippocampus (laminar)	+++	Periaqueductal gray	+
Dentate gyrus (laminar)	+++	Superior colliculi	++++
Olfactory tubercle	+	Inferior colliculi	++++
Nucleus Accumbens	++++	Dorsal raphe nucleus	++
Caudate putamen	++++	Parabrachial nucleus	+++
Globus pallidus	+	Nucleus raphe magnus	++
Medial septum	+++	Nucleus reticula	+
Thalamus periventricular nucleus	0	Nucleus tractus solitarius	++++
Thalamus Central-medial nucleus	++++	Lateral reticules nucleus	+
Thalamus reuniens nucleus	++++	Spinal trigeminal nucleus	+++
Medial habenula	+++		

Table 6-1 μOR distribution in a rat's brain
μOR are highly distributed within the neocortex, caudate-putamen, nucleus accumbens, thalamus, hippocampus, amygdala, inferior/superior colliculi and interpeduncular nucleus. Also, moderate clusters of μOR are located at the periaqueductal gray and raphe nuclei. Indeed, the μOR distribution corresponds to their role in sensory and pain regulations (Erbs et al., 2015, Mansour et al., 1988).

6.2 Study aim

To study the long-term effects of exposure to fentanyl P9-P13 on μ-opioid receptor (μOR) density within the CNS in mice.

6.3 Hypothesis

An early exposure to mu-opioid agonist (fentanyl) at the age of P9-P13 (juvenile mice) will induce a long-lasting change on the μOR density within the brain.

6.4 Methodology

6.4.1 Animals

The study was carried out under the UK Home Office regulations in accordance with the Animals (Scientific Procedures) Act, 1986. ICR mice were used in the study, and the group size was 6 female and 4 male mice, 5 control and 5 treated with fentanyl, and both groups were gender balanced. The 6 female mice were used in the first study (JUV-FEN n= 3 vs JUV-SAL n=3). The first group developed an artefact within the results and discarded; then a second group was added later, which contained 4 male mice (JUV-FEN n=2 vs JUV-SAL n=2). Pups were housed with their mother up to the age of P21, then they were placed in cages (3-4 mice per cage) according to their gender and tagged with ear piercing to identify each mouse. Food and water available ad-libitum.

6.4.2 Material and method

The mice involved in this study were reused from chapter 5, and the brain samples were collected at the terminal stage of the study. The mice had received fentanyl citrate (Janssen-Cilag, UK) (0.04 mg/kg i.p.) between P9-P13 for the JUV-FEN group (n=5). The control group (JUV-SAL) (n=5) were injected with an equivalent volume of the normal physiological saline on the same days. After that, the mice were housed in the animal house (VRF) in Garscube and euthanised at the age of 12 weeks (phenobarbital 0.1 ml intraperitoneally) (Sigma-Aldrich, UK). The brain was then dissected and immersed into isopentane at -40^{O}C for two minutes (Sigma-Aldrich, UK). See Figure 5-3 .Afterwards, the brain samples were stored in a freezer at -80^{O}C for cryostat sectioning. Before the cryostat process, the brains were retrieved from the -80^{O}C freezer, and each sample was cut coronally at the midpoint between the brainstem and cortex. Each part was fixed on a separate chuck and covered with Cryomatrix (Thermo Fisher Scientific, Cheshire, UK), for segmenting later. Sections were cut at 20 μm using a cryostat (Zeiss Microm 505E); sections were mounted on super frosted slides (6-8 sections/slide) (Thermo Fisher Scientific, UK) and stored in the -80^{O}C freezer for the autoradiography process later. See Figure 6-1.

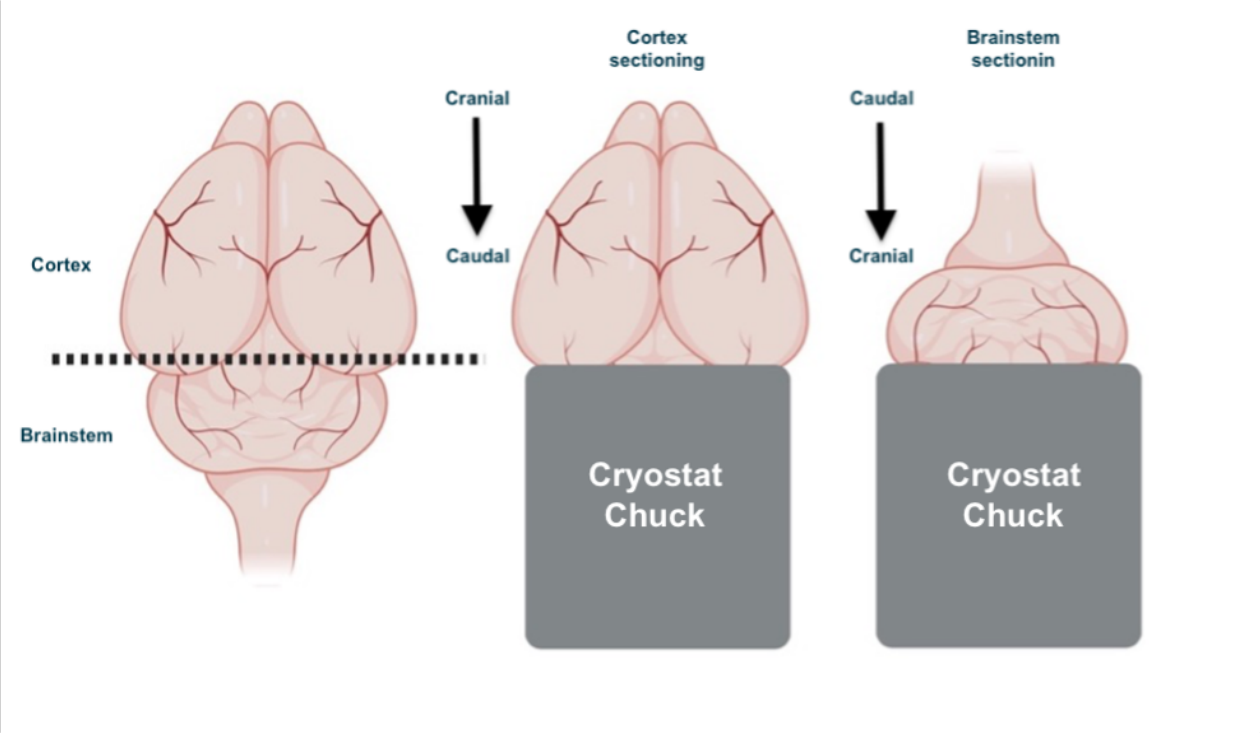

Figure 6-1 Brain samples orientation on chucks for micro-sectioning
The brain was cut into two parts (cerebral cortex and brainstem) at the level of the dotted line. Each piece was mounted on the chuck and cut individually. The cortex sectioning was done craniocaudal, and the brainstem part was cut in the caudal-cranial direction.

Forty-two slides were selected for each mouse to be involved in autoradiography analysis. Thirty slides were taken from the brainstem part, and 12 slides were selected from the brain (6 from the frontal lobe, 6 from the parietal lobe and 5 from the brainstem). The sections were taken in a continuous order caudally; the frontal lobe coronal sections started from 1.78 mm from bregma, the parietal lobe coronal sections started from –3 mm from bregma, and the brainstem coronal sections started from –5.68 mm. The slides were laid on cardboard and placed within the cassettes, facing the Kodak film (14 slides/ cassette + 1 standard slide + 1 non-specific slide). An additional time control test cassettes were included in the study, to be opened before the sample's cassettes to ensure the exposure development on films at the 9, 12 and 15 post-incubation. Once the film exposure was completed, the remaining films were taken off the cassette and developed by 50% Kodak D-19 developer. See Figure 6-3.

An additional group (second group) of mice were added later to the study, a sum of 4 (JUV-SAL, n=2 males and JUV-FEN, n=2 males). The group went through the same protocol procedures, starting from the housing until the washing part that occurred after the isotope [^{3}H] (DAMGO) incubation. However, newer slides, isotopes, films and cassettes were brought to avoid the artefact issue that developed in the first study group. The coronal sections were taken at the following areas (frontal lobe, parietal lobe and brainstem) with a determined distance in reference to Bregma, based on (Paxinos and Franklin, 2019). In the end, the slides had been exposed to films for 20 weeks (see Figure 6-2).

A pre-incubation step was taken by rinsing the slides into a 50 mM Tris-HCl buffer, 3 times/5 minutes each. Afterwards, specific binding slides (SBS) were incubated into 4 nM [^{3}H] D-Ala-MePhe-Gly-ol enkephalin (DAMGO) (Perkin-Elmer Life Sciences) for 60 minutes at room temperature. Once the incubation was completed, another wash was conducted by a Tris buffer, 3 times / 5 minutes each. Additionally, non-specific binding slides (NBS) had a 1 μM of naloxone (Sigma-Aldrich, UK) added to the 4 nM [^{3}H] (DAMGO) solution to prevent the binding of isotopes to μ-opioid receptors.

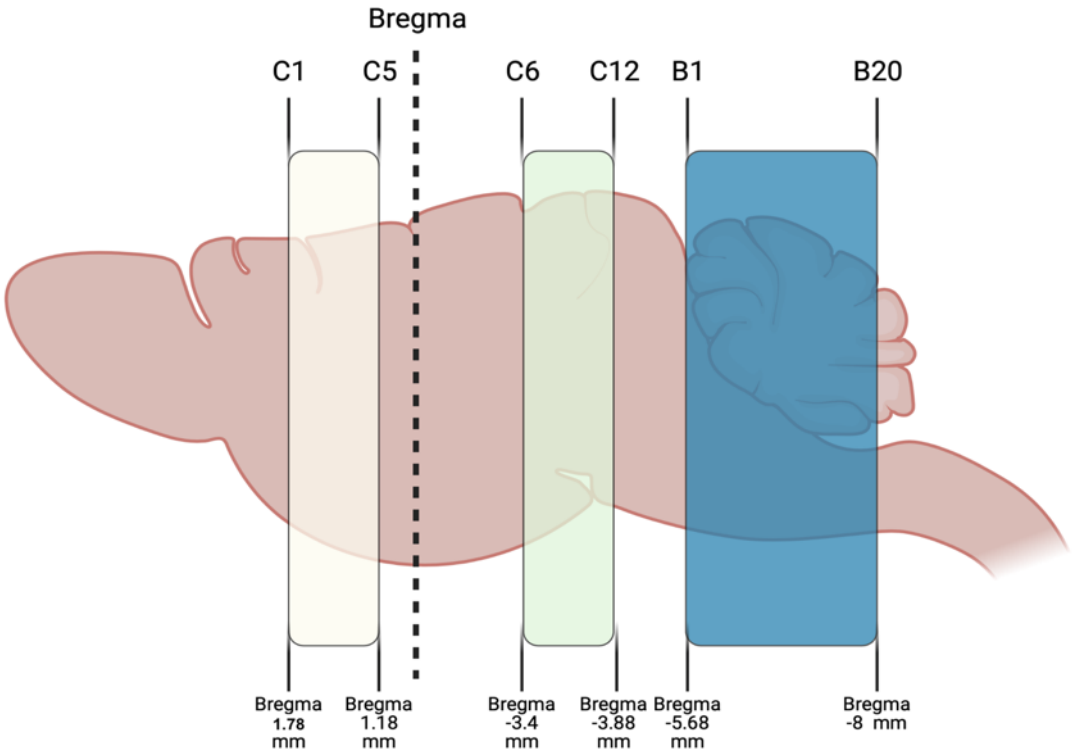

Figure 6-2 Coronal section sampling through the brain regions
The figure provides an approximate illustration of the regions included in the autoradiography study. Starting with the frontal lobe at the range of 1.18 mm to 1.78 mm from the bregma, the parietal lobe is located between -3.4 mm to -3.88 mm from the bregma. The brainstem region is identified in the following sections -5.68 mm to -8 mm from the bregma See Figure 6-3.

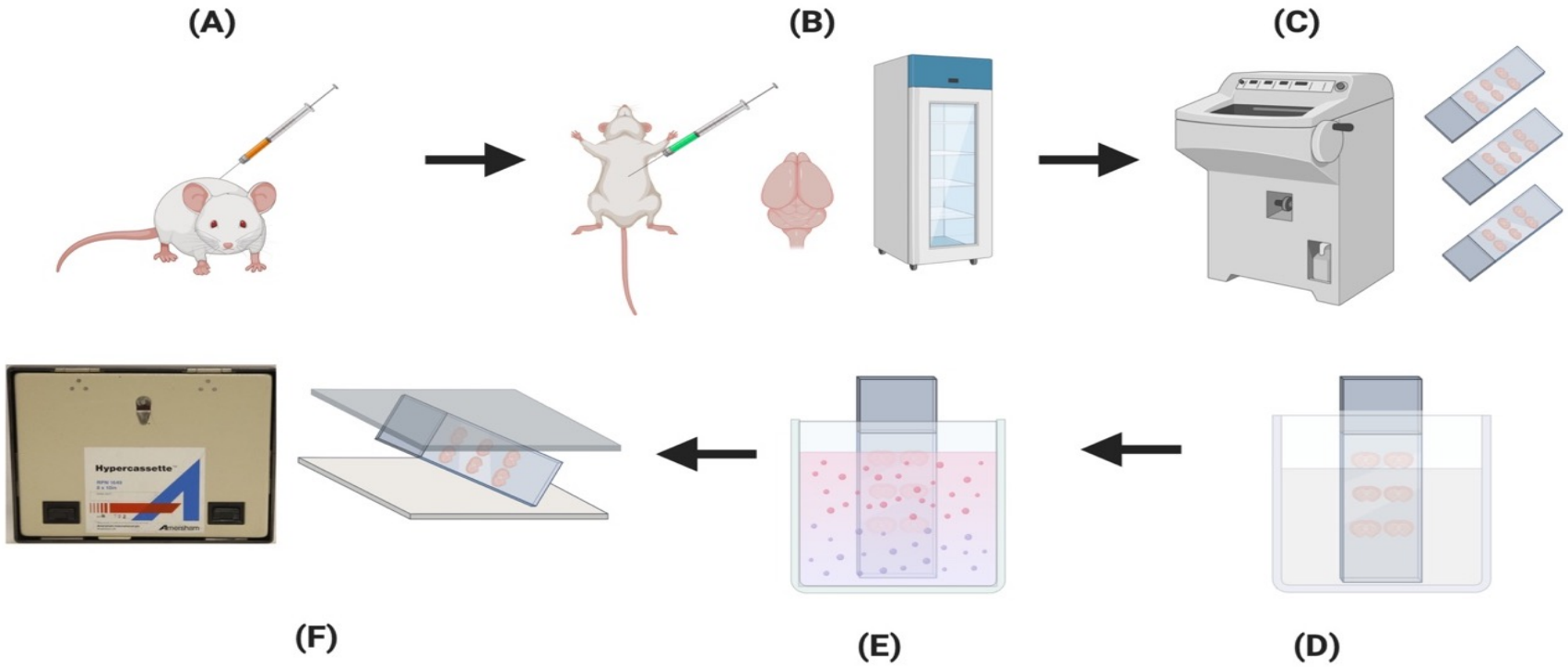

Figure 6-3 Autoradiography methodology

The experiment started at the juvenile (A) age when the mice were injected with fentanyl 0.04 mg/kg i.p. once daily from P9 to P13. After that, the mice were housed and left to thrive up to the age of 12 weeks, (B) when an injection of phenobarbital is given 0.1 ml i.p. once to euthanise the mouse. Once the mouse was euthanised, the brain was dissected and stored in -60 ^{O}C isopentane then placed in a vial and stored in a -80 ^{O}C freezer. Next, (C) the brain samples were retrieved, and a micro-section cut took place to execute 20 μm samples on several brainstem and cortex levels. Then, the samples were mounted on frosted slides (D) washed in (50 mm Tris-HCl 7.4 ph.) buffer, and (E) incubated into 4 nm [^{3}H] DAMGO. Finally, (F) slides were lined on white cards and exposed to Kodak biomax films for 12-15 weeks.

6.5 Data analysis

Films were processed by the IMC image analyser (Imaging Research, Canada), which is a video-based computerised densitometry software. A standard curve was established concerning the ^{3}H-microscale (Amersham, UK) placed beside the slides within the cassette and exposed to the film for the whole exposure period. Calibration values (femtomole/milligram) were set regarding the ^{3}H-microscale and its density that was displayed by the MCID software. The average of the sample's density was determined, referring to the standard curve based on the ^{3}H-microscale calibrated values.

6.6 Statistical analysis

Graphs were drawn using GraphPad Prism 4. Since only two samples were obtained per group, no statistical analysis was possible and preliminary data is presented

6.7 Results

6.7.1 First group

The first batch (3 control females and 3 fentanyl-exposed females) presented an artefact that affected most of the films and produced a cross-contamination, which overlapped the sections and made it difficult to analyse them. The contamination was developed due to previous samples, rat brains, placed within the same cassettes in previous studies conducted before the recent research. A leakage sign of the isotope, which could be caused by the poor hydrophobic marking of the samples, was observed in some slides. An overlap of the section developed on some films, where older sections developed on the recent slides used in the study. The films developed from this batch were excluded, and newer films were exposed for another 15 weeks, but a similar artefact and cross-contamination occurred. See Figure 6-4 and Figure 6-5.

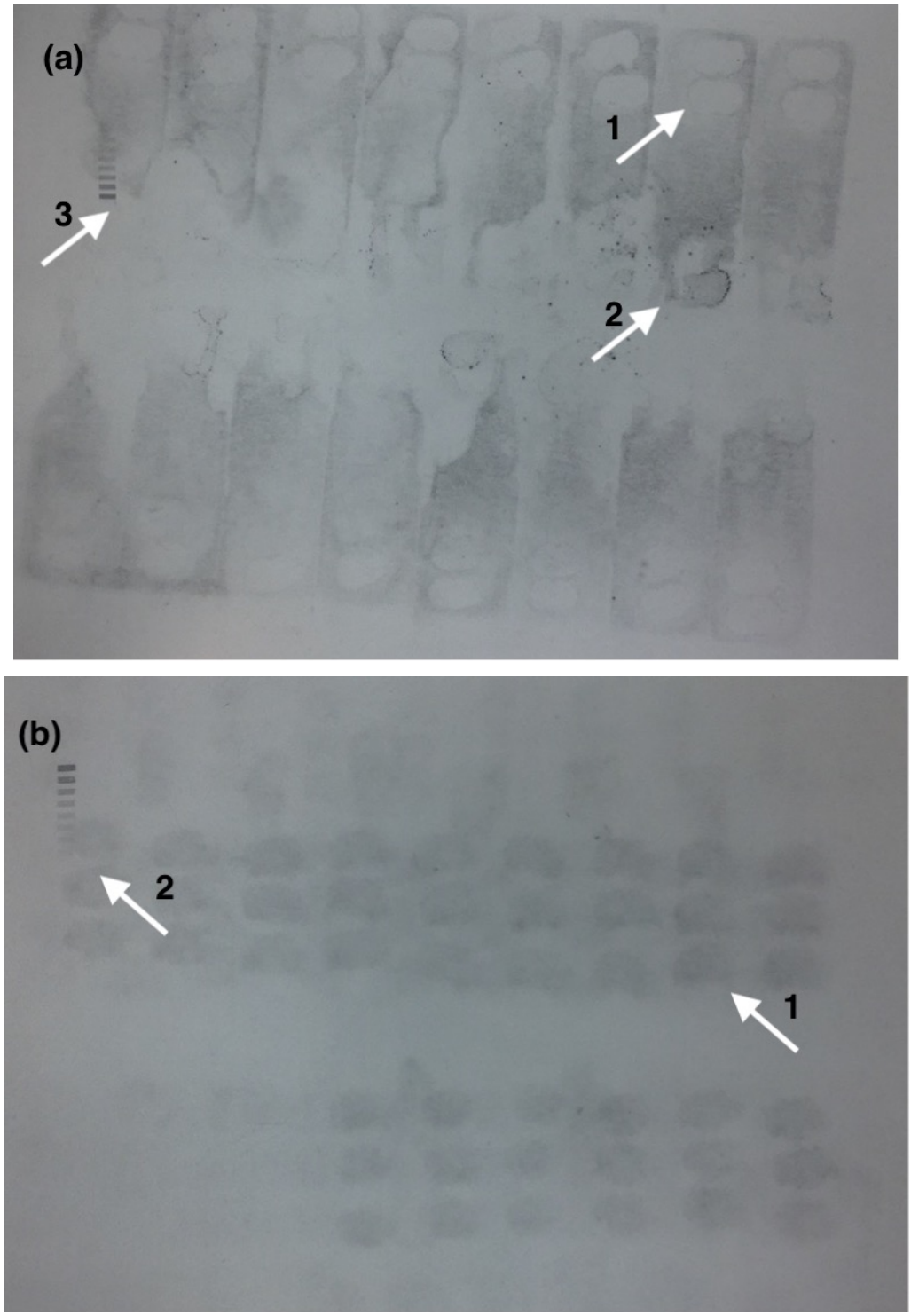

Figure 6-4 Autoradiographic artefact developed in the films
Some films were affected by an artefact that overlapped the results and made it difficult to interpret the data. Both films showed signs of maldevelopment of the isotope and so they were excluded from the study. The (a) picture shows a rat size brain sample in 1, and a leakage sign of the isotope at 2, which could be caused by the poor hydrophobic marking of the samples. Also, an arrow at 3 shows that the samples overlap with the standard, suggesting a development from previous samples or cross-contamination. Picture (b) 1 points to a rat brain sample, which is larger than the mice brain samples used in the study. Also, the samples overlap the standard at the 2 arrow, which suggests the cross-contamination of the film.

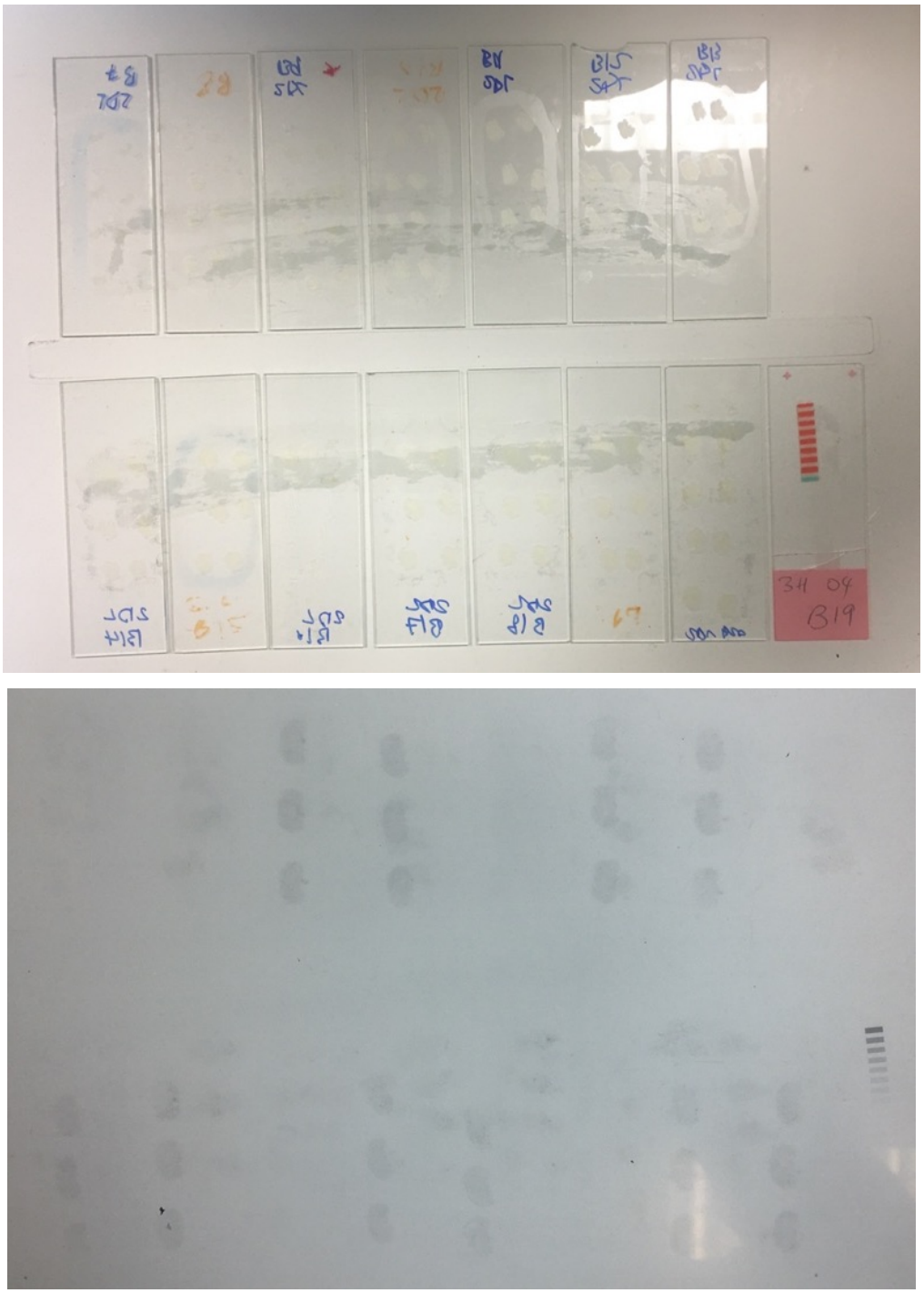

Figure 6-5 Cross-contamination of rat's brain samples that developed on the films
Some films had developed different isotope exposure to the ones we used on our sample. As shown in the pictures, the films' developed density had different arrangements from our slides. The samples' size was more prominent than the mice brain, more likely to be rat's samples that were stored in the same cassettes previously. These films were excluded from the study too.

6.7.2 Second group

Although the first batch of animals showed cross-contaminated films, the second group succeeded in developing results on the films and provided data for the designated experimental groups (JUV-SAL n=2 and JUV-FEN n=2). Some anatomical spots presented a higher density of μOR distribution through the coronal sections taken across the brain samples. For example, neocortex (NC) and nucleus accumbens (NaCC) presented a high μOR density in the sections taken from the frontal lobe (see Figure 6 6). In addition, interpeduncular nucleus (IP), amygdalopiriform transition area (ATA) and posteromedial cortical amygdaloid nucleus (PCAN) showed a higher density of μOR in the coronal sections taken from the parietal lobe (see Figure 6 7).

Brainstem samples presented an increase in μOR density at the area between -5.68 mm from bregma until -8 mm, but no certain area or nucleus could be distinguished to highlight the anatomical hotspot of μOR within the brainstem (see Figure 6 8). Some slides presented artefacts on the films and were excluded from the μOR quantitative analysis (see Figure 6 9). The numbers of slides excluded are 1 from JUV-SAL brainstem and 5, JUV-FEN brainstem and 2 from JUV-FEN cortical sections.

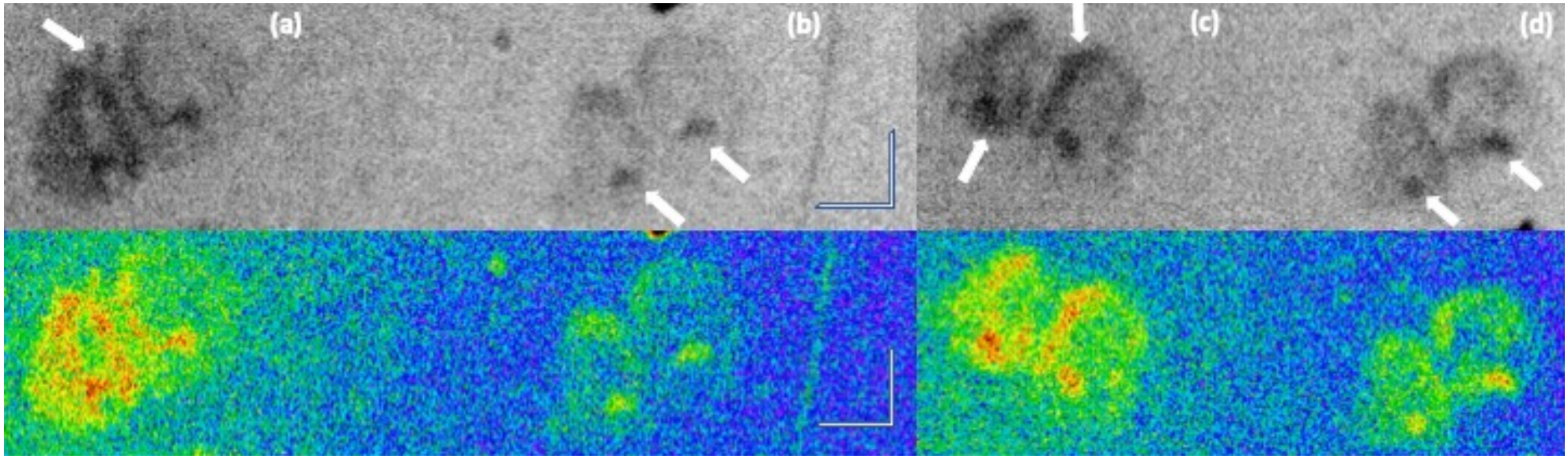

Figure 6-6 Coronal sections of frontal lobe autoradiography brain samples
The upper row presents the coronal section samples taken from the frontal lobe in monochrome resolution. The lower row is the computer-enhanced images for the same sample above. (a) shows a higher density of μOR located at the neocortex. The arrows in (b) are pointing to the nucleus accumbens (NaCC), representing a high density of μOR. Neocortex and NaCC are pointed at again on (c). Yet, a clearer image of NaCC μOR density can be obtained on (d). The calibrating measure is 1 mm each way.

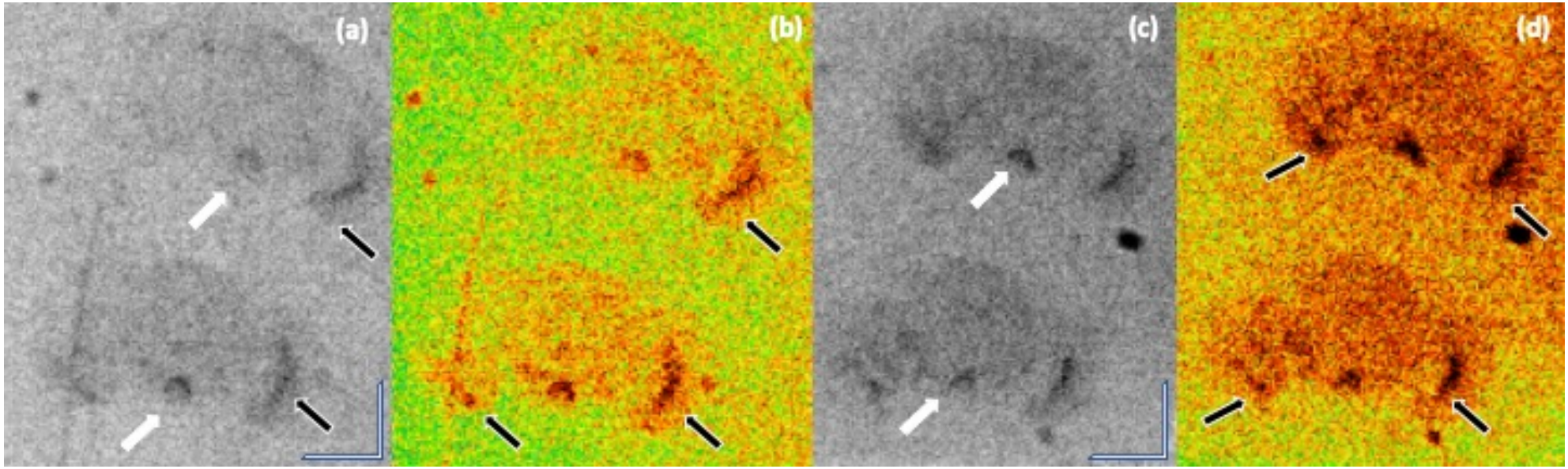

Figure 6-7 Coronal sections of parietal lobe autoradiography brain samples
The columns present coronal section samples from the parietal lobe in monochrome resolution (a) and (c), which is supplemented by the computer-enhanced images for the same samples (b) and (d). Correspondingly, an increase of μOR density is noticed in (a), and the white arrow is pointing to the interpeduncular nucleus (IP), and the black arrows point to the amygdalopiriform transition area (ATA) and posteromedial cortical amygdaloid nucleus (PCAN). Again, (ATA) and (PCAN) are highlighted by black arrows in pictures (b) and (d) while (c) represents an additional section of μOR distributed at IP, which is clear in the enhanced image (d) of the same coronal section. The calibrating measure is 1 mm in each way.

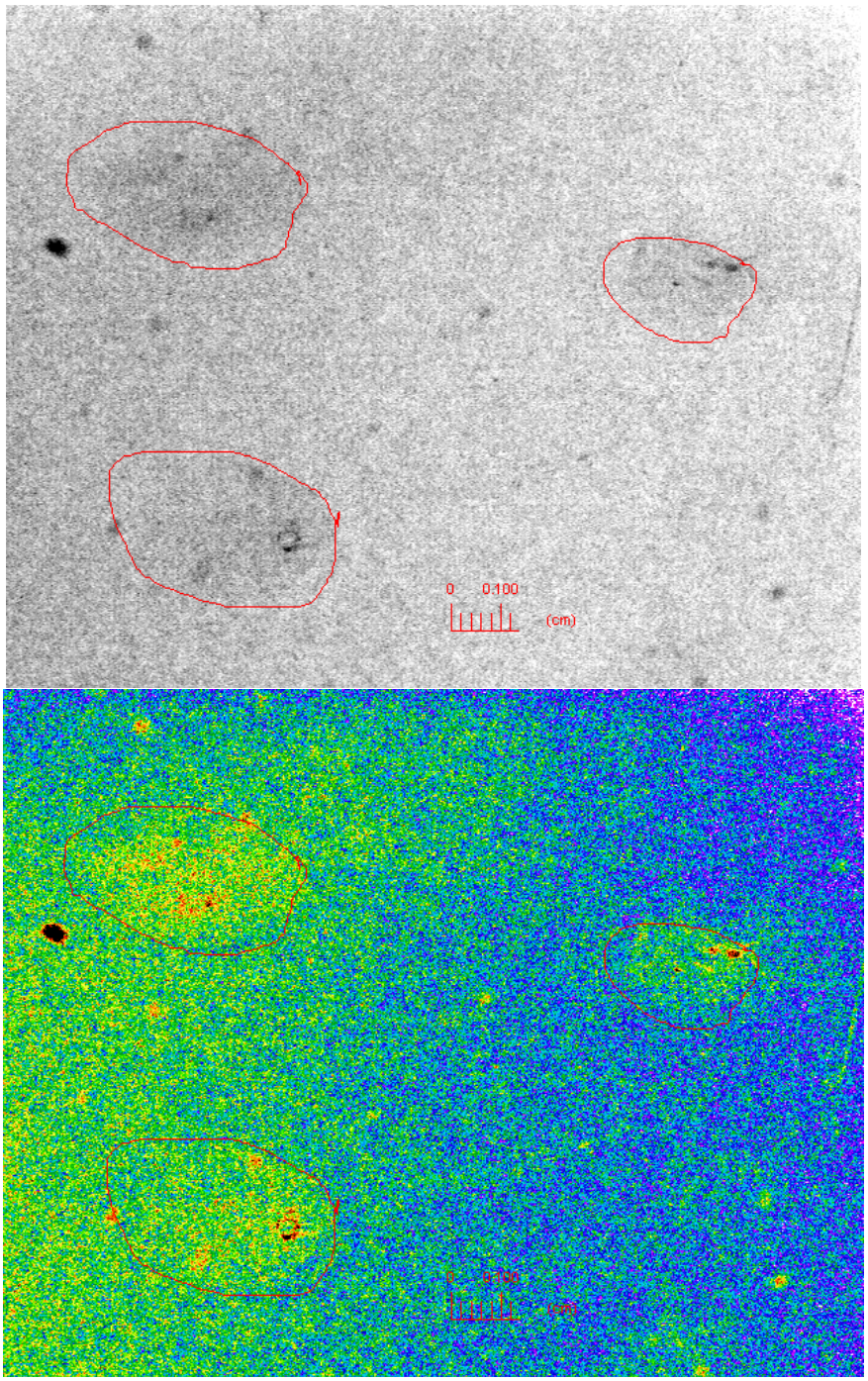

Figure 6-8 Coronal sections of brainstem autoradiography brain samples
The brainstem's coronal sections showed a density of μOR distribution through the regions of interest seen in both pictures (monochrome above photo and computer-enhanced below pictures). The coronal sections were highlighted in the pictures, and the average μOR distribution was taken for each section.

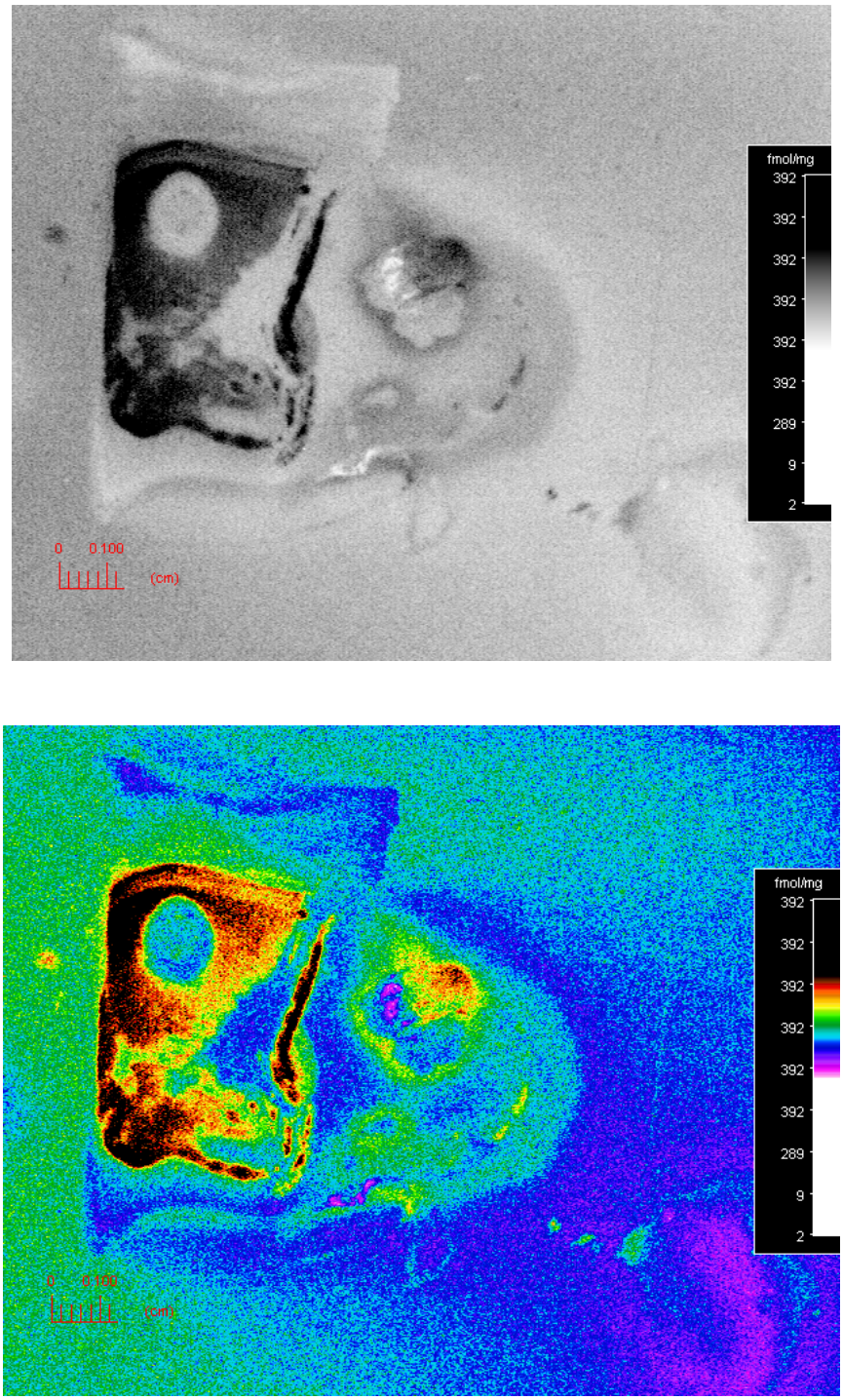

Figure 6-9 Excluded slides due to a developmental artefact during the exposure process
Some of the slides had an artefact at the time of exposure, and the sample's sections were affected. The artefact interferes with the μOR density on the films and exhibits false levels of densities in the films.

The quantitative distribution of μOR across the same coronal section of the frontal lobe, parietal lobe and brainstem are provided in the following tables: Table 6-2 Quantitative μOR distribution at the frontal lobe (1.78 to 1.18 mm from the bregma)Table 6-3 Quantitative μOR distribution at the parietal lobe (-3.4 mm to -3.88 mm from the bregma).Table 6-4 Quantitative μOR distribution at the brainstem region (-5.68 mm to -8 mm from the bregma). An increase of the μOR density is observed through the coronal section caudally to the level of 1.18 mm from the bregma in JUV-SAL (n=2). The parietal lobe showed an increase of μOR distribution obtained at the following levels -3.48- and -3.72-mm. In the brainstem, some regions present higher densities of μOR, such as -5.68 mm, -7.3 mm, and -7.88 mm. No μOR densities were obtained at -6.84 in both groups, JUV-SAL and JUV-FEN. The treated group (JUV-FEN, n=2) showed no difference in the μOR distribution across coronal sections taken from the frontal and parietal lobes compared to the JUV-SAL group. The parietal lobe presents no difference from JUV-SAL of μOR distribution at the following coronal sections -3.48 and -3.72 mm. The μOR did not develop any isotope signs at the following levels -6.49 to -6.96 mm, and from -7.19 to -7.42mm. See Table 6-4

Distance from bregma (mm)	Mice group			
	JUV-SAL		JUV-FEN	
1.78	27.24	21.43	17.11	19.19
1.63	38.12	20.59	20.4	27.06
1.48	36.46	23.02	N/A	32.01
1.33	34.82	25.66	15.99	19.32
1.18	29.81	32.76	17.11	33.32

Table 6-2 Quantitative μOR distribution at the frontal lobe (1.78 to 1.18 mm from the bregma) The table shows the μOR distribution across the coronal sections taken from the frontal lobe in both experimental groups, JUV-SAL n=2 and JUV-FEN n=2. The data is presented in fmol/mg, and the N/A refers to no development detected in the coronal section.

Distance from bregma (mm)	Mice group			
	JUV-SAL		JUV-FEN	
-3.4	29.29	22.94	20.47	27.08
-3.48	37.51	24.48	48.97	17.03
-3.56	30.74	16.45	23.49	21.35
-3.64	28.57	23.79	N/A	17.47
-3.72	38.39	22.62	38.12	20.54
-3.8	N/A	25.59	23.46	16.19
-3.88	N/A	22.88	N/A	20.26

Table 6-3 Quantitative μOR distribution at the parietal lobe (-3.4 mm to -3.88 mm from the bregma).
The table shows the μOR distribution across the coronal sections collected from the parietal lobe in both experimental groups, JUV-SAL n=2 and JUV-FEN n=2. The data is presented in fmol/mg, and the N/A refers to no development detected in the coronal section.

Distance from bregma (mm)	Mice group			
	JUV-SAL		JUV-FEN	
-5.68	40.7	19.42	N/A	7.6315
-5.8	27.7	16.64	11.39	N/A
-5.91	39.6	22.55	33.09	28.63
-6.03	22.9	24.66	17.6	32.54
-6.14	19.2	27.61	24.89	19.1
-6.26	14	24.83	N/A	14.44
-6.38	17	24.31	N/A	18.77
-6.49	26.1	17.81	N/A	N/A
-6.61	21.3	24.01	N/A	N/A
-6.72	28	N/A	N/A	N/A
-6.84	N/A	N/A	N/A	N/A
-6.96	N/A	15.84	N/A	N/A
-7.07	30.6	21.94	26.04	17.54
-7.19	25.7	25.89	N/A	N/A
-7.3	39.4	44	N/A	N/A
-7.42	25.4	22.91	N/A	N/A
-7.54	26.6	24.46	26.76	14.4
-7.65	28.9	N/A	9.43	11.64
-7.77	27.4	27.09	21.25	29.84
-7.88	35.2	N/A	N/A	13.06
-8	27.4	10.7	9.84	12.5

Table 6-4 Quantitative μOR distribution at the brainstem region (-5.68 mm to -8 mm from the bregma)
The table shows the μOR distribution across the coronal sections collected from the brainstem in both experimental groups, JUV-SAL n=2 and JUV-FEN n=2. The brainstem region showed no μOR distribution in the areas between -6.49 to -6.96 mm, and -7.19 to 7.42 mm.

6.8 Discussion

6.8.1 Autoradiography artefact

In regard to the first group introduced in the autoradiography study, artefacts were observed in the films right after development. The technical artefacts may occur due to several errors, such as contaminated isotope, variable thickness of histological sections, overpressure of the developing films laid upon the slides, and so on. The radioisotope may present false data by applying an excessive amount or concentration on the samples. This may trigger an unphysiologically reaction that affects the film's tissue development (Leblond et al., 1950). Moreover, histological processing may cause technical artefacts due to poor fixation and uneven thickness of the sampling, which had been described by (Fink, 1951, Winteringham et al., 1950). Also, the pressure effect should be considered when the films are laid into cassettes for the period of exposure, and it was addressed by (Doniach and Pelc, 1950, Yagoda and Yagoda, 1949). In addition, film developing remains a sensitive step, affecting the data and resulting in streaks and spotty effects on the film, if an error occurs through the photographic processing phase (Sonka and Grunkin, 2002). Technical artefacts may occur in any step of the autoradiography experiment, and good practice and great care must be taken through all stages of the experiment, from the beginning of section segmentation to photographic development.

Here are some recommendations by (Odeblad, 1953):

- Check the radioisotope solutions for any sort of contamination.
- Proper histological sectioning and fixation.
- Avoid touching the emulsion surface by hand.
- Avoid excessive pressure once laying the films on slides.
- Use a clear and filtered solution for film development and fixation.
- Maintain the tidiness of the dark (development room).

The recommendations for autoradiography (AR), are similar to other tissue processing and visualisation studies, such as immunohistochemistry (IHC), where precision and hygiene are the key factors for conducting a successful experiment. Nevertheless, additional steps should be considered for AR work, as mentioned above. Accordingly, this study had a long preparation period, which starts with pups being born, injected with fentanyl or saline, housed till they are 10 weeks old, euthanised, followed by brain micro-sectioning, incubation and 20 weeks of film exposure after that. Therefore, tracing artefacts' origin could lead to any technical mistake made from day 1 until the development and fixation part 9 months later. Hence, in our first batch, we exposed the slides to other films after the initial cross-contamination appeared. As mentioned in the results, similar artefacts appeared again on the films, where some technical errors had been excluded, such as excessive pressure on tissues and film development. Still, contaminated radioisotope, improper histological sectioning and contaminated cassettes were considered the triggers of the artefact that affected the first group. Therefore, the second batch of mice was introduced to the brain sectioning part. A newer radioisotope was used; different cassettes were also brought for this group, which succeeded in developing and providing the μOR distribution data brain regions.

6.8.2 μOR distribution in CNS

The additional group (JUV-SAL n=2 and JUV-FEN) successfully developed the μOR isotopes on the films. The data are presented on the following tables: Table 6-2 Quantitative μOR distribution at the frontal lobe (1.78 to 1.18 mm from the bregma)Table 6-3 Quantitative μOR distribution at the parietal lobe (-3.4 mm to -3.88 mm from the bregma).Table 6-4 Quantitative μOR distribution at the brainstem region (-5.68 mm to -8 mm from the bregma).

μ opioid receptors are densely distributed within brain regions, such as the nucleus accumbens, thalamus, hippocampus, amygdala, and inferior/superior colliculi (see Table 6-1). In the present study, μOR density increased in JUV-SAL and JUV-FEN in the same areas. In addition, the red nuclei and superior colliculus had a denser distribution of μOR. In addition μOR could be detected in all coronal sections taken from -3.4 to -3.88 mm from the bregma in both study groups (JUV-SAL and JUV-FEN). This increase was observed similarly by (Kitchen et al., 1997) at the area between -3.4 to -3.64 mm from the bregma. (See Table 6-3). In the brainstem area, which is identified between -5.68 to -8 mm from the bregma, μOR was observed in all the coronal sections taken from JUV-SAL n=2, apart from the -6.48 mm level, which showed no development of μOR. The JUV-FEN group showed an absence of μOR in several coronal sections and a reduction of μOR across the brainstem. (See Table 6-4) The brainstem region is known to have a high distribution of μOR, starting with the IP, which is followed by the parabrachial nuclei, locus coeruleus, nucleus of the lateral lemniscus, caudal subnucleus, paratrigeminal nucleus, nucleus of the solitary tract, ambiguous nucleus and inferior olivary nuclei (Ding et al., 1996, Erbs et al., 2015). The data collected from the samples remain underpowered due to the small sample size of the study groups, and no further statistical analysis was performed. This group was added to trace the artefact that produced the earlier cross-contamination on the previous samples in section 6.7.1, and the potential source of cross-contamination was discussed in section 6.8.1

The change in the μOR distribution is assumed to be triggered by the early exposure to opioids. A decrease in opioid tolerance and receptor response was found in earlier studies that investigated the long-lasting alterations of chronic opioids exposure (Matthes et al., 1996); (Zadina et al., 1995).To understand the decrease of μOR density, quantitative models were introduced in several studies to analyse μOR desensitisation triggered by opioid agonist exposure in short- and long-term treatment. Accordingly, a loss of 80-95% of μOR functional surface was accountable for the shift of the morphine concentration-response curve (Chavkin and Goldstein, 1984, Osborne and Williams, 1995, Bailey et al., 2009). Therefore, μOR tolerance (desensitisation) was measured quantitively by the loss of more than 80 % of the functional surface. Desensitisation recovery was variable concerning the exposure duration. For example, one hour was the estimated recovery duration of rapid desensitisation (Harris and Williams, 1991, Dang and Williams, 2004, Virk and Williams, 2008) while chronic opioid exposure required two phases to attain full recovery. The first phase was completed within 2 hours after disconnecting morphine administration, and the second phase persisted for several hours after that and was accompanied by tolerance (Bailey et al., 2009, Christie et al., 1987).

Concerning μOR functionality and distribution, some measures should be considered within the study. For example, receptor redistribution between cellular compartments, plasma membrane and intracellular compartments (Williams et al., 2013). Henceforth, chronic exposure to morphine produces alterations of the opioid receptors distribution across the brain region (Stafford et al., 2001, Koch and Höllt, 2008). Yet, an assay analysis for GPCR in situ after chronic heroin exposure had indicated a decrease of μOR in several brain regions, combined with an increase of total opioid receptors number (Sim-Selley et al., 2000). A limited number of studies examined the μOR distribution at the cellular level following chronic exposure to opioids. A remarkable redistribution of μOR from the plasma membrane to intracellular compartments was observed by (Drake et al., 2005) after chronic morphine treatment. Also, anatomical reallocation stated by (Van Bockstaele and Commons, 2001) once chronic opioid exposure leads to decreased opioid receptors within locus coeruleus, but internalisation of NaCC neural dendrites is triggered by an acute administration of morphine (Haberstock-Debic et al., 2003). Thus, different administration

protocol, duration, antibodies and cellular levels of analysis may produce variable results of μOR distribution; and the clear picture of the opioid exposure effect on μOR remains uncertain.

6.9 Summary

The study was designed to investigate the changes in μOR density within the brain region. This counts as a continuation of the investigation of postnatal opioid exposure. The autoradiographic μOR mapping was applied in this study, and the initial group included was 3 control (JUV-SAL) and 3 treated (JUV-FEN). The cross-contamination appeared on the films, and additional groups were involved in the study with 2 control mice and 2 treated mice. The latter showed a slight decrease of μOR density across the brain regions in the JUV-FEN group, compared to JUV-SAL. Nevertheless, the presented data was underpowered regarding the small sample size involved in this additional group.

6.10 Study limitations

Cross-contamination had affected the first study group n=6, and the slides were discarded. In the second group, I solved the technical problem but still ran out of time to include more mice and another group due to the license renewal issue, which was followed by the COVID-19 outbreak.

Chapter 7 The long-term effects of the early opioid exposure on the neural expression of μ opioid receptor within the ICR mice brainstem (Immunohistochemistry)

7.1 Introduction

Regarding the results discussed in chapter 3, early repeated exposure to opioids tends to cause a decrease of the resting respiratory rate and increase tidal volume response to awake fentanyl challenge in the NN-FEN group. Indeed, the chronic effect on breathing patterns could be triggered by the histological changes in the μOR neural expression within PreBötC, such as NK1R and μOR. Accordingly, PreBötC and RTN/pFRG are principal respiratory neural clusters (Smith et al., 1991, Onimaru and Homma, 2003, Varga et al., 2020); the histological alterations will help to understand breathing function. In addition, the systematic administration of fentanyl could trigger an indirect effect on breathing function by influencing other physiological tasks, such as the cardiovascular system (Pattinson, 2008). Repeated exposure to fentanyl was proven to alter the μOR regulation through the brain regions by developing tolerance and insensitivity to opioid exposure (Bhargava and Gulati, 1990, Bernstein and Welch, 1998, Stafford et al., 2001). Since PreBötC neurons express a high level of μOR (Montandon et al., 2011, Nagappa et al., 2017), the defect of neural expression within PreBötC leads to breathing patterns abnormalities (McKay, 2005). Therefore, repeated exposure to fentanyl could deliver the breathing pattern changes through this respiratory-related brain area by affecting the expression of μOR.

7.1 Study aims

To analyse the changes of μ opioid receptor expression within the ventrolateral respiratory column following postnatal repeated exposure to fentanyl (P9-P13), using the immunohistochemical technique.

7.2 Hypothesis

The repeated exposure to fentanyl (μ opioid agonist) at P9-P13 will result in long-lasting decrease of μ opioid receptors' neural expression within the brainstem.

7.3 COVID-19 impact

The pandemic situation affected this study. Starting with the national lockdown started in March 2020, IHC processing the naïve brain sample was carried out, and only some samples were incubated and mounted on slides at the time. As it lasted for 12 months, the non-processed samples were destroyed, and only the mounted sections were ready for microscope visualisation. As the study was carried out in March 2020, it was challenging to include the JUV-FEN group (fentanyl exposed between P9-P13) into the experimental design, due to the limited time frame and the renewal requirements for Home Office licence application. In addition, a confocal visualisation and counting of the immunopositive cells was planned. Access to the device was limited at the time of the analysis and the priority was given to essential research works at the campus. Therefore, an epifluorescence microscope was to collect images from the samples' sections.

7.4 Methodology

7.4.1 Animals

The experimental procedures were conducted under the licence from the UK Home Office in accordance with the Animals (Scientific Procedures) Act, 1986. Experiments in this chapter were performed on male ICR mice. The mice were bred at the Spinal Cord Group department (Sir James Black Building), and a total of 4 (naïve) adult mice were included. A 12-hour light/dark cycle was maintained, with food and water available ad libitum.

7.4.2 Perfusion and micro-sectioning

The mice were euthanised at the age of 6 weeks using a lethal dose of Phenobarbital 0.1 ml i.p., once. The mice were perfused transcardially with paraformaldehyde 4%, then the brain extracted and immersed into a 30% sucrose vial. After that, brain samples were rinsed with 0.3M PBS buffer and sectioned via Vibratome into 60-micrometer samples for the whole sample. Brain samples were immersed in Glycerol and stored in a freezer at -20 ^{o}C. On the day of incubation, samples were retrieved and rinsed with PBS before the IHC antibodies processing.

7.4.3 Incubation and antibody combination

The immunohistochemistry process was carried out in collaboration with Dr David Hughes' lab (Spinal Cord Group) at the main campus of Glasgow University. Samples were incubated in the primary antibody over the weekend; then, a secondary antibody was added and kept for 24 hours. Once the incubation is completed, samples were rinsed with PBS buffer, then mounted on a microscope slide (Thermo Fisher Scientific, UK) that contained glycerol and covered with a slipcover (Academy, UK). See Figure 7-1.

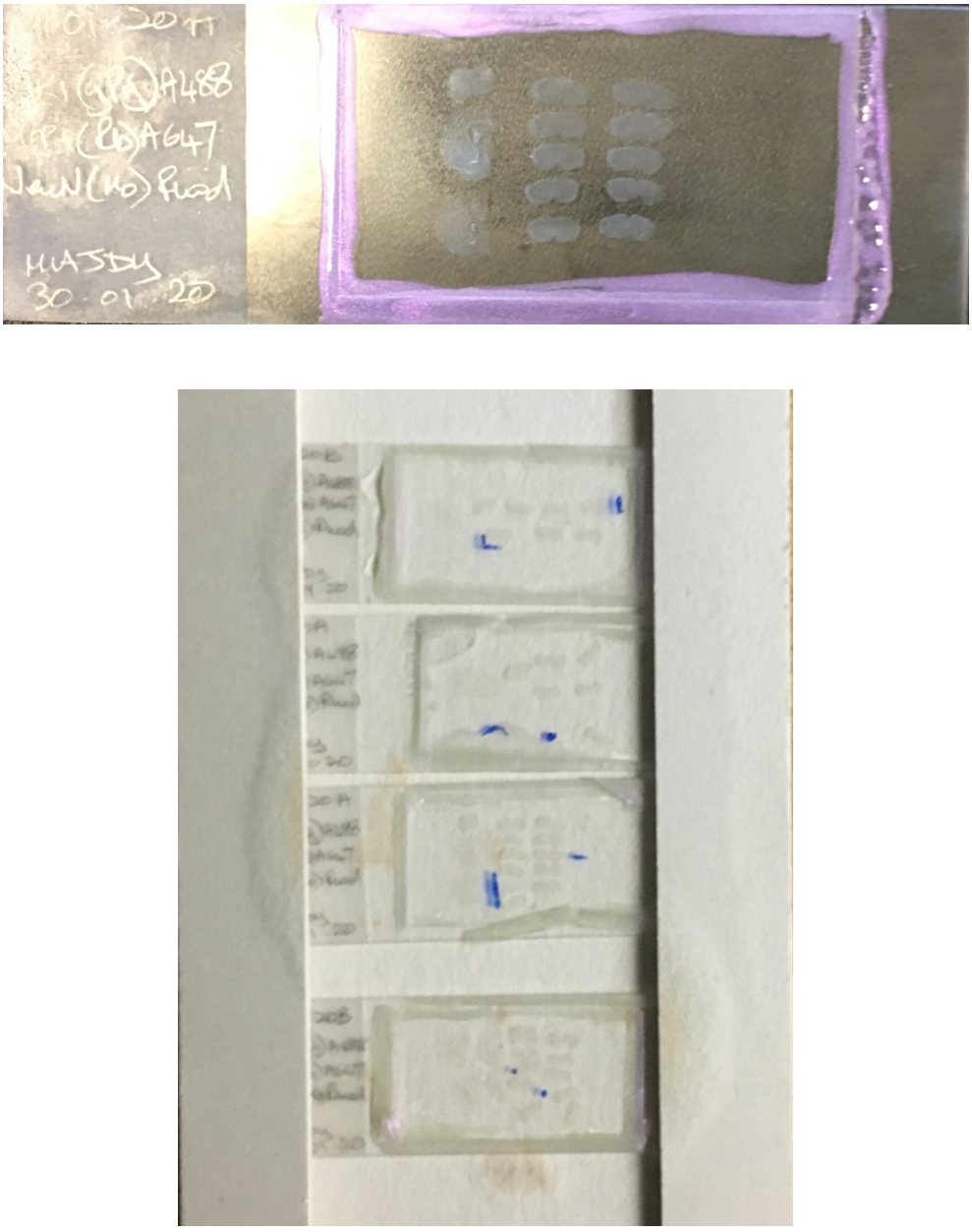

Figure 7-1 Incubated brain samples mounted on slides
The above picture shows the final product of samples collection, incubation, rinsing and sections mounting. The below picture presents the selected slides of the naïve mice, which will be visualised under the fluorescent microscope for neural expression analysis.

7.4.4 The antibody combinations

The primary antibodies used in the IHC analysis were neurokinin 1 receptor (NK1R), μ opioid receptor (μOR) and neuronal nuclear protein (NeuN). The NK1R was detected using NK1R guinea pig antibodies (1:500) (Millipore Limited, UK), and a secondary anti guinea pig antibody (1:500) (Vector Laboratories, UK). The μOR neural expression was detected utilising μOR rabbit antibodies 1:500 (Abcam, UK), and a secondary anti-rabbit antibody was added 1:500 (Vector Laboratories, UK). Monkey NeuN antibodies were included 1:1000 (Abcam, UK), and the secondary anti monkey antibodies 1:1000 (Vector Laboratories, UK) were used to detect the primary NeuN antibodies. In addition, Tyramide signal amplification was carried out (1:50) using the TSA amplification kit provided by Akoya Biosciences, UK.

7.4.5 Immunofluorescent microscope imaging

NK1R, μOR and NeuN immunopositive cells were imaged and analysed throughout the coronal sections collected from the naïve mice brain samples, using an epifluorescent microscope (Axioscop, Zeiss, UK). Coronal sections were visualised under the microscope to identify the anatomical landmarks of the ventral respiratory column (VRC). The caudal landmark was set at the rostral border of the lateral reticular nucleus (LRN), and the rostral landmark was identified by the rostral portion of the facial motor nucleus. The counting of NK1R and μOR immunopositive cells was determined to be executed through this rostrocaudal extent. In addition, to identify preBötC, nucleus ambiguous (NA) was set to be the level reference of the same coronal section. see Figure 7-2

7.5 Results

Coronal sections were collected from the 4 naïve mice, 8-10 sections per mouse. The antibodies and combined channels presented a successful IHC processing of the brain samples that helped identify several anatomical landmarks within the sections, such as preBötC and hypoglossal nucleus. (See Figure 7-2) Some examples are provided in Figure 7-3 and Figure 7-4, which are collected from the mice group regarding the clarity of the section. Each figure refer to an indiviual coronal sectoin, which is collected from a single mouse. This study was limited with the small sample size and statistical analysis was performed.

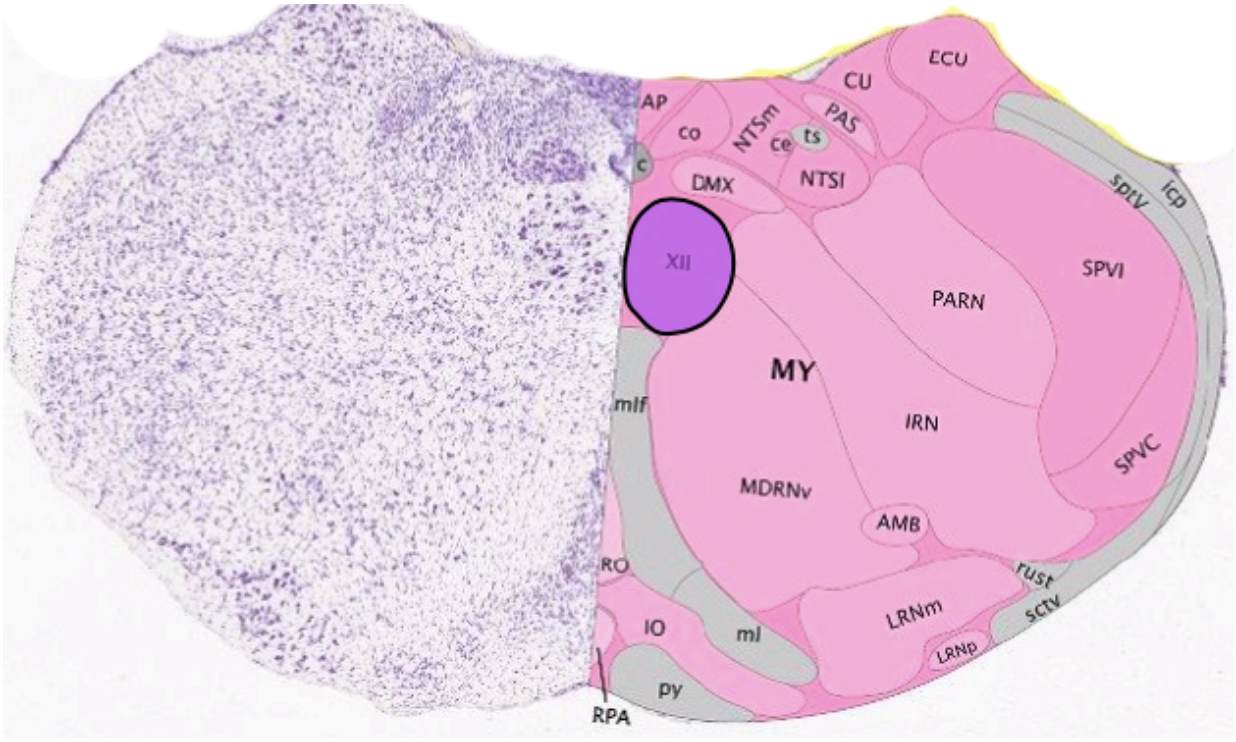

Figure 7-2 Anatomical landmarks of the coronal brainstem section
The picture shows the coronal section at the level of -6.72 mm from Bregma, where most of the anatomical structures were highlighted in the IHC study, such as hypoglossal nucleus (XII), nucleus ambiguous (AMB) and inferior olivary nucleus (IO). The picture was modified from the online Allen Mouse Brain Atlas 2012.

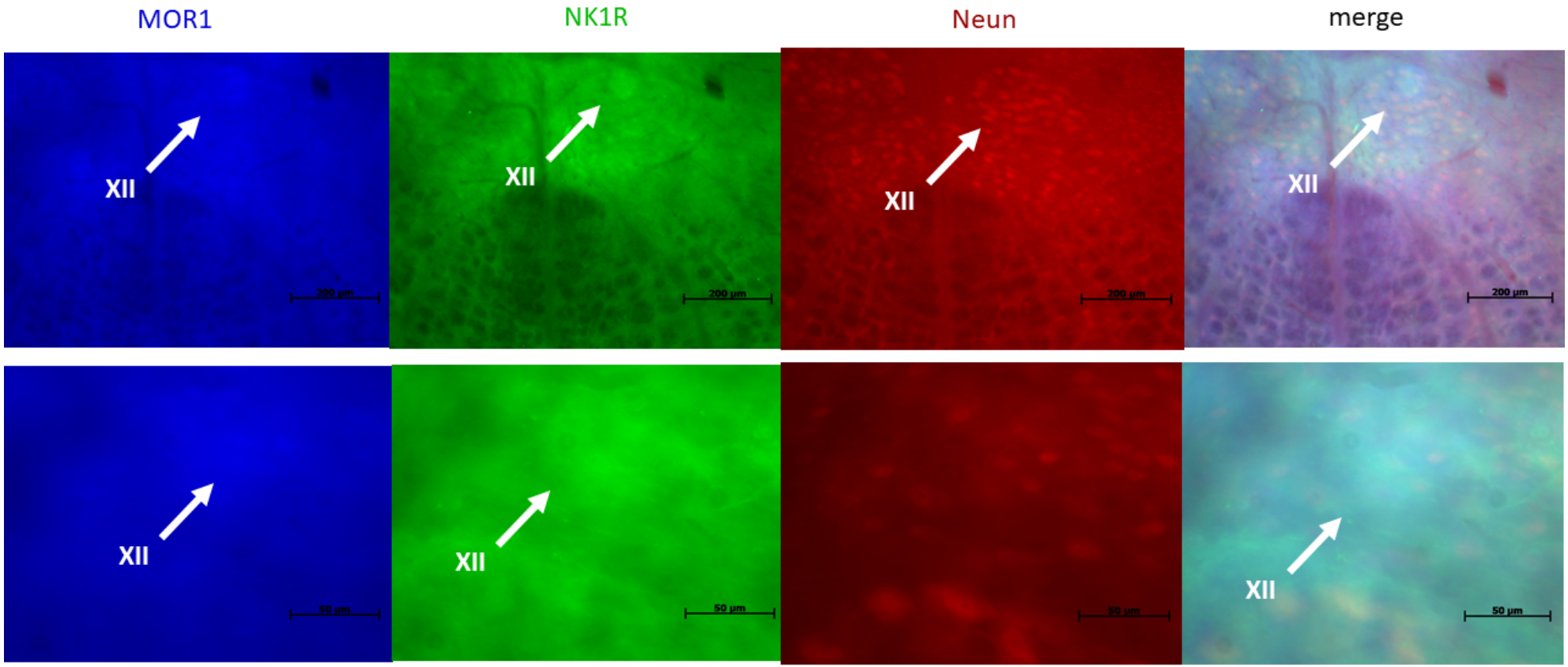

Figure 7-3 µOR expression at the hypoglossal nucleus (XII)
A single coronal section is provided in the figure, as the upper row represents 20x magnification and the lower row is 40x magnification of the same area. The blue dye highlights the MOR1 receptors; the green is for NK1R receptors, the red stands for Neun and the merged stands for all stains at the same view. The hypoglossal nucleus was identified in the dorsomedial medulla, below the central canal, and presented a high expression of the µOR (blue).

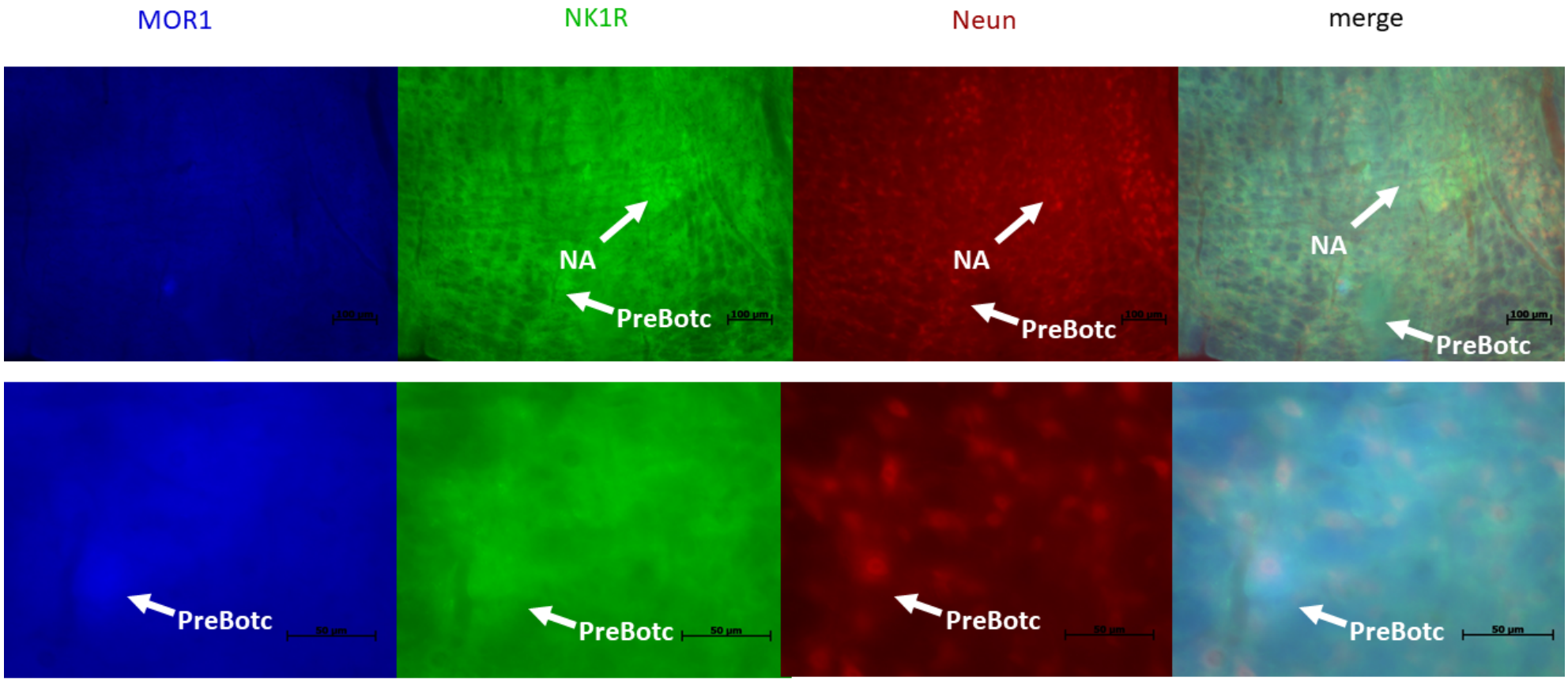

Figure 7-4 PreBötC identified at the site with a high expression of μOR and NK1R receptors
A single coronal section is provided in the figure, as the upper row represents 20x magnification and the lower row is 40x magnification of the same area. The blue dye highlights the MOR1 receptors; the green is for NK1R receptors, the red stands for Neun and the merged stands for all stains at the same view. The section highlights the ventral localisation of PreBötC toward NA at NK1R (green).

7.6 Discussion

The study was designed to investigate the chronic effect of postnatal repeated (fentanyl) exposure on the μOR neural expression across the brainstem, but a pandemic lockdown was held at the time of the study, and the samples were collected from four naïve mice. The technique succeeded in working with the samples collected from the naïve mice (Figure 7-3 and Figure 7-4), which was adapted from the previous work by (Kennedy, 2015). However, due to the covid outbreak, the study was limited to the samples the 4 naïve mice introduced. The previous work, conducted by (Kennedy, 2015) on similar study groups, showed a decrease of μOR density in the mice exposed to repeated opioid exposure early in life. (See Figure 7-5 and Figure 7-6)

The μ opioid receptors are highly expressed across preBötC and the BC in the adult rat brainstem (Lonergan et al., 2003). Dense clusters of μ opioid receptor-expressing cells are located within the facial motor nucleus. However, the density of μ opioid receptors falls in the fentanyl-exposed mice throughout preBötC and VRC (Kennedy, 2015). The mechanism of the long-term effect remains elusive, and it may be referred to as a decrease of the neural expression or downregulation of the receptors. Some studies had revealed that the repeated exposure to μ opioid receptor agonists in rodents induces a downregulation process triggered by the internalisation of the receptors (Bhargava and Gulati, 1990, Stafford et al., 2001), which reduces the functional receptors and causes tolerance. Despite the fact that downregulation may cause these long-term alterations triggered by the repeated fentanyl exposure, a decrease of the cells' number should be considered as a possible cause of the low μ opioid receptors density found in the fentanyl-exposed group. To investigate the cell count in the study group, a neuronal nuclei (NeuN) primary antibody should be used in the IHC processing. NeuN is a specified nuclear protein used as a general cell marker (Sandison and Webb, 1994). Accordingly, depletion of NeuN immunopositive cells will suggest neuronal cells loss, and unchanged NeuN expression accompanied with a decrease of μ opioid receptors would suggest a downregulation.

An epifluorescence microscope was used to observe the staining. It would be an advantageous to use a confocal microscope in our analysis. The confocal microscope has a higher resolution and contrast, due to the ability to reduce the background fluorescence (Sandison and Webb, 1994). Also, it provides the ability to produce serial optical sections that allow analysis of the samples with greater depth. Indeed, counting immunopositive cells using the epifluorescence microscope may underestimate the number of cells present within the section. The confocal microscope was set to be the first choice for the analysis in the current study. Still, due to the impact of Covid, access to the device was limited at the time of the analysis of the samples.

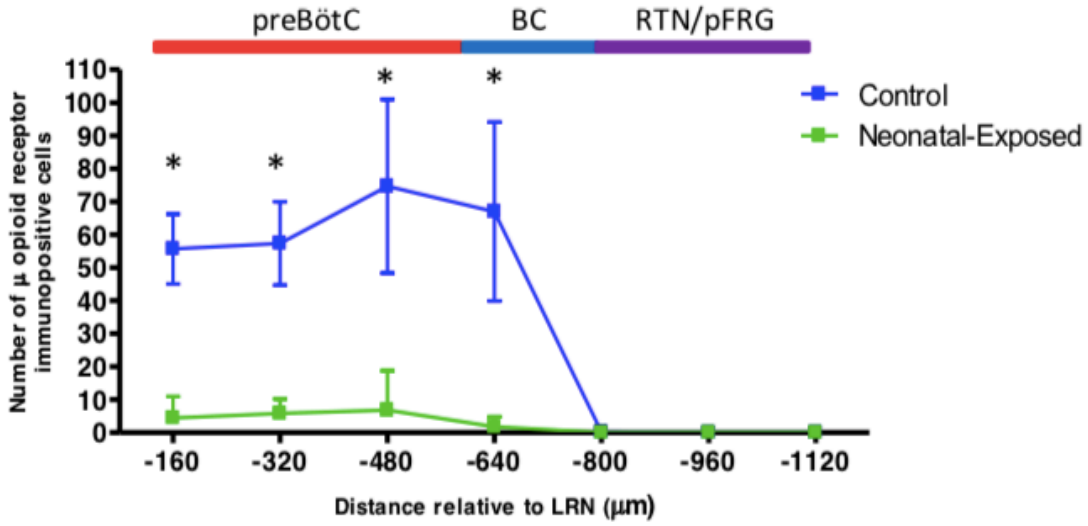

Figure 7-5 The number of μ opioid receptor immunopositive cells across VRC in fentanyl-exposed mice and control group
Fentanyl-exposed mice showed a significant decrease in μ opioid receptor immunopositive cells within the preBötC compared to the control group. In addition, no immunopositive cells were obtained at RTN/pFRG area in both control and fentanyl-exposed groups. Four control mice were included in this study, and 5 fentanyl exposed. Significant difference was denoted ($p<0.05$) between experimental groups, two-way ANOVA with Bonferroni's post-test. The graph was reproduced from (Kennedy, 2015).

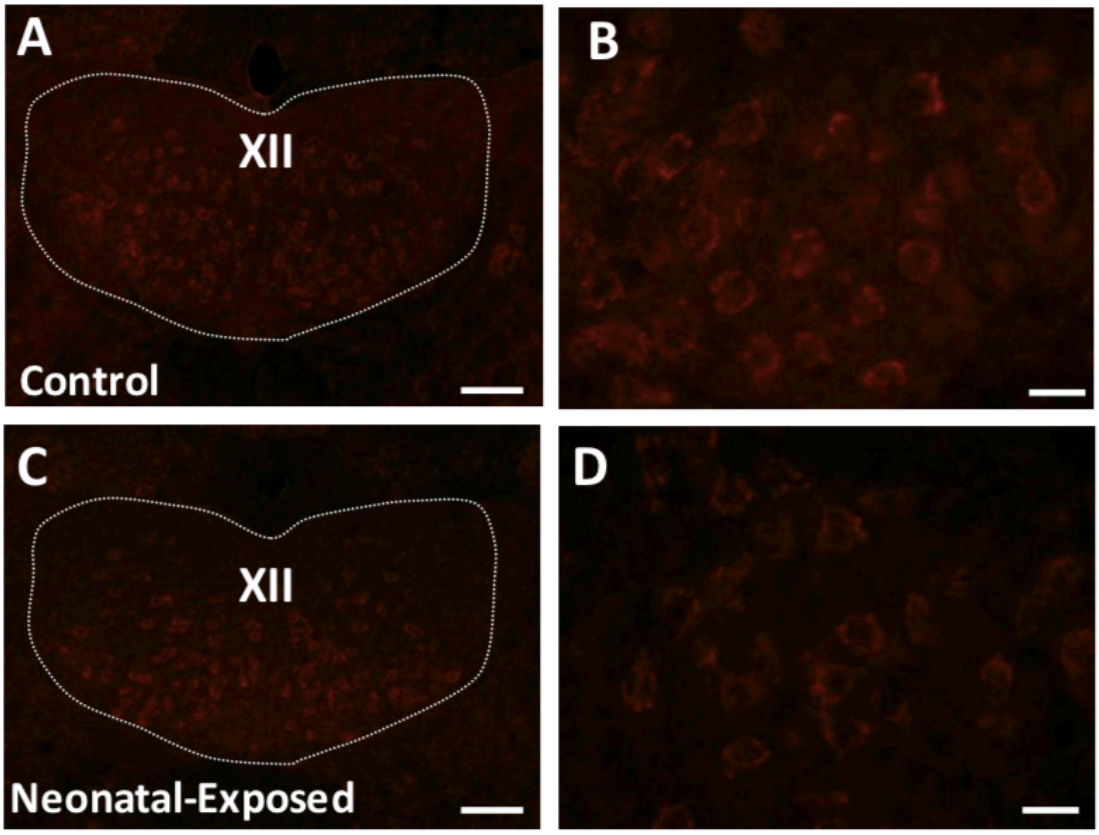

Figure 7-6 The hypoglossal nucleus (XII) μ opioid receptor immunopositive cells in neonatal fentanyl-exposed mice and control group
Magnified images of XII, captured by the epifluorescent microscope, show the μ opioid receptor clusters in control and fentanyl-exposed mice. Picture A is magnified in B; and D is referred to C. A decrease of μOR immunopositive cells is remarkable in the fentanyl-exposed group. The scale in A and C images is 100 μm and B and images is 20 μm. Pictures modified from (Kennedy, 2015).

Chapter 8 General discussion

Respiration is a critical function that is influenced by various neurological, physiological and biochemical factors. Understanding the mechanism of breathing drive and respiratory rhythm generation has become a challenge for researchers. The current research was designed to investigate the early maturation steps taken by the breathing neural oscillators at the first week of life. Accordingly, breathing is unstable and immature in the first week of life. Also, the hypothesised key oscillator of breathing at this age RTN/pFRG is opioid insensitive. To investigate the breathing maturation and neural oscillators, a μ-opioid receptor agonist, fentanyl, was introduced as a pharmacological tool to disturb the breathing maturation step taken postnatally. Fentanyl is a highly selective agonist to μ-opioid receptors located in several sites in the brain and is highly expressed within preBötC. The first week of life was targeted concerning its vulnerability and maturation period time window. It is hypothesised that the main rhythm generator of the first week of life is RTN/pFRG, which is switched to preBötC as the dominant oscillator till adulthood. Several signs of postnatal exposure to opioids were obtained during my lab work, and this will be discussed in the following sections.

8.1 The chronic effect of fentanyl exposure, at postnatal age, on breathing patterns

Experimental groups were designed to be exposed to fentanyl at postnatal age (NN) P1-P5 and (JUV) P9-P13. The breathing pattern was assessed at the age of 8-10 weeks old to investigate the chronic effect acquired after the postnatal exposure to fentanyl. The baseline of respiratory rate and minute volume were reduced in the NN fentanyl-exposed group. A similar effect of the early-life opioid exposure was observed on the respiratory rate (Kennedy, 2015); yet, the long-lasting change mechanism remains undisclosed. Although PreBötC is an opioid-sensitive respiratory oscillator, other respiratory neural centres have μ-opioid receptors such as Kolliker–Fuse nucleus (KF) (Lalley et al., 2014, Varga et al., 2020); and the effect of the early opioid exposure may extend beyond the PreBötC level, as the fentanyl was administrated systemically.

The awake fentanyl challenge was performed on the study groups to evaluate the sensitivity to μ-opioid agonist exposure at adolescence, after the postnatal exposure to opioids. The NN-FEN group showed more reduction in the respiratory rate, which is associated with a trend of tidal volume, compared to NN-SAL group, thus suggesting the long-lasting effect of the fentanyl exposure, at the age of P1-P5, on breathing pattern. Nevertheless, the alterations of tidal volume resulting from repeated opioid exposure may enhance variable responses. For example, an increase in tidal volume was observed by (Lewanowitsch et al., 2006, Leino et al., 1999, Colman and Miller, 2001), while a decrease in tidal volume was supported by (Lewanowitsch et al., 2006, Leino et al., 1999, Colman and Miller, 2001). The conflict in results could be generated by several factors, such as different opioid dose, time of exposure or underpowered studies, which may include false positive/negative data.

The juvenile groups showed a similar response to the fentanyl awake challenge, and no changes were observed in the breathing pattern. The changes in some breathing parameters imply the chronic influence of postnatal fentanyl exposure on breathing pattern. Yet, the changes may refer to several factors, such as opioid sensitivity or neural breathing centre maldevelopment, such as the ablation of PreBötC which results in sleeping disorders (McKay et al., 2005).

8.2 The vulnerability to fentanyl under anaesthesia

The awake fentanyl challenge had presented long-lasting changes in respiratory behaviour due to the repeated postnatal exposure to fentanyl. A state-dependent exaggeration of the fentanyl effect on breathing function was noted in some experimental groups exposed to fentanyl earlier in neonatal life P1-P5. The observation was attributed to the vulnerability of these mice under anaesthesia, which is state dependent. Although an anaesthetic state is known to augment the respiratory depressive effect of fentanyl (Montandon and Horner, 2019), the control groups had shown better survival rates of the same challenge. The chronic changes of postnatal exposure to fentanyl may adopt several hypotheses, such as the elimination and accumulation of unbound morphine in brain sites, once the metabolisation of opioids is not fully developed at the age of exposure P1-P5 (Bhat et al., 1990, Ainsworth, 2014). This triggers the innate pattern receptor toll-like receptor 4 (TLR4) that prompts adverse side effects of opioid addiction and sensitivity (Eidson and Murphy, 2013, Eidson et al., 2017).

The TLR4 signalling increases proinflammatory cytokines release within the CNS (Raghavendra et al, 2002; Shen et al, 2011a) including tumour necrosis factor (TNF), which enhanced the production of other cytokines, such as interlukin-6. The cytokines release disturbs the glutamate homeostasis and excitatory signalling in the CNS (Stellwagen et al, 2005). Many studies had linked the altered glutamate homeostasis to the chronic changes of opioids tolerance, as a hyperpolarisation effect (Vaughan et al, 1997; Bachtell et al, 2015). The chronic effect was observed after the postnatal exposure to fentanyl, which may get aggravated by specific anaesthetic and sleeping states. However, the sample size remains underpowered, and it is impossible to conduct a similar study design on human infants. A general recommendation could be given regarding the therapeutic use of opioids at neonatal age, which should be revised, documented and limited to avoid the unexpected outcomes of the inherited hypersensitivity to the opioids later in life.

8.3 The effect of fentanyl on cerebral blood flow

The study was dedicated to investigating the effect of opioids on CBF in both acute and chronic measures. Laser speckle technique was employed to deliver a live dynamic record of the cortical perfusion of a mouse's brain, under anaesthesia. The acute influence of fentanyl exposure on anaesthetised mice is summed up as an increase of CBF, which gradually returns to normal around 25 minutes post-exposure. The rise of CBF is a common act of opioids exposure (Franceschini et al., 2010), but the mechanism is not fully recognised. Although the respiratory rate was acquired in some samples through the study, both respiratory rate and CBF changed simultaneously, which does not provide a definite answer about the initial haemodynamic instability that follows the fentanyl administration.

The chronic effect of opioid exposure in the early days of life was assessed by introducing the postnatal fentanyl-exposed mice into the study. Some cortical regions in JUV-FEN groujp produced a trend of CBF, but the mean average of all CBF regions showed no significant changes between the experimental groups.

8.4 The impact of chronic opioid exposure on the HPA axis and corticosterone hormone

An ELISA test was used to assess the stress level in rodents, by measuring the corticosterone level in hair samples, as a chronic marker of stress level. The targeted group was exposed to a repeated dose of fentanyl at the age of P9-P13 (JUV-FEN). An increase of corticosterone was obtained that suggested the chronic effect of opioid exposure (Houshyar et al., 2001). The assessment focused on the impact of opioid exposure on the endocrine system, especially the HPA axis and stress hormone. The chronic exposure to opioid compounds, endogenous and exogenous, enhances the secretion of ACTH and alters the hypothalamic-pituitary–adrenal axis (HPA axis) to stressful stimuli (Ježová et al., 1982, Buckingham and Cooper, 1984).

8.5 The impact of chronic opioid exposure on endogenous β-endorphin levels and weight

An ELISA test was used to assess the plasma β-endorphin levels in mice exposed repeatedly to fentanyl at the age of P9-P13 (JUV-FEN), a trend toward an elevation of the endogenous β-endorphin detected in the JUV-FEN group, which accompanied with a large distribution of data. The ELISAThe β-endorphin data had presented considerable variation of data, besides a low detection level in many samples, which may refer to several factors, such as the small blood sample volume. The JUV-FEN had shown more detectable levels of plasma β-endorphin, even when a small blood volume is extracted. This may suggest the elevation of the β-endorphin level in this group compared to the JUV-SAL. Still, a larger sample would help to have a better judgmental position in future work. In regards to the literature, chronic exposure to opioids alters the hormonal levels within the plasma, such as elevating the levels of β-endorphins in plasma (Vuong et al., 2010, Victoria and Murphy, 2016). β-endorphins represent the endogenous μ-opioid agonist. Weight measures were taken from the same experimental groups, and large distribution of weight results was observed in the JUV-FEN mice beside a general trend toward an increase. Therefore, a sample of 40 mice would match the appropriate power calculation of the mice weight study and help to clarify the effect of early opioid exposure on weight gain.

8.6 The alterations of μ-opioid receptor distribution within brain regions following repeated fentanyl exposure early on in life

The long-term effect of early-life repeated fentanyl exposure on μ-opioid receptor expression throughout brain regions was analysed to understand the potential mechanisms underlying the obtained long-term respiratory changes in the same experimental group. An autoradiography study was introduced for this investigation, and [^{3}H] DAMGO was utilised to target μ-opioid receptor-expressing cells (μOR). The preliminary results showed a reduction in μOR across the brain regions in JUV-FEN n=2 vs JUV-SAL n=2. No statistical analsysi conducted due to the small group sample size. The reduction of μOR -expressing cells could be linked to several theories, such as downregulation, phosphorylation and redistribution (Ingram et al., 2008, Fyfe et al., 2010). Yet, to understand the μOR distribution, additional measures should be investigated within the study, such as receptors redistribution between cellular compartment, plasma membrane and intracellular compartments (Williams et al., 2013). μOR distribution study designed to understand the chronic physiological changes observed on the respiratory function of neonatal fentanyl exposed mice, which resulted in chronic changes of the respiratory. Additional measures were included in this study and affected by fentanyl exposure at this age, which are endogenous opioid and stress hormone levels. The latter may broaden the investigating scope on these chronic changes and help design detailed study in the future to have certain explanations of the long-lasting changes.

8.7 Study limitations and future direction

The study was affected by the Covid pandemic situation and the national lockdown rules in place by March 2020. Another group of mice (NN that received fentanyl injections between P1-P5) was planned to be included in the autoradiography study. The immunohistochemistry (IHC) study was intended to support the autoradiography investigation of μOR distribution, but it was not completed due to the effect of the pandemic Covid situation. In regard to future plans, the NN group were considered to be exposed to fentanyl early in life, besides the JUV group. Also, an additional group older than JUV mice should be involved in order to identify the early age window that exaggerates the fentanyl effect on CNS and μOR. Concerning the laser speckles study, which investigated the effect of fentanyl on CBF, detailed respiratory measures, such as the diaphragm and genioglossus muscle activities (Montandon et al., 2011), would enhance the analysis of the anaesthetised fentanyl challenge effect on breathing. However, the study time plan was long, and the surgical procedure was complex. Therefore, including an additional technique may raise the chances of mice dying before completing the fentanyl challenge due to the length and complexity of the procedure. In order to analyse the μOR distribution, two methods were suggested in this study: autoradiography and IHC. Yet, in future work, we may consider using the confocal microscope to assess the distribution of μOR. Also, evaluating the distribution of other neural expressions should be considered besides μOR. For example, investigating the delta-opioid receptors will help understand the receptors' redistribution after chronic exposure to opioids.

8.1 Conclusion

The study was designed to investigate the long-lasting effects of early opioid exposure on respiratory patterns. The long-term impact of repeated opioid exposure was observed in baseline measures of breathing patterns taken at the awake fentanyl challenge. The laser speckle (LS) experiment investigated the dynamic changes in CBF following opioid injection. LS enabled the recording of real-time, dynamic CBF changes in response to pharmacological agents. NN-FEN showed a higher CBF reactivity to fentanyl administration than NN-SAL, the control group. In addition, hypersensitivity to opioid exposure was obtained and documented under generalised anaesthesia, affecting the opioid-exposed mice's survival rate, limiting the data's analysis and conclusion.

An extended evaluation of the influence of early repeated opioid exposure on the hormone levels in mice. A trend in the corticosterone level was observed in the treated mice (JUV-FEN). The endogenous opioid levels showed a low detection level of β-endorphin in JUV-SAL and more variable traceable levels in JUV-FEN. The variability of the data would affect the statement about the β-endorphin level, and larger blood samples are recommended for future work to produce more consistent results. Weight measures were analysed as some studies backed the effect of β-endorphin on eating habits and weight gain, and opioid-exposed mice showed an increase in weight. The weight study requires a larger sample size in future (40 mice) to produce a statistically robust report regarding the effect of opioid exposure on weight gain.

In order to understand the chronic changes that were triggered by the early exposure to μ opioid agonist agent, fentanyl, an assessment was carried out to investigate the downregulation and distribution of μ opioid receptor expression across the brain. The preliminary results showed a reduction of μ opioid receptor density in JUV-FEN compared to JUV-SAL, which was limited by the sample size and time frame. Yet, this thesis provides novel information regarding the long-term effects of opioid-induced respiratory depression based on the experiments described in this study. Also, the neonatal period appears to be susceptible to the long-term adverse effects of repeated opiate exposure. The changes in the respiratory response to fentanyl may be caused by the downregulation of the

opioid receptor within the PreBötC. Therefore, a repeat of the autoradiography and immunohistochemistry studies is recommended for future work to support the data collected in the thesis and understand the extended neural effect of early opioid exposure in neonatal mice.

List of references

AASLID, R. 1987. Visually evoked dynamic blood flow response of the human cerebral circulation. *Stroke,* 18**,** 771-775.

ABADIE, V., CHAMPAGNAT, J. & FORTIN, G. 2000. Branchiomotor activities in mouse embryo. *Neuroreport,* 11**,** 141-145.

ABS, R., VERHELST, J., MAEYAERT, J., VAN BUYTEN, J.-P., OPSOMER, F., ADRIAENSEN, H., VERLOOY, J., VAN HAVENBERGH, T., SMET, M. & VAN ACKER, K. 2000. Endocrine consequences of long-term intrathecal administration of opioids. *The Journal of Clinical Endocrinology & Metabolism,* 85**,** 2215-2222.

ADAMS, M. L., BRASE, D. A., WELCH, S. P. & DEWEY, W. L. 1986. The role of endogenous peptides in the action of opioid analgesics. *Annals of Emergency Medicine,* 15**,** 1030-1035.

ADINOFF, B., DEVOUS SR, M. D., COOPER, D. C., BEST, S. E., HARRIS, T. S. & WILLIAMS, M. J. 2009. Neural response to lidocaine in healthy subjects. *Psychiatry Research: Neuroimaging,* 173**,** 135-142.

AHMADALIPOUR, A. & RASHIDY-POUR, A. 2015. Effects of treadmill running exercise during the adolescent period of life on behavioral deficits in juvenile rats induced by prenatal morphine exposure. *Physiol Behav,* 139**,** 26-33.

AILES, E. C., DAWSON, A. L., LIND, J. N., GILBOA, S. M., FREY, M. T., BROUSSARD, C. S., HONEIN, M. A., CENTERS FOR DISEASE, C. & PREVENTION 2015. Opioid prescription claims among women of reproductive age--United States, 2008-2012. *MMWR Morb Mortal Wkly Rep,* 64**,** 37-41.

AINSLIE, P. N. & DUFFIN, J. 2009. Integration of cerebrovascular CO2 reactivity and chemoreflex control of breathing: mechanisms of regulation, measurement, and interpretation. *Am J Physiol Regul Integr Comp Physiol,* 296**,** R1473-95.

AINSLIE, P. N. & OGOH, S. 2010. Regulation of cerebral blood flow in mammals during chronic hypoxia: a matter of balance. *Exp Physiol,* 95**,** 251-62.

AINSWORTH, S. B. 2014. *Neonatal formulary: drug use in pregnancy and the first year of life*, John Wiley & Sons.

AKIL, H., WATSON, S. J., YOUNG, E., LEWIS, M. E., KHACHATURIAN, H. & WALKER, J. M. 1984. Endogenous opioids: biology and function. *Annual review of neuroscience,* 7**,** 223-255.

ALHEID, G. F., JIAO, W. & MCCRIMMON, D. R. 2011. Caudal nuclei of the rat nucleus of the solitary tract differentially innervate respiratory compartments within the ventrolateral medulla. *Neuroscience,* 190**,** 207-27.

BAILE, C. A., MCLAUGHLIN, C. L. & DELLA-FERA, M. A. 1986. Role of cholecystokinin and opioid peptides in control of food intake. *Physiological Reviews,* 66**,** 172-234.

BAILEY, C. P., OLDFIELD, S., LLORENTE, J., CAUNT, C. J., TESCHEMACHER, A., ROBERTS, L., MCARDLE, C., SMITH, F., DEWEY, W. & KELLY, E. 2009. Involvement of PKC α and G – protein – coupled receptor kinase 2 in agonist – selective desensitization of μ – opioid receptors in mature brain neurons. *British journal of pharmacology,* 158**,** 157-164.

BAVIS, R. W., FALLON, S. C. & DMITRIEFF, E. F. 2013. Chronic hyperoxia and the development of the carotid body. *Respiratory physiology & neurobiology,* 185**,** 94-104.

BAVIS, R. W. & MITCHELL, G. S. 2008. Long-term effects of the perinatal environment on respiratory control. *Journal of Applied Physiology,* 104**,** 1220-1229.

BAVIS, R. W., OLSON, E. B., JR., VIDRUK, E. H., FULLER, D. D. & MITCHELL, G. S. 2004. Developmental plasticity of the hypoxic ventilatory response in rats induced by neonatal hypoxia. *J Physiol,* 557**,** 645-60.

BAVIS, R. W., OLSON JR, E. & MITCHELL, G. S. 2002. Critical developmental period for hyperoxia-induced blunting of hypoxic phrenic responses in rats. *Journal of Applied Physiology,* 92**,** 1013-1018.

BHARGAVA, H. M. & GULATI, A. 1990. Down-regulation of brain and spinal cord μ-opiate receptors in morphine tolerant-dependent rats. *European journal of pharmacology,* 190**,** 305-311.

BHAT, R., CHARI, G., GULATI, A., ALDANA, O., VELAMATI, R. & BHARGAVA, H. 1990. Pharmacokinetics of a single dose of morphine in preterm infants during the first week of life. *J Pediatr,* 117**,** 477-81.

BISGARD, G., OLSON JR, E., WANG, Z.-Y., BAVIS, R., FULLER, D. & MITCHELL, G. 2003. Adult carotid chemoafferent responses to hypoxia after 1, 2, and 4 wk of postnatal hyperoxia. *Journal of Applied Physiology,* 95**,** 946-952.

BISWAL, B. B., KYLEN, J. V. & HYDE, J. S. 1997. Simultaneous assessment of flow and BOLD signals in resting – state functional connectivity maps. *NMR in Biomedicine: An International Journal Devoted to the Development and Application of Magnetic Resonance In Vivo,* 10**,** 165-170.

BLANCHI, B., KELLY, L. M., VIEMARI, J. C., LAFON, I., BURNET, H., BEVENGUT, M., TILLMANNS, S., DANIEL, L., GRAF, T., HILAIRE, G. & SIEWEKE, M. H. 2003. MafB deficiency causes defective respiratory rhythmogenesis and fatal central apnea at birth. *Nat Neurosci,* 6**,** 1091-100.

BOLANOS, C. A., BARROT, M., BERTON, O., WALLACE-BLACK, D. & NESTLER, E. J. 2003. Methylphenidate treatment during pre-and periadolescence alters behavioral responses to emotional stimuli at adulthood. *Biological psychiatry,* 54**,** 1317-1329.

BOLLINGER, A., HOFFMANN, U. & FRANZECK, U. 1991. Evaluation of flux motion in man by the laser Doppler technique. *Journal of Vascular Research,* 28**,** 21-26.

BOR-SENG-SHU, E., KITA, W. S., FIGUEIREDO, E. G., PAIVA, W. S., FONOFF, E. T., TEIXEIRA, M. J. & PANERAI, R. B. 2012. Cerebral hemodynamics: concepts of clinical importance. *Arq Neuropsiquiatr,* 70**,** 352-6.

BOTELHO, M. F., RELVAS, J. S., ABRANTES, M., CUNHA, M. J., MARQUES, T. R., ROVIRA, E., FONTES RIBEIRO, C. A. & MACEDO, T. 2006. Brain blood flow SPET

imaging in heroin abusers. *Annals of the New York Academy of Sciences,* 1074**,** 466-477.

BOUVIER, J., THOBY-BRISSON, M., RENIER, N., DUBREUIL, V., ERICSON, J., CHAMPAGNAT, J., PIERANI, A., CHÉDOTAL, A. & FORTIN, G. 2010. Hindbrain interneurons and axon guidance signaling critical for breathing. *Nature neuroscience,* 13**,** 1066-1074.

BRIAN, J. E. 1998. Carbon dioxide and the cerebral circulation. *The Journal of the American Society of Anesthesiologists,* 88**,** 1365-1386.

BROCKHAUS, J. & BALLANYI, K. 1998. Synaptic inhibition in the isolated respiratory network of neonatal rats. *European Journal of Neuroscience,* 10**,** 3823-3839.

BRONSTEIN, D. M., DAY, N. C., GUTSTEIN, H. B., TRUJILLO, K. A. & AKIL, H. 1993a. Pre- and posttranslational regulation of beta-endorphin biosynthesis in the CNS: effects of chronic naltrexone treatment. *J Neurochem,* 60**,** 40-9.

BRONSTEIN, D. M., GUTSTEIN, H. B. & AKIL, H. 1993b. Effects of chronic morphine treatment on beta-endorphin-related peptides in the caudal medulla and spinal cord. *J Neurochem,* 60**,** 2304-7.

BUCK, M. & MARRAZZI, M. A. 1987. Atypical responses to morphine in mice: a possible relationship to anorexia nervosa? *Life Sci,* 41**,** 765-73.

BUCKINGHAM, J. C. & COOPER, T. A. 1984. Differences in hypothalamo-pituitary-adrenocortical activity in the rat after acute and prolonged treatment with morphine. *Neuroendocrinology,* 38**,** 411-417.

BURGGREN, W. W. & REYNA, K. S. 2011. Developmental trajectories, critical windows and phenotypic alteration during cardio-respiratory development. *Respiratory physiology & neurobiology,* 178**,** 13-21.

CAHILL, C. M., MCCLELLAN, K. A., MORINVILLE, A., HOFFERT, C., HUBATSCH, D., O'DONNELL, D. & BEAUDET, A. 2001. Immunohistochemical distribution of delta

opioid receptors in the rat central nervous system: evidence for somatodendritic labeling and antigen – specific cellular compartmentalization. *Journal of Comparative Neurology,* 440**,** 65-84.

CARROLL, J. L. 2003. Invited Review: Developmental plasticity in respiratory control. *Journal of Applied Physiology,* 94**,** 375-389.

CHAMBERLIN, N. L., MANSOUR, A., WATSON, S. J. & SAPER, C. B. 1999. Localization of mu-opioid receptors on amygdaloid projection neurons in the parabrachial nucleus of the rat. *Brain research,* 827**,** 198-204.

CHAVES, C., REMIÃO, F., CISTERNINO, S. & DECLÈVES, X. 2017. Opioids and the blood-brain barrier: a dynamic interaction with consequences on drug disposition in brain. *Current neuropharmacology,* 15**,** 1156-1173.

CHAVKIN, C. & GOLDSTEIN, A. 1984. Opioid receptor reserve in normal and morphine-tolerant guinea pig ileum myenteric plexus. *Proceedings of the National Academy of Sciences,* 81**,** 7253-7257.

CHEN, S. W., MAGUIRE, P. A., DAVIES, M. F., BEATTY, M. F. & LOEW, G. H. 1996. Evidence for mu1-opioid receptor involvement in fentanyl-mediated respiratory depression. *Eur J Pharmacol,* 312**,** 241-4.

CHEVILLARD, L., MEGARBANE, B., RISEDE, P. & BAUD, F. J. 2009. Characteristics and comparative severity of respiratory response to toxic doses of fentanyl, methadone, morphine, and buprenorphine in rats. *Toxicol Lett,* 191**,** 327-40.

CHRISTIE, M., WILLIAMS, J. & NORTH, R. 1987. Cellular mechanisms of opioid tolerance: studies in single brain neurons. *Molecular Pharmacology,* 32**,** 633-638.

CIPOLLA, M. J. The cerebral circulation. Colloquium Series on Integrated Systems Physiology: From Molecule to Function to Disease, 2016. Morgan & Claypool Life Sciences, 1-80.

CLAASSEN, J., THIJSSEN, D. H. J., PANERAI, R. B. & FARACI, F. M. 2021. Regulation of cerebral blood flow in humans: physiology and clinical implications of autoregulation. *Physiol Rev,* 101**,** 1487-1559.

COIRO, V., VOLPI, R., STELLA, A., VENTURI, N. & CHIODERA, P. 2011. Stimulatory effect of naloxone on plasma cortisol in human: Possible direct stimulatory action at the adrenal cortex. *Regul Pept,* 166**,** 1-2.

COLLETT, B. 1998. Opioid tolerance: the clinical perspective. *British journal of anaesthesia,* 81**,** 58-68.

COLMAN, A. S. & MILLER, J. H. 2001. Modulation of breathing by μ1 and μ2 opioid receptor stimulation in neonatal and adult rats. *Respiration physiology,* 127**,** 157-172.

CORDER, G., CASTRO, D. C., BRUCHAS, M. R. & SCHERRER, G. 2018. Endogenous and Exogenous Opioids in Pain. *Annu Rev Neurosci,* 41**,** 453-473.

CROSS, A. J., HILLE, C. & SLATER, P. 1987. Subtraction autoradiography of opiate receptor subtypes in human brain. *Brain research,* 418**,** 343-348.

CUI, Y., KAM, K., SHERMAN, D., JANCZEWSKI, W. A., ZHENG, Y. & FELDMAN, J. L. 2016. Defining preBötzinger complex rhythm-and pattern-generating neural microcircuits in vivo. *Neuron,* 91**,** 602-614.

DANG, V. C. & WILLIAMS, J. T. 2004. Chronic morphine treatment reduces recovery from opioid desensitization. *Journal of Neuroscience,* 24**,** 7699-7706.

DAS, G. 2014. Chronic heroin dependence leading to adrenal insufficiency. *Case reports in endocrinology,* 2014.

DAVIES, D. J., SU, Z., CLANCY, M. T., LUCAS, S. J., DEHGHANI, H., LOGAN, A. & BELLI, A. 2015. Near-Infrared Spectroscopy in the Monitoring of Adult Traumatic Brain Injury: A Review. *J Neurotrauma,* 32**,** 933-41.

DEBONO, M., CHAN, S., ROLFE, C. & JONES, T. H. 2011. Tramadol-induced adrenal insufficiency. *European journal of clinical pharmacology,* 67**,** 865-867.

DEL NEGRO, C. A., FUNK, G. D. & FELDMAN, J. L. 2018. Breathing matters. *Nat Rev Neurosci,* 19**,** 351-367.

DEL NEGRO, C. A., KOSHIYA, N., BUTERA JR, R. J. & SMITH, J. C. 2002. Persistent sodium current, membrane properties and bursting behavior of pre-botzinger complex inspiratory neurons in vitro. *Journal of neurophysiology,* 88**,** 2242-2250.

DEL NEGRO, C. A., MORGADO-VALLE, C., HAYES, J. A., MACKAY, D. D., PACE, R. W., CROWDER, E. A. & FELDMAN, J. L. 2005. Sodium and calcium current-mediated pacemaker neurons and respiratory rhythm generation. *Journal of Neuroscience,* 25**,** 446-453.

DELITALA, G., GROSSMAN, A. & BESSER, M. 1983. Differential effects of opiate peptides and alkaloids on anterior pituitary hormone secretion. *Neuroendocrinology,* 37**,** 275-279.

DESROSIERS, G. 2006. When opioid analgesia kills. *Perspect Infirm,* 4**,** 6-9.

DETTENBORN, L., TIETZE, A., KIRSCHBAUM, C. & STALDER, T. 2012. The assessment of cortisol in human hair: associations with sociodemographic variables and potential confounders. *Stress,* 15**,** 578-88.

DI PASQUALE, E., MONTEAU, R. & HILAIRE, G. 1992. In vitro study of central respiratory-like activity of the fetal rat. *Experimental brain research,* 89**,** 459-464.

DI PASQUALE, E., TELL, F., MONTEAU, R. & HILAIRE, G. 1996. Perinatal developmental changes in respiratory activity of medullary and spinal neurons: an in vitro study on fetal and newborn rats. *Developmental brain research,* 91**,** 121-130.

DIEGO, L., ATAYEE, R., HELMONS, P., HSIAO, G. & VON GUNTEN, C. F. 2011. Novel opioid antagonists for opioid-induced bowel dysfunction. *Expert opinion on investigational drugs,* 20**,** 1047-1056.

DING, Y. Q., KANEKO, T., NOMURA, S. & MIZUNO, N. 1996. Immunohistochemical localization of μ -opioid receptors in the central nervous system of the rat. *Journal of Comparative Neurology,* 367**,** 375-402.

DMITRIEFF, E. F., PIRO, S. E., BROGE JR, T. A., DUNMIRE, K. B. & BAVIS, R. W. 2012. Carotid body growth during chronic postnatal hyperoxia. *Respiratory physiology & neurobiology,* 180**,** 193-203.

DONIACH, I. & PELC, S. 1950. Autoradiograph technique. *The British Journal of Radiology,* 23**,** 184-192.

DONNELLY, J., BUDOHOSKI, K. P., SMIELEWSKI, P. & CZOSNYKA, M. 2016. Regulation of the cerebral circulation: bedside assessment and clinical implications. *Crit Care,* 20**,** 129.

DRAKE, C. T., AICHER, S. A., MONTALMANT, F. L. & MILNER, T. A. 2005. Redistribution of mu-opioid receptors in C1 adrenergic neurons following chronic administration of morphine. *Experimental neurology,* 196**,** 365-372.

DRORBAUG, J. E. & FENN, W. O. 1955. A barometric method for measuring ventilation in newborn infants. *Pediatrics,* 16**,** 81-87.

DUBREUIL, V., THOBY-BRISSON, M., RALLU, M., PERSSON, K., PATTYN, A., BIRCHMEIER, C., BRUNET, J. F., FORTIN, G. & GORIDIS, C. 2009. Defective respiratory rhythmogenesis and loss of central chemosensitivity in Phox2b mutants targeting retrotrapezoid nucleus neurons. *J Neurosci,* 29**,** 14836-46.

DUNN, A. K. 2012. Laser speckle contrast imaging of cerebral blood flow. *Annals of biomedical engineering,* 40**,** 367-377.

EIDSON, L. N., INOUE, K., YOUNG, L. J., TANSEY, M. G. & MURPHY, A. Z. 2017. Toll-like receptor 4 mediates morphine-induced neuroinflammation and tolerance via soluble tumor necrosis factor signaling. *Neuropsychopharmacology,* 42**,** 661-670.

EIDSON, L. N. & MURPHY, A. Z. 2013. Blockade of Toll-like receptor 4 attenuates morphine tolerance and facilitates the pain relieving properties of morphine. *Journal of Neuroscience,* 33**,** 15952-15963.

ENGSTRÖM, L., ENGBLOM, D., ÖRTEGREN, U., MACKERLOVA, L., PAUES, J. & BLOMQVIST, A. 2001. Preproenkephalin mRNA expression in rat parabrachial neurons: relation to cells activated by systemic immune challenge. *Neuroscience letters,* 316**,** 165-168.

ERBS, E., FAGET, L., SCHERRER, G., MATIFAS, A., FILLIOL, D., VONESCH, J.-L., KOCH, M., KESSLER, P., HENTSCH, D. & BIRLING, M.-C. 2015. A mu–delta opioid receptor brain atlas reveals neuronal co-occurrence in subcortical networks. *Brain Structure and Function,* 220**,** 677-702.

ERBS, E., FAGET, L., VEINANTE, P., KIEFFER, B. L. & MASSOTTE, D. 2014. In vivo neuronal co-expression of mu and delta opioid receptors uncovers new therapeutic perspectives. *Receptors Clin Investig,* 1.

ERICKSON, R. L., BROWNE, C. A. & LUCKI, I. 2017. Hair corticosterone measurement in mouse models of type 1 and type 2 diabetes mellitus. *Physiol Behav,* 178**,** 166-171.

ERMAN, T., GÖÇER, A. I., YLDZ, M. S., TUNA, M., POLAT, S. & ILDAN, F. 2004. Effect of naloxone after spinal cord injury in the rat: inducible nitric oxide synthase expression, superoxide dismutase activity, and ultrastructural changes. *Neurosurgery Quarterly,* 14**,** 249-256.

EZURE, K., TANAKA, I. & MIYAZAKI, M. 1998. Pontine projections of pulmonary slowly adapting receptor relay neurons in the cat. *Neuroreport,* 9**,** 411-4.

FACCHINETTI, F., GRASSO, A., PETRAGLIA, F., PARRINI, D., VOLPE, A. & GENAZZANI, A. 1984. Impaired circadian rhythmicity of ß-lipotrophin, ß-endorphin and ACTH in heroin addicts. *European Journal of Endocrinology,* 105**,** 149-155.

FARACI, F. M. 2011. Protecting against vascular disease in brain. *Am J Physiol Heart Circ Physiol,* 300**,** H1566-82.

FARACI, F. M. & HEISTAD, D. D. 1990. Regulation of large cerebral arteries and cerebral microvascular pressure. *Circulation research,* 66**,** 8-17.

FARACI, F. M., TAUGHER, R. J., LYNCH, C., FAN, R., GUPTA, S. & WEMMIE, J. A. 2019. Acid-sensing ion channels: Novel mediators of cerebral vascular responses. *Circulation research,* 125**,** 907-920.

FELDMAN, J. L. 1986. Neurophysiology of breathing in mammals. *Comprehensive Physiology*.

FELDMAN, J. L. & DEL NEGRO, C. A. 2006. Looking for inspiration: new perspectives on respiratory rhythm. *Nat Rev Neurosci,* 7**,** 232-42.

FELDMAN, J. L., DEL NEGRO, C. A. & GRAY, P. A. 2013. Understanding the rhythm of breathing: so near, yet so far. *Annu Rev Physiol,* 75**,** 423-52.

FERGUSON, L. M. & DRUMMOND, G. B. 2006. Acute effects of fentanyl on breathing pattern in anaesthetized subjects. *Br J Anaesth,* 96**,** 384-90.

FICHNA, J., JANECKA, A., COSTENTIN, J. & DO REGO, J.-C. 2007. The endomorphin system and its evolving neurophysiological role. *Pharmacological reviews,* 59**,** 88-123.

FIELD, L., DORRANCE, D., KRZEMINSKA, E. & BARSOUM, L. 1993. Effect of nitrous oxide on cerebral blood flow in normal humans. *BJA: British Journal of Anaesthesia,* 70**,** 154-159.

FINELLI, L. A., LANDOLT, H. P., BUCK, A., ROTH, C., BERTHOLD, T., BORBÉLY, A. A. & ACHERMANN, P. 2000. Functional neuroanatomy of human sleep states after zolpidem and placebo: A H215O – PET study. *Journal of sleep research,* 9**,** 161-173.

FINK, R. 1951. A new approach to high resolution radioautography. *Science,* 114**,** 143-149.

FIRESTONE, L. L., GYULAI, F., MINTUN, M., ADLER, L. J., URSO, K. & WINTER, P. M. 1996. Human brain activity response to fentanyl imaged by positron emission tomography. *Anesthesia & Analgesia,* 82**,** 1247-1251.

FISHER, J. T., MORTOLA, J. P., SMITH, J. B., FOX, G. S. & WEEKS, S. 1982. Respiration in newborns: development of the control of breathing. *Am Rev Respir Dis,* 125**,** 650-7.

FITTS, D. A. 2011. Ethics and animal numbers: informal analyses, uncertain sample sizes, inefficient replications, and type I errors. *J Am Assoc Lab Anim Sci,* 50**,** 445-53.

FLAMM, E. S., YOUNG, W., DEMOPOULOS, H. B., DECRESCITO, V. & TOMASULA, J. J. 1982. Experimental spinal cord injury: treatment with naloxone. *Neurosurgery,* 10**,** 227-231.

FODALE, V., SCHIFILLITI, D., PRATICO, C. & SANTAMARIA, L. 2008. Remifentanil and the brain. *Acta Anaesthesiologica Scandinavica,* 52**,** 319-326.

FODOR, A., TÍMÁR, J. & ZELENA, D. 2014. Behavioral effects of perinatal opioid exposure. *Life sciences,* 104**,** 1-8.

FOX, G., GALLACHER, D., SHEVDE, S., LOFTUS, J. & SWAYNE, G. 1993. Anatomic variation of the middle cerebral artery in the Sprague-Dawley rat. *Stroke,* 24**,** 2087-2092.

FRANCESCHINI, M. A., RADHAKRISHNAN, H., THAKUR, K., WU, W., RUVINSKAYA, S., CARP, S. & BOAS, D. A. 2010. The effect of different anesthetics on neurovascular coupling. *Neuroimage,* 51**,** 1367-1377.

FYFE, L. W., CLEARY, D. R., MACEY, T. A., MORGAN, M. M. & INGRAM, S. L. 2010. Tolerance to the antinociceptive effect of morphine in the absence of

short-term presynaptic desensitization in rat periaqueductal gray neurons. *Journal of Pharmacology and Experimental Therapeutics,* 335**,** 674-680.

GABILONDO, A. M., MEANA, J. J. & GARCIA-SEVILLA, J. A. 1995. Increased density of mu-opioid receptors in the postmortem brain of suicide victims. *Brain Res,* 682**,** 245-50.

GARCIA-PEREZ, D., LAORDEN, M. L., MILANES, M. V. & NUNEZ, C. 2012. Glucocorticoids regulation of FosB/DeltaFosB expression induced by chronic opiate exposure in the brain stress system. *PLoS One,* 7**,** e50264.

GERBER, H., BORGWARDT, S. J., SCHMID, O., GERHARD, U., JOECHLE, W., RIECHER-RÖSSLER, A., WIESBECK, G. A. & WALTER, M. 2012. The impact of diacetylmorphine on hypothalamic-pituitary-adrenal axis activity and heroin craving in heroin dependence. *European addiction research,* 18**,** 116-123.

GILLILAN, L. A. 1974. Potential collateral circulation to the human cerebral cortex. *Neurology,* 24**,** 941-8.

GLAHN, A., HEBERLEIN, A., DÜRSTELER-MACFARLAND, K. M., LENZ, B., FRIELING, H., GRÖSCHL, M., WIESBECK, G. A., KORNHUBER, J., BÖNSCH, D. & BLEICH, S. 2013. Atrial natriuretic peptide, arginine vasopressin peptide and cortisol serum levels in opiate-dependent patients. *Neuropsychobiology,* 67**,** 111-115.

GOLANOV, E. V. & REIS, D. J. 1996. Cerebral cortical neurons with activity linked to central neurogenic spontaneous and evoked elevations in cerebral blood flow. *Neuroscience letters,* 209**,** 101-104.

GRAY, P. A., HAYES, J. A., LING, G. Y., LLONA, I., TUPAL, S., PICARDO, M. C., ROSS, S. E., HIRATA, T., CORBIN, J. G., EUGENIN, J. & DEL NEGRO, C. A. 2010. Developmental origin of preBotzinger complex respiratory neurons. *J Neurosci,* 30**,** 14883-95.

GRAY, P. A., JANCZEWSKI, W. A., MELLEN, N., MCCRIMMON, D. R. & FELDMAN, J. L. 2001. Normal breathing requires preBötzinger complex neurokinin-1 receptor-expressing neurons. *Nature neuroscience,* 4**,** 927-930.

GRAY, P. A., REKLING, J. C., BOCCHIARO, C. M. & FELDMAN, J. L. 1999. Modulation of respiratory frequency by peptidergic input to rhythmogenic neurons in the preBötzinger complex. *Science,* 286**,** 1566-1568.

GUDEHITHLU, K. P., TEHWANI, G. A. & BHARGAVA, H. N. 1991. ß-Endorphin and methionine-enkephalin levels in discrete brain regions, spinal cord, pituitary gland and plasma of morphine tolerant-dependent and abstinent rats. *Brain research,* 553**,** 284-290.

GULEMETOVA, R. & KINKEAD, R. 2011. Neonatal stress increases respiratory instability in rat pups. *Respir Physiol Neurobiol,* 176**,** 103-9.

GUST, J., WRIGHT, J., PRATT, E. & BOSMA, M. 2003. Development of synchronized activity of cranial motor neurons in the segmented embryonic mouse hindbrain. *The Journal of physiology,* 550**,** 123-133.

GUYENET, P. G., SEVIGNY, C. P., WESTON, M. C. & STORNETTA, R. L. 2002. Neurokinin-1 receptor-expressing cells of the ventral respiratory group are functionally heterogeneous and predominantly glutamatergic. *J Neurosci,* 22**,** 3806-16.

HABERSTOCK-DEBIC, H., WEIN, M., BARROT, M., COLAGO, E. E., RAHMAN, Z., NEVE, R. L., PICKEL, V. M., NESTLER, E. J., VON ZASTROW, M. & SVINGOS, A. L. 2003. Morphine acutely regulates opioid receptor trafficking selectively in dendrites of nucleus accumbens neurons. *Journal of Neuroscience,* 23**,** 4324-4332.

HAN, S., SOLEIMAN, M. T., SODEN, M. E., ZWEIFEL, L. S. & PALMITER, R. D. 2015. Elucidating an affective pain circuit that creates a threat memory. *Cell,* 162**,** 363-374.

HARRIS, G. & WILLIAMS, J. 1991. Transient homologous mu-opioid receptor desensitization in rat locus coeruleus neurons. *Journal of Neuroscience,* 11**,** 2574-2581.

HARTKAMP, M. J., VAN DER GROND, J., VAN EVERDINGEN, K. J., HILLEN, B. & MALI, W. P. 1999. Circle of Willis collateral flow investigated by magnetic resonance angiography. *Stroke,* 30**,** 2671-2678.

HASHEMI, S. M., MAHMOODI, R. & AMIRJAMSHIDI, A. 2013. Variations in the Anatomy of the Willis' circle: A 3-year cross-sectional study from Iran (2006-2009). Are the distributions of variations of circle of Willis different in different populations? Result of an anatomical study and review of literature. *Surg Neurol Int,* 4**,** 65.

HEISTAD, D. D. 1980. Protection of cerebral vessels by sympathetic nerves. *Physiologist,* 23**,** 44-9.

HERMANSON, O. & BLOMQVIST, A. 1995. Enkephalinergic and catecholaminergic neurons constitute separate populations in the rat Kölliker-Fuse/A7 region. *Neuroscience letters,* 190**,** 57-60.

HERMANSON, O. & BLOMQVIST, A. 1997. Preproenkephalin messenger RNA-expressing neurons in the rat parabrachial nucleus: subnuclear organization and projections to the intralaminar thalamus. *Neuroscience,* 81**,** 803-812.

HILAIRE, G. & DURON, B. 1999. Maturation of the mammalian respiratory system. *Physiol Rev,* 79**,** 325-60.

HOCHBERG, U., OJEDA, A., BRILL, S. & PEREZ, J. 2019. An Internet – Based Survey to Assess Clinicians' Knowledge and Attitudes Towards Opioid – Induced Hypogonadism. *Pain Practice,* 19**,** 176-182.

HOLADAY, J. W., HITZEMANN, R. J., CURELL, J., TORTELLA, F. C. & BELENKY, G. L. 1982. Repeated electroconvulsive shock or chronic morphine treatment increases the number of 3H□ D□ ALA2, D□ LEU5□ enkephalin binding sites in rat brain membranes. *Life sciences,* 31**,** 2359-2362.

HOLLEY, H. S., BEHAN, M. & WENNINGER, J. M. 2012. Age and sex differences in the ventilatory response to hypoxia and hypercapnia in awake neonatal, pre-

pubertal and young adult rats. *Respiratory physiology & neurobiology,* 180**,** 79-87.

HOLZER, P. 2009. Opioid receptors in the gastrointestinal tract. *Regulatory peptides,* 155**,** 11-17.

HOUSHYAR, H., COOPER, Z. & WOODS, J. 2001. Paradoxical effects of chronic morphine treatment on the temperature and pituitary – adrenal responses to acute restraint stress: a chronic stress paradigm. *Journal of neuroendocrinology,* 13**,** 862-874.

HUCKSTEPP, R. T., HENDERSON, L. E., CARDOZA, K. P. & FELDMAN, J. L. 2016. Interactions between respiratory oscillators in adult rats. *Elife,* 5.

HUDETZ, A. G., ROMAN, R. J. & HARDER, D. R. 1992. Spontaneous flow oscillations in the cerebral cortex during acute changes in mean arterial pressure. *Journal of Cerebral Blood Flow & Metabolism,* 12**,** 491-499.

HUNT, R. W., TZIOUMI, D., COLLINS, E. & JEFFERY, H. E. 2008. Adverse neurodevelopmental outcome of infants exposed to opiate in-utero. *Early Hum Dev,* 84**,** 29-35.

IADECOLA, C. 2017. The neurovascular unit coming of age: a journey through neurovascular coupling in health and disease. *Neuron,* 96**,** 17-42.

IGNAR, D. M. & KUHN, C. M. 1990. Effects of specific mu and kappa opiate tolerance and abstinence on hypothalamo-pituitary-adrenal axis secretion in the rat. *J Pharmacol Exp Ther,* 255**,** 1287-95.

INGRAM, S. L., MACEY, T. A., FOSSUM, E. N. & MORGAN, M. M. 2008. Tolerance to repeated morphine administration is associated with increased potency of opioid agonists. *Neuropsychopharmacology,* 33**,** 2494-2504.

INTURRISI, C. E. 2002. Clinical pharmacology of opioids for pain. *The Clinical journal of pain,* 18**,** S3-S13.

JANCZEWSKI, W. A. & FELDMAN, J. L. 2006. Distinct rhythm generators for inspiration and expiration in the juvenile rat. *J Physiol,* 570**,** 407-20.

JANSEN, A. & CHERNICK, V. 1983. Development of respiratory control. *Physiological Reviews,* 63**,** 437-483.

JENG, J.-S., YIP, P.-K., HUANG, S.-J. & KAO, M.-C. 1999. Changes in hemodynamics of the carotid and middle cerebral arteries before and after endoscopic sympathectomy in patients with palmar hyperhidrosis: preliminary results. *Journal of neurosurgery,* 90**,** 463-467.

JEŽOVÁ, D., VIGAŠ, M. & JURČOVIČOVÁ, J. 1982. ACTH and corticosterone response to naloxone and morphine in normal, hypophysectomized and dexamethasone-treated rats. *Life sciences,* 31**,** 307-314.

JIANG, M., ALHEID, G. F., CALANDRIELLO, T. & MCCRIMMON, D. R. 2004. Parabrachial-lateral pontine neurons link nociception and breathing. *Respir Physiol Neurobiol,* 143**,** 215-33.

JONES, A. K., FRISTON, K. J., QI, L. Y., HARRIS, M., CUNNINGHAM, V. J., JONES, T., FEINMAN, C. & FRACKOWIAK, R. S. 1991. Sites of action of morphine in the brain. *Lancet,* 338**,** 825.

JUNG, H. S., SUNG, T.-Y., KANG, H., KIM, J. S. & KIM, T.-Y. 2014. Cerebral blood flow change during volatile induction in large-dose sevoflurane versus intravenous propofol induction: transcranial Doppler study. *Korean journal of anesthesiology,* 67**,** 323.

KADOI, Y., KAWAUCHI, C., IDE, M., SAITO, S. & MIZUTANI, A. 2009. Differential increases in blood flow velocity in the middle cerebral artery after tourniquet deflation during sevoflurane, isoflurane or propofol anaesthesia. *Anaesthesia and intensive care,* 37**,** 598-603.

KAISTI, K. K., LÅNGSJÖ, J. W., AALTO, S., OIKONEN, V., SIPILÄ, H., TERÄS, M., HINKKA, S., METSÄHONKALA, L. & SCHEININ, H. 2003. Effects of sevoflurane, propofol, and adjunct nitrous oxide on regional cerebral blood flow, oxygen

consumption, and blood volume in humans. *The Journal of the American Society of Anesthesiologists,* 99**,** 603-613.

KANO, T., SHIMODA, O., HASHIGUCHI, A. & SATOH, T. 1991. Periodic abnormal fluctuations of blood pressure, heart rate and skin blood flow appearing in a resuscitated comatose patient. *Journal of the autonomic nervous system,* 36**,** 115-122.

KASTRUP, J., PETERSEN, P. & MD, A. D. 1990. Intravenous lidocaine and cerebral blood flow: impaired microvascular reactivity in diabetic patients. *The Journal of Clinical Pharmacology,* 30**,** 318-323.

KENNEDY, A. 2015. *An investigation of the effects of fentanyl on respiratory control*. Ph.D., University of Glasgow.

KETY, S. S. & SCHMIDT, C. F. 1948. The effects of altered arterial tensions of carbon dioxide and oxygen on cerebral blood flow and cerebral oxygen consumption of normal young men. *The Journal of clinical investigation,* 27**,** 484-492.

KITCHEN, I., SLOWE, S. J., MATTHES, H. W. & KIEFFER, B. 1997. Quantitative autoradiographic mapping of μ-, δ-and κ-opioid receptors in knockout mice lacking the μ-opioid receptor gene. *Brain research,* 778**,** 73-88.

KITTERMAN, J. A. 1988. Physiological factors in fetal lung growth. *Canadian journal of physiology and pharmacology,* 66**,** 1122-1128.

KO, J. Y., PATRICK, S. W., TONG, V. T., PATEL, R., LIND, J. N. & BARFIELD, W. D. 2016. Incidence of Neonatal Abstinence Syndrome - 28 States, 1999-2013. *MMWR Morb Mortal Wkly Rep,* 65**,** 799-802.

KOBAYASHI, K., LEMKE, R. P. & GREER, J. J. 2001. Ultrasound measurements of fetal breathing movements in the rat. *Journal of Applied Physiology,* 91**,** 316-320.

KOCH, T. & HÖLLT, V. 2008. Role of receptor internalization in opioid tolerance and dependence. *Pharmacology & therapeutics,* 117**,** 199-206.

KOIZUMI, H., MOSHER, B., TARIQ, M. F., ZHANG, R., KOSHIYA, N. & SMITH, J. C. 2016. Voltage-Dependent Rhythmogenic Property of Respiratory Pre-Botzinger Complex Glutamatergic, Dbx1-Derived, and Somatostatin-Expressing Neuron Populations Revealed by Graded Optogenetic Inhibition. *eNeuro,* 3.

KOTTICK, A., MARTIN, C. A. & DEL NEGRO, C. A. 2017. Fate mapping neurons and glia derived from Dbx1-expressing progenitors in mouse preBotzinger complex. *Physiol Rep,* 5.

KU MOHD NOOR, K. M. 2017. *Disruption of the light/dark cycle and outcome after experimental stroke*. Ph.D., University of Glasgow.

KUBIN, L., ALHEID, G. F., ZUPERKU, E. J. & MCCRIMMON, D. R. 2006. Central pathways of pulmonary and lower airway vagal afferents. *Journal of Applied Physiology,* 101**,** 618-627.

KUNKO, P. M., SMITH, J. A., WALLACE, M. J., MAHER, J. R., SAADY, J. J. & ROBINSON, S. E. 1996. Perinatal methadone exposure produces physical dependence and altered behavioral development in the rat. *J Pharmacol Exp Ther,* 277**,** 1344-51.

LABORATORY, T. J. *Body weight information for C57BL/6J (000664)* [Online]. Available: https://www.jax.org/jax-mice-and-services/strain-data-sheet-pages/body-weight-chart-000664 [Accessed 20/08/2022].

LAFERRIERE, A., COLIN-DURAND, J. & MOSS, I. R. 2005. Ontogeny of respiratory sensitivity and tolerance to the mu-opioid agonist fentanyl in rat. *Brain Res Dev Brain Res,* 156**,** 210-7.

LALLEY, P. M., PILOWSKY, P. M., FORSTER, H. V. & ZUPERKU, E. J. 2014. CrossTalk opposing view: The pre-Botzinger complex is not essential for respiratory depression following systemic administration of opioid analgesics. *J Physiol,* 592**,** 1163-6.

LAM, A., DONLON, E., ENG, C., MAYBERG, T., ROUX, L., LOYD, D., MATTA, B. & FORREST, P. 1993. The effect of lidocaine on cerebral blood flow and metabolism during normocapnia and hypocapnia in humans. *Journal of Neurosurgical Anesthesiology,* 5**,** 307.

LAPRAIRIE, J. & MURPHY, A. Z. 2009. Neonatal injury alters adult pain sensitivity by increasing opioid tone in the periaqueductal gray. *Frontiers in behavioral neuroscience,* 3**,** 31.

LAPRAIRIE, J. L. & MURPHY, A. Z. 2010. Long-term impact of neonatal injury in male and female rats: Sex differences, mechanisms and clinical implications. *Frontiers in neuroendocrinology,* 31**,** 193-202.

LARA, J. P., PARKES, M. J., SILVA-CARVHALO, L., IZZO, P., DAWID-MILNER, M. S. & SPYER, K. M. 1994. Cardiovascular and respiratory effects of stimulation of cell bodies of the parabrachial nuclei in the anaesthetized rat. *J Physiol,* 477**,** 321-9.

LAW, P. Y., ERICKSON, L. J., EL-KOUHEN, R., DICKER, L., SOLBERG, J., WANG, W., MILLER, E., BURD, A. L. & LOH, H. H. 2000. Receptor density and recycling affect the rate of agonist-induced desensitization of mu-opioid receptor. *Mol Pharmacol,* 58**,** 388-98.

LEBLOND, C. P., WILKINSON, G., BELANGER, L. & ROBICHON, J. 1950. Radio – autographic visualization of bone formation in the rat. *American Journal of Anatomy,* 86**,** 289-341.

LEE, R. M. 1995. Morphology of cerebral arteries. *Pharmacol Ther,* 66**,** 149-73.

LEINO, K., MILDH, L., LERTOLA, K., SEPPÄLÄ, T. & KIRVELÄ, O. 1999. Time course of changes in breathing pattern in morphine-and oxycodone-induced respiratory depression. *Anaesthesia,* 54**,** 835-840.

LEVINE, A., MORLEY, J., GOSNELL, B., BILLINGTON, C. & BARTNESS, T. 1985. Opioids and consummatory behavior. *Brain research bulletin,* 14**,** 663-672.

LEVITT, E. S., ABDALA, A. P., PATON, J. F., BISSONNETTE, J. M. & WILLIAMS, J. T. 2015. μ opioid receptor activation hyperpolarizes respiratory – controlling Kölliker–Fuse neurons and suppresses post – inspiratory drive. *The Journal of physiology,* 593**,** 4453-4469.

LEWANOWITSCH, T., MILLER, J. H. & IRVINE, R. J. 2006. Reversal of morphine, methadone and heroin induced effects in mice by naloxone methiodide. *Life sciences,* 78**,** 682-688.

LI, C.-X., PATEL, S., WANG, D. J. & ZHANG, X. 2014. Effect of high dose isoflurane on cerebral blood flow in macaque monkeys. *Magnetic resonance imaging,* 32**,** 956-960.

LITTLE, P. J. & KUHN, C. M. 1995. Ontogenetic studies of tolerance development: effects of chronic morphine on the hypothalamic-pituitary-adrenal axis. *Psychopharmacology,* 122**,** 78-84.

LIU, Q., FEHRING, C., LOWRY, T. F. & WONG-RILEY, M. T. 2009. Postnatal development of metabolic rate during normoxia and acute hypoxia in rats: implication for a sensitive period. *Journal of applied physiology,* 106**,** 1212-1222.

LIU, Y. Y., WONG – RILEY, M. T., LIU, J. P., WEI, X. Y., JIA, Y., LIU, H. L., FUJIYAMA, F. & JU, G. 2004. Substance P and enkephalinergic synapses onto neurokinin – 1 receptor – immunoreactive neurons in the pre – Bötzinger complex of rats. *European Journal of Neuroscience,* 19**,** 65-75.

LONERGAN, T., GOODCHILD, A. K., CHRISTIE, M. J. & PILOWSKY, P. M. 2003. Mu opioid receptors in rat ventral medulla: effects of endomorphin-1 on phrenic nerve activity. *Respiratory Physiology & Neurobiology,* 138**,** 165-178.

LONGDEN, T. A., DABERTRAND, F., KOIDE, M., GONZALES, A. L., TYKOCKI, N. R., BRAYDEN, J. E., HILL-EUBANKS, D. & NELSON, M. T. 2017. Capillary K+-sensing initiates retrograde hyperpolarization to increase local cerebral blood flow. *Nature neuroscience,* 20**,** 717-726.

LOPEZ-LARSON, M. P., BOGORODZKI, P., ROGOWSKA, J., MCGLADE, E., KING, J. B., TERRY, J. & YURGELUN-TODD, D. 2011. Altered prefrontal and insular cortical thickness in adolescent marijuana users. *Behavioural brain research,* 220**,** 164-172.

LORENZ, I., KOLBITSCH, C., SCHOCKE, M., KREMSER, C., ZSCHIEGNER, F., HINTEREGGER, M., FELBER, S., HÖRMANN, C. & BENZER, A. 2000. Low – dose remifentanil increases regional cerebral blood flow and regional cerebral blood volume, but decreases regional mean transit time and regional cerebrovascular resistance in volunteers. *British journal of anaesthesia,* 85**,** 199-204.

LOWE, M., MOCK, B. & SORENSON, J. 1998. Functional connectivity in single and multislice echoplanar imaging using resting-state fluctuations. *Neuroimage,* 7**,** 119-132.

LUCAS, S. J., BURGESS, K. R., THOMAS, K. N., DONNELLY, J., PEEBLES, K. C., LUCAS, R. A., FAN, J. L., COTTER, J. D., BASNYAT, R. & AINSLIE, P. N. 2011. Alterations in cerebral blood flow and cerebrovascular reactivity during 14 days at 5050 m. *J Physiol,* 589**,** 741-53.

LUMSDEN, T. 1923. Observations on the respiratory centres in the cat. *J Physiol,* 57**,** 153-60.

LUNDBERG, J. M., HÖKFELT, T., FAHRENKRUG, J., NILSSON, G. & TERENIUS, L. 1979. Peptides in the cat carotid body (glomus caroticum): VIP – , enkephalin – , and substance P – like immunoreactivity. *Acta Physiologica Scandinavica,* 107**,** 279-281.

LYNCH, W. J., ROTH, M. E. & CARROLL, M. E. 2002. Biological basis of sex differences in drug abuse: preclinical and clinical studies. *Psychopharmacology (Berl),* 164**,** 121-37.

MANNUZZA, S., KLEIN, R. G., TRUONG, N. L., MOULTON III, P. D., JOHN L, ROIZEN, E. R., HOWELL, K. H. & CASTELLANOS, F. X. 2008. Age of methylphenidate treatment initiation in children with ADHD and later substance

abuse: prospective follow-up into adulthood. *American Journal of Psychiatry,* 165, 604-609.

MANSOUR, A., KHACHATURIAN, H., LEWIS, M. E., AKIL, H. & WATSON, S. J. 1988. Anatomy of CNS opioid receptors. *Trends in neurosciences,* 11, 308-314.

MANZKE, T., GUENTHER, U., PONIMASKIN, E. G., HALLER, M., DUTSCHMANN, M., SCHWARZACHER, S. & RICHTER, D. W. 2003. 5-HT4 (a) receptors avert opioid-induced breathing depression without loss of analgesia. *Science,* 301, 226-229.

MARCKWALD, M. 1888. *The Movements of Respiration: And Their Innervation in the Rabbit. With a Supplement on the Relation of Respiration to Deglutition, and on the Question of the Existence of Respiratory Centres in the Spinal Cord,* Blackie & Son.

MARINA, N., CHRISTIE, I. N., KORSAK, A., DORONIN, M., BRAZHE, A., HOSFORD, P. S., WELLS, J. A., SHEIKHBAHAEI, S., HUMOUD, I. & PATON, J. F. 2020. Astrocytes monitor cerebral perfusion and control systemic circulation to maintain brain blood flow. *Nature communications,* 11, 1-9.

MARTINEZ, J. A., VARGAS, M. L., FUENTE, T., GARCIA, J. D. R. & MILANÉS, M. V. 1990. Plasma ß-endorphin and cortisol levels in morphine-tolerant rats and in naloxone-induced withdrawal. *European journal of pharmacology,* 182, 117-123.

MATTHES, H. W., MALDONADO, R., SIMONIN, F., VALVERDE, O., SLOWE, S., KITCHEN, I., BEFORT, K., DIERICH, A., LE MEUR, M. & DOLLÉ, P. 1996. Loss of morphine-induced analgesia, reward effect and withdrawal symptoms in mice lacking the μ-opioid-receptor gene. *Nature,* 383, 819-823.

MATTHEW, E., ANDREASON, P., PETTIGREW, K., CARSON, R. E., HERSCOVITCH, P., COHEN, R., KING, C., JOHANSON, C.-E., GREENBLATT, D. J. & PAUL, S. M. 1995. Benzodiazepine receptors mediate regional blood flow changes in the living human brain. *Proceedings of the National Academy of Sciences,* 92, 2775-2779.

MATTSON, C. L., SCHIEBER, L., SCHOLL, L., RUDD, R. A., SETH, P., XU, L., WILSON, N. O. & PAULOZZI, L. J. 2017. Annual surveillance report of drug-related risks and outcomes-United States. CDC National Center for Injury Prevention and Control.

MAYER, C. A., DI FIORE, J. M., MARTIN, R. J. & MACFARLANE, P. M. 2014. Vulnerability of neonatal respiratory neural control to sustained hypoxia during a uniquely sensitive window of development. *Journal of Applied Physiology,* 116**,** 514-521.

MCKAY, L. C., EVANS, K. C., FRACKOWIAK, R. S. & CORFIELD, D. R. 2003. Neural correlates of voluntary breathing in humans. *Journal of Applied Physiology,* 95**,** 1170-1178.

MCKAY, L. C., JANCZEWSKI, W. A. & FELDMAN, J. L. 2005. Sleep-disordered breathing after targeted ablation of preBotzinger complex neurons. *Nat Neurosci,* 8**,** 1142-4.

MCNICOL, E. 2008. Opioid side effects and their treatment in patients with chronic cancer and noncancer pain. *Journal of Pain & Palliative Care Pharmacotherapy,* 22**,** 270-281.

MELLEN, N. M., JANCZEWSKI, W. A., BOCCHIARO, C. M. & FELDMAN, J. L. 2003. Opioid-induced quantal slowing reveals dual networks for respiratory rhythm generation. *Neuron,* 37**,** 821-826.

MENG, L., HOU, W., CHUI, J., HAN, R. & GELB, A. W. 2015. Cardiac output and cerebral blood flow: the integrated regulation of brain perfusion in adult humans. *Anesthesiology,* 123**,** 1198-1208.

MEUNIER, J.-C., MOLLEREAU, C., TOLL, L., SUAUDEAU, C., MOISAND, C., ALVINERIE, P., BUTOUR, J.-L., GUILLEMOT, J.-C., FERRARA, P. & MONSARRAT, B. 1995. Isolation and structure of the endogenous agonist of opioid receptor-like ORL1 receptor. *Nature,* 377**,** 532.

MILICI-EMILI, G. & PETIT, J. M. 1960. Mechanical efficiency of breathing. *J Appl Physiol,* 15**,** 359-62.

MILLER, J. R., ZUPERKU, E. J., STUTH, E. A., BANERJEE, A., HOPP, F. A. & STUCKE, A. G. 2017. A subregion of the parabrachial nucleus partially mediates respiratory rate depression from intravenous remifentanil in young and adult rabbits. *Anesthesiology: The Journal of the American Society of Anesthesiologists,* 127**,** 502-514.

MONTANDON, G., BAIRAM, A. & KINKEAD, R. 2006. Long-term consequences of neonatal caffeine on ventilation, occurrence of apneas, and hypercapnic chemoreflex in male and female rats. *Pediatr Res,* 59**,** 519-24.

MONTANDON, G. & HORNER, R. L. 2019. Electrocortical changes associating sedation and respiratory depression by the opioid analgesic fentanyl. *Scientific reports,* 9**,** 1-11.

MONTANDON, G., QIN, W., LIU, H., REN, J., GREER, J. J. & HORNER, R. L. 2011. PreBotzinger complex neurokinin-1 receptor-expressing neurons mediate opioid-induced respiratory depression. *J Neurosci,* 31**,** 1292-301.

MOORE, J. D., DESCHÊNES, M., FURUTA, T., HUBER, D., SMEAR, M. C., DEMERS, M. & KLEINFELD, D. 2013. Hierarchy of orofacial rhythms revealed through whisking and breathing. *Nature,* 497**,** 205-210.

MOORE, J. D., KLEINFELD, D. & WANG, F. 2014. How the brainstem controls orofacial behaviors comprised of rhythmic actions. *Trends in neurosciences,* 37**,** 370-380.

MORLEY, J. E., BARANETSKY, N. G., WINGERT, T. D., CARLSON, H. E., HERSHMAN, J. M., MELMED, S., LEVIN, S. R., JAMISON, K. R., WEITZMAN, R. & CHANG, R. J. 1980. Endocrine effects of naloxone-induced opiate receptor blockade. *The Journal of Clinical Endocrinology & Metabolism,* 50**,** 251-257.

MOSS, I. R., BROWN, K. A. & LAFERRIERE, A. 2006. Recurrent hypoxia in rats during development increases subsequent respiratory sensitivity to fentanyl. *Anesthesiology,* 105**,** 715-8.

MULKEY, D. K., STORNETTA, R. L., WESTON, M. C., SIMMONS, J. R., PARKER, A., BAYLISS, D. A. & GUYENET, P. G. 2004. Respiratory control by ventral surface chemoreceptor neurons in rats. *Nat Neurosci,* 7**,** 1360-9.

NAMBURI, P., BEYELER, A., YOROZU, S., CALHOON, G. G., HALBERT, S. A., WICHMANN, R., HOLDEN, S. S., MERTENS, K. L., ANAHTAR, M., FELIX-ORTIZ, A. C., WICKERSHAM, I. R., GRAY, J. M. & TYE, K. M. 2015. A circuit mechanism for differentiating positive and negative associations. *Nature,* 520**,** 675-8.

NIESTERS, M., OVERDYK, F., SMITH, T., AARTS, L. & DAHAN, A. 2013. Opioid-induced respiratory depression in paediatrics: a review of case reports. *British journal of anaesthesia,* 110**,** 175-182.

O'DONOVAN, M. & LANDMESSER, L. 1987. The development of hindlimb motor activity studied in the isolated spinal cord of the chick embryo. *Journal of Neuroscience,* 7**,** 3256-3264.

O'HERRON, P., CHHATBAR, P. Y., LEVY, M., SHEN, Z., SCHRAMM, A. E., LU, Z. & KARA, P. 2016. Neural correlates of single-vessel haemodynamic responses in vivo. *Nature,* 534**,** 378-382.

OBRIG, H., NEUFANG, M., WENZEL, R., KOHL, M., STEINBRINK, J., EINHÄUPL, K. & VILLRINGER, A. 2000. Spontaneous low frequency oscillations of cerebral hemodynamics and metabolism in human adults. *Neuroimage,* 12**,** 623-639.

ODEBLAD, E. 1953. Artefacts in autoradiography. *Acta radiologica,* 39**,** 192-204.

OHTAKE, P. J., SIMAKAJORNBOON, N., FEHNIGER, M. D., XUE, Y.-D. & GOZAL, D. 2000. N-Methyl-D-aspartate receptor expression in the nucleus tractus solitarii and maturation of hypoxic ventilatory response in the rat. *American journal of respiratory and critical care medicine,* 162**,** 1140-1147.

OKUBO, S. & MORTOLA, J. P. 1988. Long-term respiratory effects of neonatal hypoxia in the rat. *J Appl Physiol (1985),* 64**,** 952-8.

ONIMARU, H. & HOMMA, I. 2002. Development of the rat respiratory neuron network during the late fetal period. *Neuroscience research,* 42**,** 209-218.

ONIMARU, H. & HOMMA, I. 2003. A novel functional neuron group for respiratory rhythm generation in the ventral medulla. *Journal of Neuroscience,* 23**,** 1478-1486.

ONIMARU, H., IKEDA, K. & KAWAKAMI, K. 2008. CO2-sensitive preinspiratory neurons of the parafacial respiratory group express Phox2b in the neonatal rat. *J Neurosci,* 28**,** 12845-50.

OREN, R. E., RASOOL, N. A. & RUBINSTEIN, E. H. 1987. Effect of ketamine on cerebral cortical blood flow and metabolism in rabbits. *Stroke,* 18**,** 441-444.

OSBORNE, P. & WILLIAMS, J. 1995. Characterization of acute homologous desensitization of μ – opioid receptor – induced currents in locus coeruleus neurones. *British journal of pharmacology,* 115**,** 925-932.

PAGLIARDINI, S., GOSGNACH, S. & DICKSON, C. T. 2013. Spontaneous sleep-like brain state alternations and breathing characteristics in urethane anesthetized mice. *PLoS One,* 8**,** e70411.

PAGLIARDINI, S., JANCZEWSKI, W. A., TAN, W., DICKSON, C. T., DEISSEROTH, K. & FELDMAN, J. L. 2011. Active expiration induced by excitation of ventral medulla in adult anesthetized rats. *J Neurosci,* 31**,** 2895-905.

PAGLIARDINI, S., REN, J. & GREER, J. J. 2003. Ontogeny of the pre-Bötzinger complex in perinatal rats. *Journal of Neuroscience,* 23**,** 9575-9584.

PALKOVITS, M. & ESKAY, R. 1987. Distribution and possible origin of ß-endorphin and ACTH in discrete brainstem nuclei of rats. *Neuropeptides,* 9**,** 123-137.

PANDIT, J. J., MOHAN, R. M., PATERSON, N. D. & POULIN, M. J. 2003. Cerebral blood flow sensitivity to CO2 measured with steady-state and Read's rebreathing methods. *Respir Physiol Neurobiol,* 137**,** 1-10.

PANERAI, A. E., MARTINI, A., DI GIULIO, A. M., FRAIOLI, F., VEGNI, C., PARDI, G., MARINI, A. & MANTEGAZZA, P. 1983. Plasma beta-endorphin, beta-lipotropin, and met-enkephalin concentrations during pregnancy in normal and drug-addicted women and their newborn. *J Clin Endocrinol Metab,* 57**,** 537-43.

PANERAI, R. B. 1998. Assessment of cerebral pressure autoregulation in humans--a review of measurement methods. *Physiol Meas,* 19**,** 305-38.

PANTALEO, T., MUTOLO, D., CINELLI, E. & BONGIANNI, F. 2011. Respiratory responses to somatostatin microinjections into the Botzinger complex and the pre-Botzinger complex of the rabbit. *Neurosci Lett,* 498**,** 26-30.

PARKIS, M., DONG, X.-W., FELDMAN, J. & FUNK, G. 1999. Concurrent inhibition and excitation of phrenic motoneurons during inspiration: phase-specific control of excitability. *Journal of Neuroscience,* 19**,** 2368-2380.

PATON, J. F., ABDALA, A. P., KOIZUMI, H., SMITH, J. C. & ST-JOHN, W. M. 2006. Respiratory rhythm generation during gasping depends on persistent sodium current. *Nature neuroscience,* 9**,** 311-313.

PATRICK, S. W., SCHUMACHER, R. E., BENNEYWORTH, B. D., KRANS, E. E., MCALLISTER, J. M. & DAVIS, M. M. 2012. Neonatal abstinence syndrome and associated health care expenditures: United States, 2000-2009. *JAMA,* 307**,** 1934-40.

PATTINSON, K. T. 2008. Opioids and the control of respiration. *Br J Anaesth,* 100**,** 747-58.

PAXINOS, G. & FRANKLIN, K. B. 2019. *Paxinos and Franklin's the mouse brain in stereotaxic coordinates*, Academic press.

PEÑA, F., PARKIS, M. A., TRYBA, A. K. & RAMIREZ, J.-M. 2004. Differential contribution of pacemaker properties to the generation of respiratory rhythms during normoxia and hypoxia. *Neuron,* 43**,** 105-117.

PERIMED. 2018. *PSI NR and HR - Perimed* [Online]. Perimed. Available: https://www.perimed-instruments.com/product/psi-nr-hr/ [Accessed 2018].

PEZAWAS, L., FISCHER, G., PODREKA, I., SCHINDLER, S., BRÜCKE, T., JAGSCH, R., THURNHER, M. & KASPER, S. 2002. Opioid addiction changes cerebral blood flow symmetry. *Neuropsychobiology,* 45**,** 67-73.

PEZAWAS, L. M., FISCHER, G., DIAMANT, K., SCHNEIDER, C., SCHINDLER, S. D., THURNHER, M., PLOECHL, W., EDER, H. & KASPER, S. 1998. Cerebral CT findings in male opioid-dependent patients: stereological, planimetric and linear measurements. *Psychiatry Research: Neuroimaging,* 83**,** 139-147.

PHILLIPSON, E. & BOWES, G. 1986. Handbook of physiology. the respiratory system. *American Physiological Society***,** 649-689.

PICARDO, M. C., WERAGALAARACHCHI, K. T., AKINS, V. T. & DEL NEGRO, C. A. 2013. Physiological and morphological properties of Dbx1-derived respiratory neurons in the pre-Botzinger complex of neonatal mice. *J Physiol,* 591**,** 2687-703.

PILAPIL, C., WELNER, S., MAGNAN, J., GAUTHIER, S. & QUIRION, R. 1987. Autoradiographic distribution of multiple classes of opioid receptor binding sites in human forebrain. *Brain research bulletin,* 19**,** 611-615.

PILOZZI, A., CARRO, C. & HUANG, X. 2020. Roles of beta-Endorphin in Stress, Behavior, Neuroinflammation, and Brain Energy Metabolism. *Int J Mol Sci,* 22.

PRKIC, I., MUSTAPIC, S., RADOCAJ, T., STUCKE, A. G., STUTH, E. A., HOPP, F. A., DEAN, C. & ZUPERKU, E. J. 2012. Pontine mu-opioid receptors mediate bradypnea caused by intravenous remifentanil infusions at clinically relevant concentrations in dogs. *J Neurophysiol,* 108**,** 2430-41.

PUTNAM, R. W., CONRAD, S. C., GDOVIN, M., ERLICHMAN, J. S. & LEITER, J. C. 2005. Neonatal maturation of the hypercapnic ventilatory response and central neural CO2 chemosensitivity. *Respiratory physiology & neurobiology,* 149**,** 165-179.

QIU, Y.-W., HAN, L.-J., LV, X.-F., JIANG, G.-H., TIAN, J.-Z., ZHUO, F.-Z., SU, H.-H., LIN, C.-L. & ZHANG, X.-L. 2011. Regional homogeneity changes in heroin-dependent individuals: resting-state functional MR imaging study. *Radiology,* 261**,** 551-559.

RAJAN, V., VARGHESE, B., VAN LEEUWEN, T. G. & STEENBERGEN, W. 2009. Review of methodological developments in laser Doppler flowmetry. *Lasers Med Sci,* 24**,** 269-83.

RAY, S. B. & WADHWA, S. 1999. Mu opioid receptors in developing human spinal cord. *J Anat,* 195 (Pt 1)**,** 11-8.

READ, D. J. & HENDERSON-SMART, D. J. 1984. Regulation of breathing in the newborn during different behavioral states. *Annu Rev Physiol,* 46**,** 675-85.

RECANT, L., VOYLES, N., WADE, A., AWOKE, S. & BHATHENA, S. 1983. Studies on the role of opiate peptides in two forms of genetic obesity: ob/ob mouse and fa/fa rat. *Hormone and metabolic research,* 15**,** 589-593.

REINSTRUP, P., RYDING, E., OHLSSON, T., SANDELL, A., ERLANDSSON, K., LJUNGGREN, K., SALFORD, L., STRAND, S. & USKI, T. 2008. Regional cerebral metabolic rate (positron emission tomography) during inhalation of nitrous oxide 50% in humans. *British journal of anaesthesia,* 100**,** 66-71.

REKLING, J. C., CHAMPAGNAT, J. & DENAVIT-SAUBIE, M. 1996. Thyrotropin-releasing hormone (TRH) depolarizes a subset of inspiratory neurons in the newborn mouse brain stem in vitro. *Journal of neurophysiology,* 75**,** 811-819.

REN, J. & GREER, J. J. 2003. Ontogeny of rhythmic motor patterns generated in the embryonic rat spinal cord. *Journal of neurophysiology,* 89**,** 1187-1195.

REVILL, A. L., VANN, N. C., AKINS, V. T., KOTTICK, A., GRAY, P. A., DEL NEGRO, C. A. & FUNK, G. D. 2015. Dbx1 precursor cells are a source of inspiratory XII premotoneurons. *Elife,* 4**,** e12301.

RITTER, B. & ZHANG, W. 2000. Early postnatal maturation of GABAA – mediated inhibition in the brainstem respiratory rhythm – generating network of the mouse. *European Journal of Neuroscience,* 12**,** 2975-2984.

ROMERO, J. R., PIKULA, A., NGUYEN, T. N., NIEN, Y. L., NORBASH, A. & BABIKIAN, V. L. 2009. Cerebral collateral circulation in carotid artery disease. *Current cardiology reviews,* 5**,** 279-288.

ROSE, M. F., REN, J., AHMAD, K. A., CHAO, H. T., KLISCH, T. J., FLORA, A., GREER, J. J. & ZOGHBI, H. Y. 2009. Math1 is essential for the development of hindbrain neurons critical for perinatal breathing. *Neuron,* 64**,** 341-54.

ROY, C. S. & SHERRINGTON, C. S. 1890. On the Regulation of the Blood-supply of the Brain. *J Physiol,* 11**,** 85-158 17.

ROY-BYRE, P., FLEISHAKER, J., ARNETT, C., DUBACH, M., STEWART, J., RADANT, A., VEITH, R. & GRAHAM, M. 1993. Effects of acute and chronic alprazolam treatment on cerebral blood flow, memory, sedation, and plasma catecholamines. *Neuropsychopharmacology,* 8**,** 161-169.

RYBAK, I. A., SHEVTSOVA, N. A., PATON, J. F., DICK, T. E., ST-JOHN, W. M., MORSCHEL, M. & DUTSCHMANN, M. 2004. Modeling the ponto-medullary respiratory network. *Respir Physiol Neurobiol,* 143**,** 307-19.

SAEED, Z. I., BANCOS, I. & DONEGAN, D. 2019. Current knowledge and practices of heath care professionals on opioid-induced adrenal insufficiency. *Endocrine Practice,* 25**,** 1012-1021.

SAFO, Y., YOUNG, M., SMITH, D., GREENBERG, J., CARLSSON, C., REIVICH, M., KEYKHAH, M. & HARP, J. 1985. Effects of fentanyl on local cerebral blood flow in the rat. *Acta anaesthesiologica scandinavica,* 29**,** 594-598.

SANDISON, D. R. & WEBB, W. W. 1994. Background rejection and signal-to-noise optimization in confocal and alternative fluorescence microscopes. *Applied optics,* 33**,** 603-615.

SAUNDERS, S. E. & LEVITT, E. S. 2020. Kölliker-Fuse/Parabrachial complex mu opioid receptors contribute to fentanyl-induced apnea and respiratory rate depression. *Respiratory physiology & neurobiology,* 275**,** 103388.

SCHEEL, P., RUGE, C. & SCHONING, M. 2000. Flow velocity and flow volume measurements in the extracranial carotid and vertebral arteries in healthy adults: reference data and the effects of age. *Ultrasound Med Biol,* 26**,** 1261-6.

SCHLAEPFER, T. E., STRAIN, E. C., GREENBERG, B. D., PRESTON, K. L., LANCASTER, E., BIGELOW, G. E., BARTA, P. E. & PEARLSON, G. D. 1998. Site of opioid action in the human brain: mu and kappa agonists' subjective and cerebral blood flow effects. *American Journal of Psychiatry,* 155**,** 470-473.

SCHLÜNZEN, L., JUUL, N., HANSEN, K. & COLD, G. 2012. Regional cerebral blood flow and glucose metabolism during propofol anaesthesia in healthy subjects studied with positron emission tomography. *Acta anaesthesiologica scandinavica,* 56**,** 248-255.

SCHUMACHER, M., BASBAUM, A. & WAY, W. 2004. Opioid analgesics and antagonists. *Basic and Clinical Pharmacology. 9th ed. New York: Lange Medical Books/McGraw-Hill,* 497-516.

SCORRANO, F., CARRASCO, J., PASTOR-CIURANA, J., BELDA, X., RAMI-BASTANTE, A., BACCI, M. L. & ARMARIO, A. 2015. Validation of the long-term assessment of hypothalamic-pituitary-adrenal activity in rats using hair corticosterone as a biomarker. *FASEB J,* 29**,** 859-67.

SHARDLOW, E. & JACKSON, A. 2011. Cerebral blood flow and intracranial pressure. *Anaesthesia & Intensive Care Medicine,* 12**,** 220-223.

SIEGEL, G. J. 1999. *Basic neurochemistry: molecular, cellular and medical aspects*.

SIM-SELLEY, L. J., SELLEY, D. E., VOGT, L. J., CHILDERS, S. R. & MARTIN, T. J. 2000. Chronic heroin self-administration desensitizes μ opioid receptor-activated G-proteins in specific regions of rat brain. *Journal of Neuroscience,* 20**,** 4555-4562.

SLUPE, A. M. & KIRSCH, J. R. 2018. Effects of anesthesia on cerebral blood flow, metabolism, and neuroprotection. *Journal of Cerebral Blood Flow & Metabolism,* 38**,** 2192-2208.

SMITH, J. C., ELLENBERGER, H. H., BALLANYI, K., RICHTER, D. W. & FELDMAN, J. L. 1991. Pre-Bötzinger complex: a brainstem region that may generate respiratory rhythm in mammals. *Science (New York, NY),* 254**,** 726.

SONKA, M. & GRUNKIN, M. 2002. Image processing and analysis in drug discovery and clinical trials. *IEEE Trans Med Imaging,* 21**,** 1209-11.

SPYER, K. M. 2009. To breathe or not to breathe? That is the question. *Exp Physiol,* 94**,** 1-10.

SQUEGLIA, L. M., JACOBUS, J. & TAPERT, S. F. 2009. The influence of substance use on adolescent brain development. *Clinical EEG and neuroscience,* 40**,** 31-38.

STAFFORD, K., GOMES, A. B., SHEN, J. & YOBURN, B. C. 2001. μ-Opioid receptor downregulation contributes to opioid tolerance in vivo. *Pharmacology Biochemistry and Behavior,* 69**,** 233-237.

STALDER, T. & KIRSCHBAUM, C. 2012. Analysis of cortisol in hair--state of the art and future directions. *Brain Behav Immun,* 26**,** 1019-29.

STEIN, C. 2007. *Analgesia,* Springer Science & Business Media.

STEIN, C. 2016. Opioid receptors. *Annual review of medicine,* 67**,** 433-451.

STEIN, C. & MACHELSKA, H. 2011. Modulation of peripheral sensory neurons by the immune system: implications for pain therapy. *Pharmacological reviews,* 63**,** 860-881.

STEIN, C. & ZOLLNER, C. 2009. Opioids and sensory nerves. *Handb Exp Pharmacol*, 495-518.

STORNETTA, R. L., MOREIRA, T. S., TAKAKURA, A. C., KANG, B. J., CHANG, D. A., WEST, G. H., BRUNET, J. F., MULKEY, D. K., BAYLISS, D. A. & GUYENET, P. G. 2006. Expression of Phox2b by brainstem neurons involved in chemosensory integration in the adult rat. *J Neurosci,* 26, 10305-14.

STORNETTA, R. L., ROSIN, D. L., WANG, H., SEVIGNY, C. P., WESTON, M. C. & GUYENET, P. G. 2003. A group of glutamatergic interneurons expressing high levels of both neurokinin-1 receptors and somatostatin identifies the region of the pre-Botzinger complex. *J Comp Neurol,* 455, 499-512.

STUNDEN, C., FILOSA, J. A., GARCIA, A., DEAN, J. B. & PUTNAM, R. W. 2001. Development of in vivo ventilatory and single chemosensitive neuron responses to hypercapnia in rats. *Respiration physiology,* 127, 135-155.

SUZUKI, J., IWABUCHI, T. & HORI, S. 1975. Cervical sympathectomy for cerebral vasospasm after aneurysm rupture. *Neurologia medico-chirurgica,* 15, 41-50.

TAKEDA, S., ERIKSSON, L. I., YAMAMOTO, Y., JOENSEN, H., ONIMARU, H. & LINDAHL, S. G. 2001. Opioid action on respiratory neuron activity of the isolated respiratory network in newborn rats. *Anesthesiology: The Journal of the American Society of Anesthesiologists,* 95, 740-749.

TAN, W., JANCZEWSKI, W. A., YANG, P., SHAO, X. M., CALLAWAY, E. M. & FELDMAN, J. L. 2008. Silencing preBötzinger complex somatostatin-expressing neurons induces persistent apnea in awake rat. *Nature neuroscience,* 11, 538-540.

TAN, W., PAGLIARDINI, S., YANG, P., JANCZEWSKI, W. A. & FELDMAN, J. L. 2010. Projections of preBotzinger complex neurons in adult rats. *J Comp Neurol,* 518, 1862-78.

TER LAAN, M., VAN DIJK, J., ELTING, J., STAAL, M. & ABSALOM, A. 2013. Sympathetic regulation of cerebral blood flow in humans: a review. *British journal of anaesthesia,* 111**,** 361-367.

THANOS, P. K., MICHAELIDES, M., BENVENISTE, H., WANG, G. J. & VOLKOW, N. D. 2007. Effects of chronic oral methylphenidate on cocaine self-administration and striatal dopamine D2 receptors in rodents. *Pharmacology Biochemistry and Behavior,* 87**,** 426-433.

THEODORE, W. H., LEIDERMAN, D., GAILLARD, W., KHAN, I., REEVES, P. & LLOYD-HONTZ, K. 1993. The effect of naloxone on cerebral blood flow and glucose metabolism in patients with complex partial seizures. *Epilepsy research,* 16**,** 51-54.

THOBY-BRISSON, M., CAULI, B., CHAMPAGNAT, J., FORTIN, G. & KATZ, D. M. 2003. Expression of functional tyrosine kinase B receptors by rhythmically active respiratory neurons in the pre-Bötzinger complex of neonatal mice. *Journal of Neuroscience,* 23**,** 7685-7689.

THOBY-BRISSON, M. & GREER, J. J. 2008. Anatomical and functional development of the pre-Botzinger complex in prenatal rodents. *J Appl Physiol (1985),* 104**,** 1213-9.

THOBY-BRISSON, M., KARLEN, M., WU, N., CHARNAY, P., CHAMPAGNAT, J. & FORTIN, G. 2009. Genetic identification of an embryonic parafacial oscillator coupling to the preBotzinger complex. *Nat Neurosci,* 12**,** 1028-35.

THOBY-BRISSON, M. & RAMIREZ, J.-M. 2001. Identification of two types of inspiratory pacemaker neurons in the isolated respiratory neural network of mice. *Journal of neurophysiology,* 86**,** 104-112.

THOBY-BRISSON, M., TRINH, J.-B., CHAMPAGNAT, J. & FORTIN, G. 2005. Emergence of the pre-Bötzinger respiratory rhythm generator in the mouse embryo. *Journal of Neuroscience,* 25**,** 4307-4318.

THORNTON, S. R. & SMITH, F. L. 1998. Long-term alterations in opiate antinociception resulting from infant fentanyl tolerance and dependence. *Eur J Pharmacol,* 363**,** 113-9.

TIMAR, J., SOBOR, M., KIRALY, K. P., GYARMATI, S., RIBA, P., AL-KHRASANI, M. & FURST, S. 2010. Peri, pre and postnatal morphine exposure: exposure-induced effects and sex differences in the behavioural consequences in rat offspring. *Behav Pharmacol,* 21**,** 58-68.

TOUBIA, T. & KHALIFE, T. 2019. The endogenous opioid system: role and dysfunction caused by opioid therapy. *Clinical obstetrics and gynecology,* 62**,** 3-10.

TRESCOT, A. M., DATTA, S., LEE, M. & HANSEN, H. J. P. P. 2008. Opioid pharmacology. 11**,** S133-53.

TRIGO, J. M., MARTIN-GARCÍA, E., BERRENDERO, F., ROBLEDO, P. & MALDONADO, R. 2010. The endogenous opioid system: a common substrate in drug addiction. *Drug and alcohol dependence,* 108**,** 183-194.

URSINO, M. & LODI, C. A. 1997. A simple mathematical model of the interaction between intracranial pressure and cerebral hemodynamics. *J Appl Physiol (1985),* 82**,** 1256-69.

VALVERDE-FILHO, J., CUNHA NETO, M. B. C. D., FONOFF, E. T., MEIRELLES, E. D. S. & TEIXEIRA, M. J. 2015. Chronic spinal and oral morphine-induced neuroendocrine and metabolic changes in noncancer pain patients. *Pain Medicine,* 16**,** 715-725.

VAN BOCKSTAELE, E. & COMMONS, K. 2001. Internalization of mu-opioid receptors produced by etorphine in the rat locus coeruleus. *Neuroscience,* 108**,** 467–477.

VANN, N. C., PHAM, F. D., HAYES, J. A., KOTTICK, A. & DEL NEGRO, C. A. 2016. Transient Suppression of Dbx1 PreBotzinger Interneurons Disrupts Breathing in Adult Mice. *PLoS One,* 11**,** e0162418.

VARGA, A. G., REID, B. T., KIEFFER, B. L. & LEVITT, E. S. 2020. Differential impact of two critical respiratory centres in opioid – induced respiratory depression in awake mice. *The Journal of Physiology,* 598**,** 189-205.

VICTORIA, N. C., KAROM, M. C. & MURPHY, A. Z. 2015. Analgesia for early-life pain prevents deficits in adult anxiety and stress in rats. *Dev Neurosci,* 37**,** 1-13.

VICTORIA, N. C. & MURPHY, A. Z. 2016. The long-term impact of early life pain on adult responses to anxiety and stress: historical perspectives and empirical evidence. *Experimental neurology,* 275**,** 261-273.

VIEMARI, J. C., BURNET, H., BÉVENGUT, M. & HILAIRE, G. 2003. Perinatal maturation of the mouse respiratory rhythm – generator: in vivo and in vitro studies. *European Journal of Neuroscience,* 17**,** 1233-1244.

VIRK, M. S. & WILLIAMS, J. T. 2008. Agonist-specific regulation of μ-opioid receptor desensitization and recovery from desensitization. *Molecular pharmacology,* 73**,** 1301-1308.

VUONG, C., VAN UUM, S. H., O'DELL, L. E., LUTFY, K. & FRIEDMAN, T. C. 2010. The effects of opioids and opioid analogs on animal and human endocrine systems. *Endocrine reviews,* 31**,** 98-132.

WALDHOER, M., BARTLETT, S. E. & WHISTLER, J. L. 2004. Opioid receptors. *Annual review of biochemistry,* 73**,** 953-990.

WALSH, K. & CUNNINGHAM, A. J. 2004. Cerebral Oxygen Vasoreactivity and Cerebral Tissue Oxygen Reactivity. *Survey of Anesthesiology,* 48**,** 77-78.

WANG, H., STORNETTA, R. L., ROSIN, D. L. & GUYENET, P. G. 2001. Neurokinin-1 receptor-immunoreactive neurons of the ventral respiratory group in the rat. *J Comp Neurol,* 434**,** 128-46.

WANG, X., HAYES, J. A., REVILL, A. L., SONG, H., KOTTICK, A., VANN, N. C., LAMAR, M. D., PICARDO, M. C., AKINS, V. T., FUNK, G. D. & DEL NEGRO, C. A.

2014. Laser ablation of Dbx1 neurons in the pre-Botzinger complex stops inspiratory rhythm and impairs output in neonatal mice. *Elife,* 3**,** e03427.

WATSON, C., PAXINOS, G. & PUELLES, L. 2012. *The mouse nervous system*, Academic Press.

WILKIN, J. K. 1986. Periodic cutaneous blood flow during postocclusive reactive hyperemia. *American Journal of Physiology-Heart and Circulatory Physiology,* 250**,** H765-H768.

WILLIAMS, J. T., INGRAM, S. L., HENDERSON, G., CHAVKIN, C., VON ZASTROW, M., SCHULZ, S., KOCH, T., EVANS, C. J. & CHRISTIE, M. J. 2013. Regulation of μ-opioid receptors: desensitization, phosphorylation, internalization, and tolerance. *Pharmacological reviews,* 65**,** 223-254.

WILLIE, C. K., COLINO, F. L., BAILEY, D. M., TZENG, Y. C., BINSTED, G., JONES, L. W., HAYKOWSKY, M. J., BELLAPART, J., OGOH, S., SMITH, K. J., SMIRL, J. D., DAY, T. A., LUCAS, S. J., ELLER, L. K. & AINSLIE, P. N. 2011. Utility of transcranial Doppler ultrasound for the integrative assessment of cerebrovascular function. *J Neurosci Methods,* 196**,** 221-37.

WILLIE, C. K., TZENG, Y. C., FISHER, J. A. & AINSLIE, P. N. 2014. Integrative regulation of human brain blood flow. *The Journal of physiology,* 592**,** 841-859.

WINTERINGHAM, F., HARRISON, A. & HAMMOND, J. 1950. Autoradiography of water-soluble tracers in histological sections. *Nature,* 165**,** 149-150.

WINTERS, B. L., GREGORIOU, G. C., KISSIWAA, S. A., WELLS, O. A., MEDAGODA, D. I., HERMES, S. M., BURFORD, N. T., ALT, A., AICHER, S. A. & BAGLEY, E. E. 2017. Endogenous opioids regulate moment-to-moment neuronal communication and excitability. *Nature communications,* 8**,** 1-15.

WONG-RILEY, M. T. & LIU, Q. 2005. Neurochemical development of brain stem nuclei involved in the control of respiration. *Respiratory physiology & neurobiology,* 149**,** 83-98.

WONG-RILEY, M. T. & LIU, Q. 2008. Neurochemical and physiological correlates of a critical period of respiratory development in the rat. *Respiratory physiology & neurobiology,* 164**,** 28-37.

WONG-RILEY, M. T., LIU, Q. & GAO, X.-P. 2013. Peripheral–central chemoreceptor interaction and the significance of a critical period in the development of respiratory control. *Respiratory physiology & neurobiology,* 185**,** 156-169.

WU, J., CAPELLI, P., BOUVIER, J., GOULDING, M., ARBER, S. & FORTIN, G. 2017. A V0 core neuronal circuit for inspiration. *Nature communications,* 8**,** 1-12.

XIE, A., SKATRUD, J. B., BARCZI, S. R., REICHMUTH, K., MORGAN, B. J., MONT, S. & DEMPSEY, J. A. 2009. Influence of cerebral blood flow on breathing stability. *J Appl Physiol (1985),* 106**,** 850-6.

YACKLE, K., SCHWARZ, L. A., KAM, K., SOROKIN, J. M., HUGUENARD, J. R., FELDMAN, J. L., LUO, L. & KRASNOW, M. A. 2017. Breathing control center neurons that promote arousal in mice. *Science,* 355**,** 1411-1415.

YAGODA, H. & YAGODA, B. H. 1949. *Radioactive measurements with nuclear emulsions*, Wiley New York.

YVERT, B., BRANCHEREAU, P. & MEYRAND, P. 2004. Multiple spontaneous rhythmic activity patterns generated by the embryonic mouse spinal cord occur within a specific developmental time window. *Journal of neurophysiology,* 91**,** 2101-2109.

ZADINA, J. E., KASTIN, A. J., GE, L.-J., GULDEN, H. & BUNGART, K. J. 1989. Chronic, but not acute, administration of morphine alters antiopiate (Tyr-MIF-1) binding sites in rat brain. *Life sciences,* 44**,** 555-561.

ZADINA, J. E., KASTIN, A. J., HARRISON, L. M., GE, L. J. & CHANG, S. L. 1995. Opiate receptor changes after chronic exposure to agonists and antagonists. *Annals of the New York Academy of Sciences,* 757**,** 353-361.

ZEILER, F. A., SADER, N., GILLMAN, L. M., TEITELBAUM, J., WEST, M. & KAZINA, C. J. 2016. The cerebrovascular response to ketamine: a systematic review of the animal and human literature. *Journal of neurosurgical anesthesiology,* 28**,** 123-140.

ZELAYA, F. O., ZOIS, E., MULLER-POLLARD, C., LYTHGOE, D. J., LEE, S., ANDREWS, C., SMART, T., CONROD, P., VENNART, W. & WILLIAMS, S. C. 2012. The response to rapid infusion of fentanyl in the human brain measured using pulsed arterial spin labelling. *Magnetic Resonance Materials in Physics, Biology and Medicine,* 25**,** 163-175.

ZHANG, F., HANSON, S. M., JARA-OSEGUERA, A., KREPKIY, D., BAE, C., PEARCE, L. V., BLUMBERG, P. M., NEWSTEAD, S. & SWARTZ, K. J. 2016. Engineering vanilloid-sensitivity into the rat TRPV2 channel. *Elife,* 5.

ZHOU, H., SUN, J., JI, X., LIN, J., TANG, S., ZENG, J. & FAN, Y.-H. 2016. Correlation between the integrity of the circle of Willis and the severity of initial noncardiac cerebral infarction and clinical prognosis. *Medicine,* 95.